

University of Warwick institutional repository: <http://go.warwick.ac.uk/wrap>

A Thesis Submitted for the Degree of PhD at the University of Warwick

<http://go.warwick.ac.uk/wrap/59800>

This thesis is made available online and is protected by original copyright.

Please scroll down to view the document itself.

Please refer to the repository record for this item for information to help you to cite it. Our policy information is available from the repository home page.

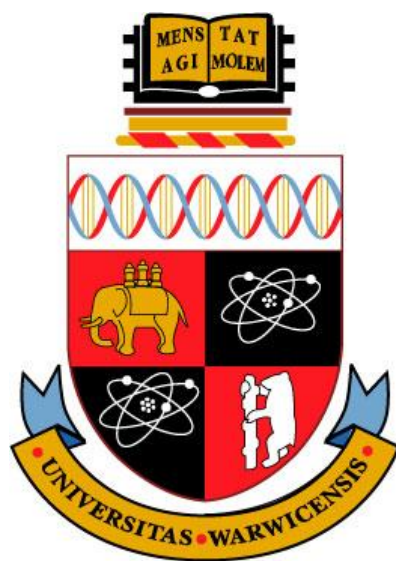
Photoactivatable Platinum(IV)

Anticancer Complexes

A Thesis Submitted for the Degree of
Doctor of Philosophy

By

Evvyenia Shaili, *M. Sc.*



University of Warwick
Molecular Organisation and Assembly in Cells
Doctoral Training Centre
September 2013

**To my parents, Evangelos and Lenia, for their unconditional
love and support throughout the years...**

Table of Contents

Acknowledgments.....	i
Declaration	iii
Conferences Attended	iv
Courses Attended	v
Abstract	vi
Abbreviations	viii
Chapter 1 Introduction	1
1.1 Cancer	2
1.2 Cisplatin	2
1.3 Cisplatin drawbacks and development of second and third generation Pt(II) agents.....	5
1.4 Non-conventional Pt(II) agents	7
1.5 Pt(IV)-prodrugs	10
1.6 Photodynamic therapy (PDT)	11
1.7 Light Delivery	14
1.8 Photophysical and photochemical properties of metal complexes	15
1.9 Non-platinum metal-based photoactivated drugs	19
1.10 Photoactivity of Pt(II) complexes	21
1.11 Photoactivity of Pt(IV) complexes.....	24
1.11.1 Pt(IV)-diiodo and Pt(IV)-diazido complexes	25
1.12 Aims	31
References	32

Chapter 2 Experimental Methods.....	40
2.1 Nuclear Magnetic Resonance spectroscopy (NMR)	41
2.2 Mass Spectrometry	42
2.2.1 Electrospray mass spectrometry (ESI-MS)	42
2.2.2 LC-MS (Liquid Chromatography-Mass Spectrometry)	43
2.3 HPLC (High Performance Liquid Chromatography).....	44
2.4 X-Ray crystallography	44
2.5 UV-VIS spectroscopy	45
2.6 pH measurements	46
2.7 Irradiation methods and devices.....	46
2.8 Light measurements	47
2.10 DFT and TDDFT calculations	48
2.11 Cell culture	48
2.12 Photo-dark toxicity testing	49
2.12.1 Neutral Red assay	50
2.12.2 MTT assay	50
References	52

Chapter 3 Axial ligand derivatisations of Pt(IV)-diazido compounds..	53
3.1 Introduction	54
3.2 Experimental	59
3.2.1 Materials	60
3.2.2 Methods and Instrumentation	60
3.2.2.1 HPLC purity test.....	60

3.2.2.2 Extinction coefficient determination	61
3.2.2.3 pKa [*] study for complex 4	61
3.2.2.4 Electron Paramagnetic Resonance	62
3.2.2.5 Computational details	62
3.2.2.6 Cell uptake studies	62
3.2.2.7 Fluorescence measurements	63
3.2.2.8 Synthesis and characterisation	64
3.3 Results	70
3.3.1 HPLC purity test	71
3.3.2 X-Ray diffraction	72
3.3.3 Aqueous solubility and stability in the dark	83
3.3.4 pKa [*] for complex 4	87
3.3.5 Extinction coefficient studies	88
3.3.6 Photoirradiation studies followed by UV-Vis	90
3.3.7 Photoirradiation studies followed by EPR.....	94
3.3.8 NMR irradiation studies	97
3.2.8.1 Photoirradiation studies of complex 4	
<i>trans, trans, trans</i> -[Pt(N ₃) ₂ (OH)(Succ)(pyr) ₂]	98
3.2.8.2 Photoirradiation studies of complex 6	
<i>trans, trans, trans</i> -[Pt(N ₃) ₂ (OH)(N-MI)(pyr) ₂]	103
3.3.9 High resolution LC-MS studies	106
3.2.9.1 LC-MS studies of complexes [Pt(N ₃) ₂ (OH)(Succ)(pyr) ₂] 4	
and [Pt(N ₃) ₂ (OH)(Succ-(RGD)f)(pyr) ₂] 7	107
3.2.9.2 LC-MS study of [Pt(N ₃) ₂ (OH)(N-MI)(pyr) ₂] 6	113
3.3.10 DFT and TDDFT calculations	117
3.3.11 Cytotoxicity and cellular uptake studies	123

3.4 Discussion	127
3.4.1 Synthesis and characterisation	128
3.4.2 Aqueous solubility and stability in the dark	132
3.4.3 Photoirradiations.....	133
3.4.3.1 UV-Vis studies	133
3.4.3.2 EPR studies.....	135
3.4.4 NMR and LC-MS studies	137
3.4.4.1 NMR and LC-MS studies of complexes $[\text{Pt}(\text{N}_3)_2(\text{OH})(\text{Succ})(\text{pyr})_2]$ 4 and $[\text{Pt}(\text{N}_3)_2(\text{OH})(\text{Succ}(\text{RGD})\text{f})(\text{pyr})_2]$ 7	137
3.4.4.2 NMR and LC-MS studies of complex $[\text{Pt}(\text{N}_3)_2(\text{OH})(\text{N-MI})(\text{pyr})_2]$ 6	141
3.4.5 Fluorescence studies	143
3.4.6 Cell studies.....	144
3.5 Conclusions	146
References	148

Chapter 4 Photoactivatable Pt(IV)-diazido complexes bearing aromatic N-heterocyclic ligands 153

4.1 Introduction	154
4.2 Experimental	156
4.2.1 Materials	157
4.2.2 Methods	157
4.2.2.1 HPLC	157
4.2.2.2 Extinction coefficient determination	158
4.2.2.3 X-Ray Diffraction.....	158
4.2.2.4 DFT calculations	158

4.2.2.5 Synthesis and characterisation.....	158
4.3 Results	172
4.3.1 Characterisation and purity test	172
4.3.2 X-Ray diffraction.....	172
4.3.3 Solubility and stability	177
4.3.4 Extinction coefficient determinations	177
4.3.5 Photoirradiation of complexes followed by UV-Vis	178
4.3.6 ¹ H-NMR of complexes <i>cis</i> -[Pt(I) ₂ (2-pic) ₂] 10 and <i>cis</i> -[Pt(Cl) ₂ (2-pic) ₂] 11	182
4.3.7 DFT-TDDFT for complex 18	183
4.4 Discussion	186
4.4.1 Synthesis, characterization and solubility.....	187
4.4.2 X-Ray crystallography	193
4.4.3 Photoirradiations monitored by UV-Vis.....	196
4.5 Conclusions	198
References	199

Chapter 5 Nucleobase binding and cellular behaviour of Pt(IV)-

diazido complexes.....	202
5.1 Introduction	203
5.2 Materials.....	205
5.3 Methods.....	206
5.3.1 5'-GMP binding studies.....	206
5.3.2 Phototoxicity testing	206
5.3.3 Light dose dependence on cell survival (Action spectra)	207
5.3.4 Yeast studies	208

5.3.5 Confocal Microscopy.....	209
5.4 Results	211
5.4.1 5'-GMP binding studies.....	211
5.4.2 Phototoxicity testing	216
5.4.3 Cell survival in <i>Schizosaccharomyces pombe</i> in response to Pt(IV)-diazido drug	218
5.4.4 Live-cell confocal microscopy	220
5.5 Discussion	223
5.5.1 5'-GMP binding studies.....	223
5.5.2 Phototoxicity and structure-activity relationships	224
5.5.3 Cell survival assessed in <i>S.pombe</i>	226
5.5.4 Live-cell confocal microscopy	230
5.6 Conclusions	232
References	234
 Chapter 6 Conclusions and future outlook	237
6.1 Conclusions	238
6.2 Future Work	243
6.2.1 Axial ligand modifications	243
6.2.2 Further work on ligand modifications	246
References	247
 Appendix.....	249

Acknowledgements

Firstly, I would like to thank Professor Peter Sadler for his guidance and supervision during my PhD. I greatly appreciate the opportunity I was given to be a member of his large research group and his exciting research.

EPSRC and MOAC are acknowledged for the funding. It has been a great experience to be a part of the MOAC DTC science community. A special acknowledgement is given to Prof Alison Rodger for her advice and encouragement throughout my PhD.

I would like to thank from the bottom of my heart all the PJS members (past and present). Special thanks to Dr Nicky Farrer for all her guidance especially at the beginning of my PhD, Miss Jennifer S. Butler for the EPR experiments, Dr Isolda Romero-Canelón for the help with the (crazy-hour!) biological work, Dr Yao Zhao for all the useful discussions, Dr Carlos Sánchez-Cano for the thesis proof-reading, the advice (and the office fun!), Dr Nicolas Barry for the general support, Miss Ruth McQuitty and Dr Ana Pizarro for the help with the HPLC. Also I would like to acknowledge our collaborators (Dr Vicente Marchan's group, University of Barcelona) for the peptide work.

Special thanks to Dr Julie Woods for the phototoxicity studies and also I am particularly grateful for allowing me to visit and work in her research facility in Ninewells Hospital (Dundee, UK). Many thanks to Dr Jacob Dalgaard and his group for the help with the yeast project and Dr Keith Leppard for the assistance with the confocal microscopy work.

I would also like to thank especially Dr Ivan Prokes for his help with the NMR, Dr Lijiang Song and Mr Phil Aston for their assistance with the mass spectrometry experiments and Dr Guy Clarkson for the X-ray crystallography.

To mi amiga, Dr María José Romero Castro, I don't think I have enough space here to express my gratitude. Thanks for listening, teaching, guiding and supporting especially towards the end where I needed you the most. You have been an impeccable friend to me and I will never forget you.

To Dr Luca Salassa (aka, the coach) thank you for the help with the DFT calculations but also for enduring a lot of DQ moments, for the advice and the

jokes! Your presence in the PJS always lit up everyone's mood, especially mine. (p.s. may the shining light be with you!).

To Dr Abraha Habtemariam, I would like to say massive thanks for always advising on chemistry and non-chemistry related matters, the interesting discussions and for always being supportive. Thank you for having faith in me and for always seeing the best in people.

Furthermore, I would like to thank Dr Julie Ann Lough for the help with the thesis, for the encouragement and for the hugs (virtual and actual).

To Khatija Bhayat, honey bee: thank you for being a shoulder to cry on, for the words of encouragement and for all those moments and memories that I will cherish.

To Joan Josep Soldevila Barreda thank you for believing in me, for the endless nights we spent in the chemistry department, your help throughout my PhD and your friendship.

To Adam Millett (aka homie) thank you for listening to my constant moaning but also the countless funny office moments!

To Nichola Smith, thank you for being a photoactivatable buddy and for allowing me to keep the radio on in our "dark side" of the lab and also joining in for magnificent musical duets!

To Luke Taylor and Vicky Marlow: thank you for being true friends from the MSc year. You have left me with wonderful memories.

To Andrew-what can I say! Thank you for your patience, your kindness, your support, your loyalty, your love, for listening to my uninteresting science moans and for never doubting me. Thank you for being here in every step of the way.

Last but not least I would like to thank my parents to whom this thesis is dedicated to. Without a doubt, your love has been a constant fuel through the difficult times that I have encountered. To my sister Ioanna and my friends Polina, Stephanie, Margarita and Natalie: you are undoubtedly the best friends a girl could ask for. Our long-lasting friendship is something that I can certainly rely on throughout the rollercoaster of life!

Declaration

I hereby declare that except where specific reference is made to other sources, the work contained in this Thesis is the original work of the author. It has been composed by myself and has not been submitted, in whole or in part, for any other degree, diploma, or other qualification.

Evyyenia Shaili

September 2013

Conferences attended

- 1) Warwick Chemistry postgraduate symposia (University of Warwick, Coventry, UK):
June, 2012 (Oral presentation)
May, 2011 (Poster presentation)
May 2010 (Attendance)
- 2) MOAC Annual Conferences:
July, 2012 (Poster Presentation, Ravenstor, Peak District, England),
July, 2011 (Poster Presentation, Arnside, Lake District, England),
May, 2010 (Poster Presentation, Arnside, Lake District, England)
- 3) Inter-DTC symposia between Institute of Chemical Biology DTC (Imperial College London), White Rose DTC (University of Sheffield) and MOAC (University of Warwick):
June, 2009 (Imperial College London, Attendance)
April, 2010 (Warwick University, Poster Presentation)
- 4) Photoactivatable metals: from theory to therapy (June 2012, London, Attendance)
- 5) Photoactivatable metal complexes: exciting potential in biotechnology and medicine? (June 2012, Chicheley, Poster and Oral Presentation)
- 6) Inorganic Chemistry 2012-A joint meeting of Dalton Division Interest Groups (April 2012, University of Warwick, Poster Presentation)
- 7) 5th EuCheMS Conference on Nitrogen Ligands (September 2011, Granada, Spain, Poster Presentation)

Courses attended

- 1) Transferable skills courses in MOAC
- 2) Weekly MOAC seminars
- 3) Weekly Chemical Biology cluster talks

Research Stays

August 2011: One month stay at the Photobiology Unit of Ninewells Hospital (Dundee, Scotland, UK) to work under the supervision of Dr Julie Woods.

Abstract

In this work, *trans*-diazido Pt(IV) complexes with general formula $[\text{Pt}(\text{N}_3)_2(\text{OH})(\text{OCOR})(\text{pyr})_2]$ (where OCOR is a carboxylate axial ligand) and $[\text{Pt}(\text{N}_3)_2(\text{OH})_2(\text{L}_1)(\text{L}_2)]$ (where L_1 and L_2 are aromatic N-heterocyclic ligands) have been synthesised and characterised. The chemical and photochemical properties of these complexes, as well as their photobiological behaviour, have been studied in order to check their potential as photoactivatable anticancer drugs.

Four *trans*-diazido Pt(IV) complexes with general formula *trans, trans, trans*- $[\text{Pt}(\text{N}_3)_2(\text{OH})(\text{OCOR})(\text{pyr})_2]$ (OCOR= succinate, 4-oxo-4-propoxybutanoate, N-methylisatoate and succinate-(RGD)f peptide ligands) have been obtained by axial derivatisation of one hydroxido ligand from *trans, trans, trans*- $[\text{Pt}(\text{N}_3)_2(\text{OH})_2(\text{pyr})_2]$. The crystal structures of three axially-derivatised complexes have been determined by X-ray diffraction. Photoirradiation studies have shown an improved photoactivity of the carboxylate *versus* the dihydroxido complexes at the longer wavelengths. Release of the axial ligands was observed in the studied complexes. This fact is especially relevant in the case of the Pt(IV)-(cRGD)f complex, where the RGD was incorporated as a tumour cell targeting moiety. DFT-TDDFT calculations performed on the complex *trans, trans, trans*- $[\text{Pt}(\text{N}_3)_2(\text{OH})(\text{Succ})(\text{pyr})_2]$ showed dissociative transitions at longer wavelength, which could explain the photolability observed in these carboxylate derivatives. Studies of photoactivation of the diazido Pt(IV) complexes in the presence of 5'-GMP indicate the formation of a mono-GMP Pt(II) adduct as main photoproduct, therefore DNA could be considered a potential target site for these anticancer compounds. Additionally, EPR studies showed that azidyl radical release was observed when complexes bearing the succinate and 4-oxo-4-propoxybutanoate ligands were irradiated with green light. No such result was obtained for the dihydroxo precursor showing that these complexes could be phototoxic with longer wavelength light activation.

Seven *trans*-diazido Pt(IV) complexes, *trans, trans, trans*- $[\text{Pt}(\text{N}_3)_2(\text{OH})_2(\text{L}_1)(\text{L}_2)]$ (where L_1 and L_2 are pyridine, 2-picoline, 3-picoline, 4-picoline, thiazole or 1-methylimidazole ligands), have been obtained by oxidation of the corresponding *trans*- $[\text{Pt}(\text{N}_3)_2(\text{L}_1)(\text{L}_2)]$ precursor. The X-ray crystal

structures have been determined for four Pt(IV) diazido complexes from this family of compounds. Photoirradiation studies indicate that the incorporation of a sterically demanding ligand, e.g. *trans, trans, trans*-[Pt(N₃)₂(OH)₂(2-pic)(pyr)], greatly enhances the photoactivity in these complexes. DFT-TDDFT calculations are in agreement with these results, since higher intensity transitions were observed for such complex at longer wavelength.

Phototoxicity studies carried out on A2780, A2780cis and OE19 cell lines with the *trans, trans, trans*-[Pt(N₃)₂(OH)₂(pyridine)(n-picoline)] family concluded that steric hindrance close to the platinum centre does not favour phototoxicity. Most of the complexes were equally potent in cisplatin resistance against the ovarian cancer cell line (A2780cis), except [Pt(N₃)₂(OH)₂(3-pic)₂] and [Pt(N₃)₂(OH)₂(4-pic)₂] which exhibited some cross resistance. All of the complexes tested in both OE19 and A2780 cell lines have shown less sensitivity to OE19 than to A2780. Studies in *S. pombe* yeast strains (WT and ΔRad3) with *trans, trans, trans*-[Pt(N₃)₂(OH)₂(pyr)₂] suggest that DNA is potentially an important target for this type of compounds, although other targets are not excluded. Furthermore, live-cell confocal microscopy was performed on A2780 cells treated with the complex *trans, trans, trans*-[Pt(N₃)₂(OH)₂(pyr)₂] and irradiated with a low dose of blue light. The cell death, monitored by propidium iodide uptake, was captured occurring 2 h 30 min post activation.

Abbreviations

Å	Angstrom
ACN	Acetonitrile
<i>ca.</i>	<i>circa</i>
CDDP	Cisplatin
CDI	1,1'-carbonyldiimidazole
COSY	Correlation Spectroscopy
δ	chemical shift
d	doublet
Da	Dalton
dd	doublet of doublets
DFT	Density Functional Theory
DMF	N, N'-dimethylformamide
DMPO	5, 5-dimethyl-pyrroline N-oxide
DMSO	Dimethylsulfoxide
DNA	Deoxyribonucleic acid
D ₂ O	Deuterated water
EDTA	Ethylenediaminetetraacetic acid
EPR	Electron Paramagnetic Resonance
eq	equivalent
ESI-MS	Electrospray Ionization Mass Spectrometry
FDA	U.S. Food and Drug Administration
GMP	5'-Guanosine monophosphate

GSH	L-Glutathione or γ -L-Glutamyl-L-cysteinyl-glycine
GSSG	L-Glutathione oxidised
HOMO	Highest Occupied Molecular Orbital
HPLC	High Performance Liquid Chromatography
HSQC	Heteronuclear Single-Quantum Correlation
IC ₅₀	50% growth inhibition concentration
ICP	Inductively Coupled Plasma
ICP-MS	Inductively Coupled Plasma Mass Spectrometry
<i>i.e.</i>	<i>id est</i>
IL	Inter-ligand transitions
J	Coupling constant
λ	Wavelength
LC-MS	Liquid Chromatography-Mass Spectrometry
LED	Light-Emitting Diode
LUMO	Lowest Unoccupied Molecular Orbital
m	multiplet
MeOD	Methanol-d ₄
MLCT/LMCT	Metal-to-ligand/Ligand-to-metal Charge Transfer
mol eq	molar equivalents
m/z	mass/charge
nm	nanometers
N-MIA	N-methylisatoic acid
NMR	Nuclear Magnetic Resonance
OD	Optical Density

PBS	Phosphate buffer solution
PDT	Photodynamic Therapy
PI	Phototoxic Index
ppb	parts per billion
ppm	parts per million
ROS	Reactive Oxygen Species
rpm	revolutions per minute
RPMI	Roswell Park Memorial Institute medium
s	singlet
t	triplet
TDDFT	Time-dependent Density Functional Theory
Tempol	4-hydroxy-2, 2, 6, 6-tetramethyl-piperidine-1-oxyl
TFA	Trifluoroacetic acid
UV	Ultraviolet
UVA	Ultraviolet A
UV-Vis	Ultraviolet-Visible

Chapter 1

Introduction

1.1 Cancer

There are more than 200 types of cancer which have as a common characteristic the uncontrolled cell growth. These are generated from a series of errors in vital signalling pathways which eventually generate a survival advantage over neighbouring cells. Subsequent cell division leads to a modified group of cells (cancer) which divide autonomously since they do not obey to any anti-growth signals. This uncontrolled cell growth allows the formation of tumours, which together with the capacity to spread across different tissues and organs, can be fatal.¹ Statistics show that more than 1 in 3 people will develop some form of cancer in their lifetime, indicating an enormous prevalence.² It is the leading cause of death in developed countries and the second cause of death in developing countries.³

At the moment there are three main streams for the treatment of cancer: surgery (removal of solid tumour when localized in a specific tissue), radiotherapy (radiation with X-ray beam) and chemotherapy (use of antiproliferative drugs). Amongst the drugs used in the last category, platinum drugs are used to treat over 40% of all cancer patients.^{4,5} For this reason, new and more advanced treatments involving platinum and other metallodrugs are likely to be greatly beneficial in enhancing the survival chances of cancer patients.

1.2 Cisplatin

Cisplatin (*cis*-[PtCl₂(NH₃)₂], CDDP) was the first example of a platinum anticancer drug. Its antiproliferative effects were first reported by Rosenberg *et al.* in 1968.^{6,7} The drug was approved for clinical use by the FDA (Food and Drug Administration) in 1978, leading to an enormous improvement of survival rates of

testicular cancer from 10% to greater than 90%. Currently, it is routinely used for the treatment of bladder, advanced cervical cancer, non-metastatic non-small cell lung, ovarian carcinoma, malignant mesothelioma, head and neck squamous cell carcinoma and testicular cancer.⁸

After cisplatin is administered (in a saline solution), via blood perfusion, it remains in the neutral form due to high Cl^- concentration in the blood stream ($>100 \text{ mM}$) which suppresses hydrolysis of the chlorides. Cellular uptake occurs through passive and active transport (partly via copper transporters).⁹ Once inside a cell, where the chloride concentration drops significantly (*ca.* 20 mM), aquation occurs, leading to DNA binding (Figure 1.1).

It is widely accepted that the main target of cisplatin is cellular DNA to which it can bind to two proximal nucleobases forming intra and interstrand crosslinks. Most crosslinks are 1,2-GpG intrastrand (60-65%), whereas 1,2-ApG intrastrand account for another 20-25%. Less frequent are the 1,3-GpXpG intrastrand crosslinks (where there is another base between the two platinated guanines), the G-G interstrand crosslinks as well as monofunctional adducts.^{10,11} Formation of the 1,2-intrastrand crosslinks can kink the DNA structure, inhibiting DNA replication and transcription. These platinum-DNA lesions can be recognized by a number of nuclear proteins such as High Mobility Group-domain (HMG) proteins that protect them from nucleotide excision repair upon binding, finally leading to cell death.⁹ Recently, Lippard *et al.* illustrated that interstrand crosslinks, although low in abundance, have profound effects since they can inhibit transcription as efficiently as 1,2-intrastrand cross links and also inhibit DNA-histone sliding thus evading cellular repair.^{12,13} This suggests that this kind of lesion might have a

greater role in the antiproliferative capacities of cisplatin than previously suspected.

Other pathways might also be responsible for the cytotoxicity of the drug. CDDP causes an increase in the levels of ROS (Reactive Oxygen Species). This effect is caused by the reaction of cisplatin with thiols ($-SH$ containing molecules), which maintain the redox homeostasis within the cell.¹⁴ Furthermore, CDDP is able to block the enzyme Thioredoxin Reductase (TrxR), responsible for the reduction of disulfide bonds, and can alter the mitochondrial functioning, causing NADPH depletion, thus leading to an increase in $OH\cdot$ and $O_2^{\cdot-}$ species.¹⁵

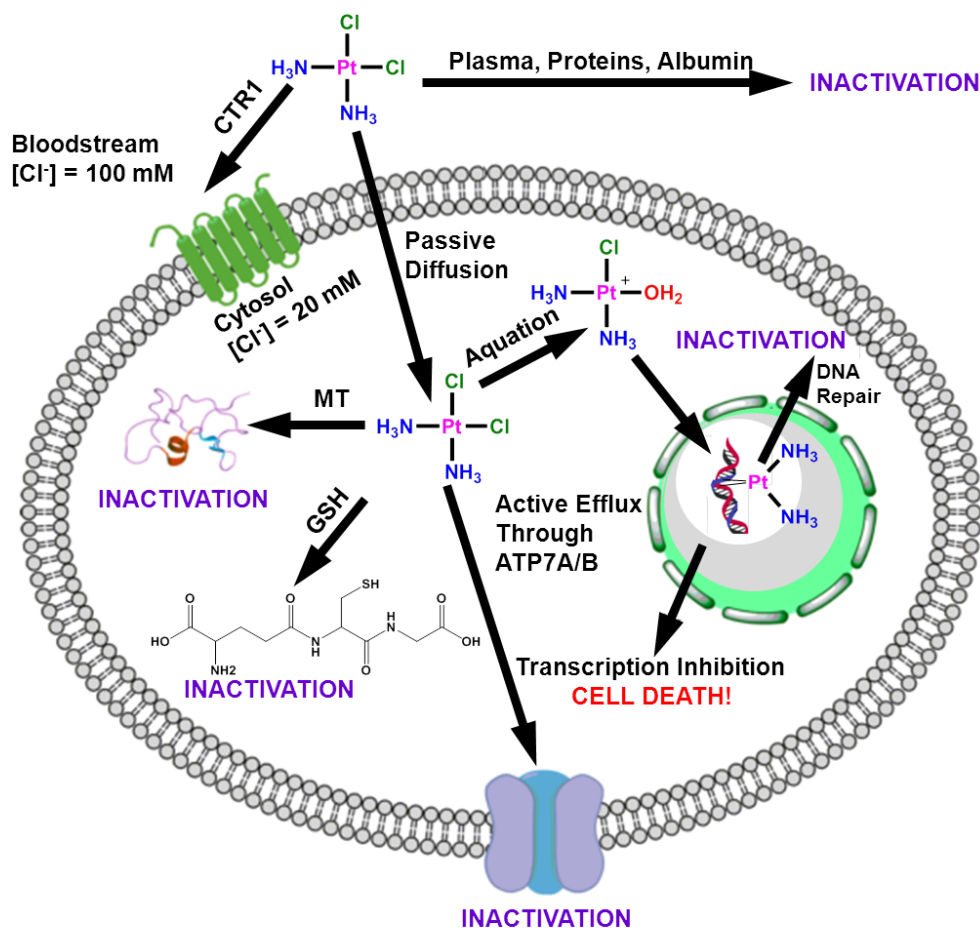


Figure 1.1: Various pathways of cisplatin: uptake, aquation and inactivation pathways. Image modified from that in reference 9.

1.3 Cisplatin drawbacks and development of second and third generation Pt(II) agents

Despite the clinical success of the drug, there are many disadvantages associated with cisplatin. One of the main drawbacks of CDDP, and other Pt(II) drugs, is the development of resistance, which can be inherent or acquired. The former is a result of spontaneous mutations occurring during cell division as part of intrinsic genetic instability and the latter is a result of initial exposure to the chemotherapeutic agent.¹⁵ The three main causes of acquired resistance are as follows:

- (a) Decreased drug uptake and/or increased efflux. It is generally accepted that active transport (e.g. via copper transporter) plays a major role in cisplatin uptake (Figure 1.1). Downregulation of these proteins or upregulation of the efflux proteins (e.g. ATP7A/B) leads to decreased sensitivity to the drug.^{16,17}
- (b) Increased DNA repair (especially nucleotide excision repair which is the main repair mechanism for 1,2-GG intrastrand crosslinks) or bypassing DNA-Pt adducts during replication leads to a decrease in apoptotic response.¹⁰
- (c) Increased drug deactivation through elevated cellular amounts of glutathione and/or metallothioneins. The high affinity of platinum for sulphur makes the drug reactive towards the sulphur-containing molecules in the cell (e.g. GSH). Formation of the inactive adducts prohibits the drug from reaction with the DNA. Furthermore cisplatin produces serious side effects, including nephrotoxicity, nausea, renal toxicity, vomiting, hair loss and asthenia.¹⁸ Ultimately the therapeutic window is narrowed, thus making necessary the development of alternative treatments. Lastly cisplatin is not orally bioavailable and it needs to be administered intravenously.⁸

Other strategies for the development of new Pt drugs have also been explored leading to the discovery of the second (changing the leaving group) and third generation (changing ammines) anticancer drugs. From all the newly-tested complexes, carboplatin, oxaliplatin, nedaplatin, heptaplatin and lobaplatin (Figure 1.2) have found clinical approval, from which the former two are globally employed whereas the latter three are mainly used in Asia.¹⁹ Carboplatin is used for the same spectrum of cancers as cisplatin, but with the advantage of fewer side effects, whereas oxaliplatin responds to a different spectrum of cancers and has found a main applicability in colorectal cancer.¹⁰ Nevertheless, these platinum drugs still suffer from disadvantages, mainly the development of resistance and severe dose limiting side-effects.⁵

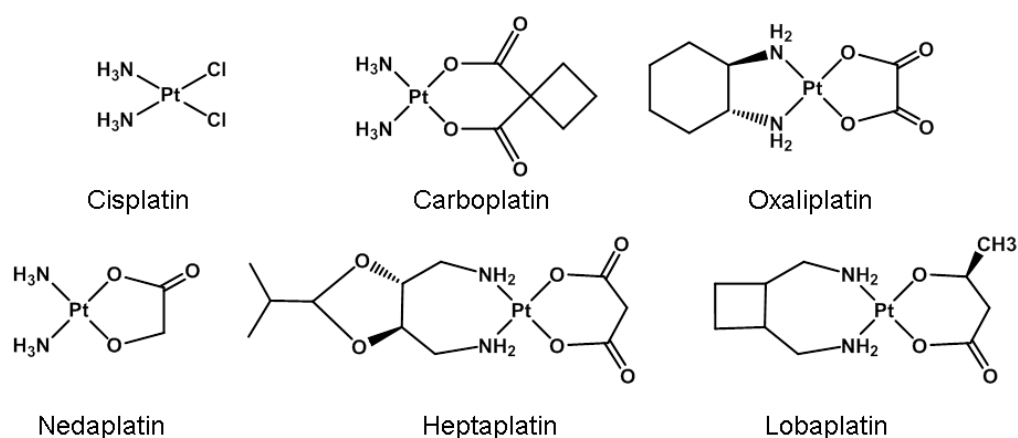


Figure 1.2: Pt(II)-anticancer drugs approved for clinical use.

Other strategies to potentiate platinum drugs are: increase delivery of the drugs to cancer cells via targeting, combination therapy, use of platinum resistance modulators or the development of new drugs that lack cross-resistance.¹⁰

1.4 Non-conventional Pt(II) complexes

The aforementioned Pt(II) complexes exert their mode of action by the formation of coordination bonds with the DNA, which are mainly 1,2-intrastrand crosslinks.¹⁸ In this section the mode of action of non-conventional Pt(II) drugs will be described, with a main focus on the monofunctional and *trans*-Pt(II) complexes.

The term monofunctional implies that the complex can bind to DNA through only one coordination site (Figure 1.3 A). Although some monofunctional complexes, such as $[\text{Pt}(\text{NH}_3)_3\text{Cl}]^+$ and $[\text{Pt}(\text{dien})\text{Cl}]^+$ are inactive, it is believed this inactivity is because they fail to alter DNA synthesis via inhibition of DNA polymerase,²⁰ Hollis and co-workers reported that replacement of one chloride with a N-heterocyclic ligand (pyridine, purine, pyrimidine, aniline) could afford compounds showing significant cytotoxicity.²¹ Further studies by Lippard *et al.* illustrated that the complex *cis*- $[\text{Pt}(\text{NH}_3)_2(\text{pyr})\text{Cl}]^+$, pyriplatin, is able to stall RNA polymerase II and has a different spectrum of activity than cisplatin.²² This molecule is uptaken by cells via Organic Cation Transporters (OCTs 1 and 2) and forms monofunctional adducts which are able to stall RNA polII.^{9, 23} These adducts can be repaired via NER mechanism (similarly to cisplatin) but less efficiently.²⁴ The interesting properties of pyriplatin spurred on the synthesis of other monofunctional complexes, of which phenanthriplatin (Figure 1.3 B) was found to be the most promising, with a 4-40 fold lower IC_{50} compared with cisplatin or oxaliplatin.²⁵

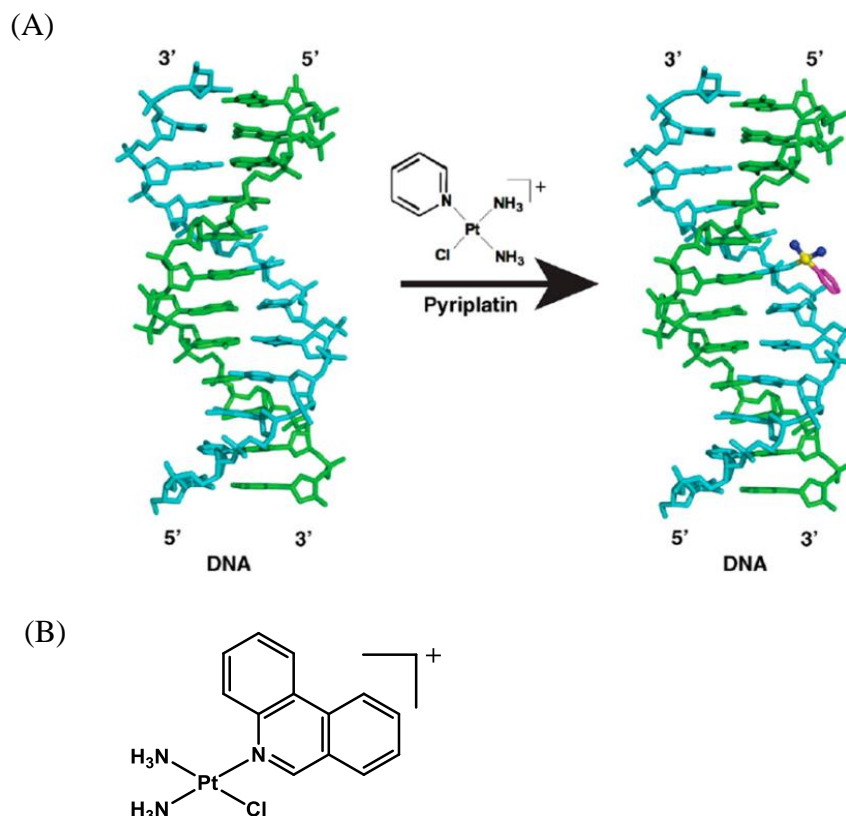


Figure 1.3: (A) Scheme illustrating the monofunctional DNA adduct formed by pyriplatin, with green and cyan representing the nondamaged and damaged strands, respectively. Taken from reference 26. (B) Structure of phenanthriplatin, developed by Lippard *et al.*

Similarly to the monofunctional Pt(II) complexes, *trans*-Pt(II) complexes were also thought to be inactive according to the initial structure-activity relationships due to inability to form 1,2-intrastrand crosslinks.

The mechanism of action for *trans* complexes follows the same principle as for the *cis* compounds, in which aquation of the chlorides needs to occur. Hydrolysis of the first chloride is fast in comparison to the second, as it is opposite to H₂O, which has a weak *trans* effect.

Replacement of one or both amines with iminoethers, aliphatic amines or heterocyclic aliphatic amines (Figure 1.4) generates a wide variety of *trans*

antitumor complexes which display cytotoxicity in cisplatin-resistant cell lines.^{27,28}

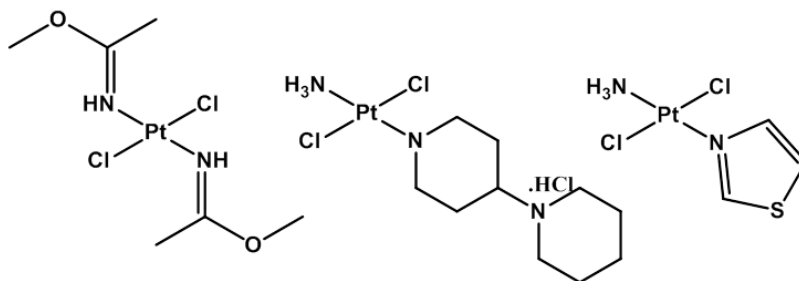


Figure 1.4: Examples of $trans$ -[PtCl₂(L)(L)'] containing iminoether, aliphatic heterocyclic amines and aromatic amines which show *in vivo* efficacy.^{29,30,31}

These complexes display a different mode of DNA binding than transplatin, but also differences amongst themselves, depending on the type and the steric bulk of the ammine. For example, $trans$ -[PtCl₂(NH₃)(thiazole)] generates an almost equal number of monofunctional, interstrand and intrastrand crosslinks, but the piperidine and piperazine complexes produce more intrastrand crosslinks. The use of two iminoether ligands, on the other hand leads to mainly monofunctional adducts.²⁸ In the case of $trans$ -[Pt(pyridine)₂Cl₂], which can be considered as a prototype of $trans$ complexes with planar aromatic ligands, it was shown that it is very efficient in forming interstrand crosslinks, despite the steric bulk created by the two pyridine ligands.³²

The interstrand crosslinks formed by these kinds of complexes are usually between two adjacent GC base pairs, resembling those formed by cisplatin, whereas transplatin's interstrand adducts are formed between G-C adjacent pairs (Figure 1.5).

Depending on the adduct type, protein recognition (e.g. by the HMG-group family) can be different, which ultimately affects downstream effects (e.g. repair).

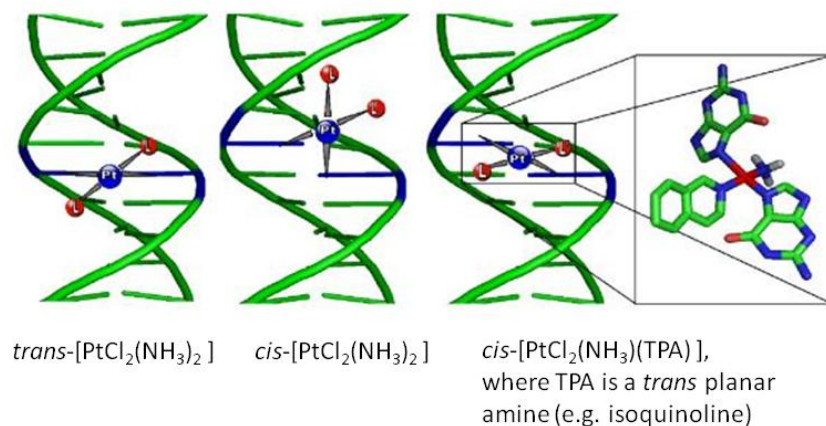


Figure 1.5: Types of interstrand DNA cross links formed by transplatin (left), cisplatin (middle) and *trans* complexes with a planar aromatic amine, using $trans-[PtCl_2(NH_3)(isoquinoline)]$ as an example. Taken from reference 28.

1.5 Pt(IV)-prodrugs

A different strategy used for the production of drugs which could potentially decrease the side effects shown by the conventional Pt(II) drugs is the development of Pt(IV) prodrugs. A prodrug is a “derivative of a drug that is metabolized or activated in the body to release or generate the active drug”.³³ The status of Pt(IV) prodrugs can be justified by the fact that these complexes enter the cells as Pt(IV) and reduction to Pt(II) is essential before any substitution reaction takes place.^{34,35}

The kinetic inertness exhibited by Pt(IV) complexes renders them less prone to undergo reactions on route to the tumour, enabling a higher therapeutic index.³⁵

The presence of two additional ligands compared to Pt(II) also allows modification of important chemical properties of the drug (e.g. lipophilicity, aqueous solubility, reduction potential)³⁶ and can be used for the incorporation of

targeting features such as nanoparticles and peptides. Furthermore, there is also the capability of a dual mode of action by the incorporation of biologically active axial ligands which can be released in the cell upon reduction.⁹

Four Pt(IV) drugs have so far entered clinical trials (Figure 1.6): iproplatin, tetraplatin, satraplatin and LA-12. The first two have been abandoned. Iproplatin showed less cytotoxicity than cisplatin and tetraplatin was too toxic³⁶, whereas satraplatin is now being trialled for combination therapy.³⁷ LA-12 is currently under phase I clinical trials.³⁸

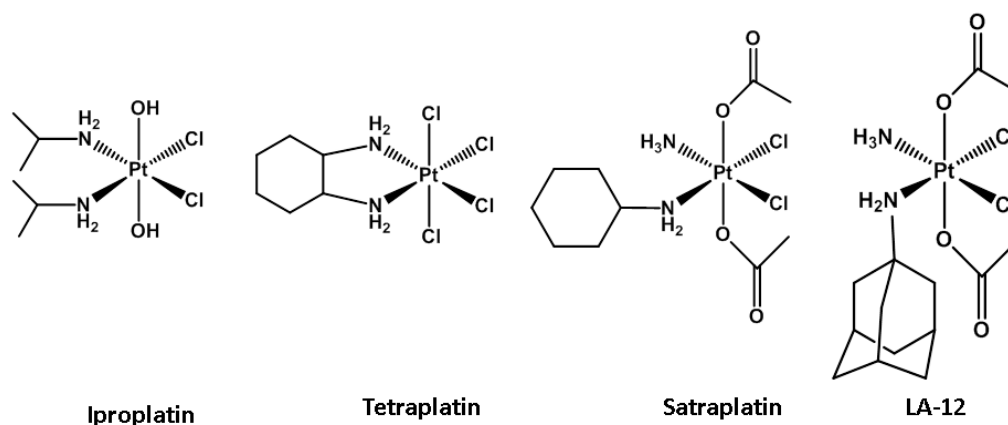


Figure 1.6: Pt(IV) complexes that have entered clinical trials.

Although the examples discussed above entail chemical activation, of special interest is the use of light to photoactivate a prodrug, which is the main concept behind photodynamic therapy.

1.6 Photodynamic therapy (PDT)

PDT is a clinical treatment for cancer based on the administration of a photosensitizer and subsequent activation using light at a wavelength where the compound absorbs. This in effect excites the photosensitizer in a higher electronic

state, causing Type I and Type II reactions. The former entails a redox reaction with subsequent formation of radicals and the second involves energy transfer to ground state molecular oxygen ($^3\text{O}_2$) to produce the highly reactive $^1\text{O}_2$ (singlet oxygen).³⁹ This species is toxic to cells and causes death via oxidative stress mechanisms, DNA damage, protein destruction and cell lysis.^{40,41} The short life time of singlet oxygen in water (3 μs) and the maximum diffusion distance of up to 100 nm within a cell, gives rise to localized cellular damage.⁴² Further to this mechanism of action, PDT can damage the vasculature associated with the tumour and also trigger an immune response.⁴⁰

The photosensitizer ideally should be activated by longer wavelength light for deeper penetration into the tissue, have good aqueous solubility, no dark toxicity, preferential accumulation in the cancer tissue, and finally a long enough half-life in the blood to reach the tumour cells in adequate concentrations.^{43,44} Most of the photosensitizers are highly conjugated macrocycles (e.g. porphyrins, chlorins, bacteriochlorins, phthalocyanines, naphthalocyanines), although research on metal-based photosensitizers has shown that they are already promising candidates for PDT.⁴⁵ Notable examples (Figure 1.7) include aluminium sulfonated phthalocyanine (Photosense), which is approved for clinical use in Russia,⁴⁶ the Motexafin Lutetium (Lu-trin or Lu-Tex) and the palladium bacteriopheophorbide (Tookad soluble), both of which are evaluated as a treatment for prostate cancer.^{47,43}

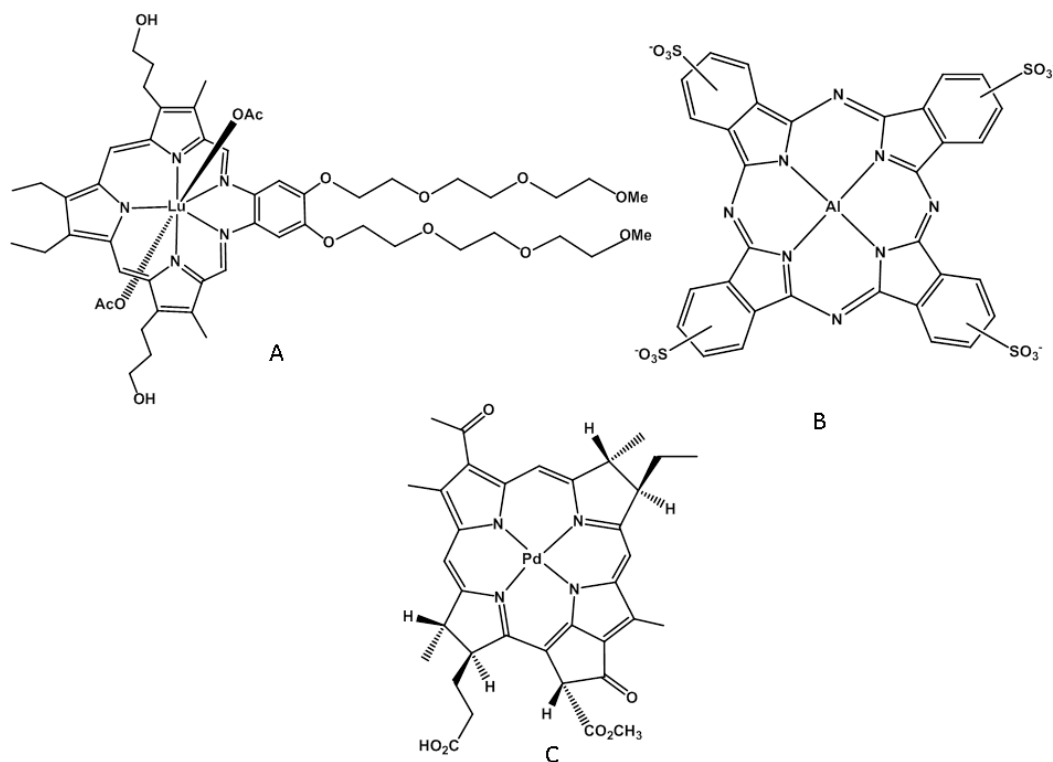


Figure 1.7: PDT agents containing metals which are either used clinically (A, Motexafin Lutetium) or under clinical evaluation (B, aluminium sulfonated phthalocyanine and C, palladium bacteriopheophorbide).

The medical benefits of PDT for the treatment of cancer and pre-cancerous conditions are the follows: (a) There is little effect on the non-living connective tissue, allowing healing without a risk of the mechanical integrity of hollow organs.⁴⁸ (b) There are no total-dose limitations, as in the case of radiotherapy.⁴³ (c) It allows excellent spatial control therefore avoiding damage to healthy cells. PDT's main drawbacks lie in the fact that it is oxygen-dependent and oxygen is scarce in hypoxic tumour environments.⁴⁹ Furthermore, porphyrin aggregation,⁵⁰ poor-solubility⁵¹ and photosensitivity after treatment⁵² are some other disadvantages associated with the current-porphyrin based PDT.

1.7 Light Delivery

Although light penetration into a specific tissue is dependent upon the competitive absorption of endogenous chromophores (e.g. melanin and haemoglobin), the optimum range is 620 nm – 850 nm. Light in the range of 600-700 nm penetrates 50-200 % deeper than in the 400-500 nm, therefore is preferentially used in the clinic (Figure 1.8).⁴⁵ However, shorter wavelength of light can be used if the target lesion is thin and the tissue surface is easily accessible.⁴³

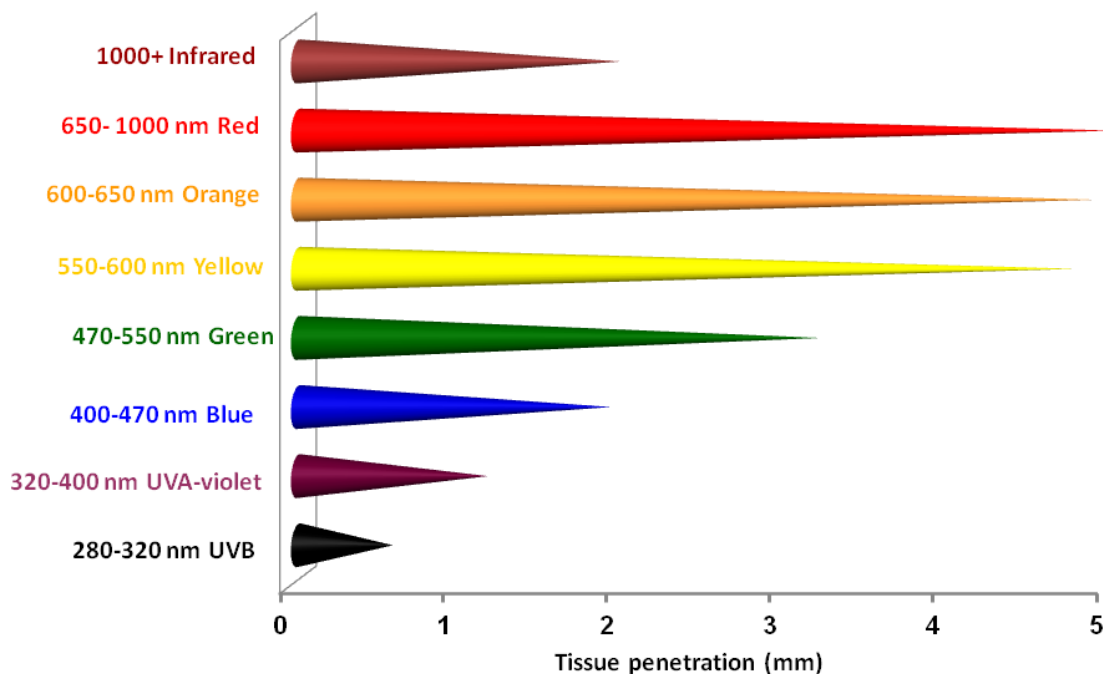


Figure 1.8: Light penetration through the tissue. Adapted from reference 53.

LED lights are used for dermatological purposes and recent advances in laser technology have enabled physicians to perform PDT in internal organs (e.g. lungs, brain, bladder, cervix and colon) via the use of optical fibres to deliver laser light.^{43,54} The use of advanced high power and tightly focused femtosecond laser systems may also enable PDT via two photon excitation in the future. This phenomenon is the near-simultaneous absorption of two photons, typically above

600 nm, to achieve excitation at shorter wavelength (approximately half).⁵⁵ As a result, metal complexes with the ability to absorb two photons (usually large with highly conjugated donor and acceptor ligands) can be activated with longer and clinically relevant wavelengths. In a recent report, Zhao *et al.* presented the first example of a Pt(II) complex containing the π -conjugated ligand 4-[2-(4-methoxyphenyl)ethynyl]pyridine for which activation with laser pulses between 600 – 740 nm yielded the same photoproducts as UV activation.⁵⁶ Furthermore, research has been carried out on the development of upconversion nanoparticles in PDT. A photosensitizer which is activated with UV or short visible wavelength is loaded onto the nanoparticle which is composed of material capable of photon upconversion (usually lanthanides, such as NaYF₄: Yb, Er⁵⁷) and upon irradiation with near-infrared light, shorter wavelength light is produced which is able to activate the photosensitizer coated on the outer shell of the NP.⁵⁸

1.8 Photophysical and photochemical properties of metal complexes^{59,60, 61,62}

Photochemistry is concerned with the effects of light in chemical systems and will be discussed here with respect to metal coordination compounds. Absorption of a photon by a molecule can cause excitation if the energy gap between the excited and the ground state matches the energy of the photon. The possibility of an electronic transition occurring depends on the transition dipole which in turn is dependent on the two following selection rules.

- (a) Spin selection rule: transitions with a change of multiplicity are not allowed ($\Delta S = 0$). This selection rule can be relaxed by the coupling of the spin and orbital angular momenta. Heavier atoms have a greater spin-orbit coupling.

(b) Laporte selection rule: in a centrosymmetric molecule the only allowed transitions are those accompanied by a change in parity (e.g. $g \leftrightarrow u$). This rule can be relaxed when the complex's symmetry departs from the perfect centrosymmetry, through natural asymmetry or through distortions occurring during vibrations.

The fact that these transitions are forbidden suggest that experimentally they will occur with low probability, hence the extinction coefficients are small.

Absorption of radiation by a molecule can lead to the population of singlet excited states, which then follow various deactivation pathways, as illustrated in the Jablonski diagram (Figure 1.9). When the population of higher electronic states (e.g. S_1 , S_2) occurs, then return to a lower singlet level can occur without radiation via internal conversion, vibrational relaxation, quenching or via a radiative process, fluorescence. Otherwise, intersystem crossing can lead to population of a triplet state which can give rise to phosphorescence (radiative process) upon return to the ground state (S_0). Phosphorescence has a longer life time than fluorescence (10^{-3} – 1 s vs 10^{-9} – 10^{-6} s),⁴¹ as the former is a spin forbidden process. A decrease in the intensity of fluorescence is commonly observed when transition metals are in close proximity to the fluorophore because they increase the rate of Intersystem-Crossing to the triplet state due to an increase in the spin-orbit coupling. This radiationless process competes with the $S_1 \rightarrow S_0$ transition, responsible for fluorescence.⁶³

The deactivation of an excited state often does not go through a physical process (e.g. luminescence) but rather causes a chemical change (e.g. isomerisation,

dissociation, redox, substitution). Nevertheless, the population of the triplet state, occurring through intersystem crossing from the singlet state, is an important step that dominates a lot of the routes of electronic excitation.

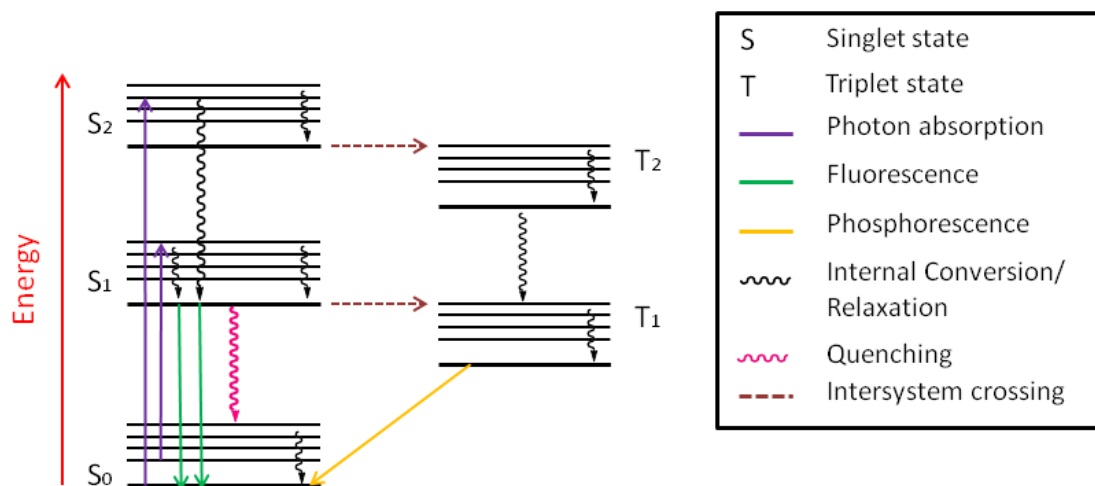


Figure 1.9: A Jablonski diagram to summarise all potential deactivation pathways of complex in an excited state. Reproduced and modified from reference 64.

Prior to discussing the various types of the excited states in a d^6 metal complex, it is important to describe the typical molecular orbital diagram for this class of compounds. In an octahedral d^6 metal complex (e.g. Pt^{IV}), the splitting of the orbitals is such that the d_{xy} , d_{yz} , d_{zx} are lower in energy than the d_{z^2} and $d_{x^2-y^2}$ orbitals, as described by crystal field theory. The energy of the ligand orbitals is lower than the metal orbitals and therefore the lower energy bonding orbitals are ligand centred, whereas the lowest energy antibonding orbitals are predominantly metal-based.

The excited state reactivity of a metal complex, as induced by light, is summarized by the following (Figure 1.10).

- 1) Metal-centred transitions (d-d transitions). These are Laporte forbidden ($g \leftrightarrow g$ transitions), hence they give rise to weak absorption band ($\epsilon \sim 1$ -

$1000 \text{ M}^{-1}\text{cm}^{-1}$. Such transitions typically lead to the occupation of antibonding orbitals, often leading to bond elongation and ligand substitution.

- 2) Charge transfer transitions (ligand-to-metal, metal-to-ligand or to-solvent) are fully allowed, giving rise to intense absorption bands. A MLCT may result if the metal is electron rich and the ligand has low lying empty orbitals. A LMCT occurs when the ligand is easy to oxidize and the metal easily reduced. A LMCT leading to a chemical change can cause change in the oxidation state of the metal, as well as ligand release by a homolytic bond cleavage to liberate radicals.
- 3) Ligand-centred transitions mainly occur in aromatic ligands with extended π and π^* orbitals and they are allowed by both spin and Laporte selection rules.

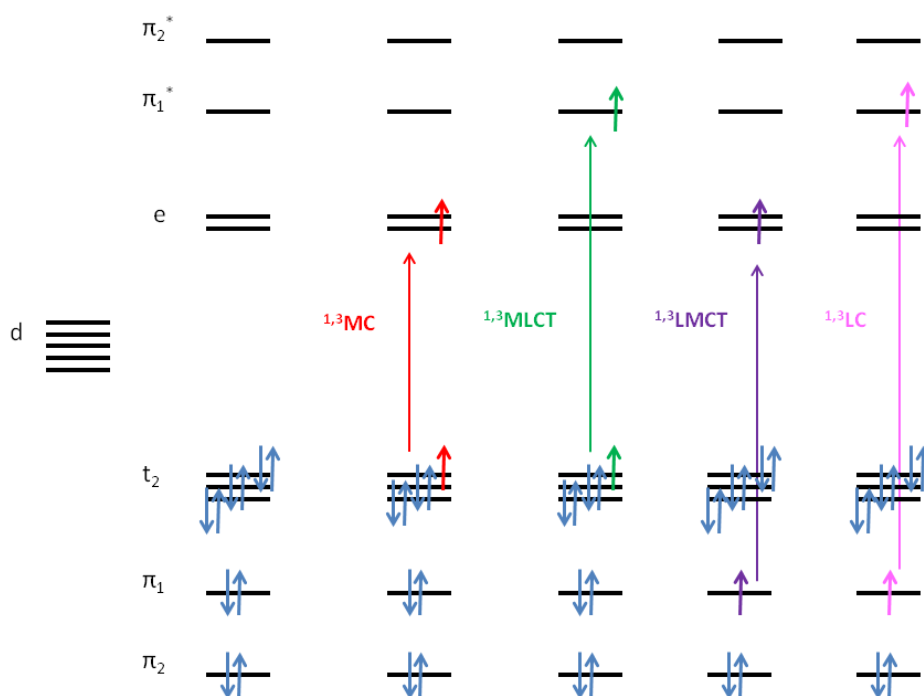


Figure 1.10: A simplified MO diagram of an octahedral d^6 complex, assuming strong crystal field splitting. The bonding orbitals π_1 and π_2 are predominantly ligand in character, whereas the t_2 are metal in character. The blue arrows represent electrons with the associated spin in the ground state, whereas the coloured arrows represent electrons involved in a transition. In the singlet and triplet states the spins are up ($\uparrow\uparrow\uparrow$) or down ($\downarrow\downarrow\downarrow$), respectively. Reproduced and modified from Farrer *et al.*⁴⁴

1.9 Non-platinum metal-based photoactivated drugs

Many transition metals (e.g. Ti, Cr, Mn, Cu, Co, Pd, Ir, Fe, V) show medically interesting photochemical properties which have been studied. A few notable examples are the oxovanadium(IV) curcumin complex $[\text{VO}(\text{cur})(\text{dppz})\text{Cl}]$ and the $\text{Fe}(\text{L})(\text{cat})\text{NO}_3$, where $\text{L} = 9\text{-[}(2,2'\text{-dipicolylamino)methyl]anthracene}$ and $\text{cat} =$ catecholate. The former was shown to have a lower IC_{50} than the FDA approved PDT agent photofrin when irradiated with visible light (400-700 nm) and its efficacy is thought to be due to its DNA photocleavage ability.⁶⁵ The latter complex can induce near IR-light induced apoptotic cell death. The anthracenyl

ligand is responsible for the fluorescent and intercalative abilities of the complex, whereas the catecholate ligand provides IR absorption.⁶⁶

Ru(II) and Rh(III) complexes have been studied the most over the years. A very prominent family is that comprising Ru-polypyridyl complexes which not only show intercalative properties via the ligand but also because the photoexcited state is a strong oxidant, capable of oxidizing DNA nucleobases.⁶⁷ Especially when tridentate ligands (e.g. 2-pyridyldipyrido-[3,2-*a*;2',3'-*c*]phenazine) were employed, quantum yields of singlet oxygen production were exceptionally high.⁶⁸ Ru-polypiridyl complexes which contain monodentate ligands can also exhibit ligand release of one or two ligands which is exploited for the uncaging of bioactive molecules (e.g. amino acids, nucleotides, neurotransmitters and genetic inducers). The photosubstitution in these complexes is enabled by the population of a d-d state from the ³MLCT, a transition which is temperature dependent.⁶⁹ Light-induced ligand substitution and subsequent nucleobase binding was also shown by Sadler and coworkers in the case of Ru(II)-arene complexes containing a pyridine monodentate ligand.⁷⁰ Furthermore, the use of polyazaaromatic ligands (e.g. 1,4,5,8,9,12-hexaazatriphenylene (HAT) and 1,4,5,8-tetraazaphenanthrene (TAP)) lead to formation of covalent adducts with nucleobases through a radical recombination process which is lethal for the cell.⁷¹ Finally, the nitrosyl bound Ru(II) complexes can also undergo ligand release but through a different mechanism (via oxidation to Ru(III)).⁷²

Rh(III) complexes with polypyridyl or phenanthroline ligands can also cause DNA cleavage on light activation. A notable example, which uses a more sterically demanding chrysi ligand (chrysi = 5,6-chrysenequinone diimine) is

$[\text{Rh}(\text{bpy})_2(\text{chrysi})]^{2+}$, complex developed by Barton *et al.*, which can specifically bind to DNA base mismatches.⁷³

1.10 Photoactivity of Pt(II) complexes

Up until now most of the photochemistry of platinum evolved around luminescent Pt(II) complexes, which have been explored thoroughly due to their useful photophysical properties. Their high efficiencies, long lifetimes of the emissive state enabled this type of complexes to be used in applications such as chemosensors,⁷⁴ photocatalysis,⁷⁵ light emitting diodes⁷⁶ and photovoltaic devices.⁷⁷

More recently, Pt(II) agents were also found to be phototoxic when coordinated to appropriate ligands. Studies carried out with transplatin (Figure 1.11, complex A) showed that upon irradiation with UVA, an enhancement in the toxicity (2-fold) was observed. This was attributed to the loss of chloride ligands and the formation of bifunctional DNA interstrand crosslinks which are unable to form in the dark.⁷⁸ A recent study has shown that a similar effect can be caused by UV irradiation of carboplatin, where a 10-fold increase in cytotoxicity and faster DNA binding kinetics was induced.⁷⁹

Brunner and co-workers, in an attempt to combine the advantages given by the preferential cellular accumulation of porphyrins in cancer cells with the cytotoxic activity of Pt(II), attached poly(ethyleneglycol)-derivatized hematoporphyrins to Pt(II) (Figure 1.11, complex B). The phototoxicity results showed that most of the complexes exhibited both cytotoxicity and phototoxicity ($\lambda = 600\text{-}730\text{ nm}$, 10 min), towards human cancer cells with a few exceptions which showed promising light-induced efficacy.⁸⁰

Franz *et al.* reported that the attachment of a photosensitive nitrophenyl group to a tetradentate ligand backbone with two pyridyl and two amide nitrogen donor sites makes the Pt(II) complex photolabile (Figure 1.11, complex C). Bond breakage occurs, accompanied by release of a Pt(II) complex prone to ligand substitution reactions as well as other nitroso side-products when exposed to UV light for a short time. The cytotoxicity of the complex was low in the dark and decreased to 68% upon irradiation.⁸¹

Chi-Ming Che *et al.* also has reported luminescent cyclometalated Pt(II) complexes with thiophene,⁸² mono⁸³ or bidentate (N-heterocyclic carbenes)⁸⁴ ligands. These complexes exhibit high emission quantum yields which enable their tracking inside a cell, via fluorescence microscopy. In the first two reports, although the complexes were very potent, they produced only a small increase in cytotoxicity when irradiated with visible light (~6 fold, Figure 1.11, complexes D and E), whereas in the latter case it was improved 30-fold in some cases (Figure 1.11, complex F). These compounds tend to accumulate in cytoplasmic structures (e.g. endoplasmic reticulum and mitochondria) rather than the nucleus, which can indicate a different mode of action than traditional anticancer Pt drugs (usually targeting nuclear DNA).

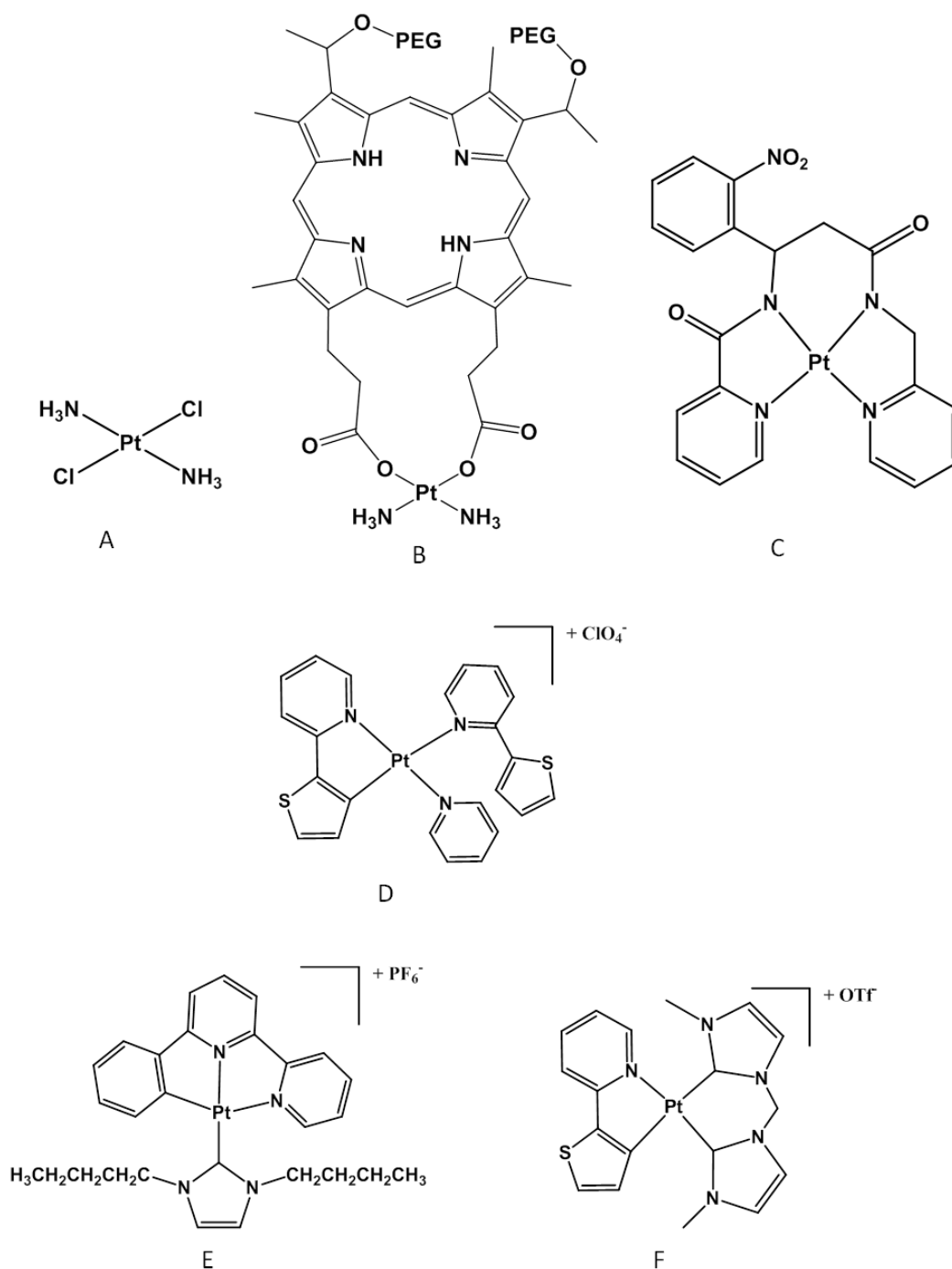


Figure 1.11: Selected complexes showing enhancement in cytotoxicity when irradiated with UV (A and C) or visible light (B and D-F).

Finally, a few dinuclear complexes of Pt(II) have been reported in recent years which exhibit promising photosensitizer characteristics. Monti *et al.* reported complexes with a dichloridopyrido Pt(II) moiety attached externally to the

porphyrazine macrocycle, where the central cavity was occupied with either Zn(II), Mg(II) or Pd(II). They were shown to generate singlet oxygen efficiently in DMF ($\lambda > 600$ nm) and also to bind to G-quadruplex structures.⁸⁵ Brewer *et al.* reported a Ru(II)-Pt(II) dinuclear complex, where the dichloro-platinum moiety is attached on a dpp ligand, where dpp=2,3- bis(2-pyridyl)pyrazine)). The other ligands on the ruthenium centre were the widely used phenanthronile ligands. Irradiation at long wavelength ($\lambda > 600$ nm) causes a MLCT excitation to the ruthenium which is transferred to PtCl₂ site, causing hydrolysis of the chlorides and DNA binding.⁸⁶

1.11 Photoactivity of Pt(IV) complexes

The phototochemical properties of Pt(IV) were documented early on, when it was shown that [PtCl₆]²⁻ can be reduced to metallic Pt or [PtCl₄]²⁻ with low-energy visible light.⁸⁷ More recently, Lippert *et al.* reported that Pt^{IV} 2,2-bipyridine complexes, e.g. *mer*-[PtCl₃(2,2-bpy)(MeNH₂)], can undergo photoreduction ($\lambda > 300$ nm) to produce the Pt(II) fragment [PtCl(2,2-bpy)(MeNH₂)] accompanied by the loss of HOCl or Cl₂ which possibly originate from the reductive elimination of the axial chlorido ligands. Surprisingly, the same result is obtained when the complex is heated at 50 °C for 24 h, showing the thermolability of the complexes.⁸⁸

1.11.1 Pt(IV)-diiodo and Pt(IV)-diazido complexes

A controlled localized reduction to a cytotoxic component is extremely beneficial to healthy cells which are prone to rapid division, such as bone marrow, GI-tract and skin, since these cells are particularly sensitive to chemotherapy.³⁸

Pt(IV) complexes, contrary to the Pt(II), are less prone to substitution reactions and therefore the selection of appropriate ligands can render them stable in the presence of high amounts of reducing agents and also create photolability.

The first generation of Pt(IV) photoactivatable anticancer drugs were diiodo complexes (Figure 1.12), with the general formula of *trans, cis*-[Pt(X)₂I₂(en)], where en = ethylenediamine and X = Cl⁻, OH⁻, acetate or methylsulfonate.⁸⁹ The ethylenediamine ligand was chosen in order to avoid photoisomerisation reactions which could lead to the formation of a *trans*-Pt(II) photoproduct which is not able to form the lethal intrastrand DNA cross-links.⁸⁹ The choice of iodides as the reducing ligands was made because they are weak field ligands and thus the LMCT transition occurs at low energy in the visible region. Indeed, the UV-Vis spectrum of the iodo complexes bears a tail which extends up to 500 nm.⁹⁰

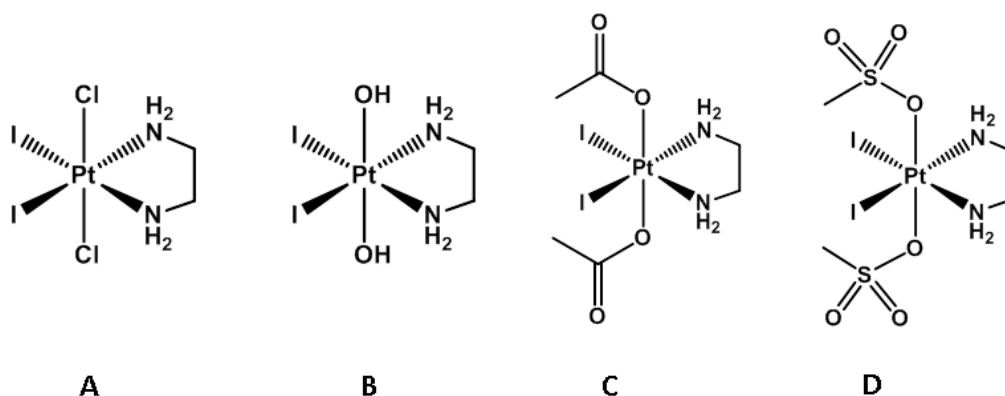


Figure 1.12: First generation photoactivatable Pt(IV) drugs with iodides as the reducing ligands, developed by Berdnaski *et al.*⁵⁴

CT-DNA binding studies illustrated that the most promising complex was C in Figure 1.12 as complexes A and D could form adducts in the dark, whereas photolysis of B led to no platination. Instead complex C led to 65% platination only after irradiation.⁹⁰

Nevertheless, cytotoxicity studies on these complexes showed no significant difference between light and dark toxicity. This might be attributable to the facile reduction of the complexes by thiols within the cellular environment.^{90,91}

Photochemical reduction of platinum(IV)-azide complexes was documented early on, by Vogler and co-workers who showed that *trans*-[Pt(CN)₄(N₃)₂]²⁻ was converted to [Pt(CN)₄]²⁻ upon excitation with UV (300 nm) via a simultaneous two-electron reduction process without a Pt(III) intermediate.⁹² Furthermore, they showed that [Pt^{II}(N₃)₄]²⁻ is also photolabile being reduced to metallic platinum leading to the production of nitrogen and azide.⁹³ Following this, the Sadler group developed a second generation of Pt(IV) photoactivatable drugs containing azides instead of iodides (Figure 1.13).

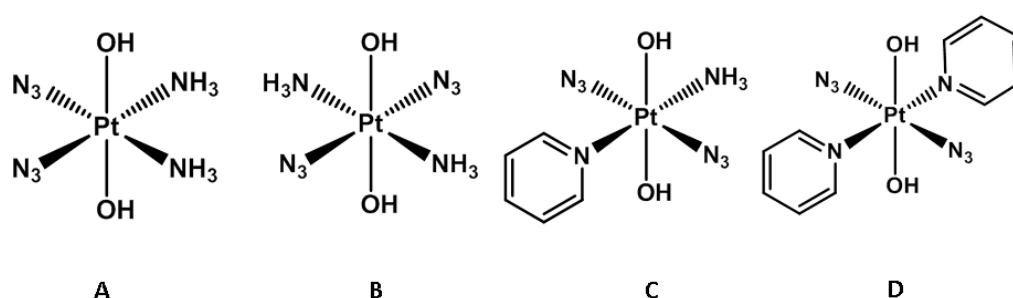


Figure 1.13: Pt(IV)-diazido complexes developed by Sadler and co-workers.^{54,94,95}

Complexes A and B in Figure 1.13 were the first synthesized and have been studied extensively. Initial experiments monitored by UV-Vis showed that A

decomposed more slowly than B under UV irradiation. This could be rationalized by the fact that the LMCT band of B is shifted towards the visible region by 29 nm and also the extinction coefficient is greater.⁹⁶ Another advantage of B over A is the higher aqueous solubility. However irradiation studies followed by ¹H and 2D [¹H, ¹⁵N] HSQC NMR spectroscopy, showed slow photoreactivity of this class of compounds since reduction to Pt(II) was seen only after 60 min of irradiation with UVA light. Instead photosubstitution/ photoisomerisation Pt(IV) products were possibly formed. Interestingly, irradiation of B in the presence of 5'-GMP (2 molar equivalents) led to the formation of *trans*-[Pt^{II}(NH₃)₂(5'-GMP-N₇)₂] adducts and reduction to Pt(II) occurred at a faster rate than in the absence of nucleotides. Furthermore, complex A was shown to generate equivalent nucleotide crosslinks when irradiated with visible light in presence of 5'-GMP or d(guanosinylphosphoguanosine) as those formed by cisplatin.⁹⁷ These results demonstrated for the first time the photoreduction of Pt(IV) to Pt(II), and also that the stereochemistry of the amines is retained after reduction to Pt(II) and subsequent binding to biomolecules.

The photochemical decomposition pathways of A and B were studied extensively by Ronconi *et al* via ¹⁴N and ¹⁵N NMR.^{98,99,100} It was discovered that the photodecomposition pathways of the two isomers are similar in the major products formed but that the experimental conditions under which the irradiation experiments were carried out affected the photoproducts: in PBS, azide release was observed, whereas in acidic conditions, N₂ was the major product. However in both conditions, O₂ and free ammonia were detected (indicating ammine release), although amine bound Pt(II) was also detected, accompanied by an

increase in pH. It was postulated that the photodecomposition to Pt(II) could involve also the formation of highly reactive Pt(IV)-nitrene intermediates, indicating a complex mechanism of photodecomposition of this class of compounds.

Although neither complexes A or B (Figure 1.13) possess dark toxicity, the *trans* isomer was slightly more active than the *cis* counterpart under irradiation (IC₅₀ 156 µM vs 176 µM in HaCaT cell line, UVA irradiation for 50 min).⁹⁶ Changes in the nuclear morphology of 5637 human bladder cells were also followed for complex A by phase-contrast and fluorescence microscopy illustrating that cells did not undergo the typical apoptotic changes (e.g. budding and cellular fragmentation). Treated cells rather ballooned and lost contact with neighbours as well as suffering disintegration of the nuclei. Furthermore, a distinctive mechanism of cell death from cisplatin became obvious.¹⁰¹

Complex C (Figure 1.13) which incorporates a pyridine in place of an ammine ligand was significantly more potent than A and B, when irradiated with UV light (IC_{50s} 6.1 and 1.9 µM in HaCaT and A2780 cell lines, respectively).⁹⁴ Photolysis experiments showed that reduction to Pt(II) occurred in the presence of biomolecules (e.g. 5'-GMP) to produce *trans*-[Pt(NH₃)(py)(5'-GMP-N7)₂] and *trans*-[Pt(N₃)(NH₃)(py)(5'-GMP-N7)]. Studies to elucidate the mechanism of action were performed for complex C by Berdnaski *et al.* showing that an elevated amount of ROS was generated after irradiation with UVA light (30 min).¹⁰² Treatment of HL60 (human promyleotic leukaemia cells) with the complex C did not yield morphological changes (Figure 1.14) that resembled those triggered by cisplatin or etoposide, which are apoptotic agents. The lack of activation of

caspase 3 or 7, combined with changes in the levels of key autophagic proteins (e.g. LC3, p62), led to postulated autophagy as the possible mechanism of cell death.¹⁰³

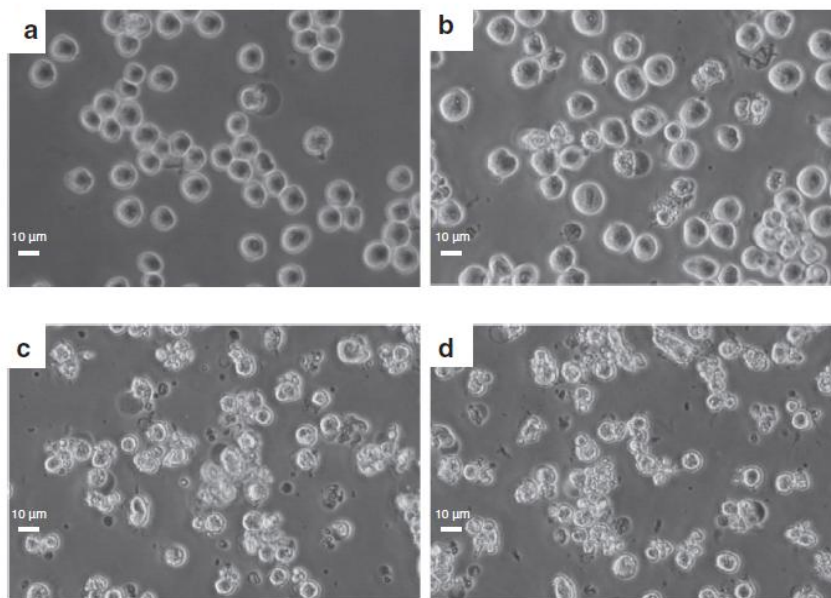


Figure 1.14: Phase contrast images of HL60 cells treated for 48 hours with untreated control (a), 68 μM of complex C activated with UVA light (b), 0.74 μM of cisplatin (c) and 0.74 μM etoposide (d).¹⁰³

The success of complex C spurred on the synthesis of *trans, trans, trans*-[Pt(N₃)₂(OH)₂(L)(L')] complexes which when compared to their *cis* analogues they were found to be more phototoxic.¹⁰⁴ This systematic study produced the first structure-activity relationship for Pt(IV)-diazido complexes.

Replacement of aliphatic amine with pyridine (complex D, Figure 1.13) resulted in photocytotoxicity (IC₅₀ 8.4 μM in OE19) with blue light (420 nm). As in the case of complex C irradiation with blue light in the presence of 5'-GMP resulted in the formation of mono and bis-5'-GMP adducts.⁹⁵ EPR studies illustrated the evolution of azide radicals and their role in the cytotoxicity of this class of

complexes was shown by the reduction in potency when IC₅₀ studies were carried out in the presence of the radical quencher tryptophan.¹⁰⁵ Azidyl radicals can cause oxidation reactions of tryptophan and tyrosine¹⁰⁶ thus potentially damaging proteins and other biomolecules.

These complexes are thought to have a dual mode of action (Figure 1.15) with azidyl radicals playing a primary role in the cytotoxicity. However binding to biomolecules is also significant. DNA binding studies of complex D demonstrated the formation of 1,3-intrastrand crosslinks as the major adduct (51%) but monofunctional lesions can form to a greater extent than cisplatin (37% vs 2%). Pracharova *et al.* also postulated that interaction of the pyridine ligand with the DNA duplex may play an important role for activity. Moreover, stalling of RNA polymerase II (responsible for transcription) is also a significant factor which can contribute to the cytotoxicity of this complex.¹⁰⁷ This result also parallels the report by Lippard *et al.* in which an X-ray crystal structure of RNA polII stalled by a monofunctional platinum-DNA adduct with pyriplatin. The structure showed that a pyridine ligand located in *cis* position to NH₃ can fit into the RNA polII active site and subsequently cause blockage of the translocation of the enzyme from this position.²⁶

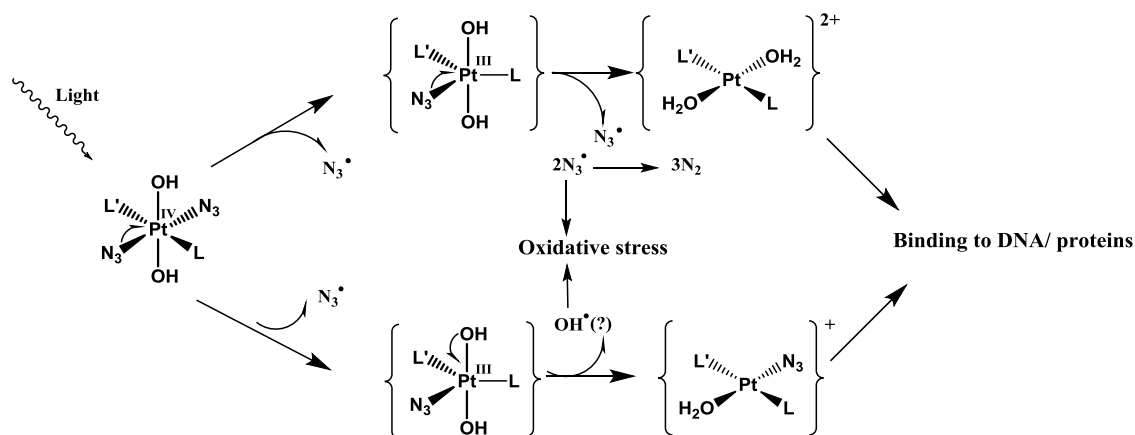


Figure 1.15: Mechanism of action of Pt(IV)-diazido complexes where L and L' are N-aromatic ligands. The scheme shows that cell death can be produced by oxidative stress caused by the generation of radicals and also by the platination of biomolecules, such as DNA and proteins.

All of these compounds were found to be stable in the dark in the presence of cellular concentrations of reducing agents such as GSH and ascorbate which is a desirable feature for photoactivatable drugs.¹⁰⁸ Together with the fact that the mechanism of action is oxygen-independent and the generally high aqueous solubility of these prodrugs, these complexes are potential candidates for photoactivated chemotherapy (PACT).

1.12 Aims

The aims of this thesis are the following.

- Synthesis and characterisation of novel complexes with planar aromatic ligands which can potentiate the phototoxicity of the Pt(IV)-diazido complexes without compromising the lack of dark toxicity.

- Synthesis and characterisation of Pt(IV)-diazido complexes with derivatization of the axial ligands so as to provide targeting and imaging features.
- Studies of the photochemistry of the new complexes, especially on the biologically relevant wavelengths, and elucidation of photoproduct pathways.
- Cellular studies in mammalian cells for the determination of phototoxicity, cell uptake as well as the employment of novel methods (confocal microscopy and survival in yeast cells) which can enable the determination of the mechanism of action.

References

1. R. J. B. King and M. W. Robins, *Cancer Biology*, Pearson Education Limited, Harlow, 2006.
2. CRUK, *Cancer Statistics key facts*, 2013.
3. A. Jemal, F. Bray, and J. Ferlay, *CA-Cancer J. Clin.*, 2011, **61**, 69-90.
4. B. Teni, A. Pantos, E. Bellis, and P. Christofis, *Cancer Therapy*, 2007, **5**, 537-583.
5. B. W. Harper, A. M. Krause-Heuer, M. P. Grant, M. Manohar, K. B. Garbutcheon-Singh, and J. R. Aldrich-Wright, *Chem. Eur. J.*, 2010, **16**, 7064-7077.
6. B. Rosenberg, L. Van Camp, and T. Krigas, *Nature*, 1965, **2**, 698-699.
7. B. Rosenberg, L. Vancamp, J. E. Trosko, and V. H. Mansour, *Nature*, 1969, **205**, 698-699.
8. S. P. Fricker, *Dalton Trans.*, 2007, 4903-17.

9. T. C. Johnstone, J. J. Wilson, and S. J. Lippard, *Inorg. Chem.*, 2013, In press.
10. L. Kelland, *Nat. Rev. Cancer*, 2007, **7**, 573-584.
11. J. M. Malinge, M. J. Giraud-Panis, and M. Leng, *J. Inorg. Biochem.*, 1999, **77**, 23-29.
12. G. Zhu, L. Song, and S. J. Lippard, *Cancer Res.*, 2013, **73**, 4451-4460.
13. M. Ober and S. J. Lippard, *J. Am. Chem. Soc.*, 2008, **130**, 2851-2861.
14. A.-M. Florea and D. Büsselberg, *Cancers*, 2011, **3**, 1351-1371.
15. I. Romero-Canelón and P. J. Sadler, *Inorg. Chem.*, 2013, In press.
16. F. Arnesano, M. Losacco, and G. Natile, *Eur. J. Inorg. Chem.*, 2013, **2013**, 2701-2711.
17. M. D. Hall, M. Okabe, D.-W. Shen, X.-J. Liang, and M. M. Gottesman, *Annu. Rev. Pharmacol. Toxicol.*, 2008, **48**, 495-535.
18. T. Boulikas, *Cancer Ther.*, 2007, **5**, 351-376.
19. J. Reedijk, *Eur. J. Inorg. Chem.*, 2009, **2009**, 1303-1312.
20. A. L. Pinto and S. J. Lippard, *Proc. Natl. Acad. Sci. USA.*, 1985, **82**, 4616-4619.
21. L. S. Hollis, A. R. Amundsen, and E. W. Stern, *J. Med. Chem.*, 1989, **32**, 128-136.
22. K. S. Lovejoy, M. Serova, I. Bieche, S. Emami, M. D'Incalci, M. Broggini, E. Erba, C. Gespach, E. Cvitkovic, S. Faivre, E. Raymond, and S. J. Lippard, *Mol. Cancer Ther.*, 2011, **10**, 1709-1719.
23. K. S. Lovejoy, R. C. Todd, S. Zhang, M. S. McCormick, J. A. D. Aquino, J. T. Reardon, A. Sancar, K. M. Giacomini, and S. J. Lippard, *Proc. Natl. Acad. Sci. USA.*, 2008, **105**, 8902-8907.
24. G. Zhu, M. Myint, W. H. Ang, L. Song, and S. J. Lippard, *Cancer Res.*, 2012, **72**, 790-800.
25. G. Y. Park, J. J. Wilson, Y. Song, and S. J. Lippard, *Proc. Natl. Acad. Sci. USA.*, 2012, **109**, 11987-11992.
26. D. Wang, G. Zhu, X. Huang, and S. J. Lippard, *Proc. Natl. Acad. Sci. USA.*, 2010, **107**, 9584-9589.

27. G. Natile and M. Coluccia, *Coord. Chem. Rev.*, 2001, **217**, 383-410.
28. S. M. Aris and N. P. Farrell, *Eur. J. Inorg. Chem.*, 2009, **2009**, 1293-1302.
29. M. Coluccia, A. Nassi, A. Boccarelli, D. Giordano, N. Cardellicchio, D. Locker, M. Leng, M. Sivo, F. P. Intini, and G. Natile, *J. Inorg. Biochem.*, 1999, **77**, 31-35.
30. Y. Najajreh, E. Khazanov, S. Jawbry, Y. Ardeli-Tzaraf, J. M. Perez, J. Kasparkova, V. Brabec, Y. Barenholz, and D. Gibson, *J. Med. Chem.*, 2006, **49**, 4665-4673.
31. N. Farrell, L. F. Povirk, Y. Dange, G. DeMasters, M. S. Gupta, G. Kohlhagen, Q. A. Khan, Y. Pommier, and D. A. Gewirtz, *Biochem. Pharmacol.*, 2004, **68**, 857-866.
32. Y. Zou, V. Houten, and N. P. Farrell, *Biochemistry*, 1993, **12**, 9632-9638.
33. F. Kratz, I. A. Müller, C. Ryppa, and A. Warnecke, 2008, 20-53.
34. M. D. Hall, G. J. Foran, M. Zhang, P. J. Beale, and T. W. Hambley, *J. Am. Chem. Soc.*, 2003, **125**, 7524-7525.
35. M. D. Hall and T. W. Hambley, *Coord. Chem. Rev.*, 2002, **232**, 49-67.
36. M. Galanski, M. A. Jakupc, and B. K. Keppler, *Curr. Med. Chem.*, 2005, **12**, 2075-2094.
37. W. D. Figg, C. H. Chau, R. A. Madan, J. L. Gulley, R. Gao, T. M. Sissung, S. Spencer, M. Beatson, J. Aragon-Ching, S. M. Steinberg, and W. L. Dahut, *Clin. Genitourinary*, 2013, In press.
38. A. M. Pizarro and P. J. Sadler, *Biochimie*, 2009, **91**, 1198-1211.
39. I. Yoon, J. Z. Li, and Y. K. Shim, *Clin. Endosc.*, 2013, **46**, 7-23.
40. A. P. Castano, P. Mroz, and M. R. Hamblin, *Nat. Rev. Cancer*, 2006, **6**, 535-545.
41. L. B. Josefsen and R. W. Boyle, *Met. Based Drugs*, **2008**, 1-24.
42. E. Skovsen, J. W. Snyder, J. D. C. Lambert, and P. R. Ogilby, *J. Phys. Chem. B*, 2005, **109**, 8570-8573.
43. S. G. Bown, *Phil. Trans. R. Soc. A*, 2013, 371:20120371.
44. N. J. Farrer, L. Salassa, and P. J. Sadler, *Dalton Trans.*, 2009, 10690-10701.

45. K. Szaciłowski, W. Macyk, A. Drzewiecka-Matuszek, M. Brindell, and G. Stochel, *Chem. Rev.*, 2005, **105**, 2647-2694.
46. O. I. Trushina, E. G. Novikova, V. V. Sokolov, E. V. Filonenko, V. I. Chissov, and G. N. Vorozhtsov, *Photodiagnosis Photodyn. Ther.*, 2008, **5**, 256-259.
47. H. Patel, R. Mick, J. Finlay, T. C. Zhu, E. Rickter, A. Keith, S. B. Malkowicz, S. M. Hahn, and T. M. Busch, *Clin. Cancer Res.*, 2008, **14**, 4869-4876.
48. W. E. Grant, P. M. Speight, a J. MacRobert, C. Hopper, and S. G. Bown, *Br. J. Cancer*, 1994, **70**, 72-78.
49. N. P. Assembly, C. S. Jin, J. F. Lovell, J. Chen, and G. Zheng, *ACS Nano*, 2013, **7**, 2541-2550.
50. H. Ali and J. E. van Lier, *Chem. Rev.*, 1999, **99**, 2379-2450.
51. R. Bonnett, *Metal Complexes for Photodynamic therapy, Comprehensive Coord. Chem. II*, Elsevier Pergamon, Oxford, 2004.
52. T. J. Dougherty and S. L. Marcus, *Eur. J. Cancer*, 1992, **28**, 1734-1742.
53. *Q Light Phototherapy*, <http://www.qlight.ch/>.
54. P. J. Bednarski, F. S. Mackay, and P. J. Sadler, *Anticancer Agents Med. Chem.*, 2007, **7**, 75-93.
55. M. Pawlicki, H. A. Collins, R. G. Denning, and H. L. Anderson, *Angew. Chem. Int. Ed.*, 2009, **48**, 3244-3266.
56. Y. Zhao, G. M. Roberts, S. E. Greenough, N. J. Farrer, M. J. Paterson, W. H. Powell, V. G. Stavros, and P. J. Sadler, *Angew. Chem. Int. Ed.*, 2012, **51**, 11263-6.
57. N. M. Idris, M. K. Gnanasammandhan, J. Zhang, P. C. Ho, R. Mahendran, and Y. Zhang, *Nat. Med.*, 2012, **18**, 1580-1585.
58. C. Wang, L. Cheng, and Z. Liu, *Theranostics*, 2013, **3**, 317-330.
59. V. Balzani, G. Bergamini, S. Campagna, and F. Puntoriero, *Top. Curr. Chem.*, 2007, **280**, 1-36.
60. C. E. Wayne and R. P. Wayne, *Photochemistry*, Oxford University Press, New York, 1996.

61. P. W. Atkins, T. L. Overton, J. P. Rourke, M. T. Weller, and F. A. Armstrong, *Inorganic Chemistry*, Oxford University Press, Oxford, Fourth., 2006.
62. C. E. Housecroft and A. G. Sharpe, *Inorganic Chemistry*, Pearson Education Limited, Harlow, England, 2nd edn., 2005.
63. D. N. Sathyanarayana, *Electronic absorption spectroscopy and related techniques*, University Press (India) Limited, Hyderabad, India, 2001.
64. W.Reusch,
<http://www2.chemistry.msu.edu/faculty/reusch/virttxtjml/photchem.htm>,
29/07/2013.
65. S. Banerjee, P. Prasad, A. Hussain, I. Khan, P. Kondaiah, and A. R. Chakravarty, *Chem. Commun.* , 2012, **48**, 7702-7704.
66. U. Basu, I. Khan, A. Hussain, P. Kondaiah, and A. R. Chakravarty, *Angew. Chem. Int. Ed.*, 2012, **51**, 2658-2661.
67. U. Schatzschneider, *Eur. J. Inorg. Chem.*, 2010, 1451-1467.
68. Y. Liu, R. Hammitt, D. A. Lutterman, L. E. Joyce, R. P. Thummel, and C. Turro, *Inorg. Chem.*, 2009, **48**, 375-385.
69. L. Zayat, O. Filevich, L. M. Baraldo, and R. Etchenique, *Phil. Trans. R. Soc. A*, 2013, **371**, 371:20120330.
70. S. Betanzos-Lara, L. Salassa, A. Habtemariam, and P. J. Sadler, *Chem. Commun.* , 2009, 6622-6624.
71. C. Moucheron, *New J. Chem.*, 2009, **33**, 235-245.
72. M. J. Rose and P. K. Mascharak, *Coord. Chem. Rev.*, 2008, **252**, 2093-2114.
73. B. A. Jackson, V. Y. Alekseyev, and J. K. Barton, *Biochemistry*, 1999, **38**, 4655-4662.
74. S. W. Thomas, K. Venkatesan, P. Müller, and T. M. Swager, *J. Am. Chem. Soc.*, 2006, **128**, 16641-16648.
75. W.-P. To, T. Zou, R. W.-Y. Sun, and C.-M. Che, *Phil. Trans. R. Soc. A*, 2013, **371**, 371:20120126.
76. J. Kalinowski, V. Fattori, M. Cocchi, and J. A. G. Williams, *Coord. Chem. Rev.*, 2011, **255**, 2401-2425.

77. M. Hissler, J. E. McGarrah, W. B. Connick, D. K. Geiger, S. D. Cummings, and R. Eisenberg, *Coord. Chem. Rev.*, 2000, **208**, 115-137.
78. P. Heringova, J. Woods, F. S. Mackay, J. Kasparkova, P. J. Sadler, and V. Brabec, *J. Med. Chem.*, 2006, **49**, 7792-7798.
79. J. Mlcouskova, J. Stepankova, and V. Brabec, *J. Biol. Inorg. Chem.*, 2012, **17**, 891-898.
80. C. Lottner, K.-C. Bart, G. Bernhardt, and H. Brunner, *J. Med. Chem.*, 2002, **45**, 2064-2078.
81. K. L. Ciesienski, L. M. Hyman, D. T. Yang, K. L. Haas, M. G. Dickens, R. J. Holbrook, and K. J. Franz, *Eur. J. Inorg. Chem.*, 2010, 2224-2228.
82. S.-W. Lai, Y. Liu, D. Zhang, B. Wang, C.-N. Lok, C.-M. Che, and M. Selke, *Photochem. Photobiol.*, 2010, **86**, 1414-1420.
83. R. Wai-Yin Sun, A. Lok-Fung Chow, X.-H. Li, J. J. Yan, S. Sin-Yin Chui, and C.-M. Che, *Chem. Sci.*, 2011, **2**, 728-736.
84. T. Zou, C.-N. Lok, Y. M. E. Fung, and C.-M. Che, *Chem. Commun.*, 2013, **49**, 5423-5425.
85. M. P. Donzello, D. Vittori, E. Viola, I. Manet, L. Mannina, L. Cellai, S. Monti, and C. Ercolani, *Inorg. Chem.*, 2011, **50**, 7391-7402.
86. S. L. H. Higgins, A. J. Tucker, B. S. J. Winkel, and K. J. Brewer, *Chem. Commun.*, 2012, **48**, 67-69.
87. N. Sciences, P. G. Programmes, K. Molnar, W. Panning, M. Andrews, and R. Whyman, *Inorg. Chem.*, 1986, **2**, 2910-2913.
88. C. Loup, A. Tesouro Vallina, Y. Coppel, U. Létinois, Y. Nakabayashi, B. Meunier, B. Lippert, and G. Pratviel, *Chemistry Eur. J.*, 2010, **16**, 11420-11431.
89. N. A. Kratochwil and P. J. Bednarski, *Arch. Pharm. Pharm. Med. Chem.*, 1999, **332**, 279-285.
90. N. A. Kratochwil, M. Zabel, and P. J. Bednarski, *J. Med. Chem.*, 1996, **2**, 2499-2507.
91. N. A. Kratochwil, Z. Guo, P. del Socorro Murdoch, J. A. Parkinson, P. J. Bednarski, and P. J. Sadler, *J. Am. Chem. Soc.*, 1998, **120**, 8253-8254.
92. A. Vogler and A. Kern, *Angew. Chem. Int. Ed.*, 1978, **1157**, 524-525.

-
93. A. Vogler, C. Quett, and H. Kunkely, *Ber. Bunsenges. Phys. Chem*, 1988, **92**, 1486-1492.
94. F. S. Mackay, J. A. Woods, P. Heringová, J. Kaspárková, A. M. Pizarro, S. A. Moggach, S. Parsons, V. Brabec, and P. J. Sadler, *Proc. Natl. Acad. Sci. USA.*, 2007, **104**, 20743-20748.
95. N. J. Farrer, J. A. Woods, L. Salassa, Y. Zhao, K. S. Robinson, G. Clarkson, F. S. Mackay, and P. J. Sadler, *Angew. Chem. Int. Ed.*, 2010, **49**, 8905-8908.
96. F. S. Mackay, J. A. Woods, H. Moseley, J. Ferguson, A. Dawson, S. Parsons, and P. J. Sadler, *Chem. Eur. J.*, 2006, **12**, 3155-3161.
97. P. Muller, B. Schroder, J. A. Parkinson, N. A. Kratochwil, R. A. Coxall, A. Parkin, S. Parsons, and P. J. Sadler, *Angew. Chem. Int. Ed.*, 2003, **42**, 335-339.
98. H. I. A. Phillips, L. Ronconi, and P. J. Sadler, *Chem. Eur. J.*, 2009, **15**, 1588-1596.
99. L. Ronconi and P. J. Sadler, *Dalton Trans.*, 2011, **40**, 262-268.
100. L. Ronconi and P. J. Sadler, *Chem. Commun.*, 2008, 235-237.
101. P. J. Bednarski, R. Grünert, M. Zielzki, A. Wellner, F. S. Mackay, and P. J. Sadler, *Chem. Biol.*, 2006, **13**, 61-67.
102. P. J. Bednarski, K. Korpis, A. F. Westendorf, S. Perfahl, and R. Grünert, *Phil. Trans. R. Soc. A*, 2013, **371**, 371:20120118.
103. A. F. Westendorf, J. A. Woods, K. Korpis, N. J. Farrer, L. Salassa, K. Robinson, V. Appleyard, K. Murray, R. Grünert, A. M. Thompson, P. J. Sadler, and P. J. Bednarski, *Mol. Cancer Ther.*, 2012, **11**, 1894-18904.
104. N. J. Farrer, J. A. Woods, V. P. Munk, F. S. Mackay, and P. J. Sadler, *Chem. Res. Toxicol.*, 2010, **23**, 413-421.
105. J. S. Butler, J. A. Woods, N. J. Farrer, M. E. Newton, and P. J. Sadler, *J. Am. Chem. Soc.*, 2012, **134**, 16508-16511.
106. A. Harriman, *J. Phys. Chem.*, 1987, **91**, 6102-6104.
107. J. Pracharova, L. Zerzankova, J. Stepankova, O. Novakova, N. J. Farrer, P. J. Sadler, V. Brabec, and J. Kasparkova, *Chem. Res. Toxicol.*, 2012, **25**, 1099-111.

108. A. F. Westendorf, A. Bodtke, and P. J. Bednarski, *Dalton Trans.*, 2011, **40**, 5342-5451.

Chapter 2

Experimental Methods

This chapter describes the main techniques used in this thesis. Specific experimental parameters and settings used on various instruments are given.

2.1 Nuclear Magnetic Resonance spectroscopy (NMR)

^1H , ^{13}C and ^{195}Pt NMR spectra were acquired at 298 K on Bruker AV-400 (^1H : 399.10 MHz), Bruker DPX-400 (^1H : 400.03 MHz) or Bruker AVIII-600 (^1H : 600.13 MHz) spectrometers. Samples were prepared by the addition of the appropriate solvent (0.6 mL) in 5 mm NMR tubes. 1D ^1H -NMR spectra were recorded using standard pulse sequences. Typically the data were acquired with 128 or 16 transients into 32 k data points over a spectral width of 14 ppm. The ^1H -NMR chemical shifts were internally calibrated with the residual peaks of solvent $\text{CHD}_2\text{COCD}_3$ ($\delta = 2.05$ ppm), CHD_2OD ($\delta = 3.31$ ppm), DMSO-d_6 ($\delta = 2.50$ ppm) or added 1,4-dioxane ($\delta = 3.75$ ppm) in the case of D_2O .¹ 2D spectra were recorded using standard pulse-pulse sequences. All the novel Pt(IV) complexes in this thesis were characterized with ^{13}C -NMR spectroscopy. The pulse sequences used were jmod (J Modulation) and PENDANT (Polarization ENhancement During Attached Nucleus Testing). In both cases, the peaks for $-\text{CH}_2$ or quaternary carbons appear to be inverted relative to those for $-\text{CH}$ or CH_3 groups. The signals of quaternary carbons were generally of low intensity.²

COSY (Correlation spectroscopy) spectra were recorded to identify pairs of nuclei which are coupled through bonds. Typically they were acquired using 8 transients into 1024 data points. [^1H , ^{13}C] HSQC (Heteronuclear Single-Quantum Correlation) 2D spectra were used for the assignment of ^{13}C NMR peaks. The spectra were acquired with 32 transients and the time domain was 1024 or 2048.

The ^{195}Pt -NMR spectra were typically obtained with pulse sequence zg (non-proton decoupled), with a relaxation delay (D1) of 0 s, using a 2 k or 65 k time domain and 20 k transients. The spectra were externally referenced with K_2PtCl_6 (15 mM in D_2O).

Water suppression was used when samples were prepared in aqueous solution. To minimise the large residual water peak, the HOD signal was suppressed by irradiating at the frequency of water in between pulse sequences.

The labelling of the atoms for the assignment of the ^1H and ^{13}C -NMR signals shown in the characterisation data (Chapters 3 and 4) are included in the Appendix.

2.2 Mass Spectrometry

2.2.1 Electrospray mass spectrometry (ESI-MS)

Positive-ion ESI spectra were obtained by preparing the samples in CH_3OH or H_2O and infusing into the mass spectrometer (Bruker Esquire 2000 Trap Spectrometer or Agilent 6130 single Quad) , using an automatic sample delivery system. The mass spectra were recorded with a scan range of m/z 500-1000 for positive ions. Data were processed using Data Analysis version 3.3 (Bruker Daltonics). The detection of platinum-containing species was aided by the distinctive isotopic distribution pattern of platinum. Platinum has 6 stable isotopes: ^{190}Pt (0.0014 %), ^{192}Pt (0.782 %), ^{194}Pt (32.967 %), ^{195}Pt (33.832 %), ^{196}Pt (25.242 %), ^{198}Pt (7.163 %). Figure 2.1 illustrates the isotopic distribution pattern for platinum.

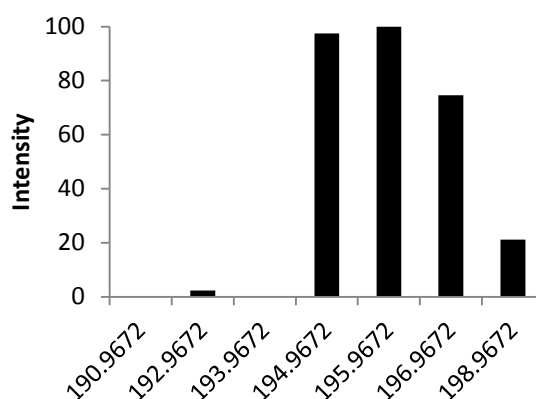


Figure 2.1: Isotopic distribution of platinum.

2.2.2 LC-MS (Liquid Chromatography-Mass Spectrometry)

LC-MS analysis was carried on a Dionex 3000RS UHPLC coupled with a Bruker MaXis Q-TOF mass spectrometer. An Agilent Zorbax Eclipse instruments plus column (C18, 100 x 2.1 mm, 1.8 μ m) were used. Mobile phases consisted of A, water with 0.1% formic acid and B, acetonitrile with 0.1% formic acid. A gradient of 5% B to 100% B in 15 minutes was employed with flow rate at 0.2 mL/min, UV detection was made at 254 nm. The mass spectrometer was operated in electrospray positive mode with a scan range 50 – 2,000 m/z. Source conditions are, end plate offset at -500 V; capillary at -4500 V; nebulizer gas (N_2) at 1.6 bar; dry gas (N_2) at 8 L/min; dry temperature 180 $^{\circ}$ C. Ion transfer conditions were: ion funnel RF at 200 Vp/p; multiple RF at 200 Vp/p; quadrupole low mass set at 55 m/z; collision energy at 5.0 eV; collision RF at 600 Vp/p; ion cooler RF at 50-350, Vp/p; transfer time set at 121 μ s; pre-pulse storage time 1 μ s. Calibration was done with sodium formate (10 mM) through a loop injection of 20 μ L of standard

solution at the beginning of each run. The spectra were processed with Bruker Daltonics Data Analysis.

2.2.3 ICP-MS (Inductively coupled plasma mass spectrometry)

ICP-MS was carried out on an Agilent 7500 Series spectrometer. Data acquisition was carried out on ICP-MS Top (version B.03.05) and analysis on Offline Data Analysis (version B.03.05). The standards were prepared from a stock of 1000 ppm Pt solutions obtained from Sigma Aldrich, in 5% HNO₃ with miliQ water at the following concentrations: 200, 50, 10, 5, 1, 0.5, 0.2, 0.05, 0.01 ppb.

2.3 HPLC (High Performance Liquid Chromatography)

HPLC was mainly used for purity assessment of the novel complexes synthesized. Specific conditions can be found in Chapters 3 and 5 and in all of the cases performed on Agilent 1200 system, with a C₁₈ column.

2.4 X-Ray crystallography

X-ray diffraction data were collected and solved by Dr Guy Clarkson at the University of Warwick.

Diffraction data were collected by the use of Mo K α radiation at a wavelength of $\lambda=0.71073$ Å on an Oxford Diffraction Gemini four-circle system with Ruby CCD area detector. The crystals were held at the following temperatures: 100 K, 150 K and 568 K (refer to specific values for each compound in Chapters 3 and 5) with the Oxford Cryosystem Cryostream Cobra. The structures were solved by direct methods using SHELXS (Sheldrick, 1990) (TREF) with additional light atoms found by Fourier methods. Hydrogen atoms were added at calculated positions and refined using a riding model. Anisotropic displacement parameters were used

for all non-H atoms except the OH; H-atoms were given isotropic displacement parameters equal to 1.2 (or 1.5 for OH and methyl hydrogen atoms) times the equivalent isotropic displacement parameter of the atom to which the H-atom is attached.

ORTEP diagrams were used to illustrate the ellipsoid form of the crystal structures and Mercury to generate the intermolecular interactions as well as the packing diagrams.

The formula used to assess whether bond distances are statistically different was the following:

Bond difference $> 3\sigma$, where

$$\sigma = \sqrt{(\sigma_1^2 + \sigma_2^2)}, \text{ where } \sigma_1 \text{ and } \sigma_2 \text{ are the bond length standard deviations}$$

2.5 UV-VIS spectroscopy

UV-Vis absorption spectra were recorded on a Varian Cary 300 UV-Vis spectrophotometer in 1 cm path-length quartz cuvettes, purchased from Starna Scientific. Before the measurement of each spectrum, a blank of the solvent was recorded for reference. The spectral width was from 200-800 nm, the bandwidth was 1.0 nm and the scan rate was set to 600 nm/min. Typically, the volume used was 450 μL . The spectra were processed using UV-Winlab software for Windows XP. Extinction coefficients were determined using the Beer-Lambert law ($A = \epsilon cl$, where ϵ is the extinction coefficient $\text{M}^{-1}/\text{cm}^{-1}$, c the molar concentration and l the path length in cm). Pt concentrations for determination of extinction coefficients were measured by ICP-MS.

2.6 pH measurements

pH measurements for the pK_a analysis in Chapter 5 were recorded at ambient temperature directly in the NMR tube with a pocket ISFET pH meter (Minilab Series), which is a solid state electrode. The meter was calibrated using standard buffer solutions (pH 7.00, pH 4.01, pH 10.01), as supplied by the provider (Minilab).

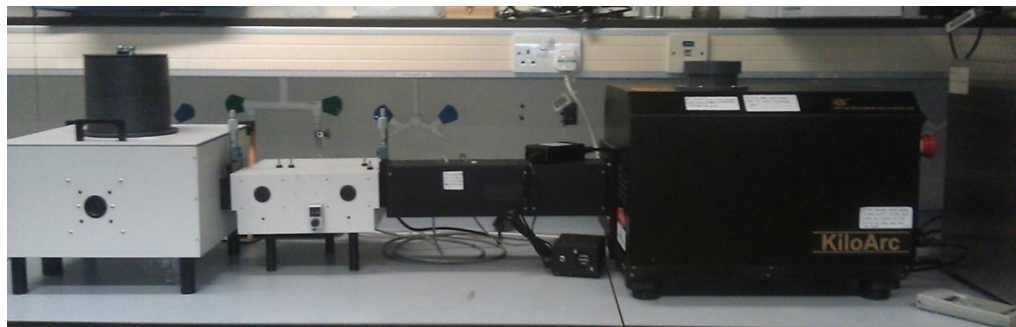
2.7 Irradiation methods and devices

Photoactivation of Pt complexes were carried out at 293 K. The light sources used were the following: (a) LZC-ICH2 photoreactor (Luzchem Research Inc.) equipped with a temperature controller and 3 UVA lamps (Hitachi, $\lambda_{\max} = 361$ nm) or 6 Luzchem LZC-420 lamps ($\lambda_{\max} = 420$ nm) with no other sources of light filtration. (b) LED light sources (BASETech model no. SP-GU10 230V~50 Hz 1.3-2.1 W) with $\lambda_{\max} = 463$ nm or 515 nm. (Refer to Appendix for the output spectra). (c) KiloArcTM broadband arc lamp monochromator, which was supplied with the appropriate filters to cut-off any unwanted lower wavelength light.

(A)



(B)



(C)

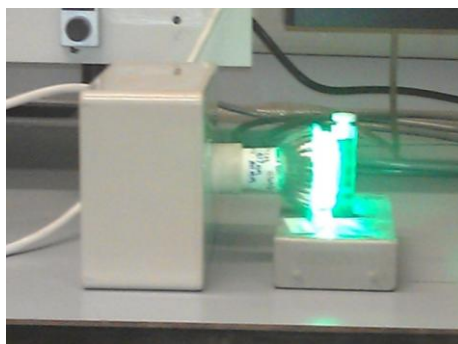


Figure 2.2: Light sources used in this thesis: A) LZC-ICH2 photoreactor (Luzchem Research Inc) equipped with 420 nm bulbs and a temperature controller. (B) KiloArc monochromator (C) Irradiation of a sample in a UV-Vis cuvette with the green LED (517 nm) fitted into a GU-10 device.

2.8 Light measurements

The light intensity used to irradiate samples was measured with an International Light Technologies Powermeter (ILT1400-A) equipped with SEL 033 detector and either a UVA/TD filter (315-390 nm) for UVA irradiations or a flat response visible filter F/W (400-1064 nm) for visible wavelengths. The output spectrum for each of the light sources discussed above was measured using the Ocean Optics USB4000-UV-Vis spectrophotometer.

The determination of the light dose in the experiments was calculated by the equation:

$$\text{Dose (mJ cm}^{-2}\text{)} = \text{Time (s)} \times \text{Irradiance (mW cm}^{-2}\text{)}$$

2.9 EPR (Electron Paramagnetic Resonance)³

The EPR spectra were recorded on a Bruker EMX (X-band) spectrometer (for more details refer to Chapter 3).

2.10 DFT and TDDFT calculations

Calculations were carried out in collaboration with Dr Luca Salassa, CIC biomaGUNE, Spain.

All calculations were performed with the Gaussian 03 (G03) program⁴ employing the DFT method, with the PBE1PBE⁵ functionals. The LanL2DZ basis set⁶ and effective core potential were used for the Pt atom and the 6-31G**+ basis set⁷ was used for all other atoms. Geometry optimizations for complex **4** and complex **4**-deprotonated (Chapter 3) and complex **18** (Chapter 4) in the ground state (S_0) and lowest-lying triplet state (T_1) were performed in the gas phase and the nature of all stationary points was confirmed by normal mode analysis. For the T_1 geometries the UKS method with the unrestricted PBE1PBE functional was employed. The conductor-like polarizable continuum model method (CPCM)⁸ with water as solvent was used to calculate the electronic structure and the excited states of complex **4** and complex **4**-deprotonated in solution (H_2O). Thirty-two singlet excited states with the corresponding oscillator strengths were determined with a Time-dependent Density Functional Theory (TD-DFT)^{9, 10} calculation.

2.11 Cell culture

The A2780 human ovarian cell line was obtained from the ECACC (European Collection of Animal Cell Culture, Salisbury, UK). Cells used for the uptake experiment were maintained in RPMI 1640 media, which was supplemented with

10% foetal calf serum (FCS), 1% L-glutamine and 1% penicillin / streptomycin.

All cells were grown at 310 K in a humidified atmosphere containing 5% CO₂.

For the determination of phototoxic activity, cells were maintained in RPMI medium containing 10% FCS, in an antibiotic free culture in a humidified atmosphere, containing 5% CO₂ and mycoplasma free.

2.12 Photo-dark toxicity testing

The photo-dark toxicity testing was carried out in collaboration with Dr Julie Woods, University of Dundee, Scotland.

The complexes were prepared in Earl's balanced salt solution just before use and filtered. Irradiations were performed using a bank of 2 × 3 ft TL03 (Philips; λ_{max} : 420 nm) light sources filtered to attenuate wavelengths below 400 nm. Irradiance was measured with an International Light meter, fitted with the appropriate detector and diffuser and calibrated using a double grating spectroradiometer (Bentham, UK) in the UKAS accredited optical physics laboratory (Photobiology Unit, Dundee). The delivered dose was 5 J/cm². The experiments were controlled for test compound and irradiation. The cytotoxicity was measured using the neutral red assay 96 or 72 hours after light exposure (i.e. recovery period). The IC₅₀ was determined by curve fitting (Graphpad). Goodness of fit was assessed by R² values and the 95% confidence interval. All cell experiments were performed in duplicate/ triplicate and repeated independently a minimum of two times.

2.12.1 Neutral Red assay

Upon cell uptake Neutral red (Figure 2.3) accumulates in lysosomes. The low pH in the lysosomal matrix of live cells causes the dye to become charged, allowing it to be retained in this organelle.¹¹ The dye is then extracted from the cells upon solubilisation and thus can be quantified.

The protocol used for this assay was the following. A stock solution of neutral red was prepared in water (4 mg/mL) and diluted 80-fold in the cell culture medium (e.g. RPMI). Prior to addition to the cells, the solution was heated to 37 °C and filtered (no. 1 Whatman paper). The growth medium was removed from the cells and the neutral red dye (100 µL) was added and the cells are incubated for 3 hours in the dark. Upon removal of the dye, the cells were rinsed with PBS (100 µL) and then the plates were shaken for 15 min with PBS (200 µL) for solubilisation. The dye concentration was quantified by measuring the absorbance at 450 nm.

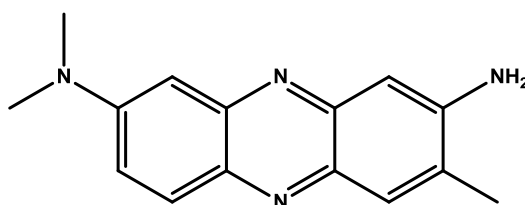


Figure 2.3: Chemical structure of 3-amino-7-dimethylamino-2-methylphenazine hydrochloride, is the dye used in the neutral red assay.

2.12.2 MTT assay

MTT (4, 5-dimethylthiazolyl)-2,5-diphenyltetrazolium bromide) assay can also be used to assess cell viability in phototoxicity experiments. The basis of this assay is that when the dye is uptaken by live cells, cytoplasmic and mitochondrial enzymes reduce the dye to the formazan form which is purple (Figure 2.4).¹²

MTT (50 μL of 1 mg/ mL stock solution prepared in PBS) was added to all the treated and control cells. Plates were incubated for 3 hours at 37 $^{\circ}\text{C}$ to allow uptake of the dye. Following this step, the medium was removed and the plates were frozen at -20 $^{\circ}\text{C}$ for 48 h. DMSO (150 μL) was added to solubilise the dye and the plates were placed on the shaker for 15 minutes to ensure a homogeneous solution. The reading was made using a plate reader at 570 nm, with a reference reading at 690 nm.

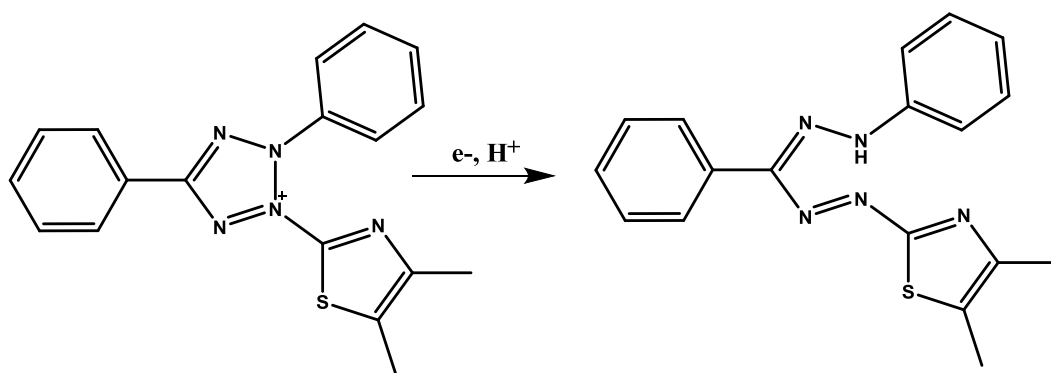


Figure 2.4: MTT assay reduction of 3-(4,5-dimethylthiazol-2-yl)-2,5-diphenyltetrazolium, which is yellow, to form the purple formazan.

References

1. H. E. Gottlieb, V. Kotlyar, and A. Nudelman, *J. Org. Chem.*, 1997, **3263**, 7512-7515.
2. J. W. Akitt and B. E. Mann, *NMR and Chemistry: An introduction to modern NMR spectroscopy*, Chapman & Hall, Cheltenham, 2000.
3. M. Brustolon and E. Giamello, *Electron Paramagnetic Resonance*, Wiley & Sons Inc., New Jersey, 2009.
4. M. J. Frisch, G. W. Trucks, and H. B. Schlegel, in *Gaussian 03, revision D 0.1*; Gaussian Inc.: Wallingford CT., 2004.
5. J. . P. Perdrew, K. Burke, and M. Ernzerhof, *Phys. Rev. Lett.*, 1996, **77**, 3865-3868.
6. P. J. Hay and W. R. Wadt, *J. Chem. Phys.*, 1985, **82**, 270-284.
7. A. D. McLean and G. S. Chandler, *J. Chem. Phys.*, 1980, **72**, 5639-5649.
8. M. Cossi, N. Rega, G. Scalmani, and V. Barone, *J. Comput. Chem.*, 2003, **24**, 669-681.
9. M. E. Casida, C. Jamorski, K. C. Casida, and D. R. Salahub, *J. Chem. Phys.*, 1998, **108**, 4439-4450.
10. R. E. Stratmann, G. E. Scuseria, and M. J. Frisch, *J. Chem. Phys.*, 1998, **109**, 8218-8285.
11. G. Repetto, A. del Peso, and J. L. Zurita, *Nat. Protoc.*, 2008, **3**, 1125-1131.
12. A. L. Niles, R. a Moravec, and T. L. Riss, *Expert Opin. Drug Discov.*, 2008, **3**, 655-669.

Chapter 3

Axial ligand derivatisation of Pt(IV)-diazido compounds

3.1 Introduction

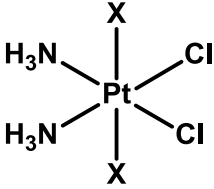
In recent years efforts have been made for the development of Pt(IV) prodrugs, which could improve the pharmacological profile of the platinum drug family due to their kinetic inertness and the various modification possibilities that they offer.¹ Amongst the 30 platinum compounds that have entered clinical trials, only three of them were Pt(IV): tetraplatin, iproplatin and satraplatin. (Chapter 1, Figure 1.6). The satraplatin-related compound LA-12 is still under clinical investigation.² Satraplatin was certainly the most promising Pt(IV) prodrug, but unfortunately there has been no significant increase of survival rates when compared to standard cisplatin treatment.^{3,4} Numerous strategies have been applied to transform the successful Pt(II) compounds into Pt(IV) prodrugs, which would exert their cytotoxic effect by the reduction into Pt(II) in the blood plasma or tissue. Pt(IV) analogs of carboplatin, picoplatin, oxaliplatin and cisplatin have been produced and they showed interesting antiproliferative properties.⁵⁻⁸ The Pt(IV) compounds are octahedral complexes, which upon reduction produce Pt(II) square-planar complexes.

By convention, axial ligands are normally considered to be those which lie above and below the plane of the amines.¹ The type of axial ligands in Pt(IV) prodrugs has always been of great interest as they affect many properties of the drug such as lipophilicity, stability, reduction rate as well as a second cytotoxic effect upon release. The work of Wee Han Ang *et al.*, is a representative example of the full exploitation of the axial ligands.⁷ By utilizing sequential acylation, Pt(IV) complexes with asymmetric axial ligands were produced. This enabled the introduction of lipophilic and hydrophilic substituents, leading to the regulation of

the pharmacological and cytotoxic properties of the prodrug.⁷ Furthermore, mitaplatin which is a cisplatin derivative containing two dichloroacetate axial ligands, can exert its pharmacological effect in a dual mode upon reduction to Pt(II) inside the cell: the first by DNA platination via cisplatin, and the other by the release of DCA (dichloroacetate) ligands. DCA alters the mitochondrial membrane potential gradient in cancer but not normal cells. As a consequence, cytochrome c is released and apoptosis inducing factor is translocated to the nucleus.⁹

The axial ligands of Pt(IV) complexes normally act as leaving groups upon reduction to Pt(II), although this rule must be handled with care.¹⁰ The reduction potential of Pt(IV) can be greatly affected by the nature of the axial ligands. In general, based on half-wave reduction potentials, the order by which reduction is facilitated is $I^- > Cl^- > OAc^- > OH^-$.¹¹ This correlates with the rate of reduction in the presence of a biological reducing agent (e.g. ascorbic acid or glutathione). An example of a result of such study is illustrated in Table 3.1, which shows values of half-wave reduction potentials in a series of Pt(IV) complexes.¹² However, a recent finding by Hambley *et al.* contradicts this expected trend: for Pt(IV) analogues of oxaliplatin (i.e. a complex with coordination sphere N_2O_2), the fastest rate of reduction does not correlate with the most positive reduction potential, with the dihydroxo compound being reduced significantly faster than the dicarboxylated compound.¹³ This indicates that the coordination sphere of the Pt(IV) plays a crucial role in the reduction mechanism of the complexes by biological reductants and therefore predicting the ease of reduction of Pt(IV) prodrugs is not straightforward.

Table 3.1: Variation of half-wave reduction potential for Pt(IV) complexes with axial ligand.

Complex	X	Reduction Potential (mV)
	-Cl ⁻	-260
	-OAc ⁻	-635
	-OH ⁻	-880

A fundamental step in the development of Pt(IV) drugs is the carboxylation of the hydroxyl groups, which greatly facilitates subsequent modification. Hydroxyl groups are common axial ligands because oxidation of the Pt(II) to Pt(IV) can be carried out through the use of hydrogen peroxide. Carboxylation by acetylation of a dihydroxo Pt(IV) was first reported by Giandomenico *et al.*^{14, 15} In a later development it was shown that functionalisation of the hydroxides can be achieved using cyclic anhydrides, which yields a free carboxylic acid for further functionalisation.¹⁶ This was first utilized by Lippard's group to bind estrogen derivatives to oxoplatin, as it was established that estrogen-receptor-positive cells are sensitized to cisplatin, due to shielding of the Pt-DNA crosslinks.¹⁷ Furthermore, more functionalities were attached such as peptides (e.g. RGD, NGR) which can recognize the integrins on the surface of tumour endothelial cells (found in angiogenic tumours) and regions of inflammation.¹⁸ Chlorotoxin (which targets glioma, prostate, lung and melanoma cell lines), TAT peptide (a cell penetrating peptide which facilitates cellular uptake) and also analogues of somatostatin and neurotensin (peptides whose receptors are upregulated in various tumours) are more examples of peptides which have been coupled to

cisplatin or oxaliplatin Pt(IV) derivatives via a carboxylic acid axial ligand.^{19, 20, 21}

In most cases the cytotoxicity of the peptide derivative is increased compared to the Pt(IV) precursor but not necessarily greater than that of the Pt(II) parent compound.¹⁹⁻²¹ Nevertheless, tumour cell targeting could give a significant advantage in terms of selectivity of the drug towards cancerous *versus* healthy tissue. More sophisticated carriers exploiting the concept of passive targeting include carbon nanotubes to which the Pt(IV) prodrug is anchored via covalent linkage, or through hydrophobic interactions and enclosure within gold nanoparticles have also been investigated.²²

Very little work has been carried out with regard to modification of the axial ligands of Pt(IV)-azido photoactivatable complexes. Since their mechanisms include photoreduction to Pt(II), their importance from a structure-activity relationship point of view is unquestionable. Early work on diiodo-Pt(IV) complexes (Figure 3.1) demonstrated that changing from dihydroxo to diacetato axial ligands affects the photochemistry of the compound. For example photoirradiation studies followed by NMR showed that complex **A** undergoes photosubstitution instead of reduction and thus cannot bind to 5'-GMP whereas **B** is able to (Figure 3.1).²³ Also photolysis of **A** did not show any measurable calf thymus-DNA platination whereas photolysis of **B** resulted in 65%.²⁴

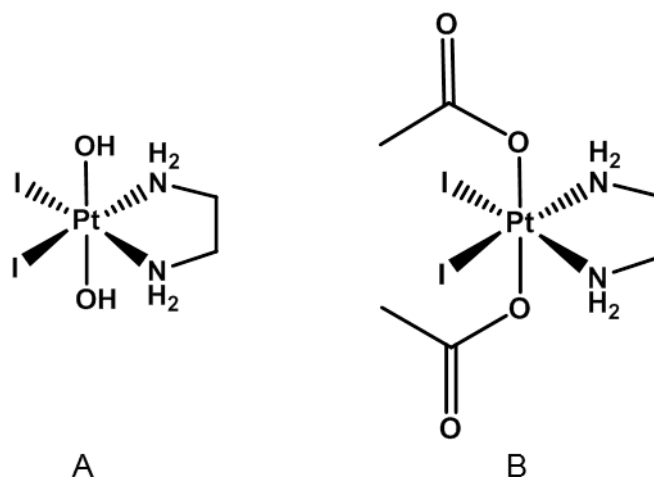


Figure 3.1: Diiodo-Pt(IV) complexes differing in the axial ligands. Complex **A** does not show evidence of DNA platination upon UV irradiation unlike compound **B**.

Computational work carried out by Sadler *et al.*²⁵ systematically studied the effect that various ligands or substituents would have on the UV-visible electronic absorption properties and photochemistry of *trans*-Pt(IV) compounds, including the modification of the axial ligands. Changing the OH⁻ axial ligand to I⁻ or to OAc⁻ critically influences the electronic transitions of the complex. Time-dependent density functional theory (TDDFT) calculations demonstrated that replacing both OH⁻ with OAc⁻ extends the strongest absorption band as well as the tail of the absorption spectrum to longer wavelengths. This is achieved by lowering the energy of the LUMO and LUMO+1, therefore lowering the energy gap between the HOMO and LUMO. However it was anticipated that this modification could also lead to more facile reduction within the cell under dark conditions.²⁵

The work in this chapter investigates the effect of axial ligand modifications on the photochemistry and photobiology of *trans*-Pt(IV) azido compounds. It describes the synthesis, characterisation, photoirradiation and biological studies of

the following novel compounds (Figure 3.2): *trans, trans, trans*-[Pt(N₃)₂(pyr)₂(OH)(succ)] (Complex 4), *trans, trans, trans*-[Pt(N₃)₂(pyr)₂(OH)(Succ-Pr)] (Complex 5), *trans, trans, trans*-[Pt(N₃)₂(pyr)₂(OH)(N-MI)] (Complex 6), in comparison with reference *trans, trans, trans*-[Pt(N₃)₂(OH)₂(pyr)₂] (Complex 3). The incorporation of cancer-cell targeting features is also presented and discussed.

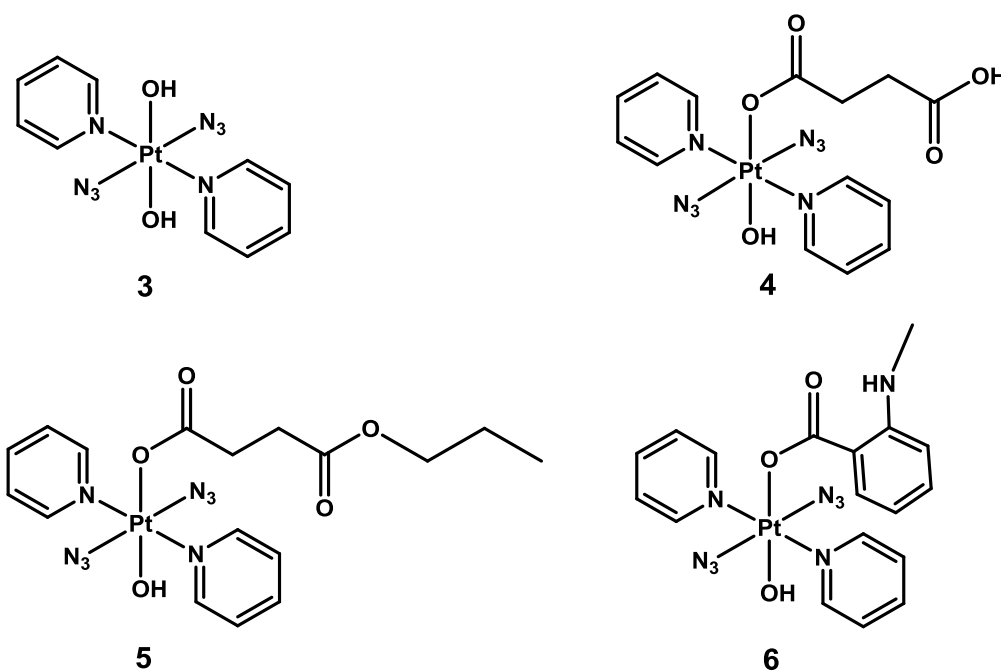


Figure 3.2: Complexes synthesized and studied in this chapter.

3.2 Experimental

Caution! Heavy metal azides are known to be shock sensitive detonators. Although no problems were encountered during this work, platinum azide compounds should be handled with care. Any syntheses or handling of platinum azide complexes was carried out under faint lighting conditions.

3.2.1 Materials

All materials were used as obtained from commercial sources unless otherwise stated. K_2PtCl_4 was purchased from Precious Metal Online. Pyridine, HCl and all solvents for common use were analytical reagent grade and were bought from Fisher Scientific and used as supplied. AgNO_3 , NaN_3 , H_2O_2 (30%), succinic anhydride, 1,1'-carbonyldiimidazole (CDI), N-methylisatoic anhydride (N-MIA), 5'-guanosine monophosphate and glutathione were purchased from Sigma Aldrich. 5,5-dimethyl-pyrroline N-oxide (DMPO) was bought from Enzo Life Sciences. PBS was purchased from Sigma Aldrich as tablets and one tablet dissolved in water (200 mL) yields a solution of 0.01 M phosphate, 0.0027 M KCl, 0.137 M NaCl at pH 7.4. Distilled water was purified using a Milipore water purification system. Water used in ICP-MS was purified using Purelab UHQ water purification system.

3.2.2 Methods and Instrumentation

3.2.2.1 HPLC purity test

The purity of the compounds was determined on an Agilent 1200 system with a VWD and 100 μL loop. The column was an Agilent ZORBAX Eclipse Plus C18, with dimensions of $250 \times 4.6 \text{ mm}^2$ and a 5 μm pore size. The injected volume was at 45 μL with needle washes. The mobile phase used was H_2O 0.1 % TFA / ACN 0.1% TFA. The flow rate was set to 1 mL/min and the method used is depicted in Table 3.2.

Table 3.2: HPLC method for purity tests on complexes. Solvent B is ACN (0.1% TFA) and solvent A is H₂O (0.1% TFA).

Time (min)	%B
0	10
30	80
40	80
41	10
55	10

Complexes **4** and **5** were dissolved in water and complex **6** in 10% MeOH/ 90% H₂O. The concentration used was 60 μ M.

3.2.2.2 Extinction coefficient determination

The extinction coefficient was estimated as described in Chapter 2 (section 2.6). The solvent used for **4**, **5** and compound **3** was H₂O; 95% H₂O / 5% DMSO (v/v) was used for **6** due to the poor solubility of the complex. The extinction coefficients for complexes **3** and **4** at longer wavelengths were measured using higher concentrations.

3.2.2.3 pK_a measurement

The pK_a^{*} (pK_a from D₂O measurements) of complex **4** (1.1 mM) was determined by following the changes in the chemical shifts of the pyridine protons, according to changes in pH^{*}. The pH^{*} was measured as described in Chapter 2 and it was adjusted to the desired value by using 0.01 M, 0.05 M, 0.1 M KOD and 0.1 M, 0.05 M, 0.001 M DCIO₄ solutions. ¹H-NMR spectra were recorded at 25 °C on a 600 MHz NMR spectrometer. Dioxane was used as a chemical shift reference.

3.2.2.4 Electron Paramagnetic Resonance

The EPR spectra were recorded on a Bruker EMX (X-band) spectrometer by Jennifer S. Butler at the University of Warwick. A cylindrical T_{M10} mode cavity (Bruker 4103 TM) was used and samples were placed in spectrosil quartz tubes of inner diameter 1.0 mm and outer diameter of 1.2 mm (Wilmad Labglass) sealed with J-Blue Tac. The tube was placed inside a larger quartz tube so the sample could be more accurately positioned inside the resonator. Using the y-incremental sweep mode of 24 with an accumulation of 10 scans in the X dimension, selected key parameters applied during the experiment were the following: modulation amplitude 2.0 G, microwave power 0.63 mW, modulation amplitude 0.2 mT, receiver gain 1.0×10^4 , sweep gain 41.94 s. The green LED (517 nm) was placed at a distance of 8.5 cm from the tube in the EPR cavity. The irradiation lasted for 35 minutes and the spectra represented are at 7 minute intervals. The spin adduct concentration was determined using a calibration curve (SigmaPlot) obtained from standard solutions of 4-hydroxy-2,2,6,6-tetramethyl-piperidine-1-oxyl (Tempol) in the corresponding solvent and the processing was carried out using Bruker WINEPR software.

3.2.2.5 Computational details

DFT and TDDFT calculations were carried out, as described in Chapter 2 (section 2.10).

3.2.2.6 Cell uptake studies

A2780 cells were seeded at a density of 5×10^5 cells/mL in each well and were allowed to adhere for 36 h. Before the drugs were added, the cells were washed with PBS (1 mL). The stock concentration of the drugs was confirmed via ICP-

MS analysis before exposure to the cells to mitigate any discrepancies in the added drug. The drugs (20 μM , 2 mL in PBS) were added and cells and incubated for 1 hour in the dark at 37 $^{\circ}\text{C}$. Following the uptake of the drug, the cells were washed with PBS (1 mL) and a solution of trypsin/ EDTA (2%) was added (0.5 mL) and incubated at 37 $^{\circ}\text{C}$ for 3 minutes, then neutralized with cell culture medium-RPMI (2 mL). Cells were transferred into falcon tubes and broken into a single cell suspension via vigorous pipetting to enable counting followed by addition of more RPMI (2 mL) to dilute the cells. Cells were counted in duplicate and an average was taken. Then, they were centrifuged at 1000 rpm at 22 $^{\circ}\text{C}$ for 5 minutes. The supernatant was removed and the cells were resuspended in PBS (1 mL) for a further wash. The cell pellet was kept at -20 $^{\circ}\text{C}$ until the Pt content was analysed via ICP-MS. Digestion of the cell pellet was carried out overnight in concentrated nitric acid (73%) at 70 $^{\circ}\text{C}$. The resulting solutions were diluted to 5% v/v HNO_3 , using doubly ionised water and then filtered through an inorganic membrane filter to remove any insoluble cell debris. The platinum content was measured by ICP-MS, as described in Chapter 2 (section 2.2.3). Temperature-dependent cell uptake experiments were performed for complexes **3** and **6**, at 4 $^{\circ}\text{C}$, 25 $^{\circ}\text{C}$ and 37 $^{\circ}\text{C}$, after 1 h of drug exposure in the dark. Concentration-dependent cell uptake experiments were performed at concentrations of 5, 10, 20, 40 and 60 μM for complexes **3** and **6**, after 1 h of incubation in the dark. Each experimental condition was carried out in triplicate.

3.2.2.7 Fluorescence measurements

Fluorescence measurements for complex **6** were performed on a Jasco FP-6500 spectrofluorimeter at a concentration of 26 μM in H_2O and using quartz cuvettes

with 1 cm path length. Spectra were acquired using the following parameters: excitation wavelength at 320 nm, excitation and emission slits at 10 nm and 5 nm respectively. The response was set to medium and the scanning rate to 200 nm/min.

3.2.2.8 Synthesis and characterisation

Complexes **1**, **2** and **3** have been synthesized as reported previously with an agreement in the characterization data.²⁶

3.2.2.8.1 *trans*-[PtCl₂(pyr)₂] (**1**)

K₂PtCl₄ (4 g, 9.64 mmol) was dissolved in H₂O (100 mL) and pyridine was added (15 mL, 193 mmol, 20 eq). The solution was stirred at 85 °C for 1.5 h after which point it became transparent. The solution was allowed to cool down and the solvent was rotary-evaporated to dryness to yield a white solid which was washed with diethyl ether for the removal of excess pyridine. HCl (2 M, 100 mL) was added and the solution was heated at 75 °C overnight to give *trans*-[PtCl₂(pyr)₂] as a yellow solid which was filtered off and washed with ice-cold water, ethanol and diethyl ether (Yield = 3.75 g, 8.86 mmol, 92%).

¹H-NMR (acetone-d₆, 400 MHz, ppm): δ= 8.87 (dd, ³J_{1H1H}= 6.83 Hz, ³J_{195Pt1H} = 31.07 Hz, 4Ho), δ= 8.02 (t, ³J_{1H1H} = 7.70 Hz, 2Hp), δ= 7.52 (t, ³J_{1H1H} = 7.46, 4Hm).

3.2.2.8.2 *trans*-[Pt(N₃)₂(pyr)₂] (**2**)

This complex was prepared as previously reported.²⁶ *Trans*-[PtCl₂(pyr)₂] (**1**) (3.75 g, 8.85 mmol) was suspended in water (500 mL), AgNO₃ (3.008 g, 2 eq) was added and the reaction was stirred at 60 °C overnight. The grey precipitate was

filtered through celite over a frit to obtain a pale yellow solution which was then further passed through an IM filter. Then NaN_3 (5.75 g, 10 eq) was added and the reaction was stirred overnight at room temperature. The yellow precipitate was filtered and washed with ice-cold water, ethanol and diethyl ether (3.48 g, 90%). The solid was recrystallised from pre-warmed pyridine at 40 °C at a ratio of 1 g/37 mL of pyridine and following hot filtration it was allowed to crystallise at -20 °C. The yellow solid was filtered, washed and dried under vacuum (Yield = 2.44 g, 70%).

^1H -NMR (acetone- d_6 , 400 MHz, ppm): δ = 8.86 (dd, $^3J_{\text{H1H1H}}$ = 6.76 Hz, $^3J_{195\text{Pt1H}}$ = 37.30 Hz, 4Ho), δ = 8.13 (tt, $^3J_{\text{H1H1H}}$ = 7.67 Hz, $^4J_{\text{H1H1H}}$ = 1.38 Hz, 2Hp), δ = 7.67 (t, $^3J_{\text{H1H1H}}$ = 7.15 Hz, 4Hm).

3.2.2.8.3 *trans, trans, trans*-[Pt(N₃)₂(OH)₂ (pyr)₂] (3)

The title product was obtained by oxidation of *trans*-[Pt(pyr)₂(N₃)₂], **2**. *Trans*-[Pt(N₃)₂(pyr)₂] (2.00 g, 4.56 mmol) was suspended in H_2O_2 (160 mL, 30%) and allowed to react at 45 °C for 4 hours, producing a yellow solution. This was filtered (IM) and transferred to a larger flask to which H_2O (340 mL) was added. The solution was lyophilized, yielding a yellow solid which was recrystallised from 2:1 ethanol/ methanol and the product precipitated by addition of diethyl ether at -20 °C. The solid was filtered and dried under vacuum (Yield = 1.6 g, 80%).

^1H -NMR (D_2O , 400 MHz, dioxane, ppm): δ = 8.80 (dd, $^3J_{\text{H1H1H}}$ = 6.68 Hz, $^3J_{195\text{Pt1H}}$ = 26.88 Hz, 4Ho), δ = 8.28 (tt, $^3J_{\text{H1H1H}}$ = 7.78 Hz, $^3J_{\text{H1H1H}}$ = 1.30 Hz, 2Hp), δ = 7.82 (t, $^3J_{\text{H1H1H}}$ = 7.11 Hz, 4Hm).

$\epsilon_{294\text{ nm}}$ = 17467 $\text{M}^{-1}\text{cm}^{-1}$, $\epsilon_{260\text{ nm}}$ = 12297 $\text{M}^{-1}\text{cm}^{-1}$ (H_2O).

3.2.2.8.4 *trans, trans, trans*-[Pt(N₃)₂(OH)(Succ)(pyr)₂] (4)

Carboxylation of one of the axial ligands was prepared by modification of a published method.²⁷ *Trans, trans, trans*-[Pt(N₃)₂(pyr)₂(OH)₂] **3** (0.150 g, 0.318 mmol) was dissolved in anhydrous DMSO (1.8 mL) under N₂, in the presence of activated molecular sieves. Succinic anhydride (1.1 eq, 0.035 g) was added and the reaction stirred in the dark at 40 °C for 48 h. The suspension was filtered and water (~2 mL) was added. The yellow solution was allowed to stand at room temperature until a crystalline solid precipitated (3–4 hours). The remaining solution was decanted and the crystalline precipitate was washed with diethyl ether and then filtered (Yield = 0.096 g, 52%). Crystals suitable for single-crystal X-ray diffraction were obtained by slow diffusion of water into the DMSO reaction mixture at room temperature.

¹H-NMR (D₂O, 600 MHz, pH 5.18, ppm): δ= 8.77 (dd, ³J_{1H1H}=5.78 Hz, ³J_{195Pt1H}= 11 Hz, 4H, H_o), δ=8.27 (t, ³J_{1H1H}= 7.64 Hz, 2H, H_p), δ=7.80 (t, ³J_{1H1H}= 7.04 Hz, 4H, H_m), δ=2.58 (t, ³J_{1H1H}= 6.90 Hz, 2H, H₁), δ=2.48 (t, ³J_{1H1H}= 6.90 Hz, 2H, H₂).

¹³C-NMR (MeOD-d₄, 150 MHz, ppm): δ=178.7, (C_a), δ=177.57 (C_d), δ=150.89, (C_e), δ=143.15 (C_g), δ=127.37 (C_f)

¹⁹⁵Pt-NMR (D₂O, 129 MHz): δ= 1059 ppm.

ESI-MS: [M+Na]⁺ (*m/z*) Calc., 594.0; Found, 593.9.

ε_{299 nm}=17251 M⁻¹cm⁻¹, ε_{260 nm}= 11584 M⁻¹cm⁻¹ (H₂O).

3.2.2.8.5 *trans, trans, trans*-[Pt(N₃)₂(OH)(Succ-Pr)(pyr)₂] (5)

Trans, trans, trans-[Pt(N₃)₂(OH)(Succ-Pr)(pyr)₂] **4** (0.100 g, 0.176 mmol) was pre-dried using P₂O₅ and then dissolved in dry DMF (1 mL) under argon. A stock solution of CDI (1,1'-carbonyldiimidazole) in DMF (0.194 M) was prepared under

dry conditions and 1.2 mL was added (1.2 eq) to the solution of the platinum complex and allowed to stir at 50 °C for 20 minutes, under continuous purging with argon. Then, sodium propanolate (2 mL), formed by the dissolution of sodium metal (0.02 g) in absolute propanol (20 mL), was added and the reaction carried out at room temperature for 48 hours. DMF was removed under vacuum and the crude product was purified by column chromatography (eluent: EtOAc: MeOH, 11:1). After solvent removal from the combined fractions, the solid was recrystallised from DCM/diethyl ether (Yield = 0.060 g, 56%). Crystals suitable for X-ray crystallography were grown by slow evaporation from water at ambient temperature.

^1H -NMR (D_2O , 600 MHz, dioxane, ppm): $\delta=8.76$ (dd, $^3J_{\text{IH1H}}=5.64$ Hz, $^3J_{\text{I195Pt1H}}=25.40$ Hz, 4H, H_6), $\delta=8.28$ (t, $^3J_{\text{IH1H}}=7.73$ Hz, 2H, H_7), $\delta=7.81$ (t, $^3J_{\text{IH1H}}=7.14$ Hz, 4H, H_8), $\delta=3.95$ (t, $^3J_{\text{IH1H}}=6.72$, 1H, H_3), $\delta=2.64, 2.63$ (m, 2H, $\text{H}_{1,2}$), $\delta=1.54$ (s, $^3J_{\text{IH1H}}=7.28$ Hz, 1H, H_4), $\delta=0.84$ (t, $^3J_{\text{IH1H}}=7.50$ Hz, 1H, H_5).

^{13}C -NMR (D_2O , 150 MHz, dioxane, ppm): $\delta=179.29$ (C_d), $\delta=176.22$ (C_a), $\delta=149.84$ (C_h), $\delta=143.31$ (C_j), $\delta=127.64$ (C_i), $\delta=67.90$ (C_e), $\delta=31.78$ (C_b), $\delta=30.88$ (C_c), $\delta=21.91$ (C_f), $\delta=10.17$ (C_g).

^{195}Pt -NMR (D_2O , 107 MHz, dioxane): No signal was obtained with ns = 32768, sw = 902.14, olp = 1000 .

ESI-MS: $[\text{M}+\text{Na}]^+$ (m/z) Calc. 636.1; Found, 636.2.

$\epsilon_{300\text{nm}}=16565 \text{ M}^{-1}\text{cm}^{-1}$, $\epsilon_{260\text{nm}}=10602 \text{ M}^{-1}\text{cm}^{-1}$ (H_2O).

3.2.2.8.6 *trans, trans, trans*-[Pt(N_3)₂(OH)(N-MI)(pyr)₂] (6)

Trans, trans, trans-[Pt(N_3)₂(pyr)₂(OH)₂] **3** (0.086 g, 18.25 mmol) was dissolved in anhydrous DMSO (2 mL) and N-methylisatoic anhydride (0.162 g, 91.23 mmol, 5

mol eq) was added. The reaction was carried out for 72 h at 40 °C under nitrogen with an outlet to allow the release of CO_{2(g)}. The isolation of the product was achieved by the addition of water (10 mL) at which point the compound precipitated. For the removal of excess ligand, repeated washing with diethyl ether was necessary and carried out via centrifugation (Yield = 0.020 g, 18%).

Crystals suitable for X-ray diffraction were grown by slow evaporation of a solution in DCM/MeOH at ambient temperature.

¹H-NMR (DMSO-d₆, 500 MHz, ppm): δ= 8.86 (dd, ³J_{1H1H} =5.54 Hz, ³J_{195Pt1H} =27.00 Hz, 4H, H₇), δ=8.30 (t, ³J_{1H1H} =7.56 Hz, 2H, H₉), δ=7.88 (m, 5H, 4H₈, H₄), δ=7.62 (q, ³J_{1H1H} =5.07 Hz, 1H, H₅), δ=7.26 (t, ³J_{1H1H} =7.78 Hz, 1H, H₃), δ=6.53 (d, ³J_{1H1H} =7.53 Hz, 1H, H₁), δ= 6.51 (t, ³J_{1H1H} = 7.53 Hz, 1H, H₂), δ= 3.88 (d, ²J_{195Pt1H} = 14.8 Hz, H₁₀), δ= 2.70 (d, ³J_{1H1H} = 5.00 Hz, 3H, H₆).

¹³C-NMR (DMSO-d₆, 125 MHz, ppm): δ=171.26 C_a, δ= 150.82 C_c, δ= 149.73 C_b, δ=149.38 C_i, δ=142.18 C_k, δ=132.86 C_g, δ=132.09 C_f, δ=126.42 C_j, δ=113.74 C_d, 110.00 C_e, δ=29.07 C_h.

¹⁹⁵Pt-NMR (DMSO-d₆, 107 MHz): δ= 990 ppm.

ESI-MS: [M+H]⁺ (*m/z*) Calc. 605.1; Found, 605.1.

ε_{302 nm} = 18325 M⁻¹cm⁻¹, ε_{260 nm} = 19169 M⁻¹cm⁻¹ (5% DMSO/95% H₂O).

3.2.2.8.7 N-Methylisatoic acid (N-MIA) (L1)

The open form of the N-methylisatoic anhydride was prepared by the hydrolysis and decarboxylation of N-methylisatoic anhydride.²⁸ N-MI anhydride (1.2 g, 6.77 mmol) was dissolved in a solution of KOH, 2 M (15 mL) and allowed to react for 4 h at 100 °C. The clear solution was then allowed to cool down at room temperature and then the pH was adjusted to 6-7 by the addition of HCl (3 M).

The white precipitate formed was isolated and dried under vacuo (Yield = 0.17 g, 19%). This compound was air sensitive therefore it was stored under nitrogen after preparation.

$^1\text{H-NMR}$ (75% MeOD- d_4 /25% D_2O , 400 MHz, ppm): δ = 8.45 (d, 8.29 Hz, H_1), δ = 7.39 (t, 7.74 Hz, H_2), δ = 6.78 (d, 8.21 Hz, H_3), δ = 6.66 (t, 7.57 Hz, H_4), δ = 2.87 (s, $-\text{CH}_3$).

ESI-MS: $[\text{M}+\text{Na}]^+$ (m/z) Calc. 174.0; Found, 174.0, $[\text{M}+\text{K}]^+$ (m/z) Calc. 190.0; Found, 190.0.

3.2.2.8.8 *Trans, trans, trans*-[Pt(N_3) $_2$ (OH)(Succ-(RGD)f)(pyr) $_2$] (**7**)

The Pt(IV)-(RGD)f complex, compound **7** (Figure 3.3) was prepared, purified and provided by Dr Vicente Marchan's group at the University of Barcelona, using complex **4** as starting material. The synthetic route was similar to that reported previously for coupling RGD peptide to $[(\eta^6\text{-}p\text{-cym})\text{Ru}(\text{bpm})(\text{H}_2\text{O})]^{2+}$ complex.²⁹

In summary the peptide was assembled on a 2-chlorotriyl chloride resin using standard Fmoc/tBu protection scheme on the amino group of the amino acids to form the linear peptide with sequence of $\text{H}_2\text{N-Asp}(\text{OtBu})\text{-D-Phe-Lys}(\text{Alloc})\text{-Arg}(\text{Pbf})\text{-Gly-resin}$, where OtBu, Alloc and Pbf are the side chain protecting groups. Cleavage from the solid support was undertaken with acetic acid/tetrafluoroethylene (TFE)/dichloromethane and cyclization was carried out with benzotriazol-1-yl-oxytripyrrolidinophosphonium hexafluorophosphate (PyBOP). Then the Alloc protecting group from the side chain of lysine was removed with $\text{Pd}(\text{PPh}_3)_4$ and phenylsilane. The free amino group allows the attachment of the polyethyleneglycol spacer. The protecting groups of Arg and Asp residues were removed with concentrated TFA in the presence of cation scavengers

(triisopropylsilane and water) and then the peptide was purified by reversed-phase HPLC. Attachment of complex **4** to the peptide was carried out with the HATU/DIEA coupling reagents and the Pt(IV)-c(RGD)f complex was purified by reversed-phase HPLC. The purity of the Pt-peptide complex was found to be 96% by HPLC.

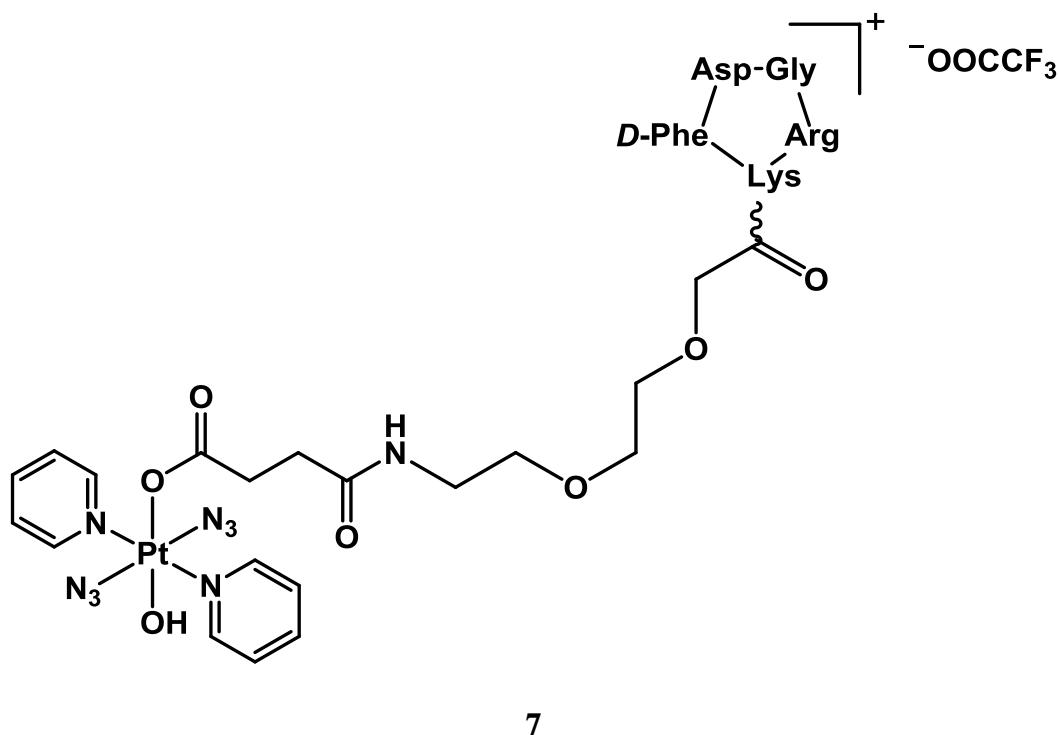


Figure 3.3: Pt(IV)-(cRGD)f peptide conjugate, complex *trans, trans, trans*-[Pt(N₃)₂(OH)(pyr)₂(Succ-(RGD)f)], **7**. This complex was formed by the attachment of the peptide to complex **4**.

3.3 Results

The compounds were characterised by ¹H, ¹³C, ¹⁹⁵Pt-NMR and mass spectrometry. In this section the assessment of compounds (in terms of purity), the X-ray crystallography, the stability and the aqueous solubility of the complexes will be presented. Furthermore, irradiation studies, which were followed by UV-Vis, EPR, NMR and mass spectrometry were carried out on complexes **3**, **4**, **5** and

6 to determine the rate of photodegradation as well as the nature of various photoproducts. Moreover, phototoxicity studies and cell uptake studies were carried out to examine in more detail the pharmacological properties of those novel potential anticancer drugs.

3.3.1 HPLC purity test

The purity of the complexes was determined via HPLC chromatography. The wavelength used for detection was set to 254 nm, which falls in the appropriate range to detect many organic and inorganic impurities. With the assumption that the same extinction coefficient applies for all platinum compounds separated, the percentage purity was calculated by the integration of the peaks using the Agilent ChemStation. The HPLC traces for the three novel compounds are presented in Figure 3.4. Complexes **4**, **5** and **6** have purities of 94%, 96% and 94%, respectively.

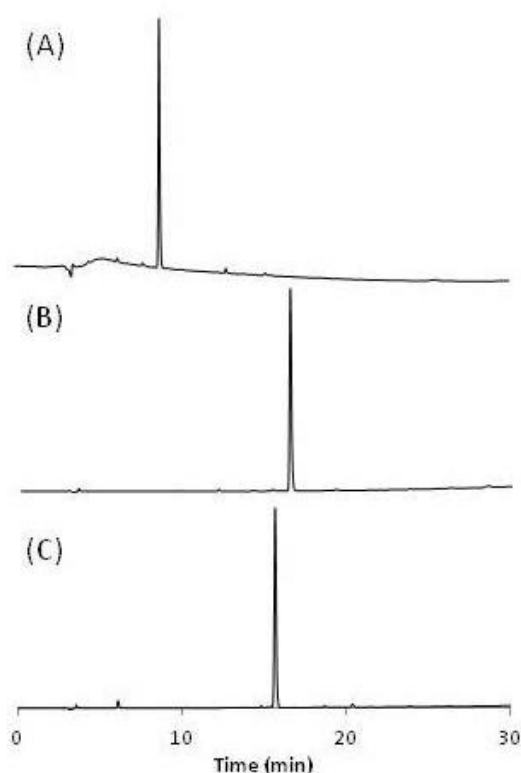


Figure 3.4: HPLC chromatographs for A) complex **4**, B) complex **5**, C) complex **6**. The conditions for the chromatographs are described in section 3.2.2.1. The Y axis is absorbance at 254 nm (omitted for clarity).

3.3.2 X-ray diffraction

This section of the chapter is focused on the bond lengths and angles of the three novel complexes as well as the intermolecular interactions, such as hydrogen bonding and π - π stacking. It is of interest to assess the type of interactions Pt(IV)-azido complexes can have on a supramolecular level, involving their ligands. These interactions can influence the various contacts a molecule can develop with biomolecules (e.g. transporters, enzymes, nucleic acids) which could then have an effect on biological activity.

A hydrogen bond, according to a IUPAC definition published in 2011³⁰ is an intermolecular or intramolecular attraction between a donor, X-H and an acceptor

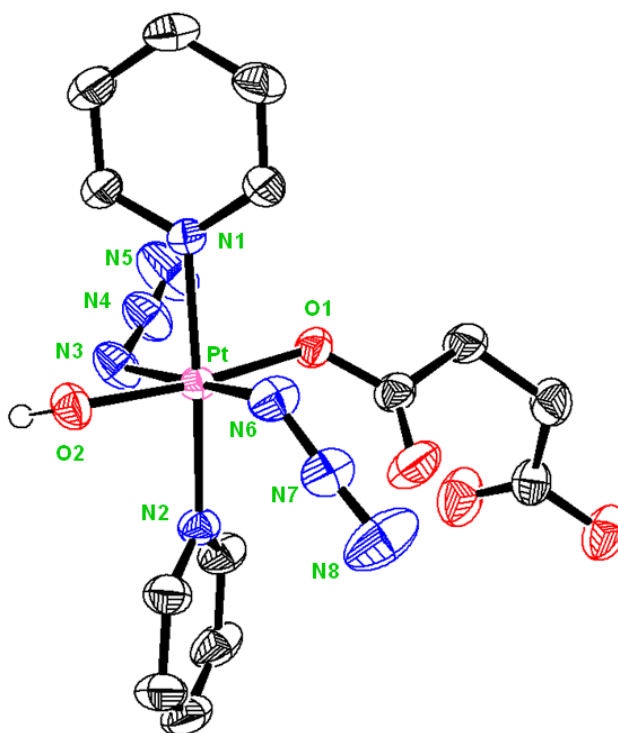
Y–Z, in which X is more electronegative than H and Y is an electron-rich region (e.g. a lone pair of electrons or a π -bonded pair of Y–Z). An ideal hydrogen bond forms an angle of 180° and the more linear, the stronger the bond is. Furthermore, a common empirical rule dictates that a strong H-bond can only exist when the H...Y bond distance is less than the sum of the Van der Waals radii of the atoms involved.³⁰ Hydrogen bonds can be classified as strong, medium or weak. As a general consideration the bond length between the donor and the acceptor can be used: below 1.5 Å, from 1.5–2.2 Å and from 2.2 to 3.2 Å are considered to be strong, moderate and weak, respectively.³¹

Two aromatic rings can form an electrostatic attraction between them, which is referred to as π - π stacking. The orientation of this interaction can vary between face-to-face stacking, face-slipped packing or a T-shaped interaction. The last two orientations are a result of a π - σ attraction.³² In the structures within this chapter, the only entities that could potentially form any π - π intermolecular interaction are the pyridine ligands or the aromatic ligands in compound **6**. Pyridine is a polarized molecule because of the electronegative nitrogen atom causing a positive net charge on the carbon atoms of the aromatic ring. In theory this could lead to a strong π - π attraction, as π -deficient rings are known to form stronger interactions than π -rich rings. The distances between centroids (Ct) of aromatic rings establishing a π - π interaction can lie up to 3.8 Å and acquire an angle of 20° .³² The C–H... π bond is normally shorter (~ 3.0 Å) and, similarly to a hydrogen bond, linearity in the edge-to-face interaction gives rise to a stronger bond.³³

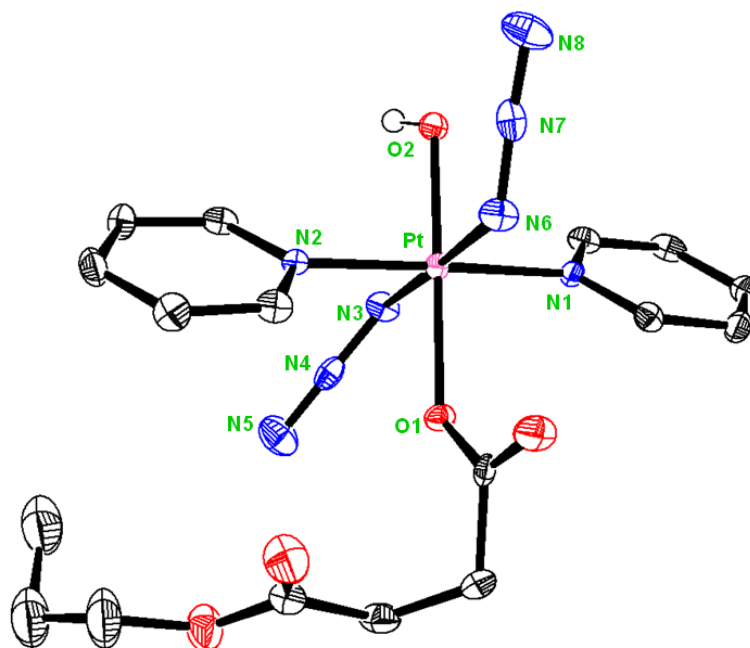
Single crystals suitable for X-ray diffraction studies were obtained for complexes *trans, trans, trans*-[Pt(N₃)₂(OH)(succ)(pyr)₂] **4**, *trans*,

trans, trans-[Pt(N₃)₂(OH)(Succ-Pr)(pyr)₂] **5** and *trans, trans, trans*-[Pt(N₃)₂(OH)(N-MI)(pyr)₂] **6** as described in section 3.2.2.8. The ORTEP diagrams of the molecular structures are shown in Figure 3.5 A, B and C, respectively. Crystallographic data of complexes **4**, **5** and **6** are summarized in Table 3.3. Selected bond distances and angles are listed in Table 3.4 including data for the precursor Pt(IV) complex *trans, trans, trans*-[Pt(N₃)₂(OH)₂(pyr)₂] **3** for comparison.

(A)



(B)



(C)

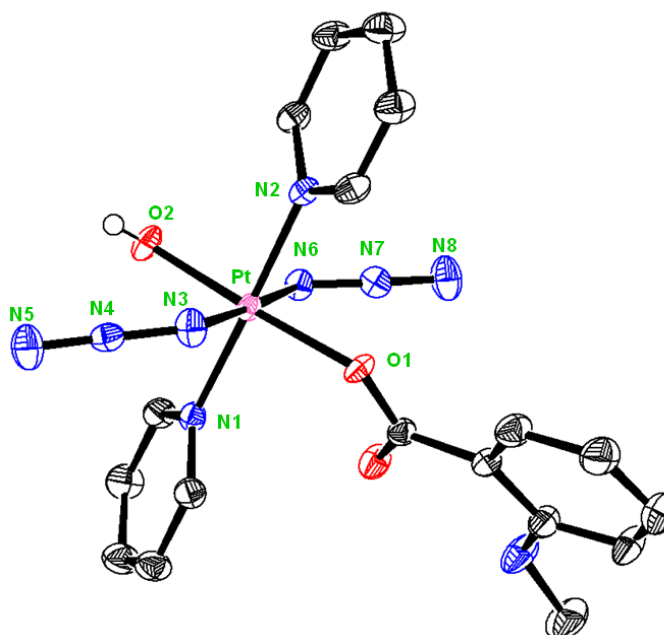


Figure 3.5: ORTEP diagrams of the complexes reported in this chapter: A) *trans, trans, trans*-[Pt(N₃)₂(OH)(Succ)(pyr)₂] **4**; B) *trans, trans, trans*-[Pt(N₃)₂(OH)(Succ-Pr)(pyr)₂] **5**; and C) *trans, trans, trans*-[Pt(N₃)₂(OH)(N-MI)(pyr)₂] **6**. The ellipsoids are set to 50% probability level. All hydrogen atoms have been omitted for clarity, except for the axial hydroxide ligand.

Table 3.3: Crystallographic data for complexes **4**, **5** and **6**.

Complex	4	5	6
Empirical formula	C ₁₄ H ₁₆ N ₈ O ₅ Pt	C ₁₇ H ₂₂ N ₈ O ₅ Pt	C ₁₈ H ₁₉ N ₉ O ₃ Pt
Formula weight	571.44	613.52	604.51
Crystal description	Colourless block	Colourless block	Brown block
Crystal system	Triclinic	Monoclinic	Monoclinic
Crystal size/ mm	0.40x0.10 x 0.10	0.40 x 0.08 x 0.08	0.30x 0.18 x 0.12
Space group	P-1	C2/c	P2(1)/c
<i>a</i> / Å	8.4300(2)	27.4103(18)	7.5372(2)
<i>b</i> / Å	10.5284(2)	12.5601(7)	35.8705(8)
<i>c</i> / Å	11.9980(4)	13.6542(8)	8.1728(2)
<i>α</i> /(°)	86.002(2)	90	90
<i>β</i> /(°)	70.799(3)	115.8(9)	109.178(2)
<i>γ</i> /(°)	68.795(2)	90	90
Volume/ Å³	936.07(4)	4252.4(4)	2086.99(9)
Z	2	8	4
D_{calc}/gcm⁻³	2.027	1.917	1.924
F(000)	548	2384	1168
μ_{calcd}/mm⁻¹	7.540	6.646	6.764
T/ K	268(2)	150(2)	150(2)
Max θ /°	30.65	31.50	32.36
Reflections collected/unique	17109/5253	14991/6340	32557/7050
[R_{int}]	[0.0377]	[0.0385]	[0.0333]
Goodness-of-fit on F²	1.061	1.007	1.400
Data/restraints/ parameters	5253/17/259	6340/14/284	7050/0/287
Final R indices	R ₁ = 0.0189,	R ₁ =0.0332,	R ₁ =0.0411,
[I>2σ(I)]	wR ₂ = 0.0469	wR ₂ = 0.0581	wR ₂ = 0.0596
R indices (all data)	R ₁ = 0.0204	R ₁ = 0.0545	R ₁ = 0.0488
	wR ₂ = 0.0461	wR ₂ = 0.0506	wR ₂ = 0.0586
Largest diff. peak and hole (eÅ⁻³)	1.178 and -1.399	1.843 and -2.190	1.807 and -3.397

Complex **4** crystallized in the triclinic space group P-1 with two molecules within a unit cell. Complexes **5** and **6** both crystallized in the monoclinic system, space groups C2/c and P2(1)/c respectively, including eight molecules of complex in the unit cell in case of compound **5** and four molecules of complex in the unit cell of compound **6**.

Compounds **4**, **5** and **6** are neutral mononuclear Pt(IV) complexes showing a distorted octahedral geometry with a [N₄O₂] hexacoordinated environment around the Pt(IV) ion. The three complexes differ in one of the oxygen donor ligands coordinated in axial positions. In all of them the equatorial plane is defined by four nitrogen atoms from two pyridine molecules *trans* to each other (N1 and N2) and two azido anions *trans* (N3 and N6), whereas an oxygen atom (O2) from a hydroxido ligand is located in an axial position. The sixth position is occupied by an oxygen atom (O1) from a monoanionic and monodentate ligand: a succinate anion in **4**, a 4-oxo-4-propoxybutanoate anion in **5** and a *N*-methylisatoate anion in the case of **6**.

The distortion from ideal octahedral geometry is shown by the axial bond angles between Pt(IV) ion and the donor atoms in *trans* (e.g. O2–Pt–O1 174.22(8)^o in complex **4**) with values smaller than 180^o. These angles are slightly smaller in comparison with the values found in the fully symmetrical precursor **3** (Table 3.4). Such an effect is observed in all the three complexes described in this section and can be attributed to the steric hindrance caused by the bulky oxygen-coordinated ligands. Along the N1–Pt–N2 axis in complex **4**, a greater distortion from the octahedral geometry than the corresponding angle in the other two

complexes is apparent, which can be attributed to the C–H... π interaction between the pyridine rings found in complex **4** but absent in **5** and **6**.

Table 3.4: Selected bond distances (Å) and angles (°) for complexes **4**, **5**, **6** and the precursor complex **3**.²⁶

Bond (Å)/ Angle (°)	4	5	6	3
Pt–O1	2.021(2)	2.056(2)	2.029(2)	1.990(3)
Pt–O2	1.984(2)	1.971(3)	1.978(2)	2.027(3)
Pt–N1	2.039(3)	2.032(3)	2.026(3)	2.047(3)
Pt–N2	2.033(3)	2.037(3)	2.036(3)	2.047(3)
Pt–N3	2.050(3)	2.057(3)	2.053(3)	2.043(3)
Pt–N6	2.041(3)	2.052(3)	2.037(3)	2.047(3)
N6–N7	1.209(4)	1.217(5)	1.214(4)	1.215(4)
N7–N8	1.139(4)	1.150(5)	1.148(4)	1.139(4)
N3–N4	1.198(4)	1.208(5)	1.210(4)	1.218(5)
N4–N5	1.133(4)	1.151(5)	1.141(4)	1.146(5)
N6–Pt–N3	175.19(10)	178.48(12)	178.01(12)	176.86(12)
N7–N6–Pt	121.8(2)	115.92(2)	116.1(2)	118.0(3)
N4–N3–Pt	118.1(2)	115.7(3)	116.9(2)	120.3(2)
N1–Pt–N2	176.83(8)	178.48(12)	178.47(11)	179.09(12)
O2–Pt–O1	174.22(8)	175.51(10)	176.50(11)	179.58(11)
N3–N4–N5	174.2(4)	175.1(4)	175.3(4)	175.3(4)
N6–N7–N8	172.9(3)	173.8(4)	175.0(4)	174.4(4)

Complex **3** has been reported previously²⁶ and has been included in Table 3.4 for comparison purposes, as it is the precursor of the rest of the complexes. The bond distances between Pt(IV) and pyridine nitrogen atoms (Pt–N1 and Pt–N2) of **4**, **5** and **6** have no significant difference when compared within the same complex or

between the aforementioned complexes. The only exception is the bond with the pyridine ligand Pt–N1 (1.978(2) Å) in complex **6**, which shows a shorter distance than Pt–N2.

The Pt–N (azido) distances for *trans*-azido, *trans*-hydroxo compounds with one pyridine or substituted pyridine ring, are reported to be between 2.026 Å and 2.069 Å.³⁴ The azide anion – although symmetrical with both N=N bonds being of equal distance – adopts a resonance structure with one bond slightly longer than the other, when it is bound to a metal ion.³⁵ Therefore it is reasonable that the N6–N7 (or N3–N4) bonds, involving coordinated donor atoms, are larger than the N7–N8 (or N4–N5) bonds. The Pt–N3 and Pt–N6 bond lengths do not have significant differences between them and fall within the expected range for Pt-azido complexes. The exception is complex **6** for which there is a significant difference between Pt–N3 (2.053(3) Å) and Pt–N6 (2.037(3) Å) bond distances.

A special remark needs to be made with regard to the Pt–O bond as these are the first reported examples of Pt-azido compounds with asymmetric axial ligands. The more closely related compound is *trans, trans, trans*-[Pt(N₃)₂(OAc)₂(pyr)₂] which shows a Pt–O bond length of 2.001 Å.³⁶ Therefore the bond distances in **4**, **5** and **6**, ranging from 1.971(3) Å to 2.056(2) Å, are close to the expected value. There is a significant difference in the bond distances between the two Pt–O axial bonds in each complex. In all the cases the Pt–O bond for the carboxylate is longer than the Pt–O bond for the hydroxido ligand, perhaps indicating a higher potential lability of this bond. Complex **3** which was also included in Table 3.4 is a symmetrical molecule and therefore no difference in the bond distances would be expected in solution. Nevertheless, a significant difference between both axial

Pt–OH bonds is also observed for compound **3** (Pt–O1 1.990(3) Å and Pt–O2 2.027(3) Å). The existence of hydrogen bond interactions could have some effect on the bond distances between the oxygen donor atoms and the metal centre. Thus the significant length difference observed in the two Pt–O axial bonds of the symmetric compound **3** (*vide supra*) is related to its packing arrangement, with one of the hydroxido ligands being involved in two hydrogen bonds (as a donor and acceptor) with another hydroxide and an azide of a neighbouring molecule, whereas the second hydroxido acts only as a donor. This appears to weaken slightly the former Pt–OH bond. For this reason, a comparative analysis of intermolecular interactions in complexes **4**, **5**, **6** with those in precursor **3** is interesting in order to explain such effects.

The intermolecular attractions which dictate the packing of complex **4** are shown in Figure 3.6 and consist of classical hydrogen bonds as well as some weak π - π and C–H $\cdots\pi$ interactions.

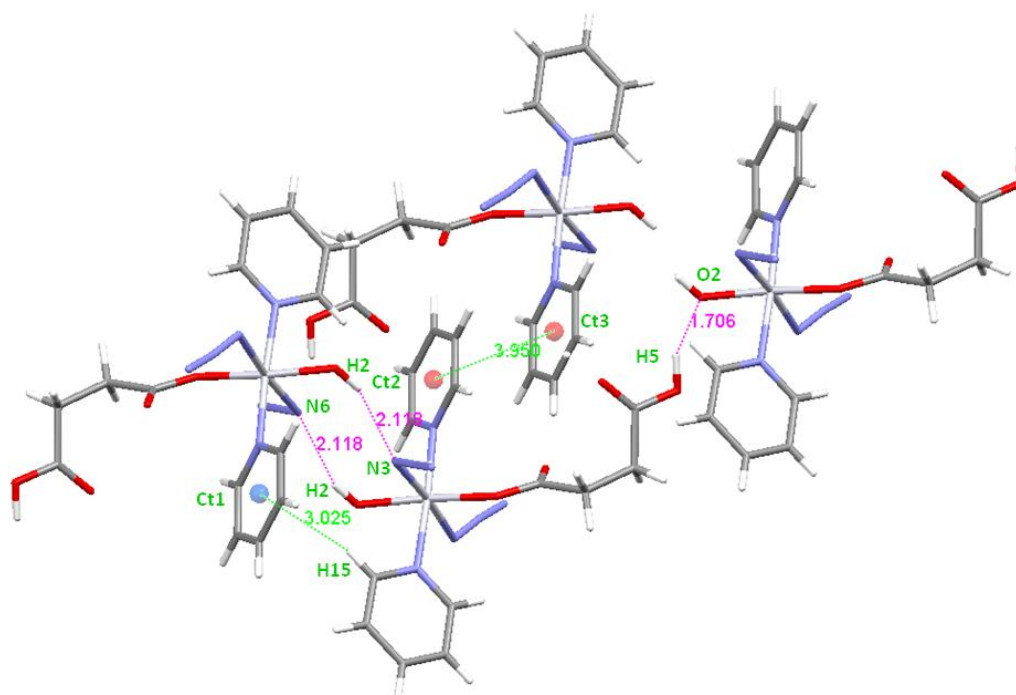


Figure 3.6: Intermolecular interactions of complex **4**. Classical H-bonds are denoted in pink whereas π - π interactions are shown in green. Bond distances are expressed in Å.

Each molecule in the unit cell is able to participate in three intermolecular hydrogen bonds: two are established with an adjacent molecule through the interaction of the hydroxido ligand and the azide nitrogen atom ($\text{O2-H2}\cdots\text{N3}$, $\text{O2-H2}\cdots\text{N6}$ 2.12 Å), while the third hydrogen bond interaction involves the OH group of the succinate ligand and the oxygen atom from the hydroxido belonging to a third molecule of complex ($\text{O-H5}\cdots\text{O2}$, 1.706 Å). Based on the distance, both hydrogen bonds can be considered strong, but the interaction with the succinate is considerably stronger.

Additionally, the pyridine rings of complex **4** interact via two different intermolecular forces: a $\text{C-H}\cdots\pi$ interaction between the ortho hydrogen of a pyridine ring and the π -cloud of another pyridine ring from a neighbouring

molecule (Ct1...H15, 3.025 Å), and also a very weak π - π stacking interaction between two pyridines with a centroid-centroid distance of 3.950 Å (Ct2-Ct3) (Figure 3.6).

Interestingly, in complex **5** the azide ligands are not involved in any hydrogen bonding. Each molecule establishes two intermolecular hydrogen bonds between the carbonyl group of the 4-oxo-4-propoxybutanoate ligand and the hydroxido group of a nearby molecule (O2-H2...O2 1.972 Å) as shown in Figure 3.7. Moreover, complex **5** shows a π - π stacking interaction between pyridine rings (3.551 Å) in the crystal packing, which is stronger in comparison with that found for complex **4**.

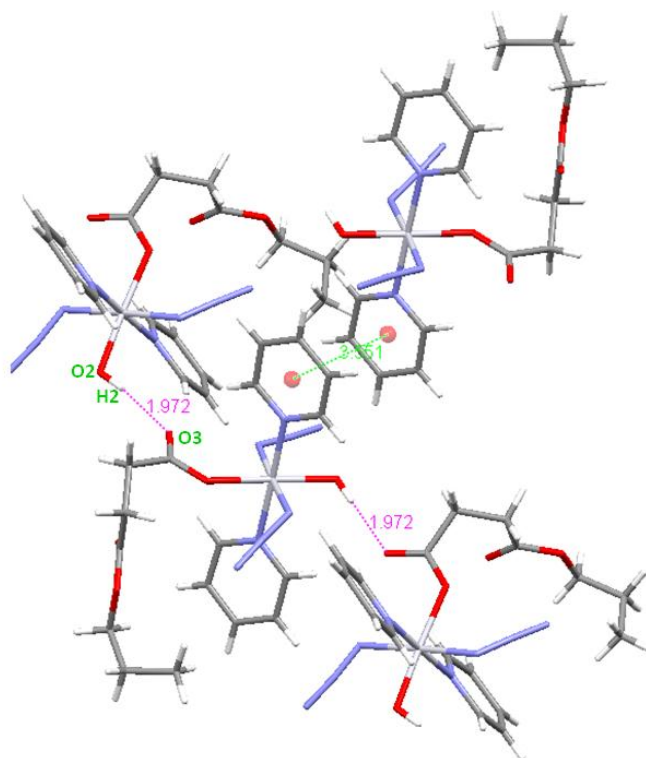


Figure 3.7: Intermolecular interactions of complex *trans, trans, trans*-[Pt(N₃)₂(OH)(Succ-Pr)(pyr)₂] complex **5**. Hydrogen bond and π - π stacking interactions are denoted with purple and green colours, respectively. Bond distances are expressed in Å.

In complex **6**, each molecule in the crystallographic unit cell is hydrogen-bonded via an azide nitrogen atom (N5) and the hydroxido group (O2–H2) to another neighbouring molecule (Figure 3.8). The strength of this bond can be considered as medium to weak as it is only 2.288 Å. It must be noted that the azido ligand in complex **6**, which participates in an intermolecular hydrogen bond shows weaker bond with the Pt(IV) ion than the second azide ligand. Moreover, this is the only complex for which a strong intramolecular hydrogen bond interaction is observed. In this case the H-bond involves the carbonyl and the NH group of the coordinated *N*-methylisatoate anion (N–H10...O3 1.096 Å), which also dictates the spatial orientation of the ligand.

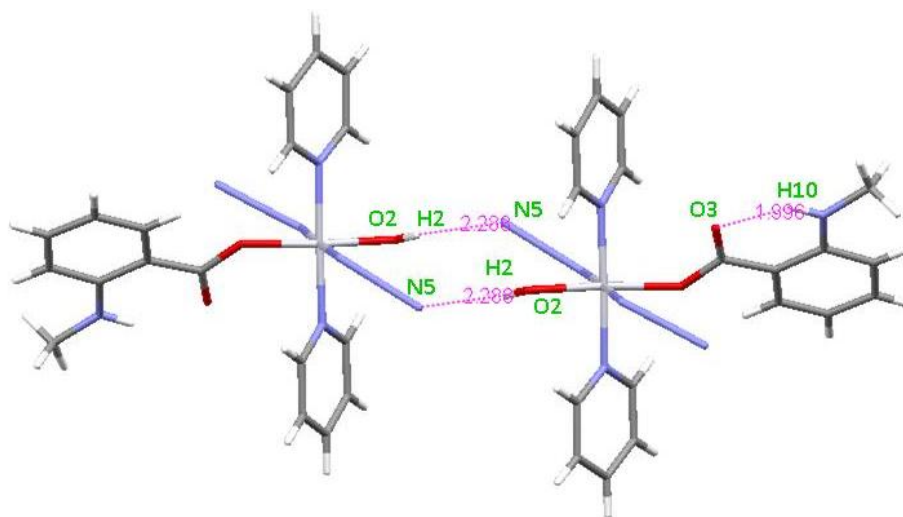


Figure 3.8: Intermolecular and intramolecular hydrogen bond interactions for complex *trans, trans, trans*-[Pt(N₃)₂(OH)(N-MI)(pyr)₂] **6**. Bond distances are expressed in Å.

3.3.3 Aqueous solubility and stability in the dark

The aqueous solubility of novel compounds is important as it greatly influences the mode of drug administration. The solubility of the compounds was determined as a saturated solution in water (for complex **4** and **5**) and in 5% DMSO/ 95%

H₂O (for complex **6**). The concentration of the latter compound was determined by ICP analysis of the platinum content (see Chapter 2 for details). The results are summarized in Table 3.5, in which complex **3** is also included for completion.

Table 3.5: Solubility of **3-6** at room temperature (*ca.* 20 °C).

Complex	Solubility (mM)	Solvent
3	34.0 ^a	H ₂ O
4	2.0	H ₂ O
5	1.5	H ₂ O
6	0.064	5% DMSO/95% H ₂ O

^a From reference 36

Before cell testing experiments are carried out, it is important to ensure the stability of the compound in the biological media, so as to verify the state of the compound before the photoactivation step. Drug exposure according to the protocol of cytotoxicity measurement of Pt(IV) compounds is 1 hour followed by irradiation. Therefore there needs to be stability in an aqueous solution in the dark for a minimum of 1 hour. Furthermore, it is of interest to check whether there is rapid reduction of the compound in the presence of a biological reducing agent such as glutathione. For these reasons, the stability of complex **4** was tested in the presence of 2 mol eq of reducing agent GSH in PBS for 24 hours at 37 °C, in the dark, as a model for the reactivity of this series of complexes. ¹H-NMR data show (Figure 3.9) that there is very little oxidation of GSH (~4 %, as quantified by NMR) over this period when compared to the GSH control.

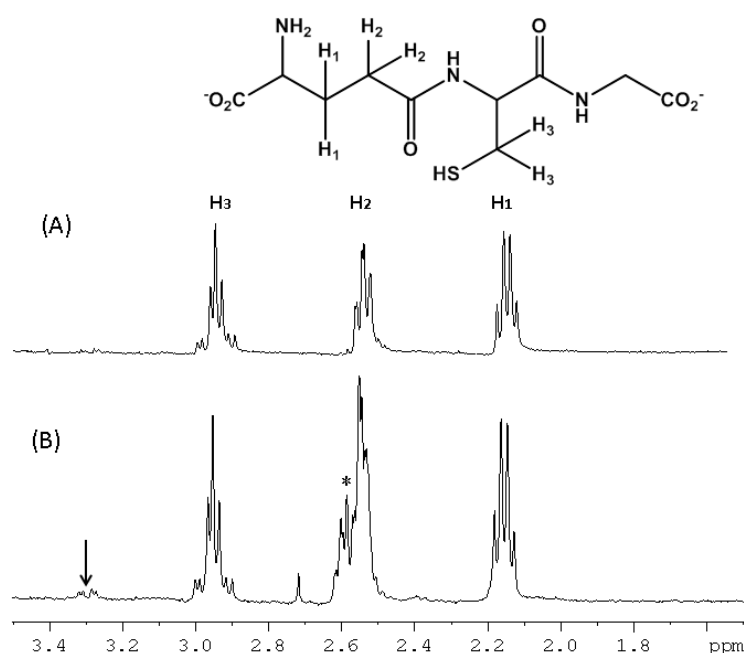


Figure 3.9: ^1H -NMR with water suppression of (A) GSH (3.8 mM) in 10 % D_2O /90% H_2O (PBS) after incubation at 37 °C for 24 h in the dark (B) Complex **4** (1.9 mM) plus 2 eq of GSH, in 10% D_2O /90 % H_2O PBS (pH 7.4) at $t=24$ h after incubation at 37 °C in the dark. The NMR spectra show the region where the GSH peaks fall (see discussion). The small peak at 3.3 ppm is assigned to GSSG³⁷ (originating from GSH oxidation) which integrates to 4%. The asterisk in spectrum B indicates peaks for the complex. The peak at 2.7 ppm is a trace of DMSO.

Compound **5** contains an ester bond, which might hydrolyse in water, and therefore it was important to check its stability in the dark in aqueous media. As shown in Figure 3.10, the compound is relatively stable as no change was observed within 3 days, but a new product formed by the second week after incubation at 37 °C.

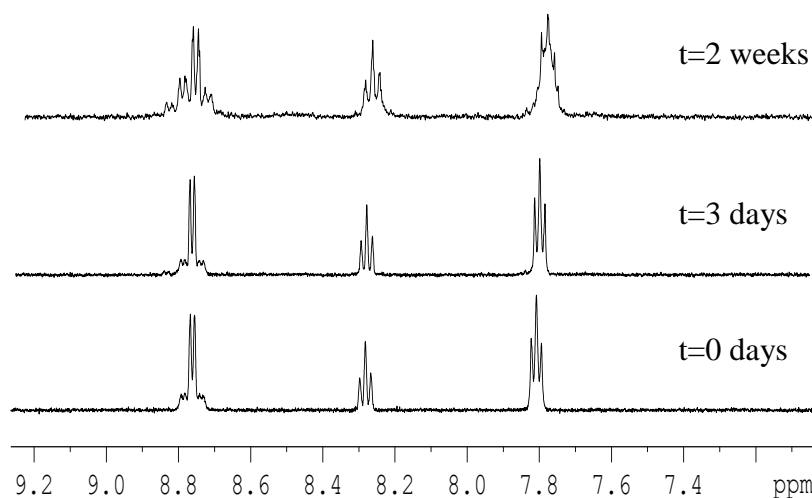


Figure 3.10: ^1H -NMR of compound **5**, in PBS (D_2O), at two different time points after incubation in the dark at 37°C . The aromatic region of the NMR spectra corresponds to the pyridine ligands. Peaks at $\delta = 8.76$ ppm, 8.28 ppm, 7.81 ppm are assigned to H_{ortho} , H_{para} , H_{meta} , respectively. After two weeks the emergence of another species becomes evident.

The stability of complex **6** was assessed by UV-Vis spectroscopy, since its aqueous solubility was too low for NMR experiments. The compound was incubated at 37°C in the dark. Also in this case, very little change was observed after 1 h 40 min (Figure 3.11), which suggests that the compound was stable enough for cell line testing.

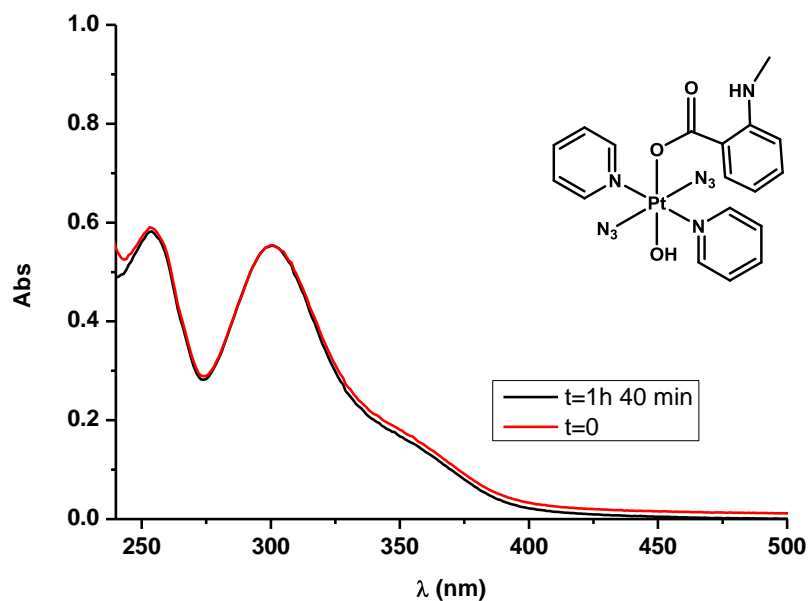


Figure 3.11: UV-Vis spectra for complex **6** in 95% H₂O and 5% DMSO at t=0 h and after 1 h 40 min of incubation at 37 °C in the dark.

3.3.4 pK_a^* study for complex **4**

To understand the speciation of the succinato complex **4** under physiological conditions, the pK_a of the carboxyl group was determined according to the method described in section 3.2.2.3. Changes in pH^* resulted in the shift of the ortho protons of the pyridine ligands as well as the protons of the succinate ligand. However, peaks for the latter merged to one peak at low pH^* and therefore the change in the shift of the pyridine protons was used to examine all the pH^* range. The data (Figure 3.12) were fitted to the Henderson-Hasselbach equation using Origin 8.5 which yielded the value of pK_a^* of 5.07. It is well established that the binding affinities of D^+ and H^+ are different and therefore it would result in different acidities. pK_a^* can be converted into the pK_a value using the relationship: $pK_a = pK_a^* \times 0.929 + 0.42$ ³⁸, which results in a pK_a of 5.13.

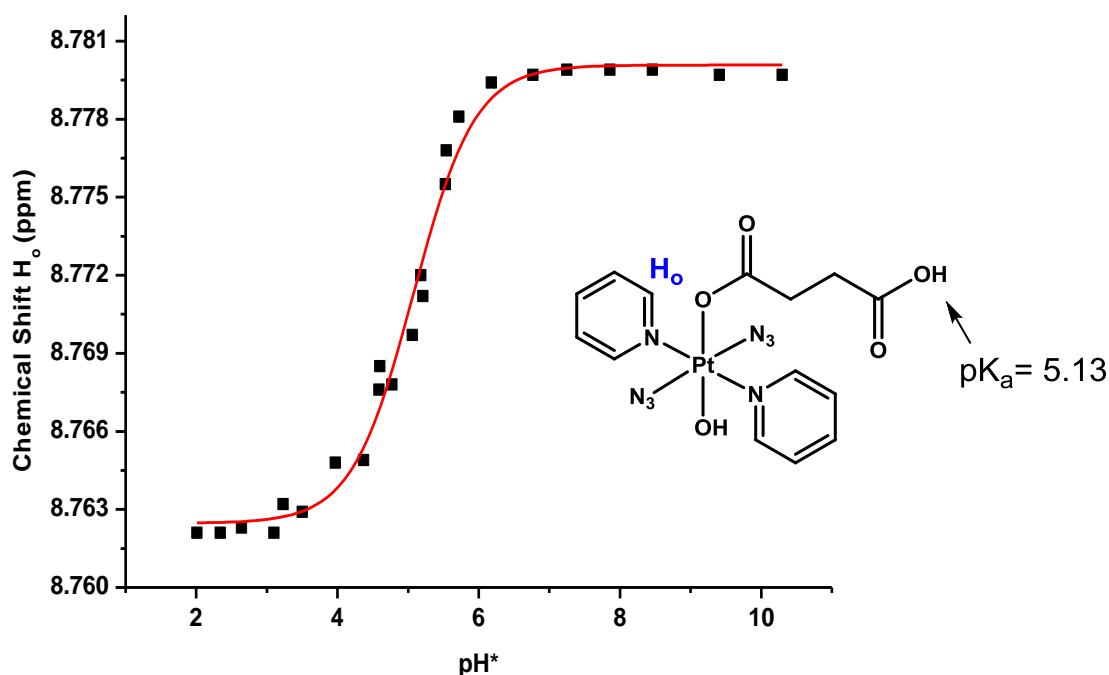


Figure 3.12: The change in chemical shift for the *ortho* protons of pyridine in complex **4** with respect to changes in pH^* . The sample was dissolved in D_2O (1.1 mM) and the pH^* was adjusted as described in section 3.2.2.3. The data were fitted to the Henderson-Hasselbalch equation (red curve), with an $r^2 = 0.99$, giving a pK_a^* of 5.07.

3.3.5 Extinction coefficient studies

Characterisation of the absorption profile of photoactivatable metal complexes is of crucial interest in the investigation of their properties. Through UV-Vis studies it is possible to obtain information about electronic transitions and excited states that can be generated upon light irradiation. Such states are involved in the chemical change of the complex into the generation of biologically active photoproducts. On this basis, the extinction coefficients of complexes **3-6** in water were determined, as described in Chapter 2 (section 2.5) and spectra are plotted in the same graph for comparative purposes in Figure 3.13. Complex **4** contains a carboxylic acid ligand and therefore it is interesting to determine the extinction

coefficient for the two different states of the coordinated ligand: protonated and deprotonated. As it was shown in section 3.3.4, the pK_a of complex **4** was found to be 5.13, hence the extinction coefficient was measured at both low and high pH (3.2 and 8.3) at *ca* 20 °C. The absorbance was identical indicating no pH dependence of the extinction coefficient. The determination of the extinction coefficient at longer wavelength for complexes **3** and **4** was achieved by the use of higher concentrations (1.4 mM and 0.95 mM for **3**, 0.87 mM and 0.57 mM for **4**) and this is illustrated in the inset graph of Figure 3.13.

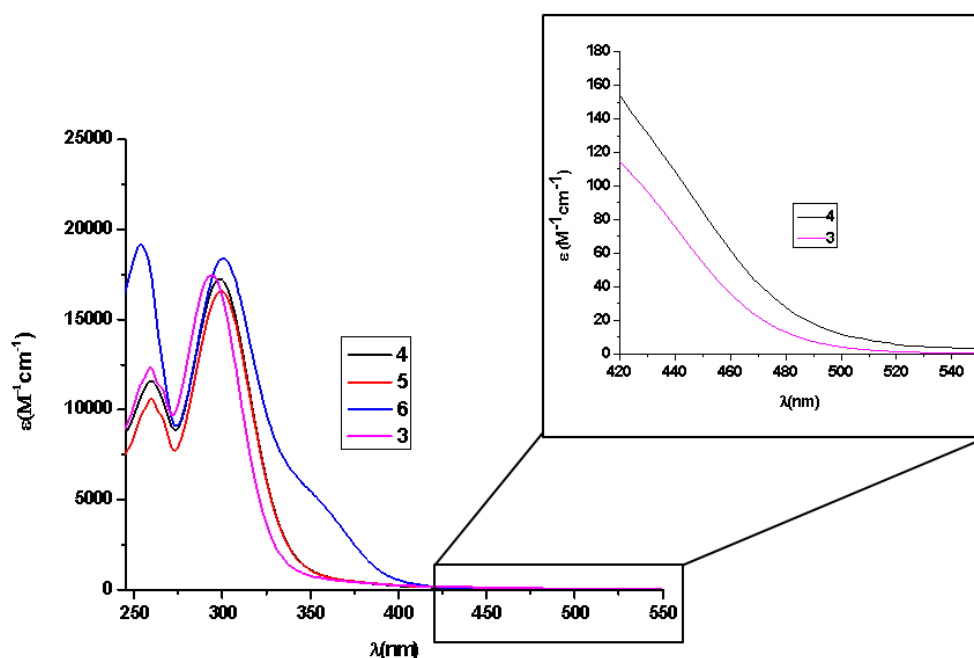


Figure 3.13: Comparison of the UV-Vis spectra of complexes **3-6**. The inset shows expansions at longer wavelength, determined using more concentrated samples (0.87 mM for **4** and 1.4 mM for **3**).

The wavelengths corresponding to the maximum absorption of those compounds follow the order of: **6** > **5** > **4** > **3**, as the values are 302 nm, 300 nm, 299 nm, 294 nm, respectively. The difference between UV-Vis spectra of these complexes is

that in the case of complex **6**, a shoulder appears at *ca.* 350 nm which is due to the presence of the aromatic ligand.

3.3.6 Photoirradiation studies followed by UV-Vis

The photoreactivity of compounds **3**, **4**, and **6** was followed by UV-Vis spectroscopy at frequent time points after irradiation of aqueous solutions of the compounds (*ca.* 60 μM) with green light (517 nm LED, 29 mW/cm^2) at ambient temperature (*ca.* 20 $^\circ\text{C}$). The photoreactivity of complex **3** has been reported before²⁶ but it was also examined here as a control compound. Green light was used, as it is clinically more preferable (see Chapter 1). Furthermore, complex **4** was also irradiated with blue (463 nm, 59 mW/cm^2) and green light (550 nm, filtered below 530 nm with GG530, 4 nm slits, 2.5 mW/cm^2), as shown in Figure 3.19 and Figure 3.20, in order to investigate the effects of shorter and longer wavelengths.

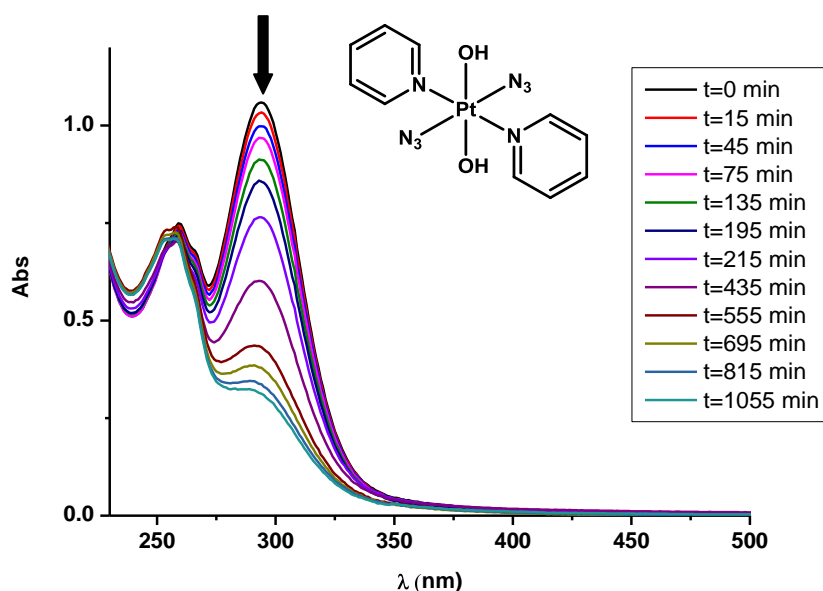


Figure 3.14: Change in the UV-Vis spectrum over time of complex **3** (60 μM , H_2O) upon irradiation with green light (517 nm). The arrow shows the decrease in absorbance of the absorption maximum, at 296 nm, with respect to time.

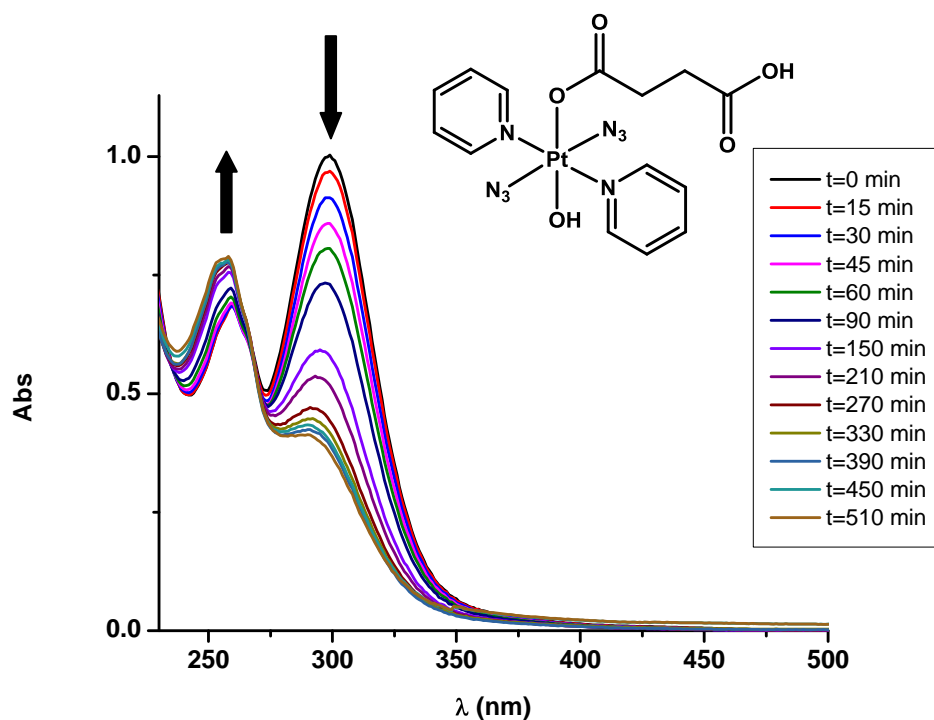


Figure 3.15: Change in the UV-Vis spectrum of complex **4** (60 μM , H_2O) upon irradiation with green light (517 nm).

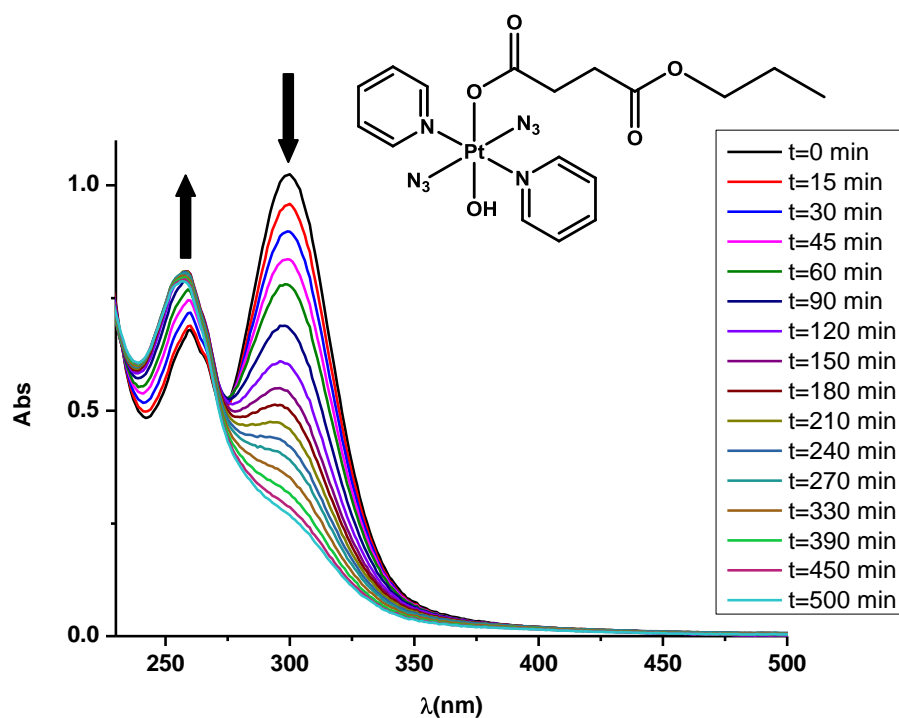


Figure 3.16: Time dependent change in the UV-Vis spectra of complex **5** upon irradiation with green light (517 nm).

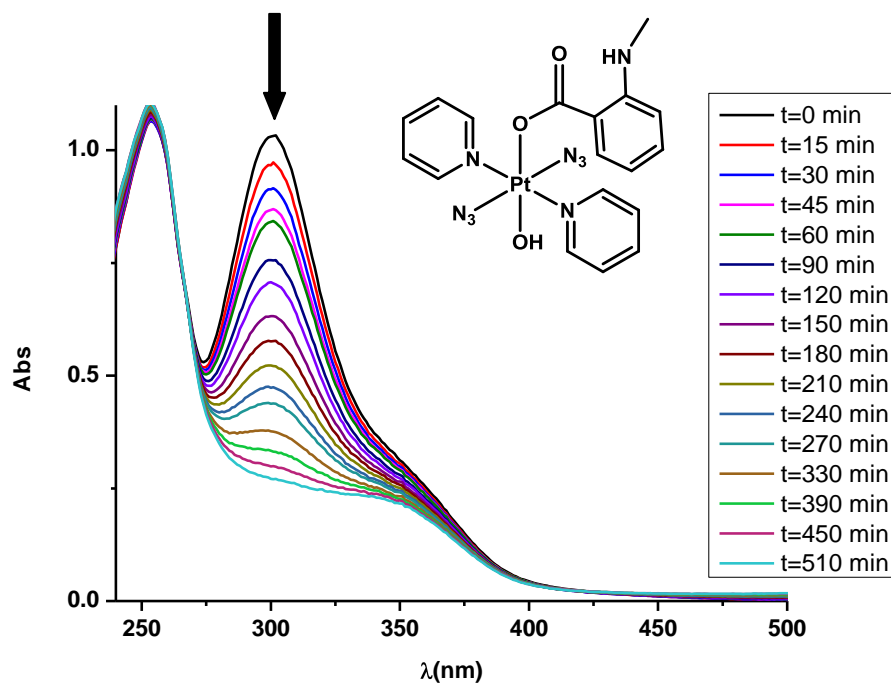


Figure 3.17: Time dependent change in the UV-Vis spectra of complex **6** (*ca* 60 μm 5% DMSO, 95% H_2O) upon irradiation with green light (517 nm).

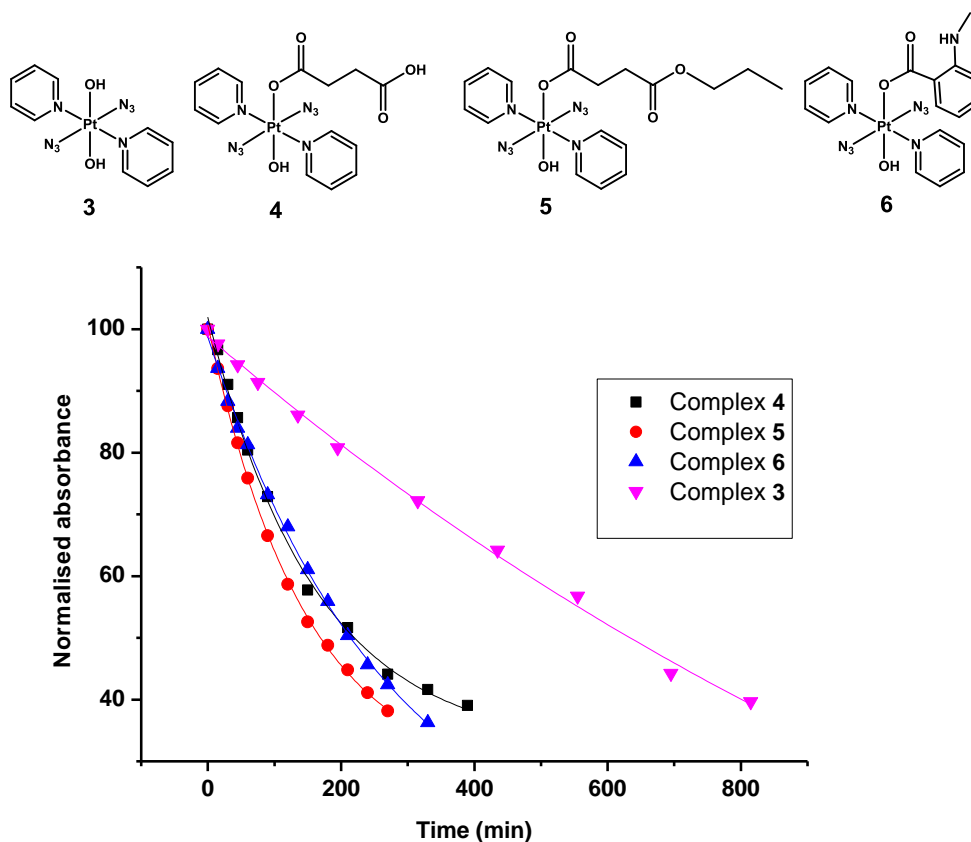


Figure 3.18: Plot of the decrease in intensity of the $\text{N}_3 \rightarrow \text{Pt}$ band (up to 38%) of compounds **3-6** versus time, when irradiated with green light (517 nm). The data were fitted to the equation $y = y_0 + Ae^{R_0 x}$.

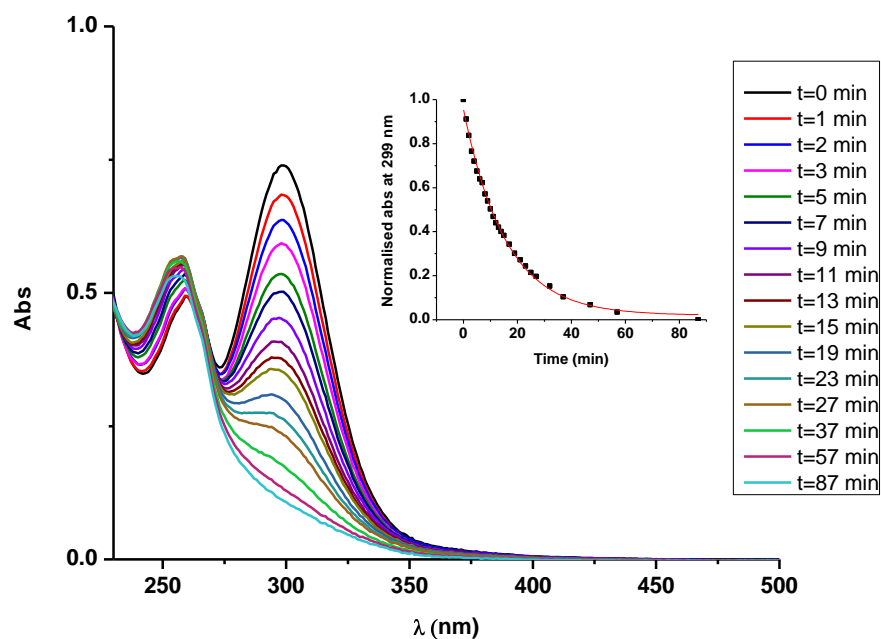


Figure 3.19: Time dependent change in the UV-Vis spectra upon irradiation of **4** (*ca* 50 μ M) with blue light, 463 nm. The fast degradation of the complex is illustrated by the short half-life of 10 min, which was extrapolated by fitting an exponential function (red line, $r^2=0.99$).

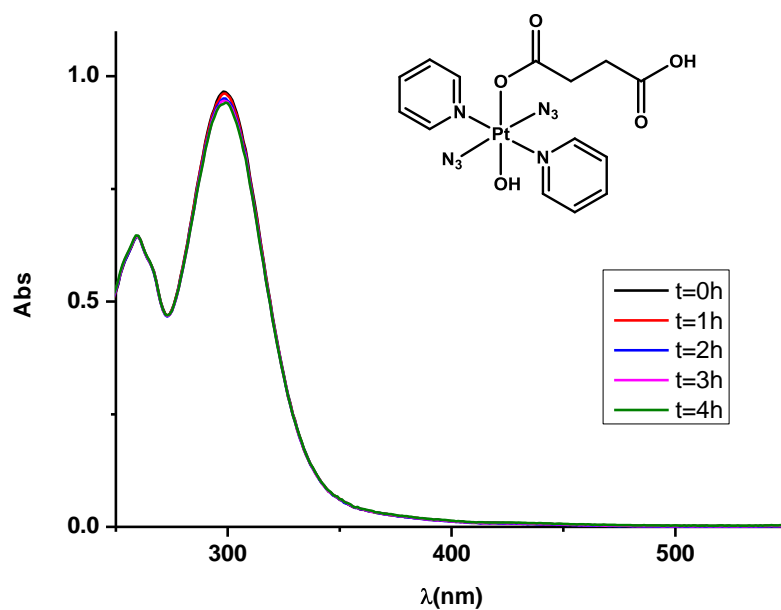


Figure 3.20: Time dependent change in the UV-Vis spectra upon irradiation of complex **4** with a low dose of 550 nm light (2.5 mW/cm^2). The spectra show very minimal change.

In Figure 3.14 -Figure 3.17, the change of the UV-Vis spectrum is recorded at different irradiation times (therefore different doses of green light). As with all of the Pt(IV)-diazido complexes, a decrease in the intensity of the azido-Pt charge-transfer band (i.e. the main UV band in the absorption spectrum of complexes at *ca.* 300 nm) is observed due to the loss of an azide. The maximum for each of the graphs was normalized so that the first spectrum ($t=0$ h, i.e. before the irradiation) has a normalized absorbance of 100%. Then by considering only the degradation of up to *ca.* 38%, the points were fitted to an exponential curve ($y=y_0+Ae^{R_0x}$) using Origin 8.5, for determination of half-life, a method used previously.³⁹ The graphs are plotted comparatively and illustrated in Figure 3.18. The half-lives of **3**, **4**, **5**, and **6** upon irradiation with green light were found to be 634 min, 220 min, 169 min, and 214 min, respectively. This shows that the photodegradation of **3** occurs 2.9 times more slowly than compound **4**, 3.7 times slower than compound **5**, and 3.0 times slower than compound **6**.

When compound **4** was irradiated with a high dose of blue light, the photoreaction was very fast with a half-life of 10.4 min (Figure 3.19). However when the compound was irradiated with the longer wavelength light (550 nm) little change was observed over the course of 4 hours (Figure 3.20).

3.3.7 Photoirradiation followed by EPR

DMPO is a widely used trapping agent which has been employed for the detection of O-, N-, S- and-less frequently- for C-centred radicals.⁴⁰ It has been used previously for the successful detection of azidyl and hydroxyl radicals.^{41, 42} On this basis, it was chosen as a suitable spin trap for the Pt(IV)-azido complexes and was used to follow the irradiation of compounds **3-6**. Free azidyl radicals have a

very short life time (10^{-5} - 10^{-6} s), therefore it is difficult to directly detect them without a spin trap.⁴³

The yield of DMPO- N_3 adduct formation was determined by the double integration of the EPR signals and quantified with respect to Tempol at each time point upon irradiation with green LED light (517 nm, 33 mW/cm²) of the compounds **3**, **4**, and **5** (1 mM, in PBS) in the presence of DMPO (2 mM). As a control, the EPR spectra were recorded in the dark and no azide radical trapping was observed. Comparing the DMPO- N_3 yields at various time points (0, 7, 21, 28, 35 min) during the irradiation of compounds **3**, **4** and **5**, it becomes evident that the two compounds with the two carboxylates can produce radicals when irradiated with green light whereas the dihydroxido compound **3** did not give rise to radical signal.

Also, the compounds were studied for their ability to yield azidyl radicals in DMF (75%) which is a suitable solvent for all complexes allowing a comparative study (Figure 3.22). The yield was estimated at various time points during the irradiation (0, 7, 14, 21, 28, 35 min) and follows a similar trend as in the buffered solution, with compounds **4** and **5** giving rise to larger EPR signals than compound **3**. Compound **6** gave an unexpected result, as the yield of azidyl radicals was as low as that found for compound **3**. To rationalize the effect of the N-MI ligand on the yield of azidyl radicals, complex **3** (2 mM, 75% DMF/ 25% H₂O) was irradiated (463 nm, 64 mW/cm²) in the presence of N-MIA (1 or 2 mol eq, 2 mM or 4 mM) and DMPO (2 eq, 4 mM) and the yield was measured at various time points (Figure 3.23).

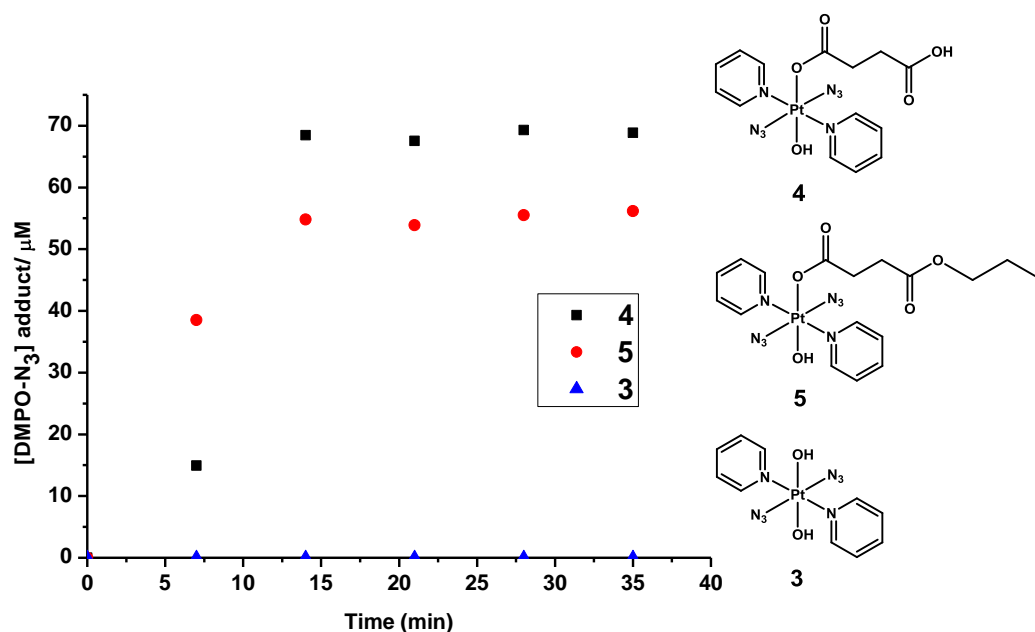


Figure 3.21: Time dependent trapping of azidyl radicals upon continuous irradiation of three Pt(IV) diazido compounds (1 mM in PBS) with green light (517 nm, 33 mW/cm²): compound 4 (black squares), compound 5 (red circles and reference compound 3 (blue triangles).

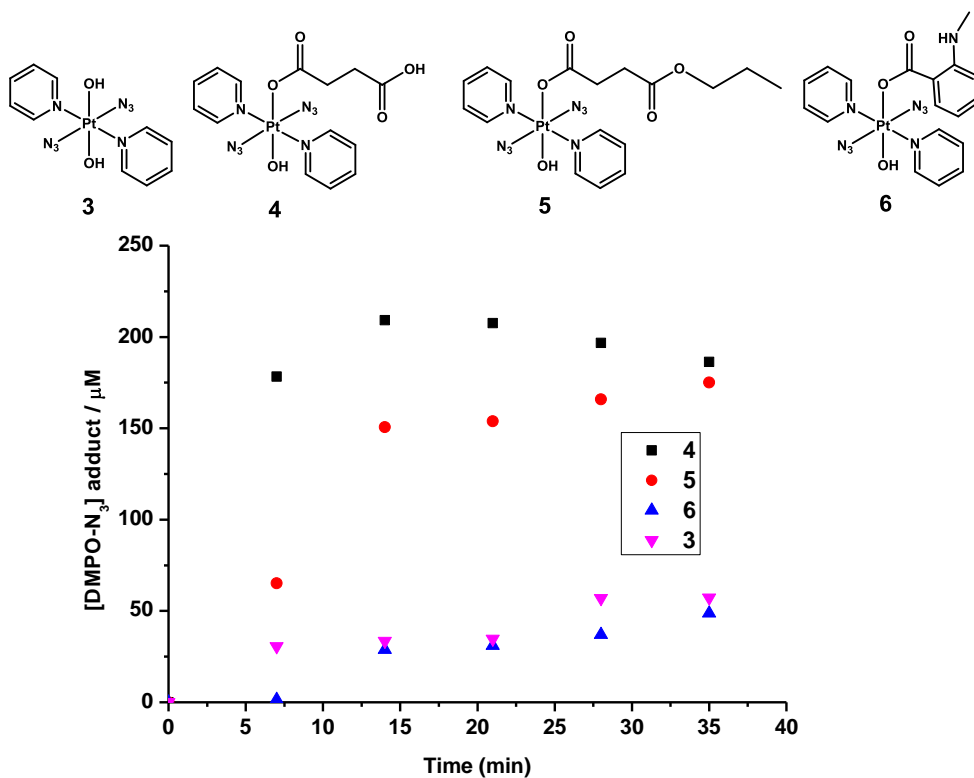


Figure 3.22: [DMPO-N₃] signal which was obtained upon irradiation with green light (517 nm, 33 mW/cm², 14 min) of complexes 3-6 (2 mM) in the presence of DMPO (2 mol eq, 4 mM) in DMF/H₂O (75%/25%, v/v).

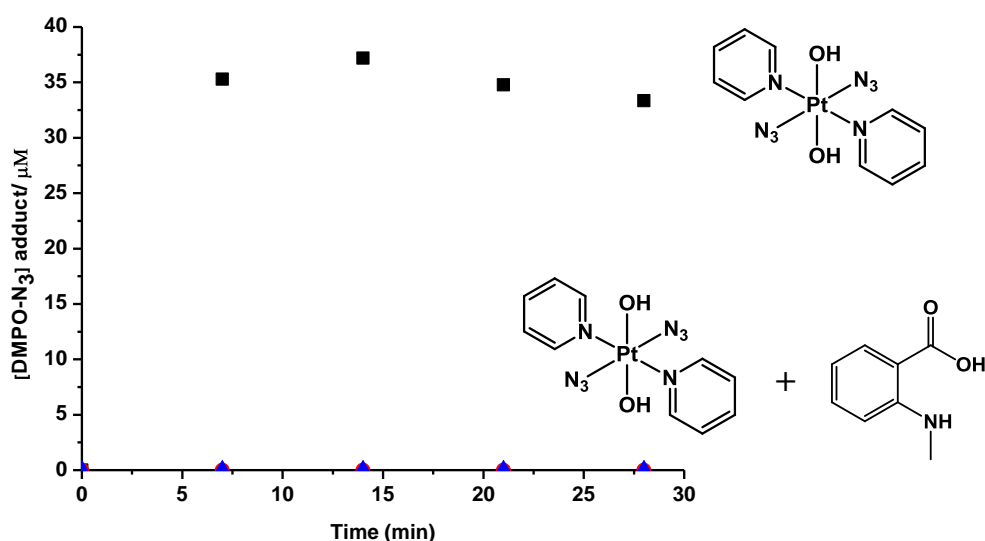


Figure 3.23: [DMPO-N₃] signal upon continuous irradiation (463 nm) of complex **3** (2 mM) alone (black squares) or in the presence of 1 and 2 eq of the N-MI ligand (red and blue triangles-overlapped) in DMF/ H₂O (75%/ 25%).

3.3.8 NMR irradiation studies

NMR is a powerful tool for the study and characterisation of photoreactions and has been used effectively in the past to characterise photoproducts of Pt(IV)-diazido photoreactions.^{23, 44-46} 1D ¹H, ¹⁹⁵Pt, ¹⁴N as well as 2D ¹⁵N-¹H HMBC are a few NMR techniques which have been used to elucidate the complicated photodissociation pathways of these compounds. Moreover it has been shown that the photoproduct production is dependent on: a) the ligands (aliphatic vs aromatic amines),^{47, 26} b) wavelength of irradiation, c) concentration, d) solvent composition, and e) presence of other molecules with affinity for platinum. Point (d) became evident in the reports by Ronconi *et al* as it was shown that in an acidic environment, the decomposition of *trans, trans, trans*-[Pt(N₃)₂(OH)₂(NH₃)₂] gave rise to the evolution of much more dinitrogen compared to when the irradiation was carried out at neutral pH.⁴⁵ Point (e) has

become evident in many reports for which the presence of a reactive molecule prohibits the formation of a precipitate during the reaction. Precipitates formed during the irradiations can be difficult to analyse due to its extreme insolubility in various solvents but are believed to consist of Pt-hydroxo bridged species.⁴⁴

Since Pt compounds can readily bind to nucleic acids or proteins once inside the cell, it is important to carry out the photoirradiation studies in the presence of biomolecules. For this reason, compounds **4** and **6** (containing aliphatic and aromatic carboxylate ligands respectively) were irradiated in the presence of guanosine monophosphate (5'-GMP), using a wavelength of irradiation at 463 nm (or 420 nm) to ensure a fast reaction. Additionally, the use of the fluorophore N-MIA as coordinating ligand in complex **6**, allowed the photostability of this complex to be followed by fluorescence emission spectroscopy.

3.3.8.1 Photoirradiation studies of complex 4 *trans,trans,trans*-[Pt(N₃)₂(OH)(Succ)(pyr)₂]

Complex **4**, as compounds **3**, **5** and **6**, was found to be stable in the dark, as shown in section 3.3.3. The release of the axial ligand upon irradiation is a characteristic outcome for such compounds together with the release of azide, as observed previously for *trans, trans, trans*-[Pt(N₃)₂(OAc)₂(pyr)₂].³⁶

Indeed, the release of the succinate ligand upon irradiation at 463 nm for 10 minutes was confirmed by adding an aliquot of succinic acid to the irradiated solution of **4**. Figure 3.24 shows the ¹H-NMR spectrum before and after the irradiation of complex **4**. The singlet peak at 2.4 ppm corresponds to the released succinate. No bound succinate is observed after 10 minutes of irradiation with

blue light (463 nm, 64 mW/cm²). The aromatic area shows a mixture of pyridine-containing photoproducts. The photoreaction was studied more extensively in the presence of GMP (2 mol eq).

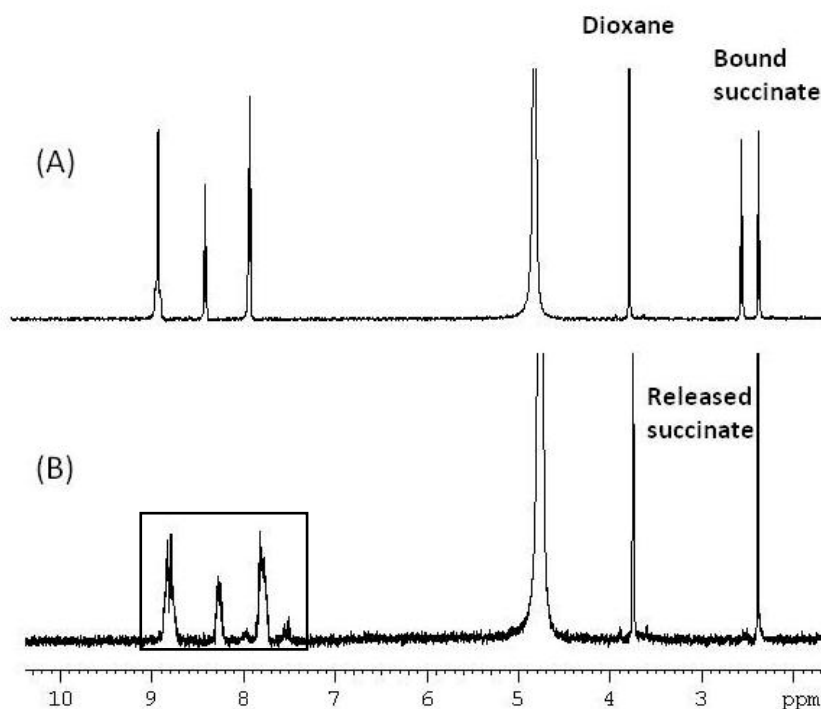


Figure 3.24: ¹H-NMR spectrum of **4** (1.5 mM, PBS/ D₂O) (A) in the dark and (B) after 10 minutes of irradiation with 463 nm light (38400 mJ/cm²). The NMR spectra were referenced with dioxane and the release of succinate becomes evident. The region labelled with a square in (B) indicates the pyridine-bound photoproducts.

In order to follow the photoreaction, NMR studies were carried out after the irradiation of the complex in the presence of 5'-GMP (1.5 mM complex **4**, and 3 mM GMP in PBS). Figure 3.25 shows the speciation at different doses of blue light (463 nm) and also the result of an irradiation with slightly shorter wavelength (420 nm). The ¹H-NMR spectra show the presence of two main products which are labelled by a circle and rhombus, the former product being assigned to the mono-azido GMP adduct, *trans*-[Pt(N₃)(GMP)(pyr)₂].

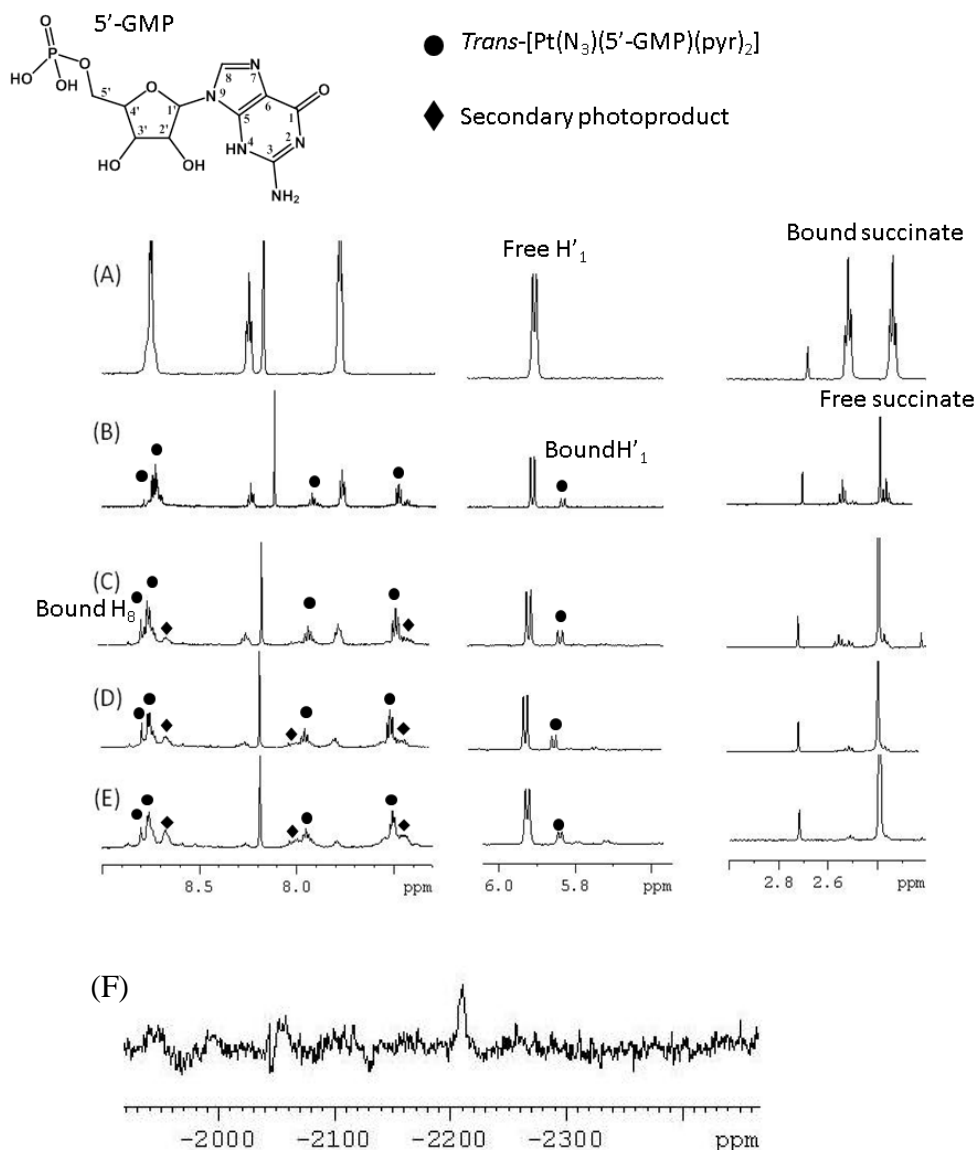


Figure 3.25: $^1\text{H-NMR}$ (500 MHz, D_2O , dioxane) and $^{195}\text{Pt-NMR}$ (129 MHz) spectra of complex **4** and GMP (2 mol eq) in PBS (pH 7.4) at the following conditions: A) Dark, B) irradiation with 463 nm, 10233 mJ/cm^2 , C) irradiation with 463 nm, 35400 mJ/cm^2 , D) irradiation with 463 nm, 70800 mJ/cm^2 , E) irradiation with 420 nm, 30510 mJ/cm^2 . The circle and the rhombus signals denote the evolution of the two main photoproducts; F) Signal of $^{195}\text{Pt-NMR}$ at -2210 ppm showing the formation of $\text{trans-[Pt(N}_3\text{)}\{5'\text{-GMP)}\{\text{pyr}\}_2\text{]}$.

Compound **3** was also photoirradiated in order to be compared with compound **4**. Interestingly the photoproducts are very similar, but one important difference is the speed of the reaction: In the case of compound **3**, 10 minutes of irradiation resulted in only 9 % of 5'-GMP binding whereas compound **4** gave rise to 23% (Figure 3.26), with the same power. Signals relative to the Pt-bound 5'-GMP were assigned and quantified (by the NMR H'_1 integration) only in the case of *trans*-[Pt(N_3)(GMP)(pyr) $_2$], as this is the main photoproduct. This assignment is confirmed by the LC-MS studies (section 3.3.9.1) and also by the chemical shift of the signal in the ^{195}Pt -NMR spectrum which was previously reported for this species.²⁶ The other GMP photoproducts are too weak to be integrated accurately.

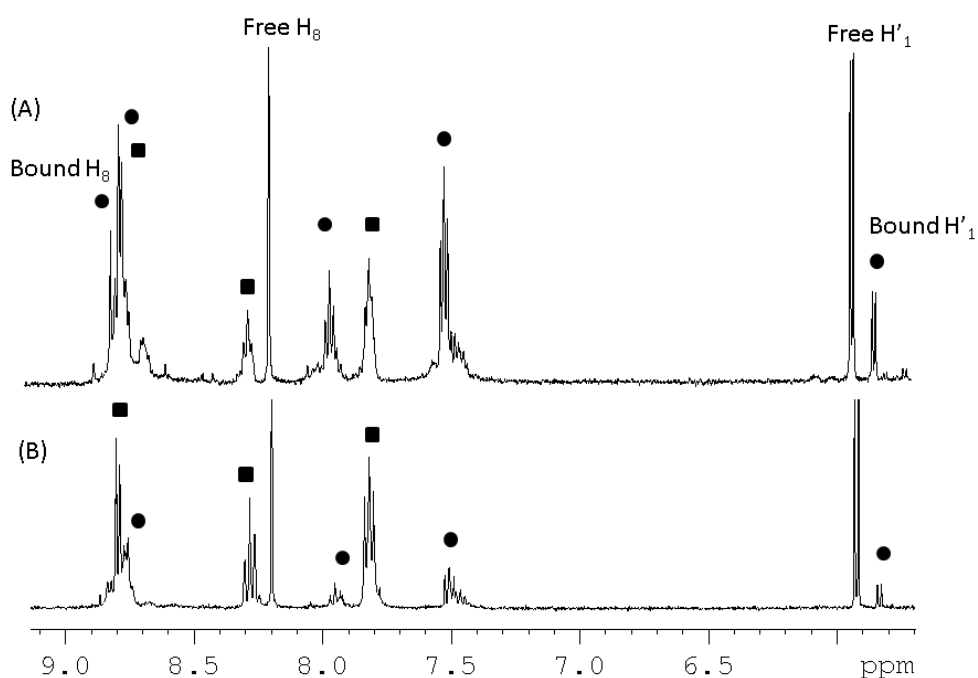


Figure 3.26: ^1H -NMR spectrum of A) Compound **4** (1.5 mM, PBS (D_2O) plus GMP (2 mol eq), and B) Compound **3** (1.5 mM, PBS/ D_2O) plus 5'-GMP (2 mol eq) after 10 minutes of irradiation with 463 nm ($64 \text{ mW}/\text{cm}^2$). The signals denoted with circles and squares represent the mono-GMP adduct (*trans*-[Pt(N_3)(GMP)(pyr) $_2$]) and starting materials, respectively.

With the aim of following the kinetics of the photodissociation in the presence and absence of 5'-GMP, the release of succinate was monitored by irradiating a sample of complex **4** (1.5 mM, PBS, pH* 7.4) in the presence and absence of GMP (2 mol eq). The release of succinate was estimated by following the photoreaction by ^1H -NMR and the percentage of release was plotted and fitted to the exponential function: $y=y_0+Ae^{R_0x}$ (Figure 3.27). It was shown that the photoreaction proceeds three times faster in the absence of 5'-GMP.

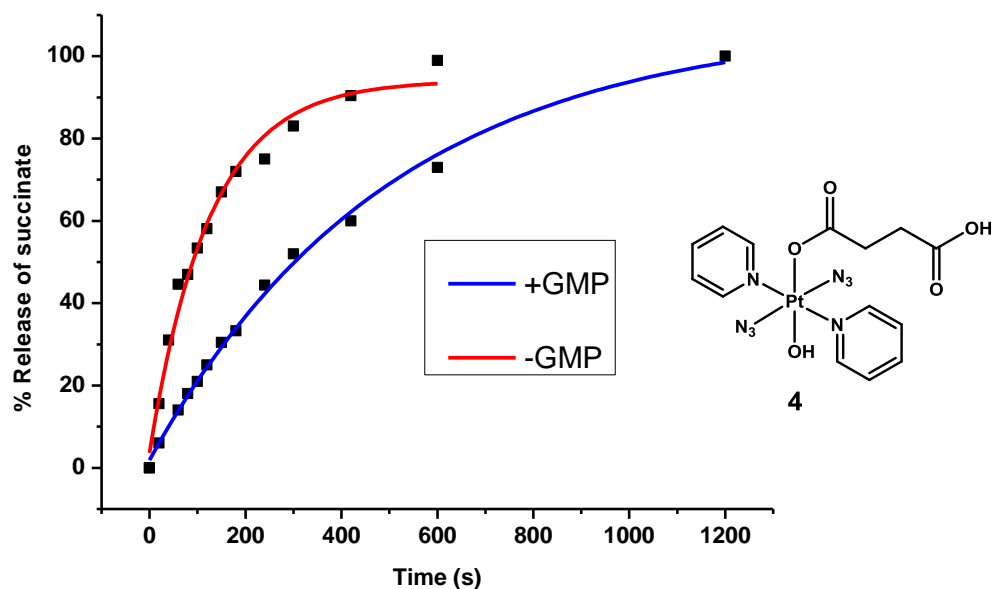


Figure 3.27: Time dependent release of succinate upon irradiation with blue light (463 nm, 64 mW/cm²) of **4** (1.5 mM, PBS, D₂O, pH* 7.4) in the presence (blue) and absence (red) of GMP (2 mol eq, 3 mM). Black dots denote the experimental data whereas the blue and red lines denote the fitted exponential function ($r^2=0.98$ for red and $r^2=0.996$ for blue).

3.3.8.2 Photoirradiation studies of complex **6** *trans, trans, trans*- [Pt(N₃)₂(OH)(N-MI)(pyr)₂]

Photoirradiation studies of compound **6** were carried out in the presence of 5'-GMP. The poor aqueous solubility of **6** prevented a study by ¹H-NMR to be carried out in water. Therefore a mixture of 75% MeOD and 25% D₂O (v/v) was used. Irradiation of **6** at 420 nm for 40 min resulted in a colour change from yellow to brown. This is likely due to the release of the axial ligand (N-MIA), as will be shown in the following sections. Furthermore, a change in the pH had occurred after the irradiation as a shift of the peaks (including the water peak) is observed (Figure 3.28). Accurate pH* measurement was not possible due to the high percentage of methanol. This effect prohibited a direct comparison of the chemical shift between the free N-MIA ligand (synthesized in section 3.2.2.8.7) and the photoproducts. Irradiation of compound **6** with blue light (420 nm, 45 min, 11.3 mW/cm²) did not result in the complete photodissociation of the complex, as there was still present 35% of bound N-MI ligand as well as 13% of another species containing this ligand (Figure 3.28 B). In the aromatic region, the evolution of a pyridine-containing species was observed which constitutes the main photoproduct of this reaction. Strikingly, irradiation of **6** (1.5 mM) with a very low dose of UVA light (1440 mJ/cm²) resulted in the complete photodissociation of the complex, as it is shown by the presence of only one ligand methyl peak, which can be assigned to the free N-MIA ligand. One of the main photoproducts in this case was interestingly found to be free pyridine, which was proved by spiking the sample with pyridine (Figure 3.28 D). Irradiation with 420 nm resulted in only a small release of pyridine; however higher doses of light

would result in the complete photodissociation of the complex and an even larger amount of pyridine release. Interestingly, irradiation with either 420 nm or UVA light did not result in the production of a 5'-GMP adduct. With the purpose of establishing whether this is an effect of the compound or the solvent, the previously studied complex **3**, *trans,trans,trans*-[Pt(N₃)₂(OH)₂(pyr)₂], was also irradiated under the same solvent conditions, i.e. 75% MeOD, 25% D₂O. The results show that 5'-GMP adducts formed in a small percentage (see small adducts at 5.8 ppm) when the compound was irradiated with either 420 nm or UVA light (Figure 3.29).

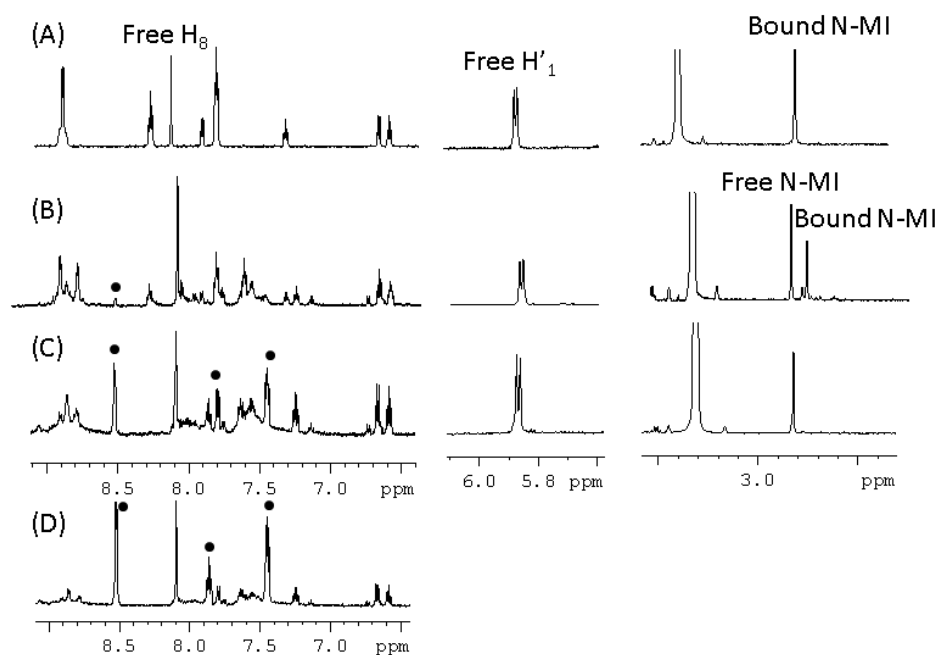


Figure 3.28: ¹H-NMR spectra (500 MHz, ns = 256) of complex **6** and 5'-GMP (2 mol eq) in MeOD (75%) and D₂O (25%) (v/v) at the following conditions: A) Dark, B) 420 nm, 30510 mJ/cm², C) UVA, 1440 mJ/cm², D) Sample C spiked with pyridine.

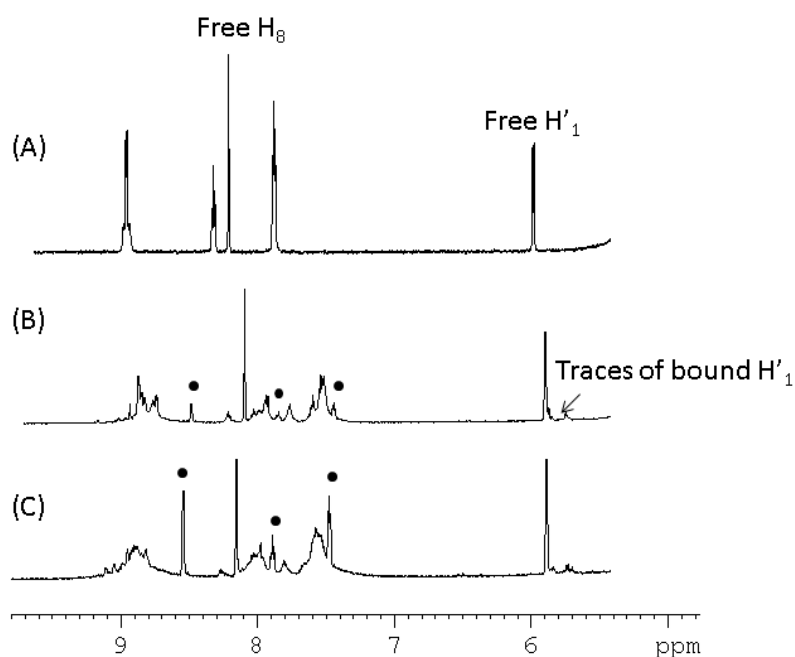


Figure 3.29: ^1H -NMR spectra of complex **3** (1.5 mM, MeOD (75%) /H₂O (25%)) and 5'-GMP (2 mol eq) at A) Dark, B) irradiation with 420 nm, 30510 mJ/cm² C) irradiation with UVA, 1440 mJ/cm². The dots signify the release of free pyridine ligand.

The incorporation of the fluorescent ligand, N-methylisatoic acid in its deprotonated form provides the possibility of complex **6**, *trans, trans, trans*-[Pt(N₃)₂(OH)(N-MI)(pyr)₂] to be studied with fluorescence emission spectroscopy by exciting the sample at 320 nm. Compound **6** has a strong absorption band at 300 nm (Figure 3.13). Therefore exciting the compound at 320 nm can potentially cause the photodissociation of the compound and release of the axial ligand N-MIA. Each measurement (200 nm/min, 377 nm spectral range) resulted in light exposure for 113 seconds, which was enough to generate structural changes in the compound without any further irradiation (Figure 3.30). The fluorescence spectra show a maximum at 420 nm (hence emission in the blue region). With the aim of identifying whether the increase in fluorescence is due to the release of the ligand,

the fluorescence of free N-MIA ligand was recorded; the fluorescence maximum was almost identical for both compounds.

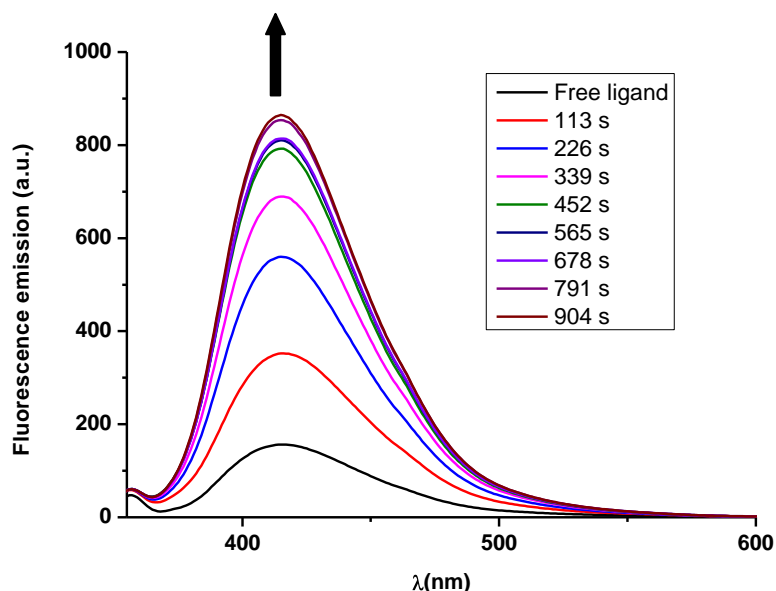


Figure 3.30: Fluorescence emission of the free N-MIA ligand (0.26 μM , 5% DMSO/95% H_2O) and the increase in fluorescence emission of complex **6** (26 μM , 5% DMSO/95% H_2O) upon consecutive measurements, by excitation at 320 nm. The irradiation times (in seconds) were determined by the scanning rate and the spectral range.

3.3.9 High resolution LC-MS studies

Liquid chromatography coupled to mass spectrometry is a useful technique for the separation and identification of photoproducts. HPLC coupled to mass spectrometry was used previously by Bednarski *et al.* to identify the photoproducts from *trans, trans, trans*- $[\text{Pt}(\text{N}_3)_2(\text{OH})_2(\text{NH}_3)_2]$ and *trans, trans, trans*- $[\text{Pt}(\text{N}_3)_2(\text{OH})_2(\text{pyr})(\text{NH}_3)]$.⁴⁸ One advantage offered by such a technique is that a minimal amount of sample is required, which makes it ideal when only small quantities of sample can be obtained, such as compound **7** studied in this chapter (see experimental section 3.2.2.8.8). Liquid chromatography was used to

separate the mixture of photoproducts before analysis by high resolution mass spectrometry (MaXis) for an accurate assignment of the species.

3.3.9.1 LC-MS studies of complexes $[\text{Pt}(\text{N}_3)_2(\text{OH})(\text{Succ})(\text{pyr})_2]$ **4** and $[\text{Pt}(\text{N}_3)_2(\text{OH})(\text{pyr})_2(\text{Succ-(RGD)f})]$ **7**

The irradiation of compounds **4** and **7** in the presence of 5'-GMP was carried out in H_2O (0.5 mM) with 2 mol equiv. 5'-GMP (1 mM), after irradiation with 420 nm (30510 mJ/cm^2) at 37°C , using the LuZchem photoreactor. The irradiated solutions were analyzed directly without any further dilution. The method employed for the separation of the products is described in Chapter 2 (Section 2.2.2). The characterisation of each peak is given in Table 3.6.

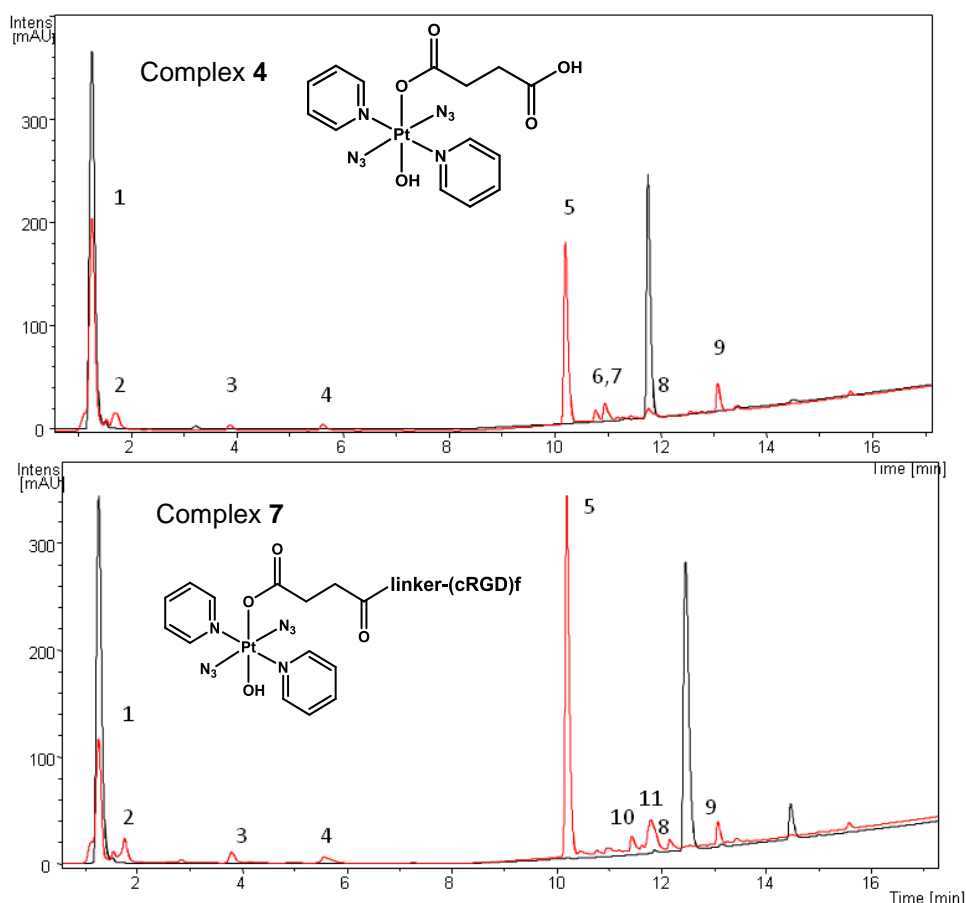
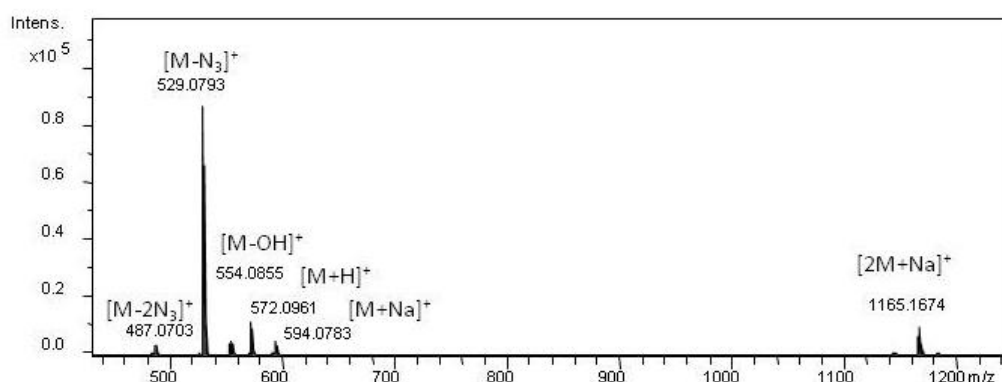


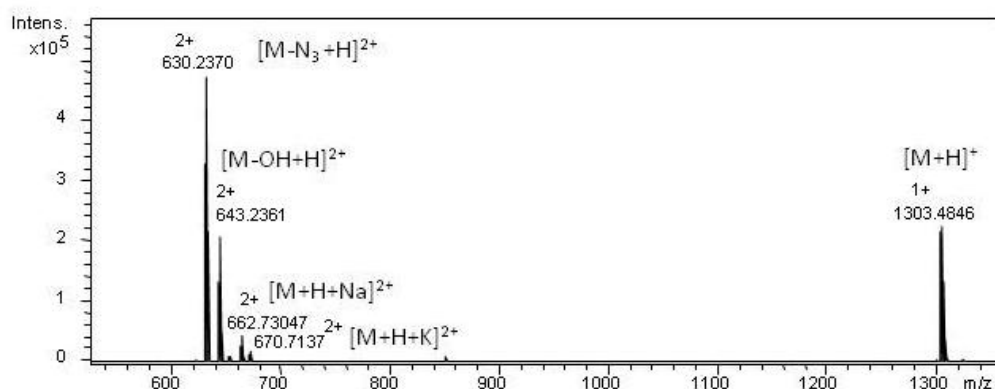
Figure 3.31: Chromatogram of the complexes **4** and **7** with 5'-GMP (2 mol eq) in the dark (black) and after the photoirradiation (red) of A) complex **4** and B) Pt(IV)-(RGD)f peptide **7**. The numbering corresponds to the various species detected, the assignments of which are summarized in Table 3.6.

The mass spectra of complexes **4** and **7** are shown in Figure 3.32. Compound **4** elutes as one peak in the chromatograph and the corresponding mass spectrum (ESI-MS) contains the molecular ion peaks with low intensity, including a proton or sodium ion. The dominant peaks corresponds to the $[M-N_3]^+$ ion, which indicates the ease by which the azide ion dissociates from the complex, under electrospray ionisation. Compound **7** gives two peaks (see Figure 3.31 B) indicating the presence of another species. The latter was assigned to the Pt(IV)-(RGD)f conjugate in which the axial $-OH$ has been replaced with trifluoroacetate (used in the initial HPLC purification of the compound).

(A)



(B)



(C)

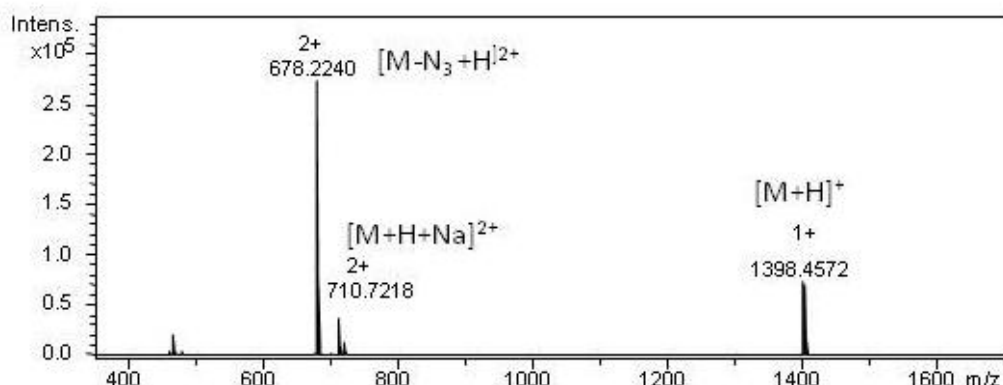
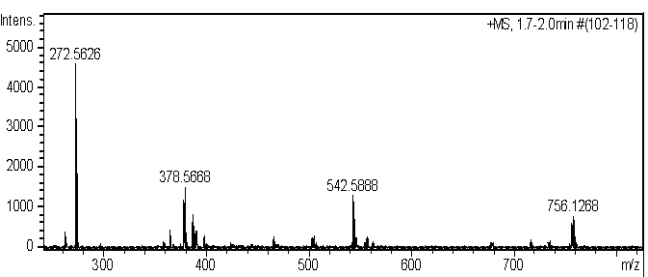
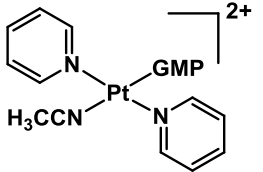
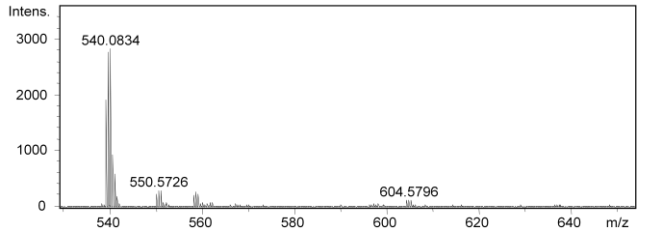
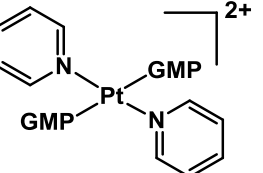
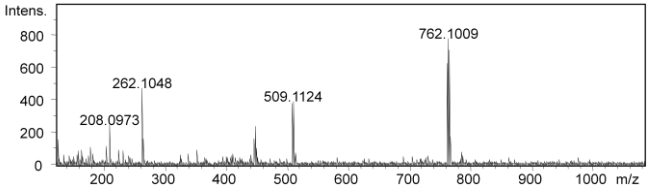
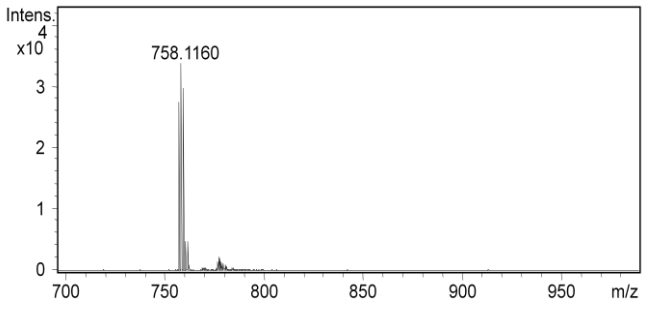
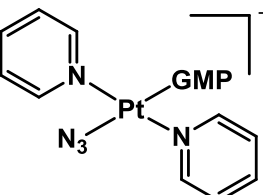
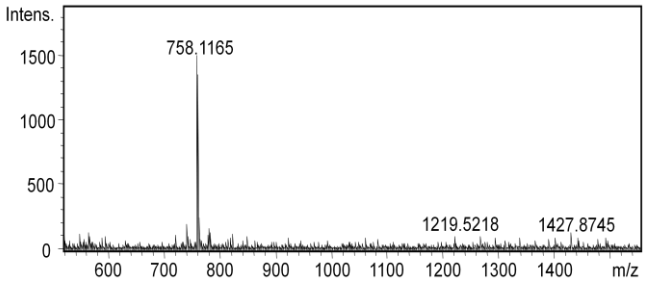
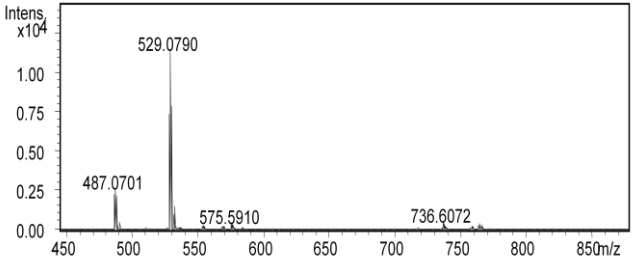
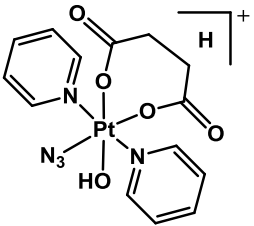
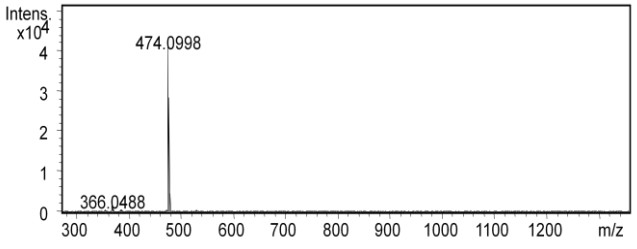
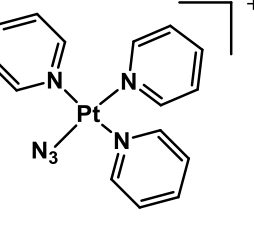
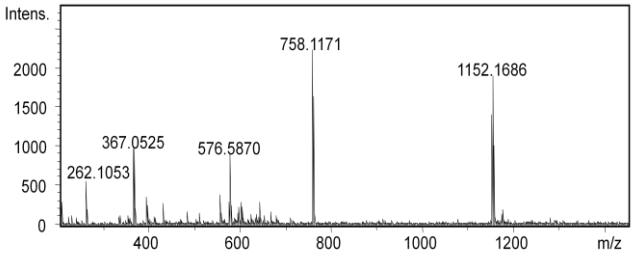
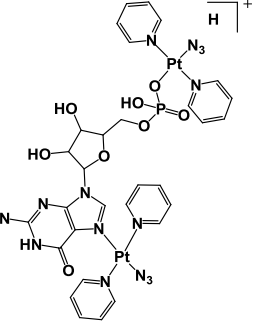
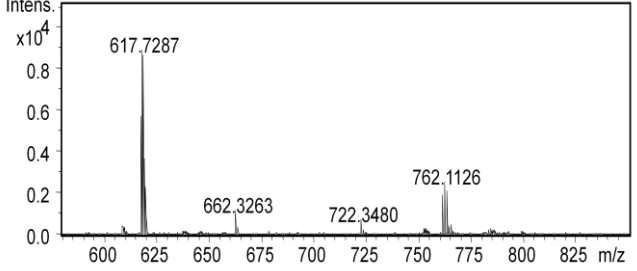


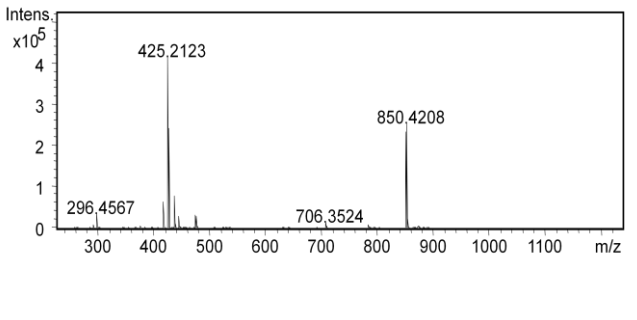
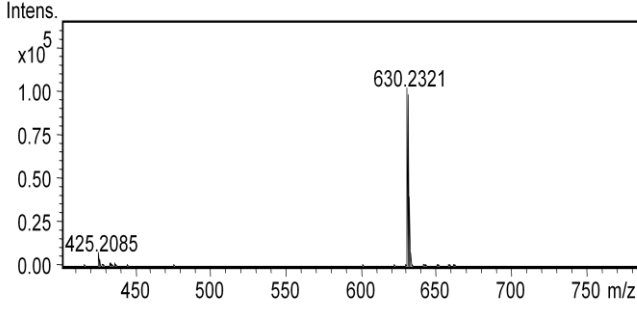
Figure 3.32: ESI-MS of dark samples of compound **4** (A) and the Pt(IV)-(RGD)f peptide **7** (B and C). The spectrum B corresponds to the main peak of the chromatograph (Figure 3.31) whereas spectrum C corresponds to the minor peak. Theoretical assignments for peaks: (A) $[M-N_3]^+$, $C_{14}H_{16}N_5O_5Pt^+$, 529.0799 m/z , where M is compound **4**. (B) $[M-N_3+H]^+$, $C_{47}H_{67}N_{15}O_{14}Pt^{2+}$, 630.2314 m/z where M is the Pt(IV)-(RGD)f as shown in Figure 3.3. (C) $[M-N_3+H]^+$, $C_{49}H_{66}F_3N_{15}O_{15}Pt^{2+}$, 678.2227 m/z , where M is the Pt(IV)-(RGD)f-peptide which the axial $-OH$ has been substituted with a trifluoroacetate.

Table 3.6: Assignment of the various species detected after the irradiation of compounds **4** and **7**. The peak number corresponds to the peak labelling in the chromatographs of Figure 3.31. The m/z values given in the assignment column correspond to the theoretical values.

Peak	Mass Spectrum	Assignment	Error in ppm
1		$[2GMP+H]^+$ $m/z = 727.1246$	1.1
		$[GMP+H]^+$ $m/z = 364.0658$	0.3
		 $m/z = 152.0588$	5.3

2		 <p>$m/z = 378.5667$</p>	0.3
3		 <p>$m/z = 539.5820$</p>	0.2
4		Unknown	NA
5		 <p>$m/z = 758.1164$</p>	0.5
6		<p>Structural isomer of mono-GMP adduct (above)</p> <p>$m/z = 758.1164$</p>	0.1

7		 <p>$m/z = 529.0799$ $[M-N_3-N_3]^+ = 487.0707$</p>	<p>1.7</p> <p>1.2</p>
8		 <p>$m/z = 474.1006$</p>	<p>1.7</p>
9		 <p>$m/z = 1152.1727$</p>	<p>3.5</p>
10		<p>Unknown</p>	<p>NA</p>

11		$[C_{37}H_{58}N_{10}O_{13}]^{2+}$ $m/z = 425.2087$ $[C_{37}H_{57}N_{10}O_{13}]^+$ $m/z = 850.4107$ peptide entity	1.6 3.4
12		$[C_{47}H_{67}N_{15}O_{14}Pt]^+$ $m/z = 630.2316$ (i.e. $[M-N_3+H]^{2+}$)	0.8

Irradiation of **4** (1.5 mM with 463 nm, 40 min) in PBS yielded very similar photoproducts to the ones obtained in H₂O, as shown in Figure 3.33. The main differences lie in the type of 5'-GMP adducts. Irradiation in the absence of PBS forms preferably *trans*-[Pt(ACN)(GMP)(pyr)₂], *trans*-[Pt(GMP)₂(pyr)₂], and a third unknown GMP adduct. However, irradiation in the presence of PBS (which contains a total of 0.140 M Cl⁻ concentration), yields a peak at 10 minutes which corresponds to the *trans*- [PtCl(pyr)₂(GMP)]⁺ species.

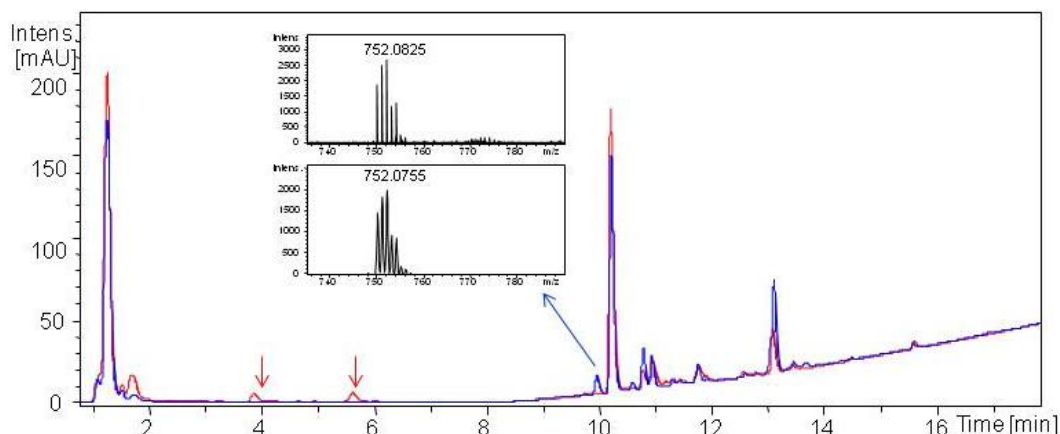


Figure 3.33: LC-MS chromatogram of **4** (1.5 mM) irradiated with blue light (463 nm) in the presence of GMP (2 mol eq) in PBS ($[\text{Cl}^-] = 139 \text{ mM}$) (blue line) or in H_2O (red line). The inset represents the experimental (bottom) and simulated (top) peak which corresponds to $[\text{Pt}(\text{pyr})_2(\text{GMP})\text{Cl}]^+$. The arrows point out GMP photoproducts which are not formed in the presence of PBS.

3.3.9.2 LC-MS study of $[\text{Pt}(\text{N}_3)(\text{OH})(\text{N-MI})(\text{pyr})_2]$ **6**

Irradiation of compound **6** (1.5 mM) plus 5'-GMP (2 mol eq) was carried out in a mixture of MeOH: H_2O (75%: 25%, v/v), to match the NMR experiments. Firstly, compound **6** was irradiated at a concentration of 1.5 mM for 45 minutes at 420 nm, using the photoreactor. The products were injected into the LC-MS system without any further dilution. A dark sample was also analyzed as control. Results are shown in Figure 3.34 and the assignment of the photoproducts is included in Table 3.7.

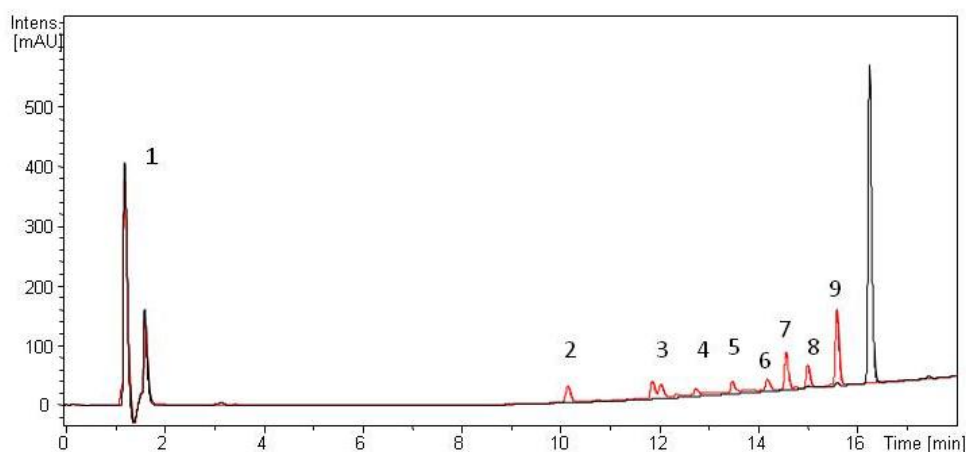


Figure 3.34: HPLC chromatogram of compound **6** in the dark (black line) and after irradiation with 420 nm (red line). The peaks were labelled and assigned in Table 3.7).

The mass spectrum of the non-irradiated sample (Figure 3.35) shows that the base peak corresponds to the molecule minus an azide anion, as in the case of compound **4**. The intensity of the molecular ion peak was low and corresponded to the protonated molecular ion.

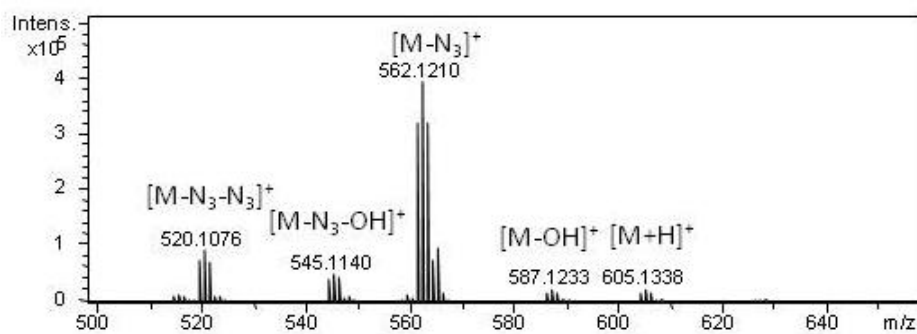
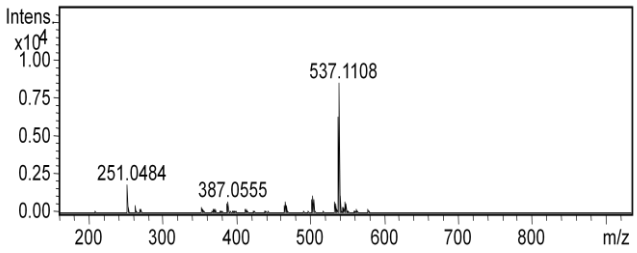
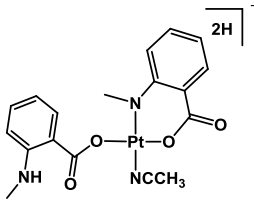
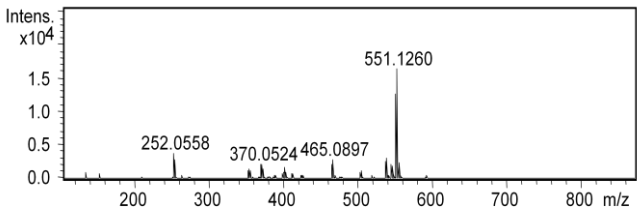
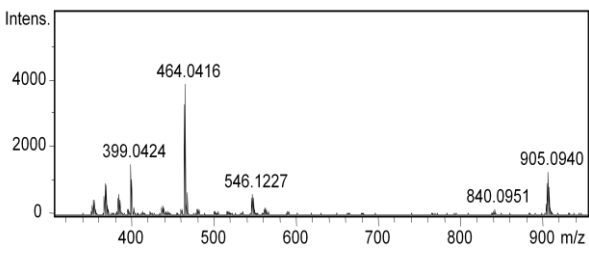
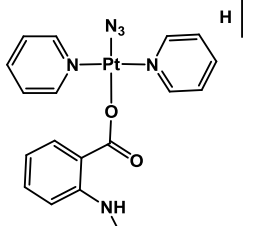
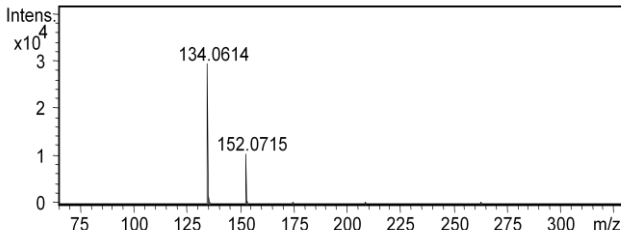
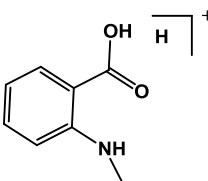
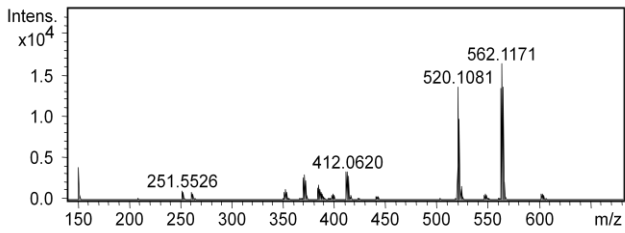
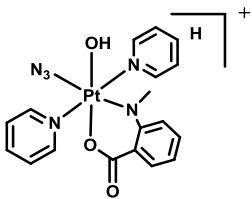
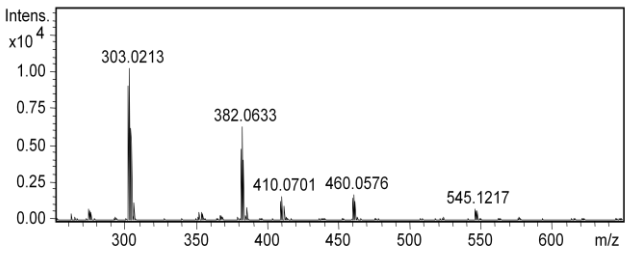
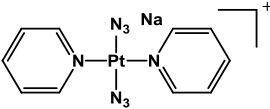
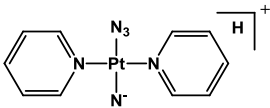
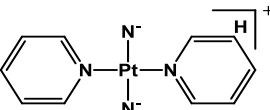
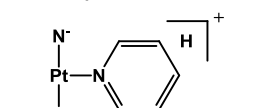


Figure 3.35: High resolution ESI-MS of compound **6** in the dark. Theoretical assignments are as follows: $[M+H]^+$, $C_{18}H_{20}N_9O_3Pt$, 605.1337 m/z ; $[M-N_3]^+$, $C_{18}H_{19}N_6O_3Pt$, 526.1166 m/z ; $[M-OH]^+$, $C_{18}H_{18}N_9O_2Pt$, 587.1231 m/z .

Table 3.7: Assignment of the various species detected after the irradiation of compound **6** with blue light (420 nm). The peak number corresponds to the peak labelling in the chromatograms in Figure 3.34. The m/z ratio reported in the assignment column refers to the theoretical values.

Peak	Mass Spectrum	Assignment	Error in ppm
1		$a = [2\text{GMP} + \text{H}]^+$ $m/z = 727.1246$ $b = [\text{GMP} + \text{H}]^+$ $m/z = 364.0658$ $c = 152.0588$	1.5 2.2 7.9
2		 $m/z = 758.1164$	0.5
3		 $m/z = 436.0849$ $m/z = 395.0584$ 367.0516 unknown	1.1 0.8 NA

4		 $m/z = 537.1102$	0.7
5		Unknown	NA
6		 $m/z = 546.1217$ 464.0416 unknown	1.8
7		 $m/z = 152.0712$	2.0

8		 <p>$m/z = 562.1166$</p> <p>$[M-N_3]^+ = 520.1074$</p>	0.9 1.3
9		 <p>$m/z = 460.0574$</p>  <p>$m/z = 410.0693$</p>  <p>$m/z = 382.0631$</p>  <p>$m/z = 303.0209$</p>	0.4 1.9 0.5 1.3

3.3.10 DFT and TDDFT calculations

As demonstrated previously, DFT calculations can provide insights into the photochemistry of platinum-azido photoactivatable complexes.²⁵ DFT and TDDFT calculations were performed as described in section 2.10 (Chapter 2) in order to characterise the electronic transitions composing the absorption spectrum of complex **4** and rationalize its enhanced photoactivity when compared to complex **3**. Bond lengths of **4** in the protonated state seem to correlate better with the experimental bond distances, as the crystallised complex is in fact in the

protonated state (Figure 3.5A). The ground state geometry optimizations were performed in both the protonated and deprotonated state, as well as in the lowest lying state geometry, as summarized in Table 3.8.

Table 3.8: Selected experimental and calculated bond lengths (in Å) for compound **4** in the protonated (*trans, trans, trans*-[Pt(N₃)₂(pyr)₂(OH)(C₄H₅O₄)]) as well as the deprotonated form (*trans, trans, trans*-[Pt(N₃)₂(pyr)₂(OH)(C₄H₄O₄)]). The theoretical bond lengths were calculated in both the ground as well as in the lowest lying triplet state.

Bond Lengths	Distance in X-ray structure (Å)	Ground-state geometry (deprot)	Lowest lying geometry	Ground-state geometry (prot)	Lowest lying geometry
Pt–N _α	2.050	2.088	2.359	2.085	2.985
Pt–N _α	2.041	2.069	2.508	2.069	2.326
Pt–(OH)	1.984	2.015	2.015	1.994	1.992
Pt–O(CO)	2.021	2.048	2.065	2.061	2.076
Pt–N(py)	2.039	2.068	2.053	2.043	2.035
Pt–N(Py)	2.033	2.027	2.040	2.039	2.058
N _α –N _β	1.209	1.213	1.200	1.218	1.183
N _α –N _β	1.198	1.211	1.189	1.214	1.204
N _β –N _γ	1.139	1.149	1.164	1.145	1.173
N _β –N _γ	1.133	1.148	1.170	1.146	1.158

As commonly observed for DFT,^{49, 50} the bond lengths of the ground state are overestimated, the largest discrepancy being the two Pt-azide bonds, with differences of 0.035 and 0.028 Å. This could result from the fact that the geometry optimization occurs in the gas phase, or the fact that there are intermolecular interactions between the molecules in the crystal structures.

The excited states of transition metal complexes usually undergo intersystem crossing (IC) to triplet states. In particular, the nature of the lowest-lying triplet state is crucial, since such a state is significantly populated before the molecule relaxes to the ground state. Hence the photochemistry of a metal complex highly depends on the lowest lying-triplet state. Elongation of bonds is indicative that

they could undergo bond-breaking upon light excitation, and therefore suggestive of which ligands are likely to be released. The difference between the lowest lying geometry and the ground state in the case of deprotonated and protonated systems follows the same trend: both Pt-azide bonds show the biggest elongation. The Pt-OH bond is either shortened (protonated) or stays intact (deprotonated), the Pt-succinate bond is elongated, and one of the Pt-pyridine bonds is elongated whereas the other is shortened.

The UV-Vis spectra were simulated by calculation of 32 singlet states using water as a solvent (cpcm)⁵¹ and the TDDFT method. The theoretical UV-Vis maxima appear at 286 nm ($33748 \text{ mol}^{-1}\text{cm}^{-1}$) in the case of the deprotonated state and 288 nm ($26217 \text{ mol}^{-1}\text{cm}^{-1}$) in the case of the protonated state. The experimental maximum is located at 299 nm ($\epsilon = 17251 \text{ mol}^{-1}\text{cm}^{-1}$). TDDFT calculations therefore seemed to slightly underestimate the absorption maximum by *ca.* 10 nm and overestimate the value of the extinction coefficient. The method used for these TDDFT calculations is the same as that used for **3**, for which a closer match between the theoretical and the experimental extinction coefficient was found. Therefore the larger difference in the case of **4** can be ascribed to the presence of the succinate ligand. Although functional and basis set benchmarking testing might improve the agreement between calculated and experimental transitions, the results obtained are satisfactory as they help to characterise the nature of the UV-Vis bands.

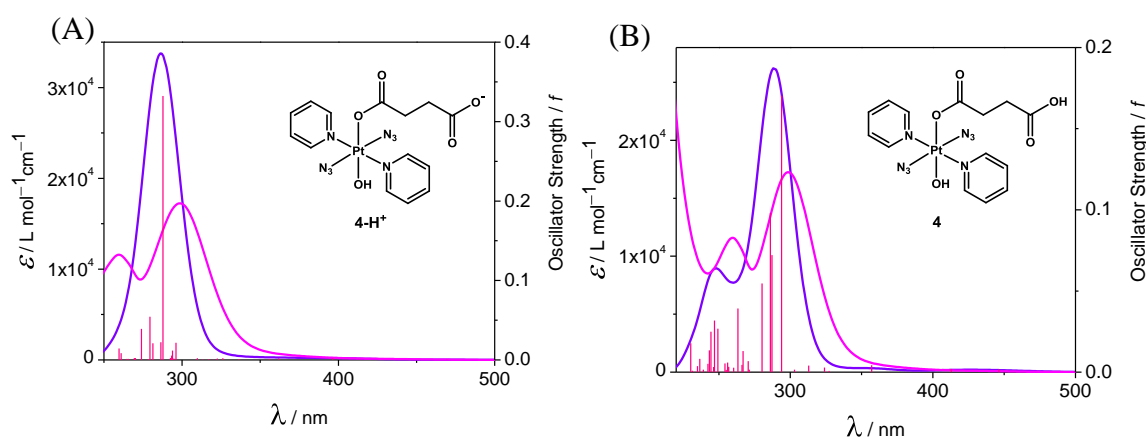


Figure 3.36: Experimental (pink) and theoretical (purple) UV-Vis spectra of compound **4** in the deprotonated (A) and protonated (B) states. The vertical bars represent the oscillator strength of the excited states.

The main focus in the description of the excited states will be on the deprotonated state as it has been established before (section 3.3.4) that at physiological pH, complex **4** will be deprotonated. The excited states as well as the percentage contribution in each case are summarized in Table 3.9. It should be noted that the longer wavelength transitions in this complex extend up to 469 nm, whereas in *trans, trans, trans*-[Pt(N₃)₂(OH)₂(pyr)₂] **3** they reach to 414 nm. The longer wavelength transitions S1, S2 and S3, which occur at wavelengths greater than 400 nm, show that there is a transfer of electron density from the succinate to the platinum centre (¹LMCT) and also contain ¹IL (inter-ligand transitions) character. In the S1 (LMCT), electron density migrates from the succinate to the Pt centre and in the second case (IL) to the hydroxyl and azide groups, but not to the pyridines. All these transitions (S1, S2, S3) as well as some of the higher energy involve the LUMO, which is antibonding in character with regard to the four equatorial ligands but mainly the azides. Interestingly the LUMO+1, to which electron density is promoted in the higher wavelength transitions (e.g. S8, S14) is orthogonal with respect to the LUMO, making it strongly antibonding mostly

towards the pyridines and also the hydroxido and the succinate ligand. This suggests that occupation of the LUMO or LUMO+1 could potentially lead to dissociation of two out of the six ligands. These two ligands would be in *trans* to each other. The HOMO is mainly ligand-based, with the major contribution from the succinate and very little on the pyridine (see Figure 3.37) which explains the LMCT character of the low energy transitions. Interestingly, the molecular orbitals of complex **4** in the protonated state show that the HOMO involves all the equatorial ligands as well as platinum, excluding the pyridines (Figure not shown), but the LUMO and LUMO+1 orbitals are very similar in character between the two species.

UV transitions (e.g. S14, S19) occur from lower energy HOMOs and can be assigned to $^1\text{LMCT}$ / ^1IL transitions. In general all transitions for complex **4** show some d-d character, as metal orbitals always contribute to the frontier molecular orbitals. Most of the ligands are involved in these transitions, which could suggest larger variability in the photoproducts when the complex is irradiated at a short wavelength.

Table 3.9: Selected calculated (TD-DFT) singlet transitions for complex *trans, trans, trans*-[Pt(N₃)₂(pyr)₂(OH)(Succ)] **4** in the deprotonated state.

Transition	Energy (eV)	Wavelength (nm)	Oscillator Strength	Major composition
S1	2.64	469	0.0004	HOMO-3 → LUMO (63%) HOMO-2 → LUMO (28%)
S2	3.00	413	0.0005	HOMO-1 → LUMO (80%) HOMO → LUMO (17%)
S3	3.07	404	0.0002	HOMO-1 → LUMO (15%) HOMO → LUMO (81%)
S4	3.13	396	0.0019	HOMO-4 → LUMO (75%)
S5	3.43	362	0.0019	HOMO-7 → LUMO (28%) HOMO-5 → LUMO (53%)
S6	3.48	356	0.0011	HOMO-3 → LUMO (30%) HOMO-2 → LUMO (64%)
S8	3.80	326	0.0022	HOMO-7 → LUMO+2 (10%) HOMO-5 → LUMO+1 (10%) HOMO-5 → LUMO+2 (16%) HOMO-1 → LUMO+1 (13%) HOMO-1 → LUMO+2 (10%)
S9	3.84	322	0.0018	HOMO-7 → LUMO (46%) HOMO-6 → LUMO (29%)
S14	4.19	296	0.0216	HOMO-3 → LUMO+1 (34%) HOMO-3 → LUMO+2 (13%) HOMO-2 → LUMO+1 (12%) HOMO-2 → LUMO+2 (12%)
S19	4.31	288	0.3322	HOMO-7 → LUMO (12%) HOMO-6 → LUMO (33%) HOMO-5 → LUMO (13%)
S22	4.437	279	0.0543	HOMO-12 → LUMO (10%) HOMO-11 → LUMO (31%) HOMO-10 → LUMO (20%)
S32	4.77	260	0.0145	HOMO-5 → LUMO+1 (48%) HOMO-5 → LUMO+2 (31%)

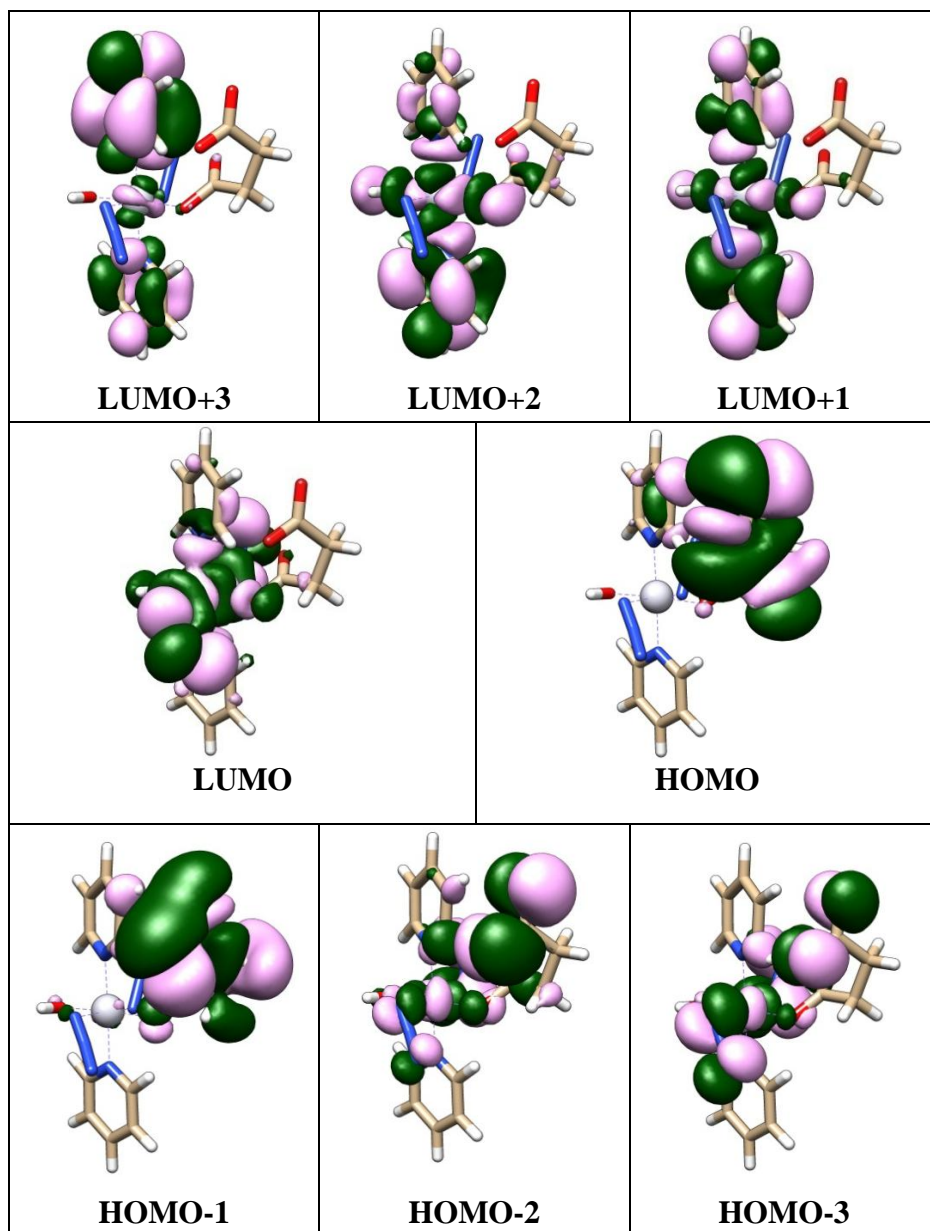


Figure 3.37: Selected molecular orbitals of compound **4** (deprotonated) in the ground-state geometry.

3.3.11 Cytotoxicity and cellular uptake studies

The determination of IC_{50} values in the dark and also upon irradiation is important to estimate the phototherapeutic window of these novel complexes. The IC_{50} values were determined as described in Chapter 2 in collaboration with Dr Julie Woods, in A2780 (ovarian cancer cell line) and in one case in A2780cis (A2780

cisplatin resistant) cell lines. The complexes were exposed to the drugs for one hour in the dark and irradiated with a low light dose of 5 J/cm² at 420 nm. The 95% confidence interval indicates that the value of IC₅₀ lies between the ranges provided. The phototoxic index (PI) is the ratio between the dark and light IC₅₀, and a high ratio is more desirable for clinical application. Compounds **4** and **5** have very similar IC₅₀ values and **6** shows the lowest toxicity. The reported IC₅₀ of **3** is an average of two independent values: 8.3 µM (CI: 3.4-20.4 µM)⁵² and 5.1 µM (CI: 3.7-6.9 µM).

Table 3.10: Summary of phototoxicity and dark toxicity IC₅₀ values of **3**, **4**, **5** and **6** on A2780 human ovarian cancer cell line. The irradiation was carried out at 420 nm.

Complex	A2780					A2780cis				
	IC ₅₀ 420 nm (µM)	95% CI	R ²	IC ₅₀ Dark (µM)	PI	IC ₅₀ 420 nm (µM)	95% CI	R ²	IC ₅₀ Dark	PI
3	6.7*	3.6-13.7	0.890	>200	>45	ND	ND	ND	ND	ND
4	3.6	3.5-3.8	0.984	>175	>48.6	ND	ND	ND	ND	ND
5	3.7	3.0-4.6	0.811	>163	>44.1	ND	ND	ND	ND	ND
6	12.1	7.3-19.9	0.909	>67	>5.5	10.8	7.6-15.3	0.926	>65	>6

Cell uptake studies are highly informative from a pharmacological perspective, since they can disclose important information on the mechanism of action of anticancer agents. Such studies were performed in A2780 cell line, in the conditions used as described in section 3.2.2.6 (Figure 3.38). The concentration used for the uptake of all of the drugs was 20 µM, since at this concentration no dark toxicity is observed and is above the IC₅₀ for all of them. The uptake of the compounds (from highest to lowest) follows the order: **6** (300 ng/10⁶ cells) >> **3**

(32 ng/10⁶ cells) > **CDDP** (29 ng/10⁶ cells) > **5** (25 ng/10⁶ cells) > **4** (15 ng/10⁶ cells).

Furthermore cell uptake mechanisms have always been important for the development of new anticancer drugs, as impaired cellular uptake could be one of the reasons which lead to development of resistance.⁵³ In general terms, cell uptake occurs by either passive (no energy required) or active (involving energy consumption) transport. Therefore it is of interest to see how the uptake of these metallodrugs is affected by different temperatures and drug concentrations.

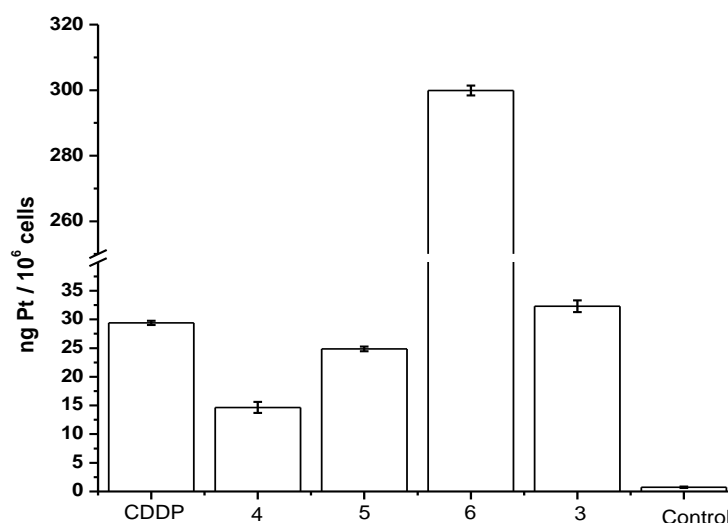


Figure 3.38: Cell uptake studies (expressed in ng Pt/10⁶ cells) of compounds **3-6** with cisplatin as comparison.

The temperature-dependence of cell uptake was studied by measuring the uptake at 4, 18 and 37 °C (Figure 3.39) for **6** and for **3**. Both compounds follow the same trend, at which the uptake is increasing with increasing temperature. The concentration dependence experiment (Figure 3.40) was carried out in order to explore whether the system reaches saturation. Uptake of Pt for compound **6** reaches saturation at 40 μM and for **3** at 20 μM.

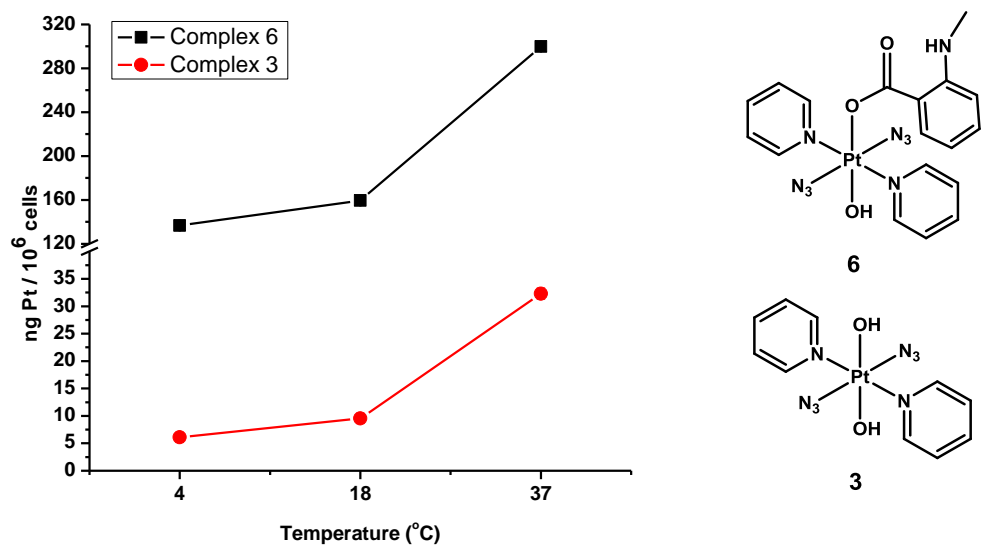


Figure 3.39: Temperature dependence on the cell uptake of complexes **3** and **6**, after 1 hour drug incubation in the dark.

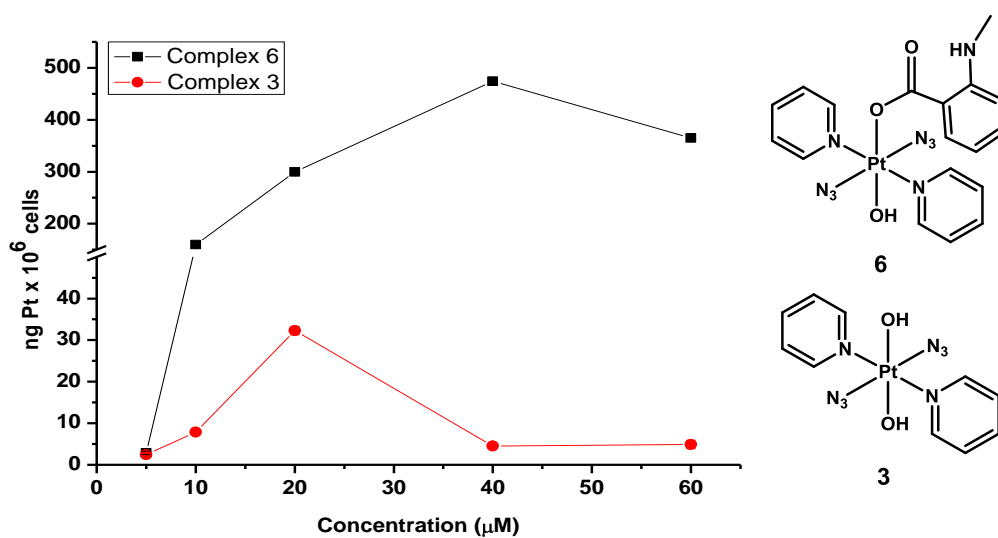


Figure 3.40: Concentration dependence on the cell uptake of complexes **3** and **6**, after 1 hour drug incubation at 37°C , in a 5% CO_2 humidified atmosphere.

3.4 Discussion

3.4.1 Synthesis and characterisation

The Pt(IV) *trans* dihydroxo complexes are reactive towards derivatisation. There are literature reports which suggest that such functionalisation can be achieved by the use of anhydrides or acid chlorides,⁵⁴ pyrocarbonates, and isocyanates to form carboxylates, carbonates and carbamates, respectively.^{14,55,56}

The three novel complexes **4-6** were successfully synthesized, using the aforementioned approach, albeit the yield for all of them was relatively low (18-56%). The succinate and N-methylisatoate axial ligands, in compounds **4** and **6** respectively, were incorporated by reaction of the precursor **3** with the corresponding anhydride through a ring-opening reaction (Figure 3.41). The ligand 4-oxo-4-propoxybutanoate in complex **5** was obtained via esterification of the succinate ligand in complex **4**.

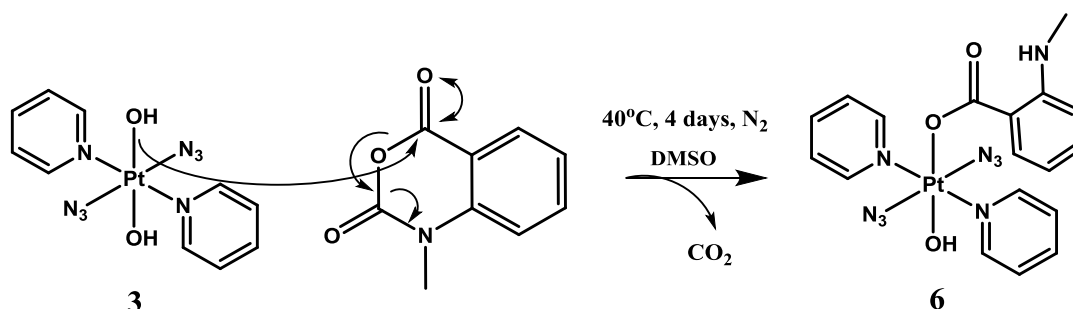


Figure 3.41: Synthetic route to compound **6** using N-methylisatoic anhydride and compound **3**, as starting materials.

The synthesis of compound **6** was attempted in anhydrous reagent grade DMF as well as in DMF with the presence of LiOH (1 mol eq) but it was unsuccessful. Reaction in DMSO with an excess of the ligand yielded the monosubstituted

Pt(IV) complex. This indicates that the polarity of the solvent plays an important role in this type of reaction (DMSO more polar than DMF) and also that reaction with the second –OH is not favourable.

Esterification of the carboxylic acid in complex **4** to obtain complex **5** was carried out by standard coupling chemistry. The esterification was considered beneficial as the cell uptake could potentially be hindered by a negative charge on the complex. Furthermore previous reports have shown that different ester derivatives influence the cytotoxicity of the complex. Two examples will be mentioned here: (a) Keppler and co-workers reported a family complexes of Pt(IV) analogue of carboplatin which are axially-derivatised with carboxylic acids, amides or esters. The ester derivatives significantly lower IC_{50} values when compared to the carboxylic acids with increased lipophilicity favouring higher cytotoxicity;⁵ (b) A similar study was conducted by the axial modification of Pt(IV) analogues of oxaliplatin and it was again discovered that the ester length had an effect on the IC_{50} of the compounds. In both cases, the cytotoxicity did not correlate with the hydrophobicity trend.⁵⁷

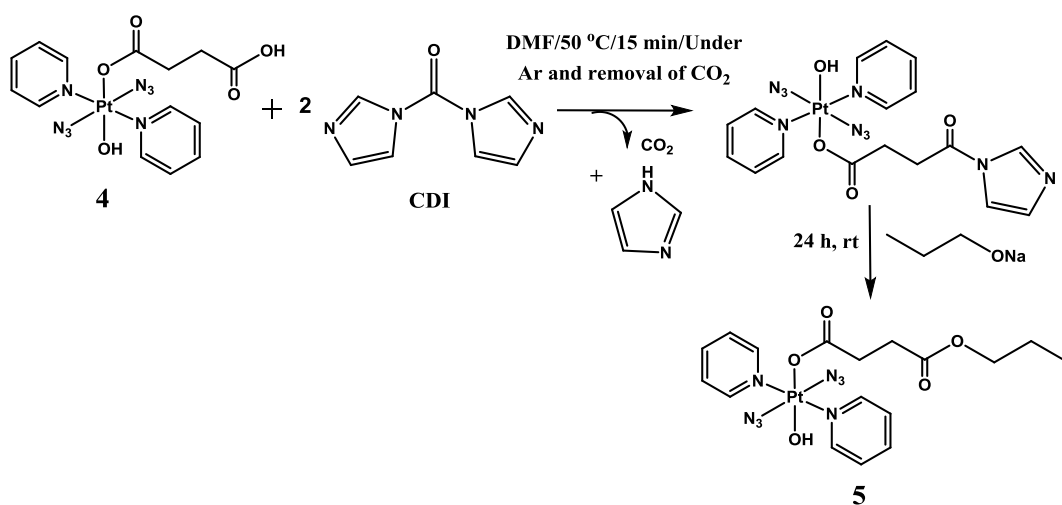


Figure 3.42: Synthetic scheme for the synthesis of compound **5**, using CDI and sodium propionate in DMF.

The synthesis of compound **5** was achieved by the use of CDI (1,1'-carbonyldiimidazole), which is a well known coupling agent used for peptide synthesis (Figure 3.42).⁵⁸ The CDI reacts with the carboxylate group to form a reactive acylimidazole intermediate, and in the presence of an alcohol the esterification takes place with the release of imidazole, as a side product. This route can be used for the formation of an amide bond, which can also be exploited for the synthesis of peptide conjugates.⁵⁸

A cRGD peptide was coupled to *trans,trans,trans*-[Pt(N₃)₂(OH)₂(Succ)(pyr)₂], **4** to yield complex **7** (section 3.2.2.8.8). The RGD sequence is recognized by a number of integrins, which are heterodimeric membrane glycoproteins (composed of α and β subunits) which recognize extracellular matrix proteins. They are involved in angiogenesis, which is an essential step in the metastasis and survival of the tumour cells.⁵⁹ There are 24 integrins most of which can recognize an RGD segment on the protein sequence, but a strong binder of this sequence is $\alpha_v\beta_3$. A crystal structure representing the complexation of RGD with $\alpha_v\beta_3$ has been published by Arnaout *et al.*⁶⁰ Besides the involvement of integrins in angiogenesis, there are strong evidence of their over expression in cancer cells and for this reason RGD peptides can be utilized as tumour targeting peptides, as diagnostic tools but also as integrin inhibitors for therapeutic purposes.⁵⁹ Attachment of a cargo onto an RGD peptide can result in the internalization of the cargo via endocytosis, thus enabling increased uptake of the molecule attached to the RGD.⁵⁹ Thus, enhanced and targeted uptake can be achieved by the incorporation of such moieties. Although light-activation provides a form of selective cytotoxicity, the conjugation to a targeting feature should potentiate it.

The synthesis of the peptide-Pt(IV) conjugate was carried out using HATU/ DIEA (*O*-(7-azabenzotriazol-1-yl)-*N,N,N',N'*-tetramethyluronium hexafluorophosphate), which is another set of commonly used coupling reagents.⁵⁸ An interesting finding during the synthesis of peptide conjugates was the reactivity of the Pt(IV) complex towards TFA, which is commonly used for the deprotection of reactive moieties (in this case Boc-protected amino acids). In order to show that the hydroxyl groups are reactive towards TFA, compound **3** was allowed to react with TFA/DCM (1:1). The product isolated was the bis-triflated adduct, as shown by mass spectrometry and ¹⁹F-NMR.

¹⁹⁵Pt-NMR spectroscopy was used for the characterisation of compounds **4** and **6**; although for **6** DMSO-*d*₆ was employed instead of D₂O for solubility reasons. The chemical shifts of the Pt(IV) signal observed for **4** and **6** fall at 1059 ppm and 990 ppm, respectively, while for reference compound **3** it was reported to be at 942 ppm.²⁶ Chemical shift comparisons can be made only between **4** and **3** as they were measured in the same solvent. The higher chemical shift in the case of complex **4** indicates that the ¹⁹⁵Pt nucleus is more deshielded, even though both complexes exhibit a [N₄O₂] coordination environment around the metal centre. Noticeably, lengthening of the Pt–P bond in the case of platinum complexes containing phosphine ligands was found to increase the Pt chemical shift.⁶¹ As reported in subsection 3.3.2., the Pt–O bonds with the carboxylate ligands are longer than the Pt–OH bond, which might account for the increase in the chemical shift.

As previously stated, the analysis of the UV-Vis spectra of photoactivatable complexes is important to understand and exploit their photochemistry. The bands

in the spectra of Pt(IV)-diazido compounds can be estimated with the aid of theoretical calculations. All complexes discussed in this chapter (**3-6**) show two absorption bands at *ca.* 260 nm and 300 nm. These are composed mainly of transitions with $^1\text{LMCT}$ character. Since in phototherapy longer wavelength light is ideally desirable for greatest penetration into tissues, the longer wavelength absorption bands are of great interest for photoactivatable metallodrugs. The absorption bands in compounds **4-6** are red-shifted in comparison with those in the precursor **3**, indicating that modification of the axial bond enhances the photolability of Pt(IV)-diazido prodrugs. Figure 3.43 shows the difference in colour between compound **4** and compound **3**, the former having a more intense yellow colour.



Figure 3.43: Comparison of colour between compound **4** (orange-right) and compound **3** (yellow-left).

The largest red shift corresponds to compound **6**, which has a visible absorbance between 350 nm and 400 nm. This is not surprising since this compound bears a benzyl ring and it was predicted by DFT calculations that the replacement of the $-\text{OH}$ group with $-\text{OPh}$ would result in a red shift, and also more transitions appear in the visible region of the spectrum.⁶²

3.4.2 Aqueous solubility and stability in the dark

Regarding the aqueous solubility of complexes **4-6**, an evident conclusion is that the introduction of carboxylate axial ligands greatly influences in the hydrophobicity and hence in their water solubility. Replacing one of the hydroxyl groups with a succinate ligand clearly made the complex more hydrophobic as the solubility was reduced 17-fold and also the HPLC retention time increased from 6.3 (compound **3**) to 8.8 min (compound **4**). The increase in the chain length (from *trans, trans, trans*-[Pt(N₃)₂(pyr)₂(OH)(Succ)] **4** to *trans, trans, trans*-[Pt(N₃)₂(pyr)₂(OH)(Succ-Pr)] **5**) lead to a slight decrease in the aqueous solubility as observed in complex **5**. Strikingly the attachment of a phenyl ring in complex [Pt(N₃)₂(OH)(N-MI)(pyr)₂] **6** produces a compound which is very poorly soluble in water. These results illustrate the effects that derivatisation of these two hydroxyl groups can have on water solubility of these Pt(IV) complexes.

The stability of compound **4** was assessed in the presence of 2 mol eq of GSH, as two molecules of GSH would be required to provide 2 electrons to reduce Pt(IV) to Pt(II). It is significant to test reactivity with biological reductants, as Pt(IV) photoactivatable prodrugs need to be stable in the dark and activated only in the presence of light. Biological reducing agents in the cell and in the blood plasma include ascorbate, glutathione as well as metallothioneins (small proteins having 20 cysteines per molecule).⁶³ Ascorbic acid has a concentration of *ca.* 1 mM in the cytosol and 50-150 μ M in the blood plasma, whereas GSH is found at 2-8 mM in the cytosol and 850 μ M in the blood plasma.⁶³ It was shown that complexes with axial acetates are a lot easier to be reduced than those with hydroxyl groups. For example, a recent study by Dabrowiak *et al* showed that the monocarboxylato

Pt(IV) analogue of oxoplatin (i.e. the complex *cis, trans, cis*-[PtCl₂(OH)₂(NH₃)₂]) reduces faster in the presence of GSH than oxoplatin.⁶³ Also some carboxylato complexes e.g. *cis, trans, cis*-[Pt(NH₃)(2-pic)(OAc)₂(Cl)₂] can be completely reduced within 4 hours when co-incubated with GSH.⁶⁴ The fact that these Pt(IV)-azido monocarboxylato compounds are stable in the presence of GSH (as shown in Figure 3.9, section 3.3.3) is significant for their possible development as phototherapeutic candidates.

3.4.3 Photoirradiations

3.4.3.1 UV-Vis studies

UV-Vis spectroscopy allows the photoreduction of Pt(IV)-diazido compounds to be monitored as a decrease of the N₃→Pt charge transfer band (at *ca.* 300 nm) is observed due to the loss of an azide. Irradiation of compound **3** results only in a decrease in intensity of this LMCT band, whereas for compounds **4** and **5**, there is an apparent increase in intensity of the band at *ca.* 250 nm (refer to Figure 3.15 and Figure 3.16, section 3.3.6). In case of compound **3**, similarly to **6**, no increase of intensity occurs for the band at 250 nm but a slight shift of the maximum wavelength is observed. This result could be explained in two ways: either the electronic transitions of the attached ligand are not mixing with the transitions of the platinum centre therefore absorbance of the former is similar to the free ligand or the release of the ligand is very slow in comparison to the release of the azide. Most reduction profiles of Pt(IV) complexes,⁶⁵ as found for compounds **3-6**, follow an exponential decay profile. This is illustrated in Figure 3.18 which shows plots of the absorbance of the N₃→Pt band, as a function of time. Mechanistic

studies of the chemical reduction of other Pt(IV) prodrugs in the presence of reducing agents such as GSH and L-ascorbate have shown that the reduction is second-order and proportional to the concentration of the Pt(IV) complex as well as the reducing agent.⁶⁶ In the case of the photoreductions carried out on **3-6**, it was observed a decrease in the reduction rate when the concentration of the sample was increased, upon the same light exposure (Figure 3.44).

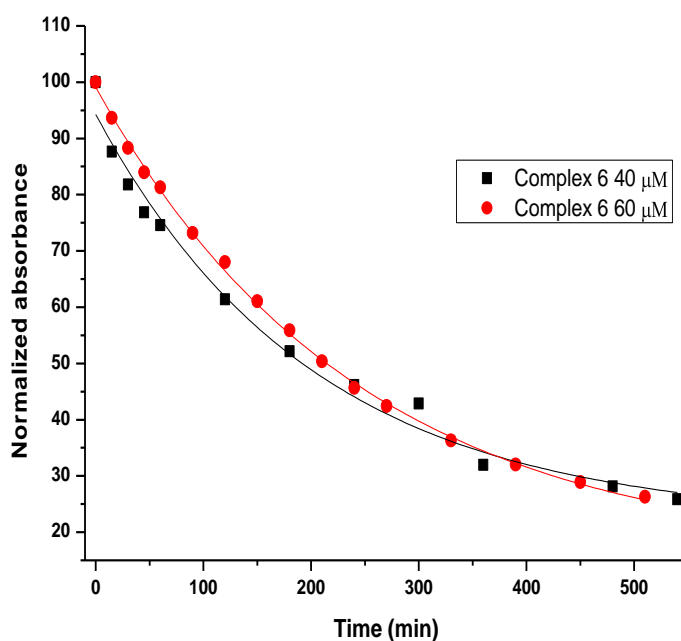


Figure 3.44: Time dependent photoreduction of complex **6** at 40 μ M ($t_{1/2}$ = 192 min) and 60 μ M (214 min) concentration in 5% DMSO/95% H_2O . The photoirradiation was carried out with green light (517 nm).

The photoreactions proceed at different rates depending on the complex ($t_{1/2}$ = 634 min for **3**, 220 min for **4**, 169 min for **5** and 214 min for **6**). Evidently, the half times of the compounds decrease by up to ~4 times less (e.g. compound **5**) as compared to the dihydroxo compound **3**. This suggests that the carboxylate functionality enhances the photoreactivity of these complexes. All three show

much faster kinetics in comparison to compound **3**. Furthermore compound **5**, the fastest complex in photodegradation, shows the longest Pt–O (carboxylate) bond, which photodissociates upon light exposure. Observing an effect on the reduction rate of Pt(IV) prodrugs with an increasing chain length of the functionality on the carboxylate ligand is not unusual (although the chain is distant from the Pt centre). Ravera *et al* showed that the reduction potential decreased for a longer carbon chain, in *cis,trans,cis*-[PtCl₂(mpy)(NH₃)(RCOO)₂], where R= CH₃(CH₂)_n, n=0-4.⁸ The increased rate of photodegradation in the case of compound **4** *versus* compound **3** correlates with the extinction coefficients, higher for **4** at the longer wavelengths (Figure 3.13). Compound **4** underwent very little activation with yellow light (550 nm, 2.5 mW/cm²), as judged by the change in the absorbance of the band at *ca.* 300 nm.

3.4.3.2 EPR studies

The formation of azidyl radicals when Pt-diazo compounds are irradiated may play a role in the mechanism of action of these prodrugs.⁵² Therefore the amount of azidyl radicals produced on photoactivation of the complexes studied here was determined.

The first experiment was carried out with 1 mM solutions of compounds **3**, **4**, and **5** in PBS in the presence of DMPO (spin-trap). The results of this study showed that no radicals were trapped in the case of **3** whereas **4** and **5** yielded radicals up to 68 μM and 55 μM, respectively (Figure 3.21). The identity of the trapped radical was confirmed to be the DMPO-N₃ by matching the hyperfine splitting constants (HFSC) to the theoretical data reported previously (Figure 3.45).^{43, 41}

Hydroxyl or carboxylate radicals, which could potentially be released from the Pt(IV) complex, would give a 1:2:2:1 pattern when trapped by DMPO. This signal however, was not detected in the spectrum. Even though compound **4** was found to have a slightly lower photodissociation rate than compound **5**, the azidyl radical yield after 14 minutes of irradiation was in fact slightly higher for the former. However the initial production of radicals (e.g. after 7 min of irradiation) was lower for **4** than for **5**.

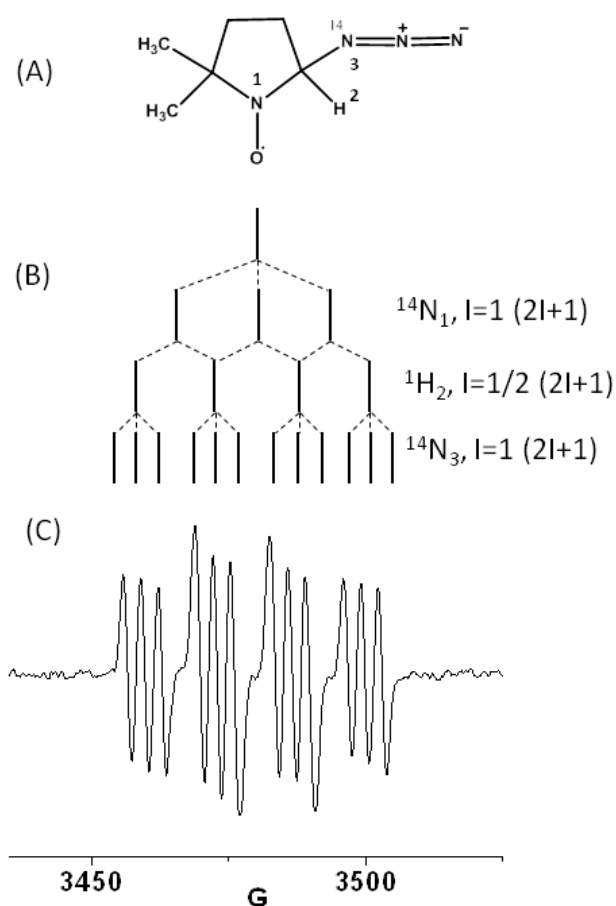


Figure 3.45: (A) The structure of the spin-adduct DMPO \cdot -N₃ adduct formed by the addition of N₃ \cdot to DMPO. (B) The origin of the hyperfine splitting pattern from the coupling of the unpaired electron to nitrogen (atom 1), hydrogen (atom 2) and nitrogen (atom 3). (C) EPR signal of an irradiated sample of compound **4** in DMF/H₂O (75 %, 25%, v/v) in the presence of DMPO (2 mol eq) at 20 °C.

A similar experiment was carried out using DMF as the solvent. Compounds **3**, **4**, and **5** in DMF gave similar results as in PBS, with compound **4** giving the highest and compound **3** the lowest azidyl radical yield. Surprisingly, compound **6** produced a similar amount of radicals as **3** although the rate of photodegradation is ~3-fold higher. A plausible explanation for this fact is that the released N-methylisatoate ligand (axially bound in **6**) could act as a radical scavenger. In order to confirm this hypothesis, complex **3**, *trans, trans, trans*-[Pt(N₃)₂(OH)₂(pyr)₂], was irradiated ($\lambda = 463$ nm, 64 mW/cm²) in the presence of N-methylisatoic acid (1 or 2 mol eq). The production of azidyl radicals was entirely quenched by N-MIA suggesting that upon release, this ligand can readily react with N₃[•]. The reactivity of similar molecules with reactive oxygen species has been established recently where it was shown that methyl anthranilate, structurally related to N-methylisatoate ligand, can quench singlet oxygen due to the presence of the anilinic moiety.⁶⁷

3.4.4 NMR and LC-MS studies

As described in sections 3.3.8, irradiation studies were carried out in the presence of 5'-GMP, as DNA is considered to be a possible target site for platinum anticancer drugs.

3.4.4.1 NMR and LC-MS studies of complexes [Pt(N₃)₂(OH)(Succ)(pyr)₂] **4** and [Pt(N₃)₂(OH)(Succ-(RGD)f)(pyr)₂] **7**

The irradiation of complexes **3** and **4** with 5'-GMP (2 mol eq) in PBS yielded the mono-GMP Pt(II) adduct in both cases. However 23% of GMP was bound to platinum in the case of **4**, whereas only 9% was bound in the case of compound **3**.

This result, along with the UV-Vis and EPR studies shows the enhanced photoactivity of the carboxylate *versus* the dihydroxo complexes. DFT calculations gave an insight into the enhanced photoactivity by showing that indeed this compound has dissociative transitions which can extend up to 469 nm. The photoproducts from the irradiation of compound *trans, trans, trans*-[Pt(N₃)₂(OH)(Succ)(pyr)₂] **4** at 463 nm (blue light) were characterised by ¹H-NMR, ¹⁹⁵Pt-NMR as well as LC-MS. As described previously, the release of succinate as well as azidyl radicals was observed (Figure 3.25 and Figure 3.21). The reduction of Pt(IV) to Pt(II) requires the gain of two electrons. However, the only radical detected by EPR was the azidyl radical. The loss of both azidyl radicals is excluded since the major product generated after irradiation is a mono-azido Pt(II) compound. Therefore, the second electron could originate from either the hydroxyl or the carboxylate ligands which could react rapidly with another radical or solvent molecule and thus be quenched.

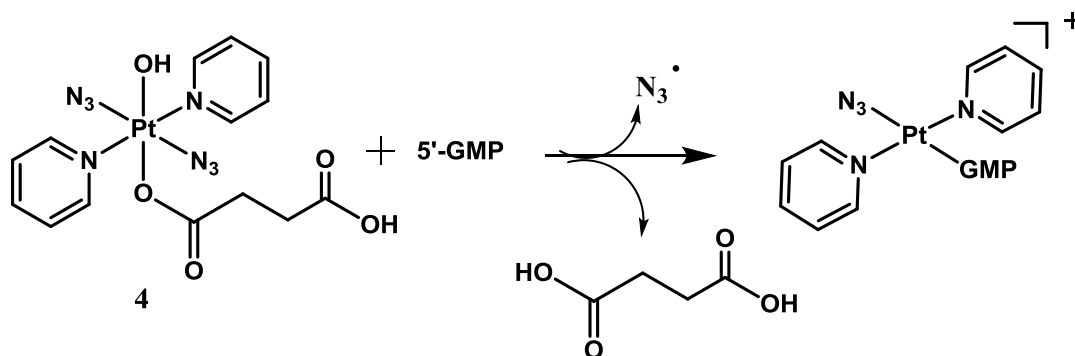


Figure 3.46: Scheme for the decomposition pathway of compound **4** leading to the major photoproduct which is the mono-azido GMP Pt(II) adduct.

The mono-GMP Pt(II) adduct *trans*-[Pt(N₃)(pyr)₂(GMP)] is formed in the first 10 minutes of the irradiation to an extent of 30% (refer to Figure 3.29). The assignment was easily confirmed as the ¹H and ¹⁹⁵Pt-NMR match those chemical

shifts assigned previously for *trans*-[Pt(pyr)₂(GMP)(N₃)].²⁶ Notably, in this reaction two products were formed: the first was the mono-azido GMP Pt(II) adduct which formed immediately after the light exposure. Further irradiation caused the percentage of this adduct to increase but also the appearance of a second product. Interestingly the intensity of the mono-azido GMP Pt(II) adduct reached a maximum of 30% and then it stayed intact upon further irradiation. This suggests that the Pt(II) mono-azido GMP adduct is not photolabile in the presence of blue light. This is an important result as it indicates that if DNA is photoplatinated in this way, the Pt(II)-DNA adducts will be stable.

The second photoproduct does not contain GMP, as there were no corresponding GMP resonances in the ¹H-NMR spectra. Moreover, it was observed that further irradiation produced an increase in the second photoproduct which was difficult to quantify due to the overlap and the broadness of the ¹H-NMR peaks.

It should be noted that irradiation with slightly shorter wavelength (420 nm *vs* 463 nm) did not result in any significant change in the photoproducts. Similar to the results obtained upon excitation at 463 nm, apart from the major GMP adduct, only very low intensity signals corresponding to other GMP adducts become visible in the ¹H-NMR spectra. When GMP was irradiated alone under similar conditions as a control, no change in its spectrum was observed (results not shown).

In order to aid the identification of the other photoproducts, an LC-MS analysis was carried out in the dark and after the irradiation of compound **4** in the presence of 2 mol equivalents of GMP. The majority of the HPLC peaks were assigned (Figure 3.31), with the exception of the peaks with *m/z* of 762.1009 (peak 4) and

762.1126 (peak 10). The 5'-GMP adducts observed after irradiation are listed below and are ordered from high to low peak abundance:

- *trans*-[Pt(N₃)(GMP)(pyr)₂]⁺, *m/z* 758.1164 (obs.=758.1160)
- *trans*-[Pt(ACN)(GMP)(pyr)₂]²⁺ or *trans*-[Pt(ACN)(GMP-H)(pyr)₂]⁺, *m/z* 378.5667 and 756.1259, respectively (obs.= 378.5668 and 756.1268). The acetonitrile was used as a solvent for the HPLC. In biological medium, this position could be occupied by another reactive molecule with affinity for platinum.
- *trans*-[Pt(GMP)₂(pyr)₂]²⁺, *m/z* 539.5820 (obs.= 539.5834))
- *trans*-[Pt₂(N₃)₂(GMP)(pyr)₄]⁺, *m/z* 1152.1727 (obs.= 1152.1686), in which GMP bridges between two platinum centres.

A different outcome occurs when the photoirradiation takes place in PBS, which contains 139 mM chloride. This prohibited the formation of a bis- GMP adduct since upon release of the second azide ligand, a chloride readily binds instead of a second 5'-GMP molecule (refer to Figure 3.33). Bednarski *et al* showed that the amount of platinated DNA was significantly reduced when the irradiation of *trans, trans, trans*-[Pt(N₃)₂(OH)₂(NH₃)₂] was carried out in the presence of 100 mM of Cl⁻, which reflects the extracellular chloride concentration.⁴⁸

Interestingly, another product identified by LC-MS was the [Pt(N₃)(pyr)₃]⁺, which can correlate with the presence of a pyridine containing photoproduct in the ¹H-NMR spectrum (assigned with rhombus in Figure 3.25). Furthermore, it is worth mentioning that after irradiation, the peak with the retention time corresponding to the starting complex 4 (at 11.9 min) is depleted. Peak 7 in Figure 3.31

corresponds to a $[M-N_3]^+$ species with m/z of 529.0750. The formation of such a species was observed in the mass spectrum even before irradiation, probably due to fragmentation in the mass spectrometer (Figure 3.32 A for the mass spectrum in the dark) but the molecular ion $[M+H]^+$ was still observed under those conditions. The lack of the aforementioned peak ($[M+H]^+$) after irradiation suggests that the azide was lost as an anion. The detected $[M-N_3]^+$ species appears at different retention time (11.0 min) than that observed in the dark (11.9 min). In this case, it may indicate a different coordination mode of the succinate, possibly acting as bideprotonated and bidentate chelating ligand to generate a metallacyclic Pt(IV) complex which would elute differently on the column. This could suggest that the azide is more labile than the axial ligands and its loss would occur before the dissociation of an axial ligand.

Photoirradiation of **7** showed that the peptide tethered to the succinate completely dissociates from the Pt(IV) complex after irradiation and elutes at 11.8 min. This is a significant result, as it shows that if the compound is delivered to tumour cells in the dark, then after irradiation the peptide will be released, allowing the azidyl radicals and the platinum centre to exert the cytotoxic mechanism. This result also shows that the release of the axial ligand will occur regardless of the type of functionality tethered at the end of the carboxylic acid.

3.4.4.2 NMR and LC-MS studies of compound *trans, trans, trans*- $[Pt(N_3)_2(OH)(N-MI)(pyr)_2]$ **6**

Irradiation of compounds **6** and *trans,trans,trans*- $[Pt(N_3)_2(OH)_2(pyr)_2]$ **3** (section 3.3.8.2), which were followed by 1H -NMR in a mixture of MeOD (75%) and D₂O

(25%) v/v, gave rise to some unexpected results. Firstly a very small percentage of GMP binding was observed and the release of pyridine occurred, especially upon irradiation with UVA. Pyridine release was not observed when complex **3** was irradiated with UVA light in an aqueous solution.²⁶

This stresses the effect of the solvent and the environment on the photodecomposition pathways of Pt(IV)-diazido anticancer drugs, suggesting that if these drugs accumulate in a hydrophobic, non-aqueous environment within the cell (e.g. membrane) different photoproducts can be expected. The release of pyridine from these drugs is not unexpected as DFT calculations performed on compound **3** had shown that the LUMO and LUMO+1 are strongly antibonding towards all ligands.

Assignment of irradiation photoproducts of **6** was aided by LC-MS, which detected as a product a $[M-N_3]^+$ species. Taking into account its charge, this can be assigned to a Pt(III) complex or to a metallacyclic product in which the N-methylantranilate ligand is bideprotonated and coordinates the Pt(IV) ion in a bidentate chelating mode. Pt(III) intermediates are not unusual in mass spectrometry, but the fact that this complex elutes from the HPLC column suggests that it is stable, and therefore may correspond to a metallacyclic Pt(IV) complex (as illustrated in Table 3.7). The major photoproducts detected by LC-MS were assigned to the axial ligand (N-MI) as well as to the $[Pt(pyr)_2(N_3)_2]$. Figure 3.47 summarizes a proposed scheme for the irradiation of compound **6**.

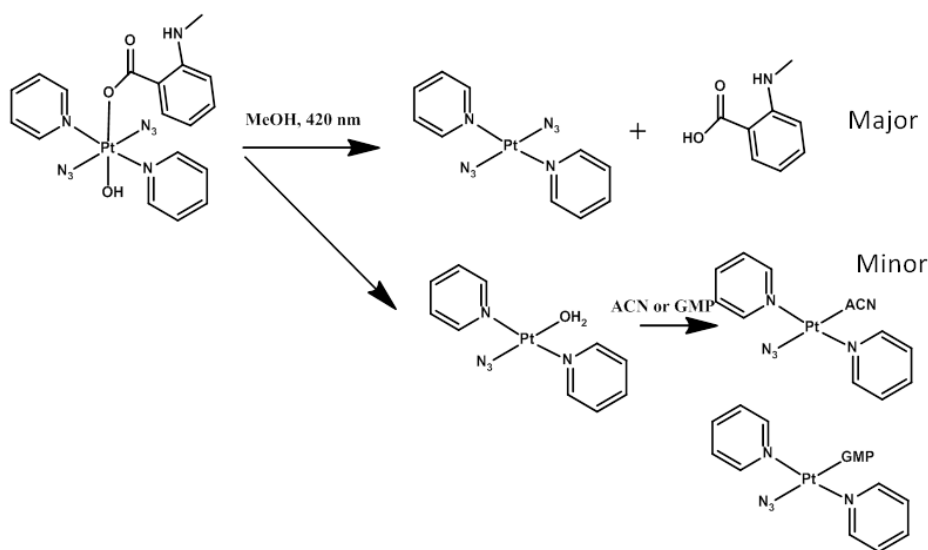


Figure 3.47: Scheme showing the photoproducts of the irradiation of compound **6** in MeOH as detected by LC-MS.

3.4.4.3 Fluorescence studies

The attachment of fluorescent tags to platinum compounds is useful to study their temporal and spatial distribution in living cells. Furthermore, fluorescent tags can act as antennas for light harvesting which can be useful in the development of phototherapeutic agents.⁶⁸ Frequently, the attachment of fluorescent tags to Pt(IV) occurs on the equatorial position and it results in fluorescence quenching. However when reduced to Pt(II), within the cell, fluorescence enhancement occurs.^{69,70}

Complex **6** bears a fluorescent tag (N-MI) in the axial position. The fluorescence emission spectrum of complex **6** shows a single broad band with maximum at 420 nm, similar to the maximum emission wavelength of the free ligand N-MIA. This band is independent of the excitation monitoring wavelength which suggests a

single emissive species in the excited state. These seem to indicate that the fluorescence of the ligand is quenched because of its binding to platinum. This becomes evident as there is an enhancement in the fluorescence emission at 420 nm upon repeated excitation at 320 nm due to the release of the ligand (Figure 3.30).

3.4.5 Cell studies

Complexes **4** *trans, trans, trans*-[Pt(N₃)₂(OH)₂(Succ)(pyr)₂] and **5** *trans, trans, trans*-[Pt(N₃)₂(OH)(Succ-Pr)(pyr)₂] showed promising photo-cytotoxicity towards ovarian cancer cells (A2780) using a low dose of blue light (420 nm, 5 J/cm²). The phototoxicity of **4** and **5** increased by 2-fold higher compared to compound **3**, *trans, trans, trans*-[Pt(N₃)₂(OH)₂(pyr)₂]. This suggests that although the photoproducts from complexes **3**, **4** and **5** are similar, the enhanced photoactivity that the carboxylate confers can result in greater amounts of the active Pt(II) products for a given irradiation dose. Complex **6**, *trans, trans, trans*-[Pt(N₃)₂(OH)(N-MI)(pyr)₂] was the least phototoxic with an IC₅₀ value of 12.1 μM. This is surprising as complex **6** shows *ca.* 10-fold greater uptake in comparison to the rest of the compounds. The reduced IC₅₀ may be related to the low yield of azidyl radicals or to the potential accumulation of the drug in hydrophobic environment within the cell (e.g. membranes) which could give rise to different photoproducts. In order to confirm the mechanism further, experiments would need to be carried out such as determining the subcellular distribution of the drug in comparison with a less hydrophobic drug, as well as azidyl radical quantification within cells. Cell uptake of **5** is *ca.* 2-fold higher than that of **4** in A2780 cells (from 15 to 25 ng/10⁶), which can be attributed to the

increased hydrophobicity from the propyl ester functionality in **5**. However an improvement in the cytotoxicity is not observed as the IC_{50} of these compounds is very close (3.6 μ M for **4** and 3.7 μ M for **5**). Interestingly, compound **4** produced a higher yield of azidyl radicals than **5** as determined by EPR experiments, which may compensate for the decreased cell uptake.

There is some correlation between the hydrophobicity of complexes **4-6** and increasing cell uptake. However compound **3** (dihydroxo) is the most hydrophilic-water-soluble complex in the series and yet its uptake surpasses that of complexes **4** and **5**.

The transport of molecules across the membrane of a cell can be either active (energy dependent) or passive (no energy dependent).⁷¹ Platinum drugs are generally thought to be taken up by both passive and active transport. Extensive efforts have been made to discover the uptake mechanisms for cisplatin and it was found that a family of copper transporters (Ctr1), which is used for the uptake of Cu, plays a major role.^{53,72,73} Organic cation transporters also constitute another class of transporters, responsible for the uptake of picoplatin in mice.⁷⁴ The importance of passive transport was for example exploited in the case of satraplatin, which may be the reason for circumventing cisplatin resistance by increased cellular uptake.⁵³

There is very little uptake of cisplatin (0.005 ng of Pt per 10^6 cells) over the range at 4 °C which shows that influx is energy-dependent.⁷⁵ However, complexes **3** and **6** were taken at a low temperature and with increasing temperature (from 4 °C to 18 °C), the influx increases. These results demonstrate that the uptake of these diazido drugs is a combination of passive and active transport. Passive transport is

enhanced greatly by the incorporation of an aromatic ligand in the axial position, as shown by complex **6**.

The net cellular accumulation of drugs into cells is a result of equilibrium between influx and efflux. Many efflux transporters are involved in the export of drugs. These include ATP7A, ATP7B, ES-X (Pt-glutathione conjugates), and the MDR efflux pump.^{76, 77} In order to estimate the optimum concentration at which maximum uptake occurs, concentration-dependent experiments were carried out. This can have significant implications in photodynamic therapy since pulsed light therapy is considered to be a clinical advantage compared to continuous light therapy.⁷⁸ With such a short light exposure, it is important to obtain the highest amount of drug within a cell. The optimum concentration for uptake for complexes **3** and **4** is 20 μM and 40 μM , respectively.

3.5 Conclusions

In this chapter complexes of the type *trans, trans, trans*-[Pt(N₃)₂(OH)(OCOR)(pyr)₂] (**4**, **5** and **6**), where OCOR is succinate, 4-oxo-4-propoxybutanoate and N-methylisatoate ligands have been synthesized and characterised by NMR, MS, UV-Vis and X-ray crystallography. Photoactivation studies comparing the three novel complexes with respect to the dihydroxo precursor *trans, trans, trans*-[Pt(N₃)₂(OH)₂(pyr)₂] **3** indicate a three-fold faster degradation kinetics when irradiated with green light (517 nm). EPR studies performed on equimolar aqueous solutions of complexes **3**, **4** and **5** showed that azidyl radicals were not produced in the case of **3** but produced to a concentration up to 69 and 56 μM for **4** and **5**, respectively. Complex **4** was also able to bind to 5'-GMP to an extent of 2.6 times greater than **3** when irradiated with the same

dose of 463 nm light (23% vs 9%). Incorporation of the cRGD-peptide moiety onto the free carboxylic acid of complex **4** yielded complex **7**. LC-MS studies undertaken on these two complexes upon blue light irradiation (420 nm) resulted in the release of the axial ligands (succinate for **4** and succinate-(RGD)f for **7**) yielding very similar photoproducts, with $[\text{Pt}(\text{N}_3)(\text{pyr})_2(5'\text{-GMP})]$ being the major.

Complex **6** bears the fluorescent ligand N-methylisatoate. Continuous fluorescent measurements, by exciting aqueous solution at 320 nm, resulted in an increase in fluorescence of the band at 420 nm possibly due to the release of the ligand. The complex has very low solubility in water (0.065 μM) thus prohibiting NMR or EPR studies in aqueous solutions. Irradiation studies (420 nm or UVA) in MeOD resulted in a mixture of products. The release of the axial ligand and pyridine (especially with UVA irradiation) was observed but no significant 5'-GMP binding.

Cellular uptake studies of complexes **3**, **4**, **5** and **6** on A2780 cells showed a dramatic increase in uptake of complex **6** (10-fold) with respect to **3** and a 1.7-fold when comparing **4** and **5**. Temperature dependence studies on **3** and **6** to elucidate whether passive or active transport takes place showed that active transport facilitates the influx of the drugs, as there is an increase in uptake upon increasing the temperature from 4 to 18 to 37 °C.

Phototoxicity studies with 420 nm irradiation on A2780 cells showed that complexes **4** and **5** (IC_{50} = 3.6 and 3.7 μM) were ~2-fold more active than **3** (IC_{50} = 6.7 μM) but complex **6** was the least active (12.1 μM). The lack of activity of the

latter could be attributed a low yield of azidyl radicals, as the N-MI ligand has the ability to quench those radicals.

References

1. M. D. Hall, C. T. Dillon, M. Zhang, P. Beale, Z. Cai, B. Lai, A. P. J. Stampfl, and T. W. Hambley, *J. Biol. Inorg. Chem.*, 2003, **8**, 726-32.
2. N. J. Wheate, S. Walker, G. E. Craig, and R. Oun, *Dalton Trans.*, 2010, **39**, 8113-8127.
3. *G.B. Inc, Orplanta, USA Food and Drug Administration*, 2007.
4. *Withdrawal assessment report for oplanta, European Medicines Agency*, 2008, 1-37.
5. H. P. Varbanov, S. M. Valiahdi, C. R. Kowol, M. A. Jakupec, M. Galanski, and B. K. Keppler, *Dalton Trans.*, 2012, **41**, 14404-14415.
6. J. Z. Zhang, E. Wexselblatt, T. W. Hambley, and D. Gibson, *Chem. Commun.*, 2012, **48**, 847-849.
7. C. F. Chin, Q. Tian, M. I. Setyawati, W. Fang, E. S. Q. Tan, D. T. Leong, and W. H. Ang, *J. Med. Chem.*, 2012, **55**, 7571-7582.
8. M. Ravera, E. Gabano, I. Zanellato, I. Bonarrigo, E. Escibano, V. Moreno, M. Font-Bardia, T. Calvet, and D. Osella, *Dalton Trans.*, 2012, **41**, 3313-3320.
9. S. Dhar and S. J. Lippard, *Proc. Natl. Acad. Sci. USA.*, 2009, **106**, 22199-22204.
10. A. Nemirovski, I. Vinograd, K. Takrouri, A. Mijovilovich, A. Rompel, and D. Gibson, *Chem. Commun.*, 2010, **46**, 1842-1844.
11. L. T. Ellis, H. M. Er, and T. W. Hambley, *Aust. J. Chem.*, 1994, **48**, 793-806.
12. M. D. Hall, S. Amjadi, M. Zhang, P. J. Beale, and T. W. Hambley, *J. Inorg. Biochem.*, 2004, **98**, 1614-1624.

13. J. Z. Zhang, E. Wexselblatt, T. W. Hambley, and D. Gibson, *Chem. Commun.*, 2012, **48**, 847-849.
14. C. M. Giandomenico, M. J. Abrams, B. a Murrer, J. F. Vollano, M. I. Rheinheimer, S. B. Wyer, G. E. Bossard, and J. D. Higgins, *Inorg. Chem.*, 1995, **34**, 1015-1021.
15. L. R. Kelland, B. A. Murrer, G. Abel, L. R. Rolland, C. M. Giandomenico, P. Mistry, and K. R. Harrap, *Cancer Res.*, 1992, **52**, 822-828.
16. A. Alvarez-Valdes, J. M. Perez, I. Lopez-Solera, R. Lannegrand, J. M. Continente, P. Amo-Ochoa, M. J. Camazon, X. Solans, M. Font-Bardia, and C. Navarro-Ranninger, *J. Med. Chem.*, 2002, **45**, 1835-1844.
17. K. R. Barnes, A. Kutikov, and S. J. Lippard, *Chem. Biol.*, 2004, **11**, 557-564.
18. S. Mukhopadhyay, C. M. Barnés, A. Haskel, S. M. Short, K. R. Barnes, and S. J. Lippard, *Bioconjugate Chem.*, 2008, **19**, 39-49.
19. N. Graf, T. E. Mokhtari, I. A. Papayannopoulos, and S. J. Lippard, *J. Inorg. Biochem.*, 2012, **110**, 58-63.
20. S. Abramkin, S. M. Valiahdi, M. A. Jakupiec, M. Galanski, N. Metzler-Nolte, and B. K. Keppler, *Dalton Trans.*, 2012, **41**, 3001-3005.
21. L. Gaviglio, A. Gross, N. Metzler-Nolte, and M. Ravera, *Metallomics*, 2012, **4**, 260-266.
22. X. Wang and Z. Guo, *Chem. Soc. Rev.*, 2013, **42**, 202-224.
23. P. J. Bednarski, F. S. Mackay, and P. J. Sadler, *Anticancer Agents Med. Chem.*, 2007, **7**, 75-93.
24. N. A. Kratochwil, M. Zabel, and P. J. Bednarski, *J. Med. Chem.*, 1996, **2**, 2499-2507.
25. H.-C. Tai, Y. Zhao, N. J. Farrer, A. E. Anastasi, G. Clarkson, P. J. Sadler, and R. J. Deeth, *Chem. Eur. J.*, 2012, **18**, 10630-10642.
26. N. J. Farrer, J. A. Woods, L. Salassa, Y. Zhao, K. S. Robinson, G. Clarkson, F. S. Mackay, and P. J. Sadler, *Angew. Chem. Int. Ed.*, 2010, **49**, 8905-8908.
27. S. Dhar, W. L. Daniel, D. A. Giljohann, C. A. Mirkin, and S. J. Lippard, *J. Am. Chem. Soc.*, 2009, **131**, 14652-14653.

28. A. Conte, H. Kuehne, T. Luebbers, P. Mattei, C. Maugeais, W. Mueller, and P. Pflieger, 2008, PCT/EP2007/050815.
29. F. Barragán, P. López-Senín, L. Salassa, S. Betanzos-Lara, A. Habtemariam, V. Moreno, P. J. Sadler, and V. Marchán, *J. Am. Chem. Soc.*, 2011, **133**, 14098-14108.
30. E. Arunan, G. R. Desiraju, R. A. Klein, J. Sadlej, S. Scheiner, I. Alkorta, D. C. Clary, R. H. Crabtree, J. J. Dannenberg, P. Hobza, H. G. Kjaergaard, A. C. Legon, B. Mennucci, and D. J. Nesbitt, *Pure Appl. Chem.*, 2011, **83**, 1637-1641.
31. J. W. Steed and J. L. Atwood, *Supramolecular Chemistry*, Wiley & Sons Inc., Chichester, 2nd edn., 2009.
32. C. Janiak, *Dalton Trans.*, 2000, 3885-3896.
33. M. Nishio, Y. Umezawa, K. Honda, S. Tsuboyama, and H. Suezawa, *CrystEngComm*, 2009, **11**, 1757-1788.
34. F. S. Mackay, S. A. Moggach, A. Collins, S. Parsons, and P. J. Sadler, *Inorg. Chim. Acta*, 2009, **362**, 811-819.
35. A. G. Sharpe, *Inorganic Chemistry*, Longman, London, New York, 1981.
36. F. S. Mackay, N. J. Farrer, L. Salassa, H.-C. Tai, R. J. Deeth, S. A. Moggach, P. A. Wood, S. Parsons, and P. J. Sadler, *Dalton Trans.*, 2009, **7**, 2315-2325.
37. V. P. Munk and P. J. Sadler, *Chem. Commun.*, 2004, **1**, 1788-1789.
38. A. Krežel and W. Bal, *J. Inorg. Biochem.*, 2004, **98**, 161-166.
39. B. S. Howerton, D. K. Heidary, and E. C. Glazer, *J. Am. Chem. Soc.*, 2012, **134**, 8324-8327.
40. K. Makino, T. Hagiwara, and A. Murakami, *Radiat. Phys. Chem.*, 1991, **37**, 657-665.
41. R. S. Partridge, S. M. Monroe, J. K. Parks, K. Johnson, J. Parker, W. Davis, G. R. Eaton, and S. S. Eaton, *Arch Biochem Biophys.*, 1994, **310**, 210-217.
42. G. R. Buettner, *Free Radic. Biol.*, 1988, **5**, 259-303.
43. M. Branch, *Can. J. Chem.*, 1980, **58**, 1592-1595.
44. H. I. A. Phillips, L. Ronconi, and P. J. Sadler, *Chem. Eur. J.*, 2009, **15**, 1588-1596.

45. L. Ronconi and P. J. Sadler, *Dalton Trans.*, 2011, **40**, 262-268.
46. A. F. Westendorf, J. A. Woods, K. Korpis, N. J. Farrer, L. Salassa, K. Robinson, V. Appleyard, K. Murray, R. Grünert, A. M. Thompson, P. J. Sadler, and P. J. Bednarski, *Mol. Cancer Ther.*, 2012, **11**, 1894-18904.
47. F. S. Mackay, J. A. Woods, H. Moseley, J. Ferguson, A. Dawson, S. Parsons, and P. J. Sadler, *Chem. Eur. J.*, 2006, **12**, 3155-3161.
48. A. F. Westendorf, A. Bodtke, and P. J. Bednarski, *Dalton Trans.*, 2011, **40**, 5342-5451.
49. L. Salassa, T. Ruiiu, C. Garino, A. M. Pizarro, F. Bardelli, D. Gianolio, A. Westendorf, P. J. Bednarski, C. Lamberti, R. Gobetto, and P. J. Sadler, *Organometallics*, 2010, **29**, 6703-6710.
50. A. Vlček and S. Zális, *Coord. Chem. Rev.*, 2007, **251**, 258-287.
51. M. Cossi, N. Rega, G. Scalmani, and V. Barone, *J. Comput. Chem.*, 2003, **24**, 669-681.
52. J. S. Butler, J. A. Woods, N. J. Farrer, M. E. Newton, and P. J. Sadler, *J. Am. Chem. Soc.*, 2012, **134**, 16508-16511.
53. M. D. Hall, M. Okabe, D.-W. Shen, X.-J. Liang, and M. M. Gottesman, *Annu. Rev. Pharmacol. Toxicol.*, 2008, **48**, 495-535.
54. M. Galanski and B. K. Keppler, *Inorg. Chem.*, 1996, **35**, 1709-1711.
55. W. H. Ang, S. Pilet, R. Scopelliti, F. Bussy, L. Juillerat-Jeanneret, and P. J. Dyson, *J. Med. Chem.*, 2005, **48**, 8060-9069.
56. J. J. Wilson and S. J. Lippard, *Inorg. Chem.*, 2011, **50**, 3103-3115.
57. B. R. Hoffmesiter, M. S. Adib-razavi, M. A. Jakupiec, M. Galanski, and B. K. Keppler, *Chem. Biodiversity*, 2012, **9**, 1840-1848.
58. G. T. Hermanson, *Bioconjugate Techniques*, Elsevier Academic Press, Amsterdam, 2008.
59. F. Danhier, A. Le Breton, and V. Préat, *Mol. Pharm.*, 2012, **9**, 2961-2973.
60. J.-P. Xiong, T. Stehle, R. Zhang, A. Joachimiak, M. Frech, S. L. Goodman, and M. A. Arnaout, *Science*, 2002, **296**, 151-155.
61. B. M. Still, P. G. A. Kumar, J. R. Aldrich-Wright, and W. S. Price, *Chem. Soc. Rev.*, 2007, **36**, 665-686.

62. A. Y. Sokolov and H. F. Schaefer, *Dalton Trans.*, 2011, **40**, 7571-7582.
63. Y. Shi, S.-A. Liu, D. J. Kerwood, J. Goodisman, and J. C. Dabrowiak, *J. Inorg. Biochem.*, 2012, **107**, 6-14.
64. M. Ravera, E. Gabano, I. Zanellato, I. Bonarrigo, E. Escribano, V. Moreno, M. Font-Bardia, T. Calvet, and D. Osella, *Dalton Trans.*, 2012, **41**, 313-120.
65. S. Jovanović, B. Petrović, Z. D. Bugarčić, and R. van Eldik, *Dalton Trans.*, 2013, **42**, 8890-88906.
66. S. Senapati, S. P. Das, and A. K. Patnaik, *Adv. Phys. Chem.*, 2012, **2012**, 1-5.
67. C. Gambetta, J. Natera, W. A. Massad, and N. A. García, *J. Photochem. Photobiol. A*, 2013, **269**, 27-33.
68. Q.-X. Zhou, W.-H. Lei, Y.-J. Hou, Y.-J. Chen, C. Li, B.-W. Zhang, and X.-S. Wang, *Dalton Trans.*, 2013, **42**, 2786-2791.
69. J. J. Wilson and S. J. Lippard, *Inorg. Chim. Acta*, 2012, **389**, 77-84.
70. E. J. New, R. Duan, J. Z. Zhang, and T. W. Hambley, *Dalton Trans.*, 2009, 3092-39101.
71. S. P. Oldfield, M. D. Hall, and J. A. Platts, *J. Med. Chem.*, 2007, **50**, 5227-5237.
72. D. Sinani, D. J. Adle, H. Kim, and J. Lee, *J. Biol. Chem.*, 2007, **282**, 26775-26785.
73. S. Ishida, J. Lee, D. J. Thiele, and I. Herskowitz, *Proc. Natl. Acad. Sci. USA.*, 2002, **99**, 14298-14302.
74. S. S. More, S. Li, S. W. Yee, L. Chen, Z. Xu, D. M. Jablons, and K. M. Giacomini, *Mol. Cancer Ther.*, 2010, **9**, 1058-1069.
75. I. Romero-Canelón, A. M. Pizarro, A. Habtemariam, and P. J. Sadler, *Metallomics*, 2012, **4**, 1271-1279.
76. Y. Jung and S. J. Lippard, *Chem. Rev.*, 2007, **107**, 1387-1407.
77. W. Jäeger, *Int. J. Clin. Pharmacol. Ther.*, 2009, **47**, 46-48.
78. I. Yoon, J. Z. Li, and Y. K. Shim, *Clin. Endosc.*, 2013, **46**, 7-23.

Chapter 4

**Photoactivatable Pt(IV)-
azido complexes bearing
aromatic N-heterocyclic
ligands**

4.1 Introduction

Early structure-activity relationships concluded that cytotoxic Pt(II) drugs should contain amines in *cis* geometry, the leaving group should be adequately bound (but not too strong) and that higher activity could be obtained with complexes having amine ligands with fewer substituents (NH_3 , primary or secondary amines).¹ These rules were revised when it was discovered that the use of pyridine-like ligands or substituted amines conferred cytotoxic activity in cisplatin resistant cell lines.^{1, 2} Examples of some promising pyridyl Pt(II) complexes are illustrated in Figure 4.1.

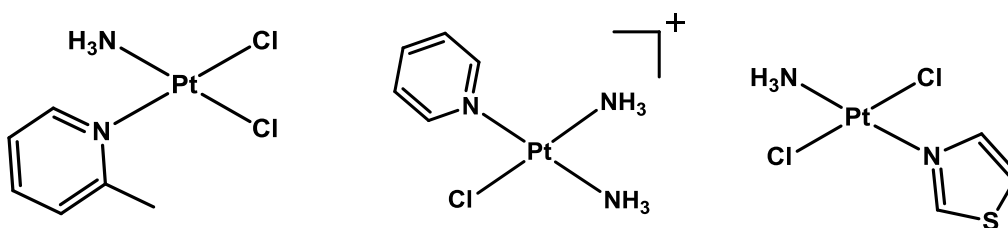


Figure 4.1: Potent Pt(II) compounds (picoplatin, pyriplatin and *trans*-(dichloroaminethiazole) platinum (II) with useful cytotoxic properties.

Picoplatin (AMD 473) was designed and synthesized specifically to tackle the problem of platinum drug deactivation due to reactions with S-donor molecules, such as glutathione, an effect which eventually leads to chemoresistance. A bulky 2-methylpyridine group close to the platinum centre reduced the rates of side reactions which diminish the potency of a drug.³ Picoplatin was designated as an orphan drug for the treatment of small cell lung cancer carcinoma in 2007.⁴

Pyriplatin has been studied in recent years by Lippard *et al*, where it was shown that it is significantly cytotoxic in a number of tumour cell lines. The

monofunctional adducts inhibit transcription and also elude DNA repair. Additionally its positive charge confers an uptake mechanism different to cisplatin (via organic cation transporters rather than copper transporters).⁵

Trans-[PtCl₂(NH₃)(thiazole)] developed by Farrell⁶ has shown the best combination of cytotoxicity and aqueous solubility and *in vivo* activity amongst compounds in this general structural family.⁷

Furthermore, it was shown by Gibson *et al.* that sterically-hindered complexes such as *trans*-[PtCl₂(4-pic)(piperazine)]HCl are very cytotoxic towards cancer cells and also have a mechanism of action distinctive from cisplatin.⁸

The aforementioned compounds illustrate the significance of planar heterocyclic ligands in affording Pt(II) drugs with different pharmacological properties (e.g. uptake, solubility, type of DNA lesions) and consequent overcoming multifactorial cisplatin resistance.

In the case of Pt(IV)-diazido photoactivatable complexes, it was established that the molecules with the N-donor ligands in *trans* geometry were more cytotoxic than their *cis* isomers.⁹ Moreover, replacing aliphatic amines with pyridines was extremely beneficial for extending the phototoxic activity of the molecule to longer -and consequently more clinically relevant- wavelengths of activation. *Trans, trans, trans*-[Pt(pyr)₂(N₃)₂(OH)₂] and *trans, trans, trans*-[Pt(pyr)(NH₃)(N₃)₂(OH)₂] are phototoxic with blue and UVA light, respectively.^{10,11} These structure-activity relationships demonstrated that having N-heterocyclic amines in a *trans* geometry is a promising combination that needs to be explored for the development and the fine-tuning of this class of compounds. Furthermore, upon irradiation (and reduction from Pt(IV) to Pt(II)), the N-

heterocyclic aromatic ligands remain coordinated to the Pt(II) centre, which is thought to be important for retention of the anticancer activity of the Pt(II) species. Hence in this present study Pt(IV) diazido complexes were designed with N-heterocyclic ligands, which if retained in Pt(II) photoproducts could have advantageous cytotoxic properties.

The aims of this chapter was to synthesize a variety of Pt(IV)-diazido complexes, bearing planar N-heterocyclic amine ligands and to study their photodecomposition. Some of the planar amines chosen (e.g. pyridine, 2-picoline, 4-picoline, thiazole and 1-methylimidazole) were inspired by those in known cytotoxic Pt(II) compounds. In this chapter, the synthesis, characterisation and photodecomposition studies of the following complexes (structures can be found in Appendix) will be described: *trans,trans,trans*-[Pt(N₃)₂(OH)₂(2-picoline)(pyridine)]-**18**, *trans,trans,trans*-[Pt(N₃)₂(OH)₂(3-picoline)(pyridine)]-**19**, *trans,trans,trans*-[Pt(N₃)₂(OH)₂(4-picoline)(pyridine)]-**20**, *trans,trans,trans*-[Pt(N₃)₂(OH)₂(3-picoline)₂]-**23**, *trans,trans,trans*-[Pt(N₃)₂(OH)₂(4-picoline)₂]-**26**, *trans,trans,trans*-[Pt(N₃)₂(OH)₂(thiazole)₂]-**29**, *trans,trans,trans*-[Pt(N₃)₂(OH)₂(1-methylimidazole)₂]-**32**.

4.2 Experimental

Caution! While no problems were encountered during this work, heavy metal azides are known to be shock sensitive detonators; therefore it is essential that any Pt-azido compound is handled with care. The Pt-diazido complexes were handled under dim lighting conditions.

4.2.1 Materials

All materials were used as obtained from commercial sources unless otherwise stated. K_2PtCl_4 was obtained from Precious Metal Online and Alfa Aesar, KI, NaCl from Fisher Scientific, $AgNO_3$ from Fluka, NaN_3 , H_2O_2 (30%) and all other chemicals from Sigma-Aldrich. The solvents used were analytical reagent grade from Fisher Scientific and were used as supplied. Inorganic membrane filters were purchased from Sartorius stedim biotech.

4.2.2 Methods

4.2.2.1 HPLC

HPLC for purity testing for complexes **18-20**, **26** and **29** was carried out using the column ZORBAX Eclipse Plus C_{18} (5 μm pore size, 150 \times 4.6 mm dimensions) with 1 mL/min flow rate and 45 μl injection volume. The method employed is summarized in Table 4.1. The mobile phase was $H_2O/MeOH$ with 0.1% TFA. The wavelength of detection was 254 nm.

Purity tests for complexes **23** and **32** were carried out in the same manner as for **4-6** in Chapter 3.

Table 4.1: HPLC elution gradient for the purity testing of compounds **18-20**, **26** and **29**, where B is MeOH (with 0.1% TFA) and the rest is H_2O (0.1% TFA).

Time (min)	%B
0	7
5	7
21	90
25	90
25.01	7
30	7

4.2.2.2 Extinction coefficient determination

Extinction coefficients were determined as outlined in Chapter 2. For the shorter wavelengths, solutions of *ca.* 70 and 50 μM were used whereas for the longer wavelengths the concentrations employed were *ca.* 2 mM and 1 mM, except in the case of *trans, trans, trans*-[Pt(N₃)₂(OH)₂(tz)₂], where a solution of 0.6 mM was used.

4.2.2.3 X-Ray Diffraction

The X-ray crystal structures of **20**, **23**·CH₃OH, **26**·CH₃OH and **32**·0.5H₂O were solved by Dr Guy Clarkson, as described in Chapter 2.

4.2.2.4 DFT calculations

The DFT and TDDFT calculations for complex **18** were carried out by Dr Luca Salassa, as outlined in Chapter 2.

4.2.2.5 Synthesis and Characterisation

Complexes **8-11**, **21**, **24**, **27** and **30** have been synthesized using the Kauffman method with the use of concentrated HCl.¹² Complexes **8-11**, **21**, **24** have been reported previously by Rochon¹³ and complexes **27** and **30** have been synthesized and studied by Farrell.¹⁴

4.2.2.5.1 *Cis*-[Pt(I)₂(pyridine)₂] (**8**)

K₂PtCl₄ (0.500 g, 1.21 mmol) was suspended in H₂O (38 mL) and KI (2.0 g, 12.05 mmol) was added and allowed to react under stirring for 1 h at room temperature. Pyridine (0.194 mL, 2.41 mmol) was added and the mixture was stirred under room temperature for 24 h. The dark yellow solid was isolated via

filtration under suction and washed with ice cold water, ethanol and diethyl ether. Then it was left to dry overnight under vacuum (Yield = 0.724 g, 99 %).

$^1\text{H-NMR}$ (CD_2Cl_2 , 400 MHz, ppm): $\delta = 8.84$ (dd, $^3J_{195\text{Pt}1\text{H}} = 39.90$ Hz, $^3J_{1\text{H}1\text{H}} = 6.70$ Hz, 2H, H_o), $\delta = 7.82$ (t, $^3J_{1\text{H}1\text{H}} = 7.61$ Hz, 1H, H_p), $\delta = 7.34$ (t, $^3J_{1\text{H}1\text{H}} = 6.68$ Hz, 2H, H_m).

4.2.2.5.2 *Cis*-[Pt(Cl) $_2$ (pyridine) $_2$] (9)

Cis-[Pt(I) $_2$ (pyr) $_2$] (0.7229 g, 1.19 mmol) was suspended in H_2O (143 mL) and AgNO_3 (0.401 g, 2.36 mmol) was added. The mixture was allowed to react under reflux for 24 h at 60 °C, to yield a yellow precipitate (AgI). The AgI was removed by centrifugation, followed by filtration through celite on frit, then NaCl (0.696 g, 11.91 mmol) was added and the reaction was carried out for 24 h at room temperature. The pale yellow solid was isolated by filtration and washed with cold water, ethanol and diethyl ether (Yield= 0.39 g, 77 %).

$^1\text{H-NMR}$ (CDCl_3 , 400 MHz, ppm): $\delta = 8.76$ (dd, $^3J_{195\text{Pt}1\text{H}} = 36.54$ Hz, $^3J_{1\text{H}1\text{H}} = 6.81$ Hz, 2H, H_o), $\delta = 7.84$ (t, $^3J_{1\text{H}1\text{H}} = 7.69$ Hz, 1H, H_p), $\delta = 7.33$ (t, $^3J_{1\text{H}1\text{H}} = 6.90$ Hz, 2H, H_m).

4.2.2.5.3 *Cis*-[Pt(I) $_2$ (2-picoline) $_2$] (10)

K_2PtCl_4 (0.200 g, 0.48 mmol) was suspended in H_2O (110 mL), KI (0.800 g, 4.82 mmol) was added and the reaction was left to stir for 40 min at room temperature. 2-picoline (0.095 mL, 0.96 mmol) was added and the reaction mixture was stirred for 24 h at 40 °C. The dark yellow solid was collected by filtering under vacuum and washed with cold water, ethanol and diethyl ether (Yield=0.268 g, 88%).

^1H -NMR (acetone- d_6 , 600 MHz, ppm), $\delta = 9.26$ (dd, $^3J_{195\text{Pt}1\text{H}} = 31.5$ Hz, $^3J_{1\text{H}1\text{H}} = 6.0$ Hz, 1H, H_6 or $\text{H}_{6'}$), $\delta = 9.12$ (dd, $^3J_{195\text{Pt}1\text{H}} = 31.40$ Hz, $^3J_{1\text{H}1\text{H}} = 5.9$ Hz, 1H, H_6 or $6'$), $\delta = 7.80$ (t, $^3J_{1\text{H}1\text{H}} = 7.0$ Hz, 1H, H_4 or $4'$), $\delta = 7.79$ (t, $^3J_{1\text{H}1\text{H}} = 7.0$ Hz, 1H, H_4 or $4'$), $\delta = 7.48$ (m, $^3J_{1\text{H}1\text{H}} = 6.7$ Hz, 2H, H_3 and $3'$), $\delta = 7.37$ (t, $^3J_{1\text{H}1\text{H}} = 6.8$ Hz, 1H, H_5 or $5'$), $\delta = 7.33$ (t, $^3J_{1\text{H}1\text{H}} = 6.6$ Hz, 1H, H_5 or $5'$), $\delta = 3.34$ (s, 3H, CH_3), $\delta = 3.25$ (s, 3H, CH_3).

4.2.2.5.4 *Cis*-[Pt(Cl) $_2$ (2-picoline) $_2$] (11)

Cis-[Pt(I) $_2$ (2-pic) $_2$] (0.212 g, 0.34 mmol) was suspended in H_2O (54 mL), AgNO_3 (0.112 g, 0.66 mmol) was added and the reaction was stirred under reflux at 60°C for 24 h. The AgCl formed was removed by filtration under suction using celite on a frit and also Inorganic Membrane filter to ensure complete removal of traces of AgCl . NaCl (0.195 g, 3.34 mmol) was added and the reaction was left to stir for 24 h at ambient temperature. The pale yellow solid was isolated by filtration under suction and washed with cold water, ethanol and diethyl ether (Yield= 0.104 g, 68%).

^1H -NMR (acetone- d_6 , 400 MHz, ppm): $\delta = 9.1$ ppm (broad peak, 2H, H_6), $\delta = 7.8$ (t, $^3J_{1\text{H}1\text{H}} = 7.8$ Hz, 2H, H_4), $\delta = 7.5$ (d, $^3J_{1\text{H}1\text{H}} = 7.7$ Hz, 2H, H_3), $\delta = 7.3$ (broad peak, 2H, H_5), $\delta = 3.2$ (s, 6H, CH_3).

4.2.2.5.5 Synthesis of mixed pyridine complexes

Trans-[Pt(Cl) $_2$ (pyridine)(*n*-picoline)], where *n*=2, 3 or 4

Cis-[Pt(Cl) $_2$ (pyr) $_2$] (0.200 g, 0.47 mmol) was suspended in H_2O (60 mL) and then *n*-picoline (4 eq, 0.176 g, 1.89 mmol in the case of 2-picoline and 2 eq, 0.044 g, 0.473 mmol for 3- and 4-picolines) was added and the solution was stirred at 75°C overnight. When the solution turned colourless (~12 h for 2-picoline and 2 h

for 3- and 4-picoline), the water was removed by rotary evaporation. The residual white solid was washed with diethyl ether to remove the excess ligand. Then, HCl (2 M, 1.3 mL) and H₂O (8 mL) were added and the reaction was allowed to proceed for 4 days at 70 °C. The pale yellow solid was isolated by filtration and washed with water, ethanol and diethyl ether.

***Trans*-[Pt(Cl)₂(pyr)(2-pic)] (12)**

Yield = 0.155 g, 75%.

¹H-NMR (acetone-d₆, 600 MHz, ppm): δ = 8.94 (dd, ³J_{195Pt1H} = 16.02 Hz ³J_{1H1H} = 5.09 Hz, 2H, H₈), δ = 8.87 (d, ³J_{1H1H} = 5.53 Hz, 1H, H₆), δ = 8.02 (t, ³J_{1H1H} = 7.76 Hz, 1H, H₁₀), δ = 7.84 (t, ³J_{1H1H} = 7.67 Hz, 1H, H₄), δ = 7.52 (m, 2H, H₉, H₃), δ = 7.34 (t, ³J_{1H1H} = 6.70 Hz, 1H, H₅), δ = 3.25 (s, 3H, CH₃).

¹³C-NMR (acetone-d₆, 150 MHz, ppm): δ = 161.9 (C₂), δ = 154.4 (C₆), δ = 154.08 (C₈), δ = 139.4 (C₁₀), δ = 139.0 (C₄), δ = 126.8 (C₃), δ = 126.0 (C₉), δ = 123.2 (C₅), δ = 26.3 ppm (C_{CH3}).

[ESI-MS] = [M+Na]⁺, [2M+Na]⁺ (*m/z*) Calc., 461.0, 899.0; Found, 460.9, 898.9

***Trans*-[Pt(Cl)₂(pyr)(3-pic)] (13)**

Yield = 0.135 g, 65%.

¹H-NMR (acetone-d₆, 600 MHz, ppm): δ = 8.89 (d, ³J_{195Pt1H} = 13.20 Hz ³J_{1H1H} = 6.76 Hz, 2H, H₈), δ = 8.70 (d, ³J_{195Pt1H} = 13.53 Hz, H₂), δ = 8.68 (d, ³J_{1H1H} = 5.93 Hz, 1H, H₆), δ = 8.02 (t, ³J_{1H1H} = 7.66 Hz, 1H, H₁₀), δ = 7.83 (t, ³J_{1H1H} = 7.79 Hz, 1H, H₄), δ = 7.52 (t, ³J_{1H1H} = 6.47 Hz, 2H, H₉), δ = 7.39 (t, ³J_{1H1H} = 6.81 Hz, 1H, H₅), δ = 2.41 (s, 3H, CH₃).

^{13}C -NMR (acetone- d_6 , 150 MHz, ppm): δ =155.3 (C_8), δ =155.2 (C_2), δ =152.5 (C_6), δ =141.1 (C_2), δ =140.5 (C_{10}), δ = 136.22 (C_3), δ = 127.1 (C_9), δ =126.4 (C_5), δ =19.0 (C_{CH_3}).

[ESI-MS]= $[\text{M}+\text{Na}]^+$, $[\text{2M}+\text{Na}]^+$ (m/z) Calc., 461.0, 899.0; Found, 460.9, 898.9

***Trans*-[Pt(Cl) $_2$ (pyr)(4-pic)] (14)**

Yield = 0.140 g, 67%.

^1H -NMR (acetone- d_6 , 600 MHz, ppm): δ = 8.89 (dd, $^3J_{195\text{Pt}1\text{H}}$ = 15.77 Hz, $^3J_{1\text{H}1\text{H}}$ = 5.9 Hz, 2H, H_6), δ = 8.69 (dd, $^3J_{195\text{Pt}1\text{H}}$ = 15.22 Hz, $^3J_{1\text{H}1\text{H}}$ = 6.5 Hz, 2H, H_2), δ = 8.02 (t, $^3J_{1\text{H}1\text{H}}$ =7.8 Hz, 1H, H_8), δ = 7.51 (t, $^3J_{1\text{H}1\text{H}}$ =6.7 Hz, 2H, H_7), δ = 7.33 (d, $^3J_{1\text{H}1\text{H}}$ =6.1 Hz, 2H, H_3), δ = 2.47 (s, 3H, CH_3).

^{13}C -NMR (acetone- d_6 , 150 MHz, ppm): δ = 155.3 (C_5), δ = 154.4 (C_2), δ = 152.9 (C_4), δ = 140.5 (C_7), δ = 127.8 (C_3), δ = 127.1 (C_6), δ = 21.7 (C_{CH_3}).

[ESI-MS]= $[\text{M}+\text{Na}]^+$, $[\text{2M}+\text{Na}]^+$ (m/z) Calc., 461.0, 899.0; Found, 460.9, 898.9

4.2.2.5.6 *Trans*-[Pt(N $_3$) $_2$ (pyr)(n-pic)]

Trans-[Pt(Cl) $_2$ (pyr)(n-pic)] (0.155 g, 0.35 mmol; 0.245 g, 0.56 mmol; 0.24 g, 0.55 mmol for 2-, 3- and 4-picoline, respectively) were suspended in H_2O (204 mL per 1 g). AgNO_3 (2 mol eq) was added and the reaction was carried out at 60 $^\circ\text{C}$ for 24 h. The AgCl was removed by filtration on celite on frit and also through an Ionic Membrane (IM) filter. NaN_3 (10 mol eq) was added and the mixture was allowed to stir for 24 h at 40 $^\circ\text{C}$. The yellow solid was isolated and washed with cold water, ethanol and diethyl ether. Recrystallisation of these complexes was carried out by dissolving the solid in hot MeOH (50 $^\circ\text{C}$, ~0.5 g/L) and then allowing the solution to stand at -20 $^\circ\text{C}$.

***Trans*-[Pt(N₃)₂(pyr)(2-pic)] (15)**

Yield = 0.1029 g, 64%.

¹H-NMR (acetone-d₆, 400 MHz, ppm): δ = 9.07 (dd, ³J_{1H1H} = 6.0 Hz, ³J_{195Pt1H} = 32.0 Hz, 1H, H₄), δ = 8.77 (dd, ³J_{1H1H} = 5.5 Hz, ³J_{195Pt1H} = 39.0 Hz, 2H, H₅), δ = 8.11 ppm (t, ³J_{1H1H} = 7.5 Hz, 1H, H₇), δ = 7.96 (t, ³J_{1H1H} = 7.8 Hz, 1H, H₂), δ = 7.68 (d, ³J_{1H1H} = 7.8, 1H, H₁), δ = 7.60 (t, ³J_{1H1H} = 6.8 Hz, 2H, H₆), δ = 7.52 (t, ³J_{1H1H} = 7.0 Hz, 1H, H₃), δ = 3.31 (s, CH₃).

¹³C-NMR (acetone-d₆, 150 MHz, ppm): δ = 161.9 (C₂), δ = 154.3 (C₄), δ = 152.4 (C₈), δ = 140.0 (C₁₀), δ = 139.8 (C₄), δ = 127.5 (C₃), δ = 126.4 (C₉), δ = 124.5 (C₅), δ = 25.8 (C_{CH3}).

¹⁹⁵Pt-NMR (acetone-d₆, 129 MHz): δ = -2118 ppm.

[ESI-MS] = [M+Na]⁺ (*m/z*) Calc., 474.0; Found, 473.9.

***Trans*-[Pt(N₃)₂(pyr)(3-pic)] (16)**

Yield = 0.177 g, 70 %.

¹H-NMR (acetone-d₆, 600 MHz, ppm): δ = 8.84 (dd, ³J_{1H1H} = 5.1 Hz, ³J_{195Pt1H} = 32.0 Hz, 2H, H₈), δ = 8.68 (s, 1H, H₂), δ = 8.65 (d, ³J_{1H1H} = 5.8 Hz, 1H, H₆), δ = 8.12 (t, ³J_{1H1H} = 7.4 Hz, 1H, H₁₀), δ = 7.92 (d, ³J_{1H1H} = 7.8, 1H, H₄), δ = 7.66 (t, ³J_{1H1H} = 6.9 Hz, 2H, H₉), δ = 7.54 (t, ³J_{1H1H} = 7.1 Hz, 1H, H₅), δ = 2.46 (s, 3H, CH₃).

¹⁹⁵Pt-NMR (acetone-d₆, 129 MHz): δ = -2120 ppm.

[ESI-MS] = [M+Na]⁺ (*m/z*) Calc., 474.0; Found, 473.9.

***Trans*-[Pt(N₃)₂(pyr)(4-pic)] (17)**

Yield = 0.167 g, 66%.

¹H-NMR (acetone-d₆, 600 MHz, ppm): δ= 8.85 (dd, ³J_{1H1H}=5.7 Hz, ³J_{195Pt1H}=30.0 Hz, 2H, H₆), δ= 8.66 (dd, ³J_{1H1H}=5.8 Hz, 2H, H₂), δ= 8.11 (t, ³J_{1H1H}=7.77 Hz, 1H, H₈), δ= 7.65 (t, ³J_{1H1H}=6.5 Hz, 2H, H₇), δ= 7.48 (d, ³J_{1H1H}= 5.6, 1H, H₂), δ= 2.52 (s, 3H, CH₃).

¹⁹⁵Pt-NMR (acetone-d₆, 129 MHz): δ= -2117 ppm.

[ESI-MS]= [M+Na]⁺ (*m/z*) Calc., 474.0; Found, 473.9.

4.2.2.5.7 *Trans, trans, trans*-[Pt(N₃)₂(OH)₂(pyr)(n-pic)]

Trans-[Pt(N₃)₂(pyr)(n-pic)] (0.084 g, 0.18 mmol; 0.138 g, 0.30 mmol; 0.108 g, 0.18 mmol for 2-, 3- and 4-picoline, respectively) was suspended in H₂O₂ (30% v/v, 70 mL per 1 g) and the reaction was allowed to proceed at 45 °C for 3 hours. A bright yellow solution formed, which was filtered using an Inorganic Membrane filter to remove any unreacted starting material or insoluble side products. Then, the H₂O₂ was removed by lyophilization. To isolate the final product, the residual yellow precipitate was suspended in the minimum amount of warm ethanol (45 °C) and then it was allowed to precipitate upon addition of diethyl ether (3-fold) at -20 °C. Crystals suitable for X-ray diffraction were obtained for **20** via this method.

***Trans, trans, trans*-[Pt(N₃)₂(OH)₂(pyr)(2-pic)] (18)**

Yield = 0.023 g, 25%.

¹H-NMR (D₂O, 700 MHz, ppm): δ= 8.78 (d, ³J_{1H1H}=6.4 Hz, 1H, H₆), δ= 8.73 (d, ³J_{1H1H}= 6.0 Hz, 2H, H₈), δ= 8.26 (t, ³J_{1H1H}= 7.1 Hz, 1H, H₁₀), δ= 8.06 (t, ³J_{1H1H}=

7.6 Hz, 1H, H₄), δ = 7.80 (t, $^3J_{\text{IH1H}}$ = 6.5, 2H, H₉), δ = 7.60 (d, $^3J_{\text{IH1H}}$ =6.8 Hz, 1H, H₃), δ = 7.56 (t, $^3J_{\text{IH1H}}$ =7.0 Hz, 1H, H₅), δ = 3.32 (s, 3H, CH₃).

^{13}C -NMR (D₂O, 175 MHz, ppm): δ = 163.3 (C₂), δ = 152.8 (C₆), δ = 149.8 (C₈), δ = 143.2 (C₁₀), δ = 142.3 (C₄), δ =130.1 (C₃), δ = 127.6 (C₉), δ = 124.8 (C₅), δ = 22.9 (C_{CH3}).

^{195}Pt -NMR (D₂O, 129 MHz): δ = 1132 ppm.

[ESI-MS]= [M+Na]⁺ (m/z) Calc., 508.0; Found, 508.1.

HPLC purity= 90%.

$\epsilon_{297\text{ nm}}$ =20091 M⁻¹cm⁻¹, $\epsilon_{268\text{ nm}}$ =16061 M⁻¹cm⁻¹ (H₂O).

***Trans, trans, trans*-[Pt(N₃)₂(OH)₂(pyr)(3-pic)] (19)**

Yield = 0.073 g, 49%.

^1H -NMR (D₂O, 600 MHz, ppm): δ = 8.83 (dd, $^3J_{\text{IH1H}}$ = 5.9 Hz, $^3J_{195\text{Pt1H}}$ = 32.0 Hz, 2H, H₈), δ = 8.64 (s, 1H, H₂), δ = 8.63 (d, $^3J_{\text{IH1H}}$ =7.0 Hz, 1H, H₆), δ = 8.31 (t, $^3J_{\text{IH1H}}$ = 7.5 Hz, 1H, H₁₀), δ = 8.14 (d, $^3J_{\text{IH1H}}$ = 7.8, 1H, H₄), δ = 7.85 (t, $^3J_{\text{IH1H}}$ = 7.0 Hz, 2H, H₉), δ = 7.72 (t, $^3J_{\text{IH1H}}$ = 7.0 Hz, 1H, H₅), δ = 2.56 (s, 3H, CH₃).

^{13}C -NMR (D₂O, 150 MHz, ppm): δ = 150.93 (C₈), δ = 150.65 (C₂), δ = 148.00 (C₆), δ = 144.58 (C₄), δ = 144.08 (C₁₀), δ = 139.64 (C₃), δ = 128.65 (C₉), δ = 127.92 (C₅), δ = 19.32 (C_{CH3}).

^{195}Pt -NMR (D₂O, 129 MHz): δ = 954 ppm.

[ESI-MS]= [M+Na]⁺ (m/z) Calc., 508.0; Found, 508.0.

HPLC purity= 88%.

$\epsilon_{294\text{ nm}}$ =18258 M⁻¹cm⁻¹, $\epsilon_{268\text{ nm}}$ =13467 M⁻¹cm⁻¹ (H₂O).

***Trans, trans, trans*-[Pt(N₃)₂(OH)₂(pyr)(4-pic)] (20)**

Yield = 0.074 g, 50%.

¹H-NMR (D₂O, 600 MHz, ppm): δ = 8.78 (dd, ³J_{1H1H} = 5.9 Hz, ³J_{195Pt1H} = 48 Hz, 2H, H₆), δ = 8.59 (d, dd, ³J_{1H1H} = 6.1 Hz, ³J_{195Pt1H} = 52 Hz, 2H, H₂), δ = 8.27 (t, ³J_{1H1H} = 6.9 Hz, 1H, H₈), δ = 7.81 (t, ³J_{1H1H} = 6.4 Hz, 2H, H₇), δ = 7.63 (d, ³J_{1H1H} = 6.1 Hz, 2H, H₃), δ = 2.60 (s, 3H, CH₃).

¹³C-NMR (D₂O, 150 MHz, ppm): δ = 158.65 (C₄), δ = 149.97 (C₆), δ = 148.94 (C₂), δ = 143.14 (C₈), δ = 128.48 (C₃), δ = 127.71 (C₇), δ = 21.14 (C_{CH3}).

¹⁹⁵Pt-NMR (D₂O, 129 MHz): δ = 957 ppm.

[ESI-MS] = [M+Na]⁺ (*m/z*) Calc., 508.0; Found, 508.1.

HPLC purity = 91%.

ε_{295 nm} = 18955 M⁻¹cm⁻¹, ε_{258 nm} = 12535 M⁻¹cm⁻¹ (H₂O).

4.2.2.5.8 *Trans*-[Pt(Cl)₂(3-pic)₂] (21)

K₂PtCl₄ (0.700 g, 1.69 mmol) was dissolved in H₂O (55 mL) and 3-picoline (50 eq, 7.51 mL) was added. The solution was allowed to react under reflux at 100 °C for 24 h. The water and excess ligand were evaporated and the white residue was washed with diethyl ether. Then HCl (2 M, 24 mL) was added and the reaction proceeded for 48 h at 85 °C. The yellow precipitate was collected by filtration (Yield = 0.706 g, 93%).

¹H-NMR (CDCl₃, 400 MHz, ppm): δ = 8.72 (s, 2H, H₂), δ = 8.69 (d, ³J_{1H1H} = 5.50 Hz, 2H, H₆), δ = 7.57 (d, ³J_{1H1H} = 8.02 Hz, 2H, H₄), δ = 7.19 (t, ³J_{1H1H} = 6.72 Hz, 2H, H₅), δ = 2.37 (s, 6H, CH₃).

4.2.2.5.9 *Trans*-[Pt(N₃)₂(3-pic)₂] (22)

Trans-[Pt(Cl)₂(3-pic)₂] (0.700 g, 1.55 mmol) was dissolved in DMF (30 mL), NaN₃ (20 eq, 2.013 g) was added and the reaction was stirred for 4 days at 35 °C. Work up of the reaction was carried out by the addition of diethyl ether (60 mL) and precipitation of the solid at -20 °C (Yield= 0.400 g, 55%).

¹H-NMR (CDCl₃, 400 MHz, ppm): δ= 8.63 (s, 2H, H₂), δ= 8.61 (d, ³J_{IH1H}= 6.45 Hz, 2H, H₆), δ= 7.66 (d, ³J_{IH1H}= 7.82 Hz, 2H, H₄), δ= 7.33 (t, ³J_{IH1H}= 6.77 Hz, 2H, H₅), δ= 2.43 (s, 6H, CH₃).

[ESI-MS]= [M+Na]⁺ (*m/z*) Calc., 488.1; Found, 488.0.

4.2.2.5.10 *Trans, trans, trans*-[Pt(N₃)₂(OH)₂(3-pic)₂] (23)

Trans-[Pt(N₃)₂(3-pic)₂] (0.350 g, 0.75 mmol) was suspended in H₂O₂ (51 mL) and the reaction allowed to react at 50 °C for 5 h, at which point the solution turned transparent. The work up of the reaction was carried out as described in section 4.2.2.5.7. Crystals suitable for X-ray diffraction were obtained by slow evaporation of a solution of the complex in MeOH/DCM at room temperature.

¹H-NMR (D₂O, 500 MHz, ppm): δ= 8.60 (s, 2H, H₂), δ= 8.59 (d, ³J_{IH1H}= 5.54 Hz, 2H, H₆), δ= 8.10 (d, ³J_{IH1H}= 7.76 Hz, 2H, H₄), δ= 7.68 (t, ³J_{IH1H}= 7.10 Hz, 2H, H₅), δ= 2.52 (s, 6H, CH₃).

¹³C-NMR (D₂O, 125 MHz, ppm): δ= 149.74 (C₁), δ= 147.04 (C₆), δ= 143.62 (C₄), δ= 138.68 (C₃), δ= 126.98 (C₅), δ= 18.38 (C_{CH3}).

¹⁹⁵Pt-NMR (D₂O, 107 MHz): δ= 971 ppm.

[ESI-MS]= [M+Na]⁺ (*m/z*) Calc., 522.1; Found, 521.9.

HPLC purity= 97%.

ε_{295 nm}=19025 M⁻¹cm⁻¹, ε_{267 nm}=13766 M⁻¹cm⁻¹ (H₂O).

4.2.2.5.11 *Trans*-[Pt(Cl)₂(4-pic)₂] (24)

K₂PtCl₄ (0.800 g, 1.93 mmol) was completely dissolved in H₂O (24 mL), 4-picoline (20 eq, 3.75 mL) was added and the solution allowed to react at 95 °C for 1 h, at which point the mixture turned into a colourless solution. The solvent was rotary evaporated to dryness and the residual white solid was suspended in HCl (2 M, 27 mL) and allowed to react for 12 h. The yellow precipitate was filtered out and washed with water, ethanol and diethyl ether (Yield = 0.697 g, 80%).

¹H-NMR (CDCl₃, 400 MHz, ppm): δ= 8.71 (d, ³J_{1H1H}= 6.87 Hz, 4H, H₂), δ= 7.11 (d, ³J_{1H1H}= 6.87 Hz, 4H, H₃), δ= 2.41 (s, 6H, CH₃).

4.2.2.5.12 *Trans*-[Pt(N₃)₂(4-pic)₂] (25)

Trans-[Pt(Cl)₂(4-pic)₂] (0.690 g, 1.53 mmol) was dissolved in DMF (35 mL), then NaN₃ (20 eq, 1.282 g) was added and the mixture was allowed to react for 4 days at room temperature in the dark. The solution was then placed at -20 °C, for the precipitation of the first crop. A second crop was collected by the addition of diethyl ether to the filtrate and then allowing further precipitation at -20 °C. Both batches were washed with excess water for removal of sodium azide (Yield = 0.605 g, 85%).

¹H-NMR (acetone-d₆, 400 MHz, ppm): δ= 8.65 (dd, ³J_{195Pt1H}= 34 Hz, ³J_{1H1H}= 6.60 Hz, 4H, H₂), δ= 7.47 (d, ³J_{1H1H}= 6.03 Hz, 4H, H₃), δ= 2.51 (s, 6H, CH₃).

[ESI-MS]= [M+Na]⁺ (*m/z*) Calc., 488.1; Found, 488.0.

4.2.2.5.13 *Trans*-[Pt(N₃)₂(OH)₂(4-pic)₂] (26)

Trans-[Pt(N₃)₂(4-pic)₂] (0.600 g, 1.29 mmol) was suspended in H₂O₂ and the mixture was stirred for 20 h at 50 °C, to give a yellow solution which was lyophilized. Recrystallisation was carried out by dissolving the solid in warm

methanol (2 mL, 55 °C) and then adding diethyl ether (20 mL). The mixture was placed at -20 °C to yield the title compound. Crystals suitable for X-ray diffraction were obtained by the slow evaporation at ambient temperature of a methanol solution (Yield= 0.193 g, 30%).

$^1\text{H-NMR}$ (D_2O , 400 MHz, ppm): δ = 8.57 (dd, $^3J_{195\text{Pt}1\text{H}}$ = 26.80 Hz, $^3J_{1\text{H}1\text{H}}$ = 6.81 Hz, 4H, H_2), δ = 7.62 (d, $^3J_{1\text{H}1\text{H}}$ = 6.16 Hz, 4H, H_3), δ = 2.60 (s, 6H, CH_3).

$^{13}\text{C-NMR}$ (D_2O , 150 MHz, ppm): δ = 156.63 (C_4), δ = 148.95 (C_2), δ = 128.46 (C_3), δ = 21.36 (C_{CH_3}).

$^{195}\text{Pt-NMR}$ (D_2O , 129 MHz): δ = 964 ppm.

[ESI-MS]= $[\text{M}+\text{Na}]^+$ (m/z) Calc., 522.1; Found, 522.1.

HPLC purity= 90%.

$\epsilon_{293\text{ nm}}=15815\text{ M}^{-1}\text{cm}^{-1}$, $\epsilon_{256\text{ nm}}=12689\text{ M}^{-1}\text{cm}^{-1}$ (H_2O).

4.2.2.5.14 *Trans*-[Pt(Cl) $_2$ (thiazole) $_2$] (27)

K_2PtCl_4 (0.800 g, 1.93 mmol) was completely dissolved in H_2O (16 mL) and thiazole (14 eq, 2.29 mL) was added. The solution was allowed to react, under reflux, at 100 °C for three hours until the mixture turned into a transparent yellow solution. The reaction passes through an orange precipitate. The solvent was rotary evaporated to dryness and the residual yellow solid was suspended in HCl (2 M, 24 mL) and allowed to react overnight (14 hours) at 85 °C. The yellow precipitate was filtered off and washed with water, ethanol and diethyl ether (Yield = 0.750 g, 89%).

$^1\text{H-NMR}$ (acetone- d_6 , 400 MHz, ppm): δ = 9.58 (dd, $^3J_{1\text{H}1\text{H}}$ = 2.36 Hz, $^3J_{195\text{Pt}1\text{H}}$ = 27 Hz, 2H, H_2), 8.32 (d, $^3J_{1\text{H}1\text{H}}$ = 3.44 Hz, 2H, H_4), 7.88 (t, $^3J_{1\text{H}1\text{H}}$ = 2.96 Hz, 2H, H_5).

[ESI-MS]= $[\text{M}+\text{Na}]^+$, $[2\text{M}+\text{Na}]^+$ (m/z) Calc., 458.9, 894.8; Found, 458.8, 894.7

4.2.2.5.15 *Trans*-[Pt(N₃)₂(thiazole)₂] (28)

Trans-[Pt(Cl)₂(tz)₂] (0.700 g, 1.61 mmol) was completely dissolved in DMF (30 mL) and NaN₃ (20 eq, 2.087 g) was added. The reaction mixture was allowed to react for 6 days at room temperature in the dark. Work up of the reaction was carried out as described in section 4.2.2.5.9 (Yield= 0.411 g, 57%).

¹H-NMR (acetone-d₆, 400 MHz, ppm): δ = 9.57 (dd, ³J_{1H1H}= 2.05 Hz, ³J_{195Pt1H}= 29 Hz, 2H, H₂), 8.26 (d, ³J_{1H1H}= 3.68 Hz, 2H, H₄), 8.04 (t, ³J_{1H1H}= 2.85 Hz, 2H, H₅).

[ESI-MS]= [M+Na]⁺ (*m/z*) Calc., 488.0; Found, 488.0.

4.2.2.5.16 *Trans, trans, trans*-[Pt(N₃)₂(OH)₂(thiazole)₂] (29)

Trans-[Pt(N₃)₂(tz)₂] (0.400 g, 0.89 mmol) was suspended in H₂O₂ (30% v/v, 45 mL) and allowed to react at 50 °C for 5 hours. The yellow solution was IM filtered and then the H₂O₂ removed by freeze drying. The resulting residual solid of the title compound was washed with ethanol and acetone, as well as cold water (Yield= 0.215 g, 50%).

¹H-NMR (D₂O, 400MHz, ppm): δ = 9.58 (dd, ³J_{1H1H}= 1.97 Hz, ³J_{195Pt1H}= 20.30 Hz, 2H, H₂), 8.30 (dd, ³J_{1H1H}= 3.85 Hz, ³J_{195Pt1H}= 15.71 Hz, 2H, H₄), 8.07 (t, ³J_{1H1H}= 2.93 Hz, 2H, H₅).

¹³C-NMR (D₂O, 150 MHz, ppm): δ= 157.8 (C₂), δ= 140.3 (C₄), δ= 123.8 (C₅).

¹⁹⁵Pt-NMR (D₂O, 129 MHz): δ= 977 ppm.

[ESI-MS]= [M+Na]⁺ (*m/z*) Calc., 506.0; Found, 505.8.

HPLC purity= 94 %.

ε_{295 nm}=16750 M⁻¹cm⁻¹ (H₂O).

4.2.2.5.17 *Trans*-[Pt(Cl)₂(1-methylimidazole)₂] (30)

K₂PtCl₄ (0.5 g, 1.21 mmol) was dissolved in H₂O (15 mL), 1-methylimidazole (7 eq, 0.672 mL, 8.43 mmol) was added and the solution was allowed to react under reflux at 90 °C. The precipitation of a yellow intermediate was observed and the solution turned colourless after 120 min. Water was removed by rotary evaporation to leave a yellow solid and excess ligand. HCl (2 M, 15 mL) was then added and the reaction was allowed to proceed for 48 h at 85 °C, to yield a yellow solid which was isolated by filtration and washed with water, ethanol and diethyl ether (Yield= 0.366 g, 71%).

¹H-NMR (acetone-d₆, 400 MHz, ppm): δ= 8.13 (s, 2H, H₂), δ= 7.38 (t, ³J_{1H1H} = 1.32 Hz, 2H, H₄), δ= 7.11 (t, ³J_{1H1H} = 1.56 Hz, 2H, H₅), δ= 3.86 (s, 6H, CH₃).

[ESI-MS]= [M+Na]⁺, [2M+Na]⁺ (*m/z*) Calc., 453.0, 883.0; Found, 452.9, 882.9

4.2.2.5.18 *Trans*-[Pt(N₃)₂(1-methylimidazole)₂] (31)

Trans-[Pt(Cl)₂(mim)₂] (0.350 g, 0.82 mmol) was dissolved in DMF (7 mL) and NaN₃ (20 eq, 1.057 g) was suspended in the solution. The reaction was allowed to proceed for 4 days at 35 °C. Work up of the reaction was executed as described in section 4.2.2.5.9 (Yield= 0.110 g, 30%).

¹H-NMR (methanol-d₄, 400 MHz, ppm): δ= 8.03 (s, 2H, H₂), δ= 7.19 (s, 4H, H₄, H₅), δ= 3.82 (s, 6H, CH₃).

[ESI-MS]= [M+Na]⁺ (*m/z*) Calc., 466.1; Found, 465.9.

4.2.2.5.19 *Trans*-[Pt(OH)₂(N₃)₂(1-methylimidazole)₂] (32)

Trans-[Pt(N₃)₂(mim)₂] (0.106 g, 0.24 mmol) was suspended in H₂O₂ (30%, 9.2 mL) and the reaction was heated to 50 °C, until the yellow solution became transparent (1.5 h). Removal of the solvent was carried out via lyophilisation after

the solution was IM-filtered. Recrystallisation in a methanol/ DCM solution allowed the growth of crystals suitable for their study by X-ray diffraction (Yield= 0.050 g, 44%).

^1H -NMR (D_2O , 500 MHz, ppm): δ = 8.22 (s, 2H, H1), δ = 7.35 (t, $^3J_{\text{H1H}}= 1.54$ Hz, 2H, H2), δ = 7.32 (t, $^3J_{\text{H1H}}= 1.62$ Hz, 2H, H3), δ = 3.92 (s, 6H, CH_3).

^{13}C -NMR (D_2O , 125 MHz, ppm): δ = 137.48 (C_2), δ = 125.54 (C_4), δ = 123.05 (C_5), δ = 35.59 (C_{CH_3}).

^{195}Pt -NMR (D_2O , 107 MHz): δ = 987 ppm.

[ESI-MS]= $[\text{M}+\text{Na}]^+$ (m/z) Calc., 500.0; Found, 499.9.

HPLC purity= 88 %.

$\epsilon_{290\text{ nm}}=18307\text{ M}^{-1}\text{cm}^{-1}$ (H_2O).

4.3 Results

4.3.1 Characterisation and purity test

The Pt(IV)-diazido complexes were characterised by ^1H , ^{13}C , ^{195}Pt -NMR, ESI-MS and the purity assessed by HPLC (see section 4.2.2.5).

4.3.2 X-ray diffraction

Single crystals suitable for X-ray diffraction studies were obtained for the novel complexes *trans, trans, trans*-[Pt(N_3)₂(OH)₂(pyr)(4-pic)] **20**, *trans, trans, trans*-[Pt(N_3)₂(OH)₂(3-pic)₂] **23**, *trans, trans, trans*-[Pt(N_3)₂(OH)₂(4-pic)₂] **26** and *trans, trans, trans*-[Pt(N_3)₂(OH)₂(mim)₂] **32**, as described in section 4.2.2.5. The ORTEP diagrams of the molecular structures are shown in Figure 4.2. Crystallographic data of complexes **20**, **26**, **23** and **32** are summarized in Table 4.2 and selected bond distances and angles in Table 4.3 and Table 4.4.

Compounds **20** and **23** crystallized in the monoclinic space group $P2(1)/n$, whereas **26** and **32** in a triclinic space group $P-1$. All the complexes show an octahedral geometry with an $[N_4O_2]$ coordination sphere around the metal center. Complexes **23**, **26** and **32** are completely symmetrical, therefore the two halves of the molecule are identical. The O–Pt–O angle is 180° indicating a perfect octahedral geometry, whereas complex **20** has a slight distortion with a N3–Pt–N6 bond angle of $178.0(3)^\circ$. The crystal structures of **23** and **26** consist of a molecule of complex solvated by one methanol molecule. The unit cell of complex **32** contains two crystallographically-independent molecules of complex and a water molecule.

Table 4.2: Crystallographic data for complexes **20**, **23**·CH₃OH, **26**·CH₃OH and **32**·0.5H₂O.

Complex	20	23 ·CH ₃ OH	26 ·CH ₃ OH	32 ·0.5H ₂ O
Empirical formula	C ₁₁ H ₁₄ N ₈ O ₂ Pt	C ₁₃ H ₂₀ N ₈ O ₃ Pt	C ₁₃ H ₂₀ N ₈ O ₃ Pt	C ₈ H ₁₅ N ₁₀ O _{2.5} Pt
Formula weight	485.39	531.44	531.44	486.36
Crystal description	Colourless block	Colourless block	Yellow block	Yellow block
Crystal system	Monoclinic	Monoclinic	Triclinic	Triclinic
Crystal size/ mm	0.24×0.20× 0.18	0.26×0.26× 0.06	0.40×0.20× 0.16	0.20×0.20× 0.06
Space group	P2(1)/n	P2(1)/n	P-1	P-1
<i>a</i> / Å	9.5981(5)	7.09413(13)	9.4526(2)	8.4781(6)
<i>b</i> / Å	9.2035(5)	11.18048(20)	9.5894(2)	8.7226(7)
<i>c</i> / Å	17.2119(8)	12.3270(2)	12.0611(2)	10.9694(5)
<i>α</i> / (°)	90	90	97.810(2)	71.064(5)
<i>β</i> / (°)	92.640(5)	90.6038(17)	105.402(2)	79.820(5)
<i>γ</i> / (°)	90	90	114.181(2)	84.869(6)
Volume/ Å³	1518.82(13)	977.67(3)	923.57(3)	754.77(8)
Z	4	2	2	2
D_{calc}/gcm⁻³	2.123	1.914	2.026	2.180
F(000)	920	548	548	472
<i>μ</i>_{calcd}/mm⁻¹	9.259	7.214	7.636	9.326
T/ K	100(2)	150(2)	100(2)	150(2)
Max <i>θ</i> /°	29.75	31.45	32.26	29.77
Reflections collected/unique [R_{int}]	8340/ 3732 [0.0710]	10712 /3001 [0.0268]	19091/ 6074 [0.0320]	6604, 3714 [0.0498]
Goodness-of-fit on F²	1.034	1.050	1.098	1.032
Data/restraints/ parameters	3732/ 0/ 200	3001/ 0/ 132	6074/ 2/ 254	3714/ 0/ 211
Final R indices [I>2σ(I)]	<i>R</i> _I = 0.050 <i>wR</i> ₂ =0.1172	<i>R</i> _I = 0.0184 <i>wR</i> ₂ =0.0405	<i>R</i> _I = 0.0240 <i>wR</i> ₂ =0.0577	<i>R</i> _I = 0.0450 <i>wR</i> ₂ =0.1159
R indices (all data)	<i>R</i> _I = 0.064 <i>wR</i> ₂ =0.1235	<i>R</i> _I = 0.0263 <i>wR</i> ₂ =0.0451	<i>R</i> _I = 0.0311 <i>wR</i> ₂ =0.0614	<i>R</i> _I = 0.0588 <i>wR</i> ₂ =0.1312
Largest diff. peak and hole (eÅ⁻³)	6.803 and -1.988	0.829 and -1.015	2.811 and -1.263	4.383 and -2.786

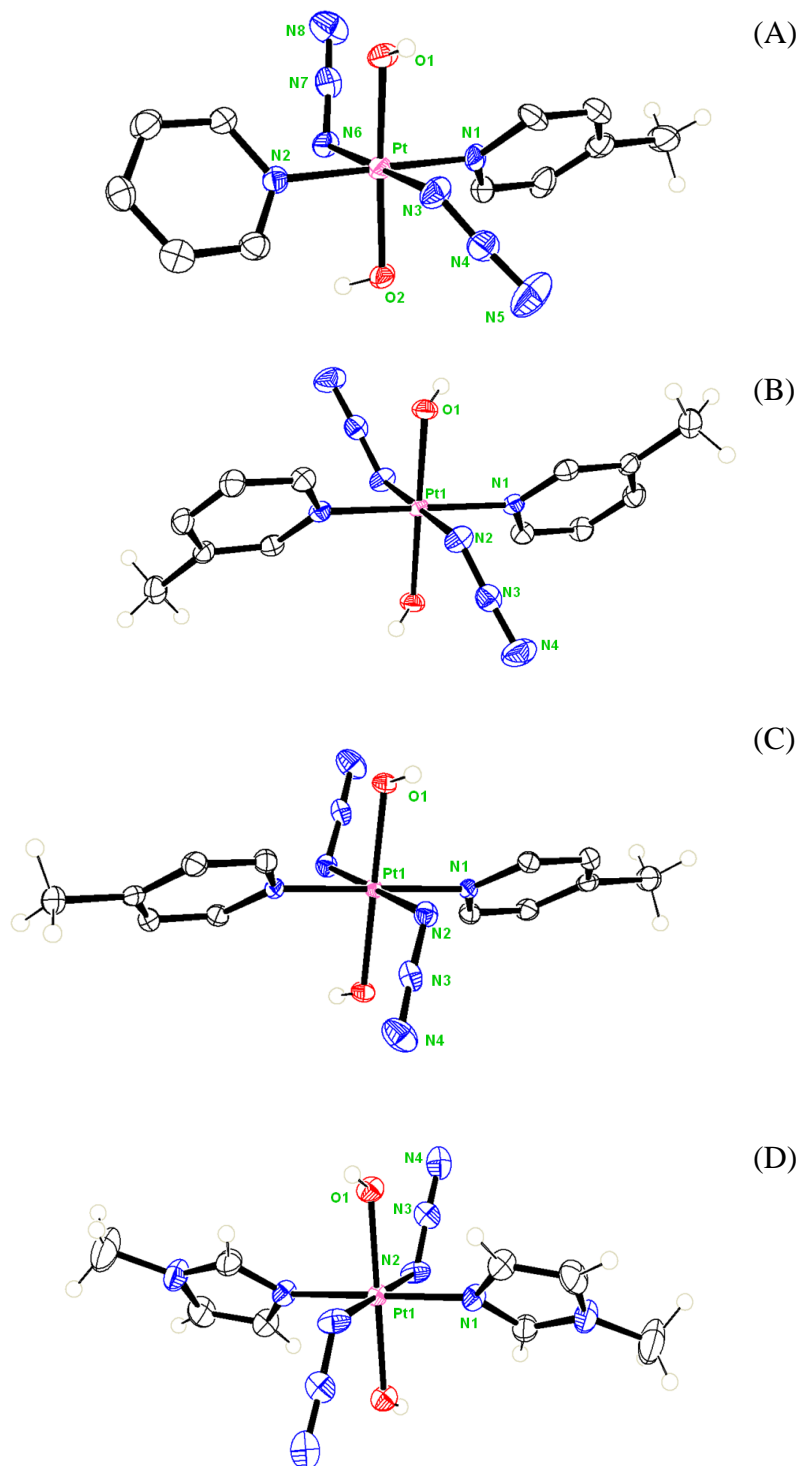


Figure 4.2: ORTEP diagrams of the complexes reported in this chapter: A) *trans, trans, trans*-[Pt(N₃)₂(OH)₂(pyr)(4-pic)] **20**; B) *trans, trans, trans*-[Pt(N₃)₂(OH)₂(3-pic)₂] **23**; C) *trans, trans, trans*-[Pt(N₃)₂(OH)₂(4-pic)₂] **26**; D) *trans, trans, trans*-[Pt(N₃)₂(OH)₂(mim)₂] **32**. The ellipsoids are set to 50% probability level.

Table 4.3: Selected bond distances (Å) and angles (°) for complex **20**.

Bond	(Å)	Angle	(°)
Pt–O1	2.003(6)	N6–Pt–N3	178.0(3)
Pt–O2	2.014(6)	N7–N6–Pt	118.0(6)
Pt–N1	2.013(7)	N4–N3–Pt	116.1(6)
Pt–N2	2.033(7)	N1–Pt–N2	179.2(3)
Pt–N3	2.052(6)	O2–Pt–O1	176.7(2)
Pt–N6	2.043(7)	N3–N4–N5	174.8(9)
N6–N7	1.197(10)	N6–N7–N8	175.6(9)
N7–N8	1.141(11)	-	-
N3–N4	1.225(10)	-	-
N4–N5	1.136(11)	-	-

Table 4.4: Selected bond distances (Å) and angles (°) for complexes **23**·CH₃OH, **26**·CH₃OH and **32**·0.5H₂O. For the latter, two independent platinum centres were found and they are represented as A and B.

Bond (Å)/ Angle (°)	23	26	32 A	32 B
Pt–O1	2.0046(19)	1.998(2)	1.997(4)	2.003(3)
Pt–N1	2.033(2)	2.036(3)	2.000(5)	2.005(5)
Pt–N2	2.048(2)	2.048(3)	2.058(5)	2.062(5)
N2–N3	1.218(3)	1.210(4)	1.198(8)	1.198(7)
N3–N4	1.147(3)	1.144(4)	1.155(10)	1.134(8)
N2–Pt–N2	180.0	180.0	180.00(19)	180.0(1)
N3–N2–Pt	115.51(15)	115.6(2)	118.7(4)	115.4(4)
N1–Pt–N1	180.0(1)	180.0(1)	180.0	180.000(1)
O1–Pt–O1	180.0	180.0	180.0(3)	180.000(1)
N2–N3–N4	174.5(2)	174.6(4)	174.2(8)	175.3(7)

4.3.3 Solubility and Stability

All compounds were stable in water in the dark at ambient temperature (20-25 °C) for at least two weeks, as examined by ^1H -NMR experiments. The solubility of the compounds in water is summarized in Table 4.5.

Table 4.5: Maximum solubility in water at *ca* 20 °C of the Pt(IV)-diazido complexes reported in this chapter.

Complex	Max Solubility (mM)
18	20.0
19	20.0
20	20.0
23	3.0
26	4.0
29	82.0
32	0.9

4.3.4 Extinction coefficient determinations

The extinction coefficients for the novel Pt(IV)-diazido complexes were determined in water and the UV-Vis spectra are depicted in the same graph for comparison (Figure 4.3).

The longest wavelength absorption maximum in these set of complexes was found for complex *trans, trans, trans*-[Pt(N₃)₂(OH)₂(pyr)(2-pic)] **18** at 297 nm, whereas the shortest absorption maximum is for compound *trans, trans, trans*-[Pt(N₃)₂(OH)₂(mim)₂] **32** with a λ_{max} of 290 nm. The absorption maxima of all other complexes, including the previously reported complex *trans, trans, trans*-[Pt(N₃)₂(OH)₂(pyr)₂],¹¹ lie between 293-295 nm. The complexes containing pyridine and/or pyridine-derivative ligands had two main absorption bands

whereas the complexes with thiazole or 1-methylimidazole showed one main band.

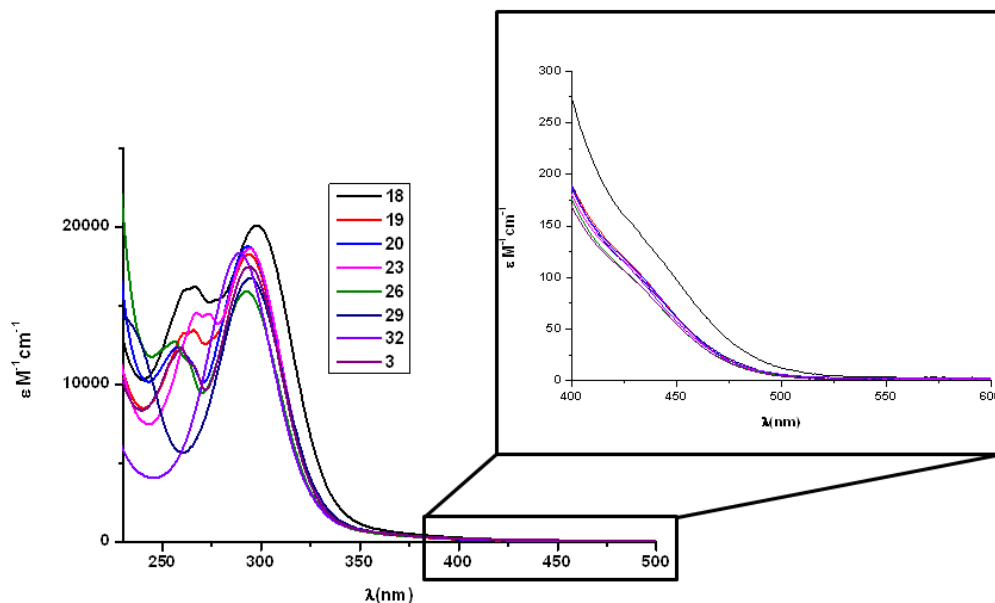
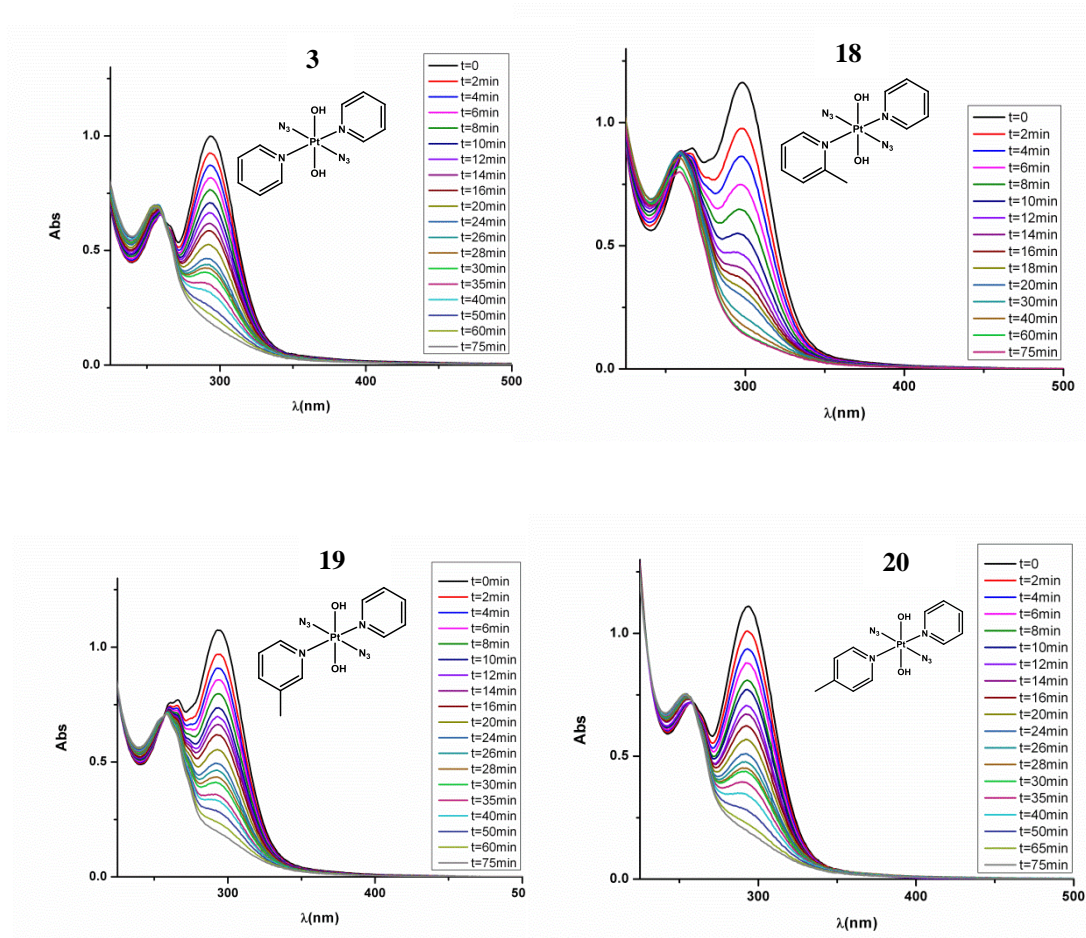


Figure 4.3: UV-Vis spectra of the Pt(IV)-diazido complexes in water. The inset in the graph shows an extension for the 400-600 nm range.

4.3.5 Photoirradiation of complexes followed by UV-Vis

Aqueous solutions of the complexes (60 μM) were irradiated with blue light (463 nm, 57 mW/cm^2), under identical conditions, and their photodegradation was followed by UV-Vis spectroscopy, at frequent time points (Figure 4.4). Although the complexes can also be activated with green light ($\lambda = 517$ nm), a comparative study was carried out with blue light activation, as the time required for the green light for substantial photodecomposition is greater than 6 hours (e.g. see Appendix). As pointed out in Chapter 3, a decrease in intensity of the $\text{N}_3 \rightarrow \text{Pt}$ band is observed upon irradiation. This exponential decrease was followed until *ca* 78% decrease for all complexes and plotted against time. The data were fitted

to the function $y = y_0 + Ae^{R_{ox}x}$, with an $r^2 > 0.98$ in all of the cases (Figure 4.5). The half lives of the complexes are depicted in Table 4.6. The fastest half life was found for complex **18** (Pt^{IV}-(pyr)(2-pic)) whereas the slowest was for complexes **23** and **26** (Pt^{IV}-(3-pic)₂ and Pt^{IV}-(4-pic)₂, respectively).



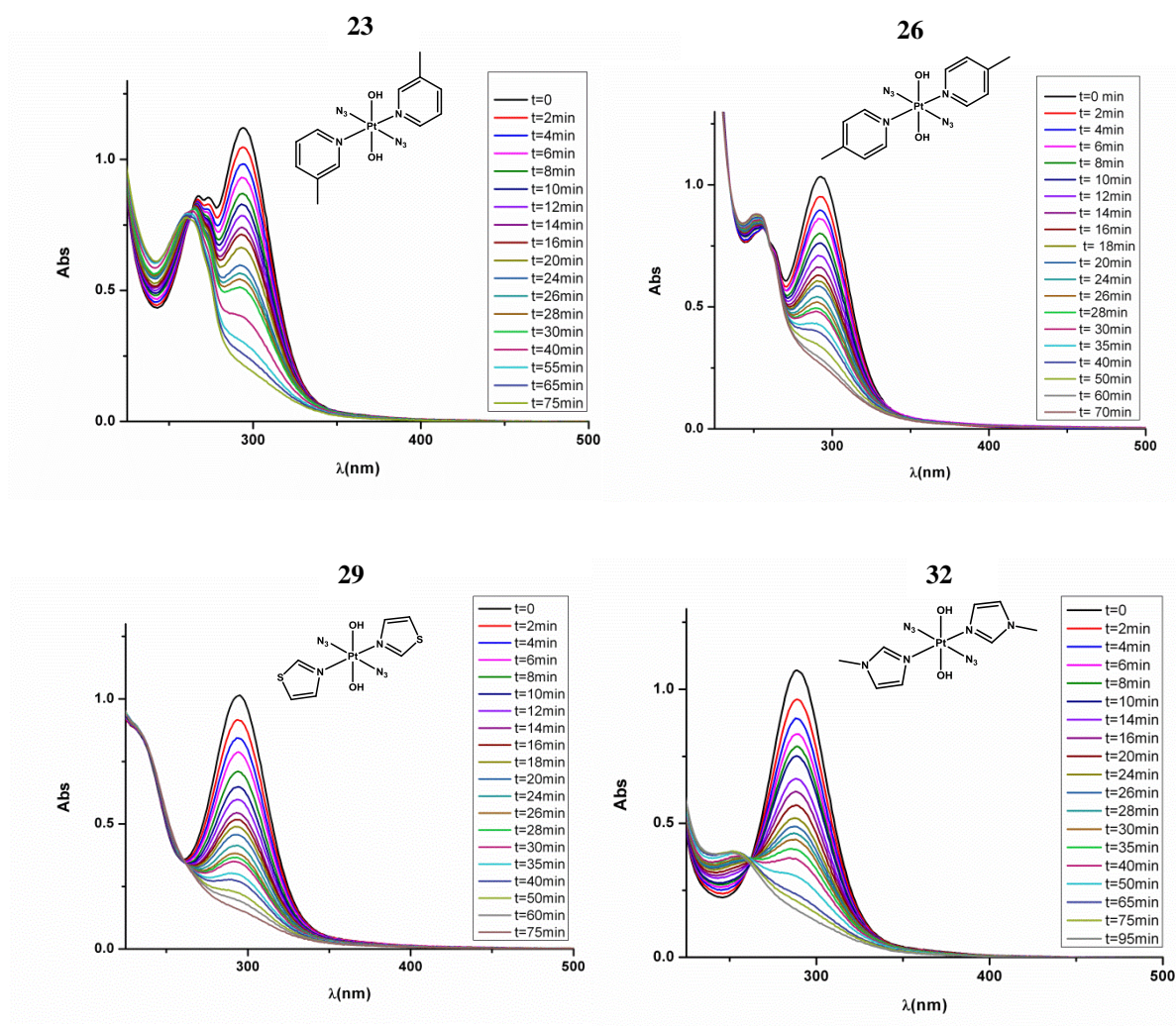


Figure 4.4: Changes in UV-Vis spectra of the complexes (60 μ M in H₂O) upon irradiation with 463 nm light.

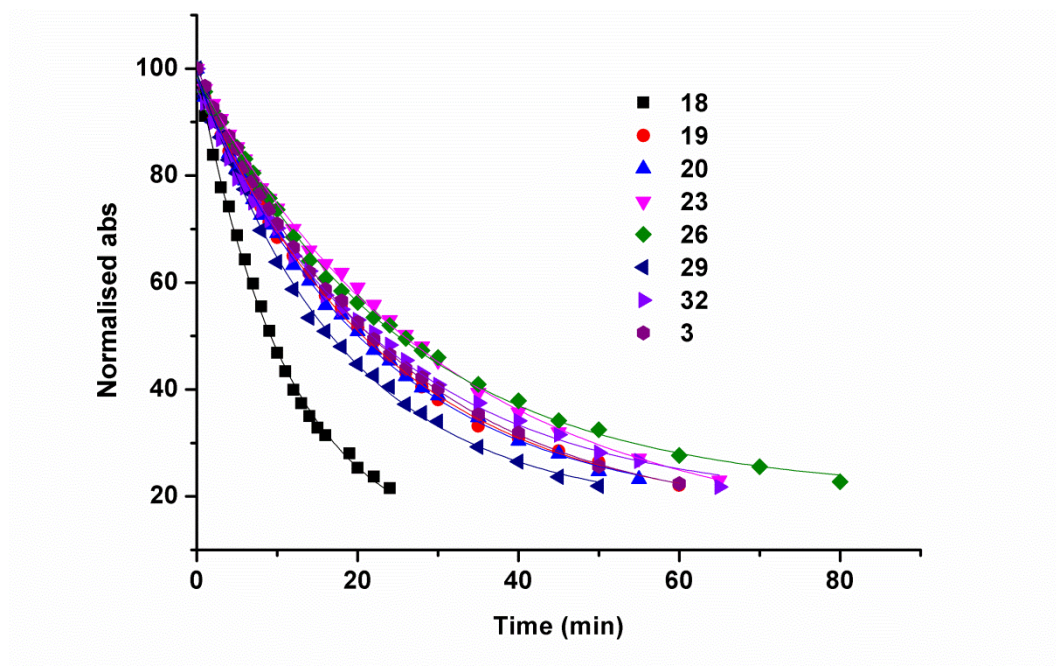


Figure 4.5: Plot of decrease of the normalised absorbance corresponding to the change of the N3→Pt band to an extent of *ca.* 22%. Irradiation was carried out with blue light (463 nm, 57 mW/cm²).

Table 4.6: Decomposition half-lives of complexes (60 μM) when irradiated with blue (463 nm) light, as measured by UV-Vis spectroscopy.

Complex	$t_{1/2}$ (min)
18	9.2
19	20.7
20	20.1
23	25.8
26	25.1
29	16.8
32	21.8
3	21.6

4.3.6 ^1H -NMR of complexes $\text{cis-}[\text{Pt}(\text{I})_2(2\text{-pic})_2]$ -**10** and $\text{cis-}[\text{Pt}(\text{Cl})_2(2\text{-pic})_2]$ -**11**

The synthesis of $\text{trans-}[\text{Pt}(\text{Cl})_2(2\text{-pic})(\text{pyr})]$ was attempted by the addition of 2 mol equivalents of pyridine to $\text{cis-}[\text{Pt}(\text{Cl})_2(2\text{-pic})_2]$ **11**. The steric strain in this molecule as well as in the precursor $\text{cis-}[\text{Pt}(\text{I})_2(2\text{-pic})_2]$ **10** was studied via ^1H -NMR. The iodo complex gives rise to a set of two peaks for each picoline ligand. Increase in temperature resulted in the peaks approaching together (Figure 4.6), especially H5 and H3. In the chlorido complex, broad peaks are generated for the H5 and H6 protons.

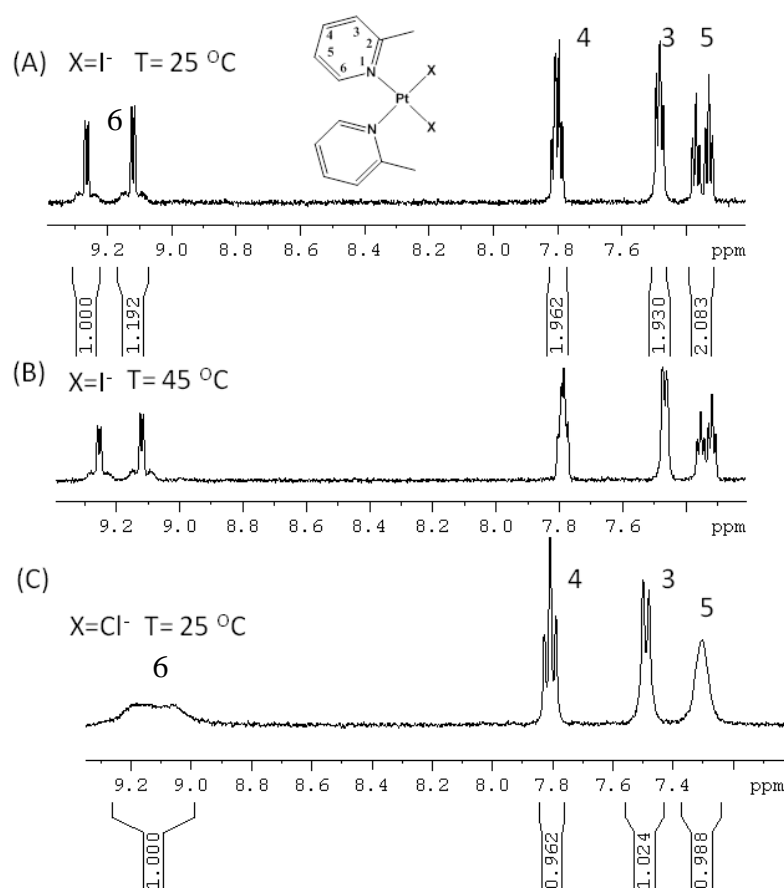


Figure 4.6: ^1H -NMR spectrum (600 MHz) of $\text{cis-}[\text{Pt}(\text{I})_2(2\text{-pic})_2]$ **10** at (A) $T=25\text{ }^\circ\text{C}$ and (B) $T=45\text{ }^\circ\text{C}$; (C) ^1H -NMR spectrum (400 MHz) of $\text{cis-}[\text{Pt}(\text{Cl})_2(2\text{-pic})_2]$ **11** at $T=25\text{ }^\circ\text{C}$. All NMR spectra were recorded in acetone- d_6 .

4.3.7 DFT-TDDFT calculations for complex **18**

Complex **18**, *trans, trans, trans*-[Pt(N₃)₂(OH)₂(pyr)(2-pic)], was found to be the most photosensitive complex in this series, with a half life decreased by 2.5, when compared to complexes from the same family. Ground-state and lowest-lying-triplet-state optimizations were performed. Furthermore, TDDFT calculations were carried out in order to simulate the electronic transitions and rationalize the photoactivity of metal complexes. A crystal structure for complex **18** was not obtained and therefore direct comparison of bond lengths in the ground state was not possible. However the theoretical UV-Vis spectrum, as shown in Figure 4.7, matches well with the experimental, with the absorption maximum underestimated by only 9 nm (experimental: 297 nm, 20091 M⁻¹cm⁻¹, theoretical: 288 nm, 19282 M⁻¹cm⁻¹) and the shoulder with only 1 nm difference (theoretical: 267 nm, 13520 M⁻¹cm⁻¹ and experimental: 268 nm, 16061 M⁻¹cm⁻¹). The UV-Vis spectra were simulated by the calculation of 32 singlet states using water as a solvent (cpcm)¹⁵ and the TDDFT method. The singlet excited states as well as the percentage contribution are presented in Table 4.8, whereas in

Figure 4.8, a representation of the contributions of each of the ligands in the most relevant molecular orbitals is provided which can help with the characterisation of the transitions. The main band is composed by ligand-to-metal charge transfer (LMCT) dissociative transitions with N₃⁻→Pt character. The transitions composing the shoulder of the spectrum contain mixed LMCT/ IL character involving the OH⁻ → Pt, pyridines.

Table 4.7: Selected bond distances for **18**, the N_α , N_β and N_γ labels denote the azide atoms.

Bond length	Ground-state (Å)	Lowest-lying excited state(Å)
Pt– N_α	2.075	2.435
Pt– N_α	2.075	2.526
Pt–OH	2.054	2.025
Pt–OH	2.031	2.010
Pt–N(Py)	2.055	2.062
Pt–N(Py-CH ₃)	2.068	2.063
N_α – N_β	1.217	1.200
N_α – N_β	1.217	1.192
N_β – N_γ	1.147	1.162
N_β – N_γ	1.147	1.167

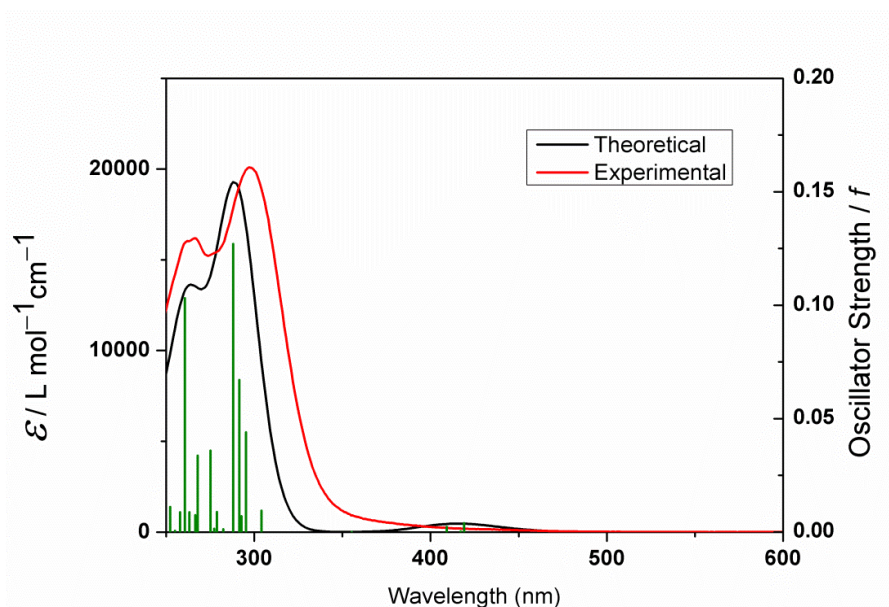
**Figure 4.7:** Calculated and experimental absorption spectra of **18**. The excited states are shown as vertical bars with heights equal to the extinction coefficients. The theoretical graph was obtained using GAUSSUM 2.2.

Table 4.8: Calculated singlet transitions for complex **18**, in H₂O.

	Energy (eV)	Wavelength (nm)	Oscillator Strength	Major contributions
1	2.96	419	0.004	H-1→LUMO (88%)
2	2.97	417	0.0003	HOMO→LUMO (94%)
3	3.03	409	0.0023	H-2→LUMO (88%)
5	4.08	304	0.0094	H-5→LUMO (57%) H-4→LUMO (26%)
8	4.25	291	0.067	H-3→LUMO (17%) H-2→L+3 (56%)
9	4.30	288	0.127	H-3→LUMO (30%) H-2→L+3 (21%) H-1→L+3 (25%)
13	4.51	275	0.0359	H-5→LUMO (32%) H-4→LUMO (54%)
17	4.76	261	0.1032	H-7→LUMO (38%) H-2→L+2 (21%)
22	5.01	248	0.0379	H-9→LUMO (18%) H-8→LUMO (47%)
30	5.39	230	0.0803	H-5→L+2 (15%) H-4→L+1 (16%) H-4→L+2 (17%) H-1→L+5 (17%)

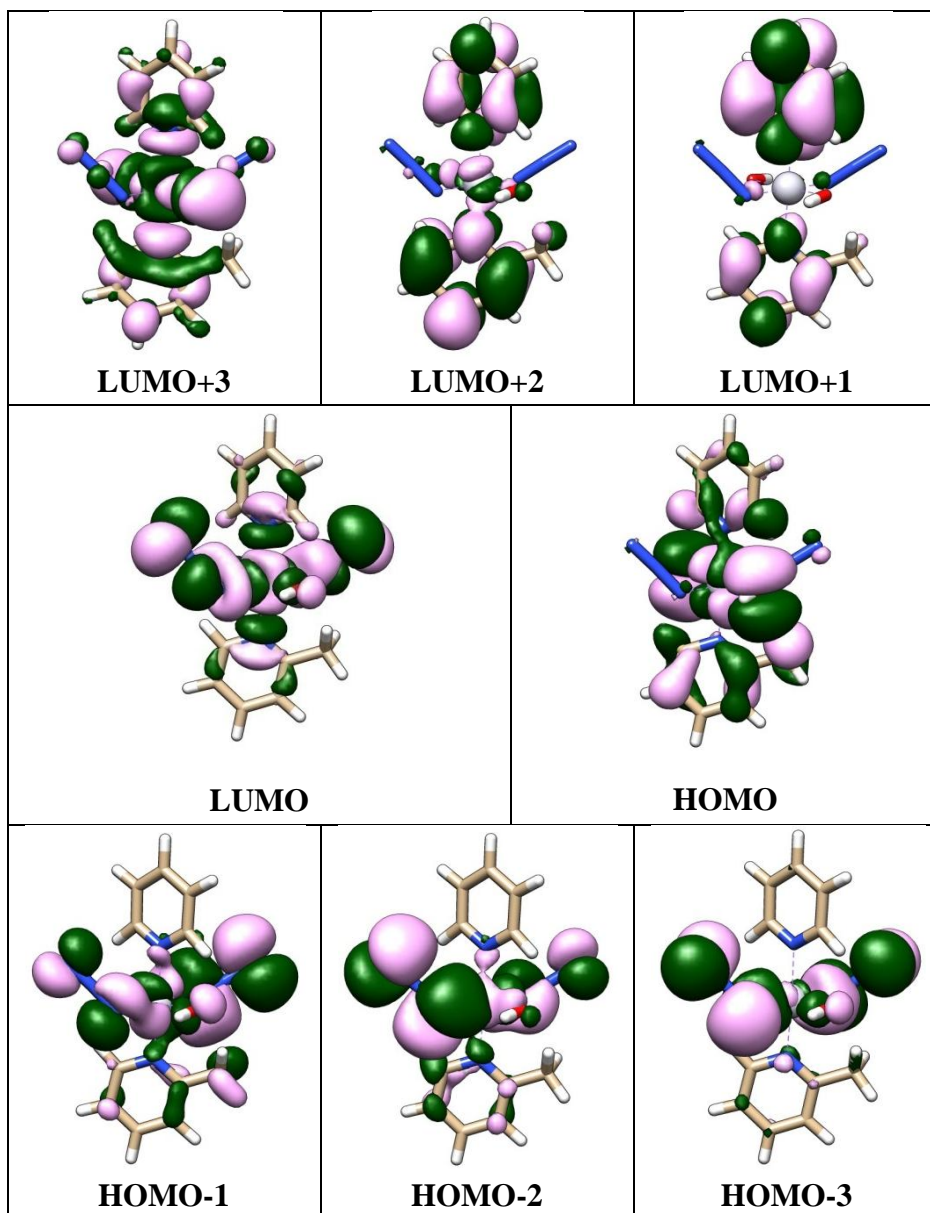


Figure 4.8: Selected molecular orbitals of complex **18**, with purple and green representing the two signs of the wavefunctions (+ and -).

4.4 Discussion

The design of novel platinum-diazido complexes with different planar-aromatic ligands, is important for the development of the Pt(IV)-diazido family of complexes, since these ligands can have an effect on the photolability as well as the phototoxicity of the complexes. Previous research^{11, 16} showed that after

photoactivation, these aromatic ligands are retained on the platinum, upon reduction to Pt(II) and therefore play a vital role in the cytotoxic properties of these complexes. Furthermore studies by Bednarski *et al.*¹⁷ showed that the bulk of the ligand also plays a vital role in the photolability of the complex. Comparative studies between piperidine and pyridine containing complexes showed that with the piperidine ligand, a faster rate of cellular death under light activation was achieved.

4.4.1 Synthesis, characterization and solubility

Cis-dichlorido compounds

In general, the synthesis of the *cis*-dichlorido diammine Pt(II) compounds, can be achieved by direct replacement of chlorides on K_2PtCl_4 , upon addition of two equivalents of the amine ligand.¹² Although this method is appealing, the purity of the products was not reproducible and also the yield was low. Previous reports also showed that contamination with the “Magnus” green salt, $[\text{PtL}_4][\text{PtCl}_4]$, is common in these procedures.¹⁸ Therefore, the method by Dhara¹⁹ for cisplatin synthesis was adopted, as illustrated in Figure 4.9.

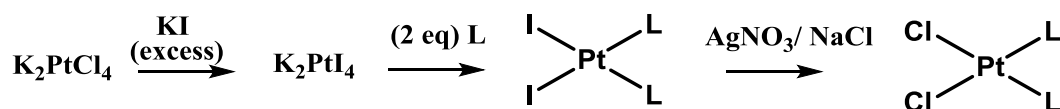


Figure 4.9: Method for the synthesis of *cis*-dichloro complexes, as developed by Dhara.¹⁹

Replacement of the chlorides with iodides (i.e. formation of K_2PtI_4) is necessary to ensure the *cis* geometry of the complex. This is promoted by the high *trans* effect of iodido ligands. In general, square-planar Pt(II) substitution chemistry is highly dependent on the *trans* effect: the effect of a ligand on the rate of substitution of the ligand *trans* to it.²⁰ Ligands with a large *trans* effect can be strong σ -donors or π -acceptors, the former characteristic affecting the ground state of the molecule and the latter influencing the transition state geometry of the ligand substitution intermediate. The order of common ligands with decreasing *trans* effect is the following²¹:

CN^- , C_2H_4 , CO > PR_3 , H^- > CH_3^- , $\text{SC}(\text{NH}_2)_2$ > C_6H_5^- , I^- , SCN^- > Br^- > Cl^- > py , NH_3 , OH^- , H_2O

Upon obtaining the *cis*-diiodido compound, conversion to the dichlorido Pt(II) complex can be easily achieved via the use of AgNO_3 and then addition of NaCl to the di-aqua intermediate.

***Trans*-Dichlorido compounds**

The synthesis of the titled compounds is based on the method of Kauffman and Thompson,¹² which involves the use of HCl in an aqueous solution of $[\text{Pt}(\text{L})_2(\text{L}')_2]^{2+}$. It was used previously for the synthesis of *trans*-Pt(II) complexes with substituted pyridines or diamines as ligands.^{22, 23} The stronger *trans* effect of Cl^- compared to the pyridine ligands ensures the formation of the *trans* isomer. When L and L' are the same ligand, then it is a two-step process (Figure 4.10 A). Ligand substitution in Pt(II) complexes normally goes through an associative mechanism,²⁴ via a pentacoordinate transition state, as illustrated in Figure 4.10 B.

Compounds **21**, **24**, **27** and **30** which contain the same planar aromatic ligand, were reported previously.^{13, 14} The synthesis of **13**, [Pt(Cl)₂(pyr)(3-pic)], and **14**, [Pt(Cl)₂(pyr)(4-pic)], was more challenging due to the formation of the respective *trans*-[Pt(Cl)₂(n-pic)₂] as side product. This complication was avoided by the use of exactly 2 molar equivalents of the second ligand. If a slight excess is employed then the formation of *trans*-[Pt(Cl)₂(n-pic)₂] occurs, which due to its similarity to the target compound, is difficult to purify by crystallisation (e.g. from 0.1 M HCl).

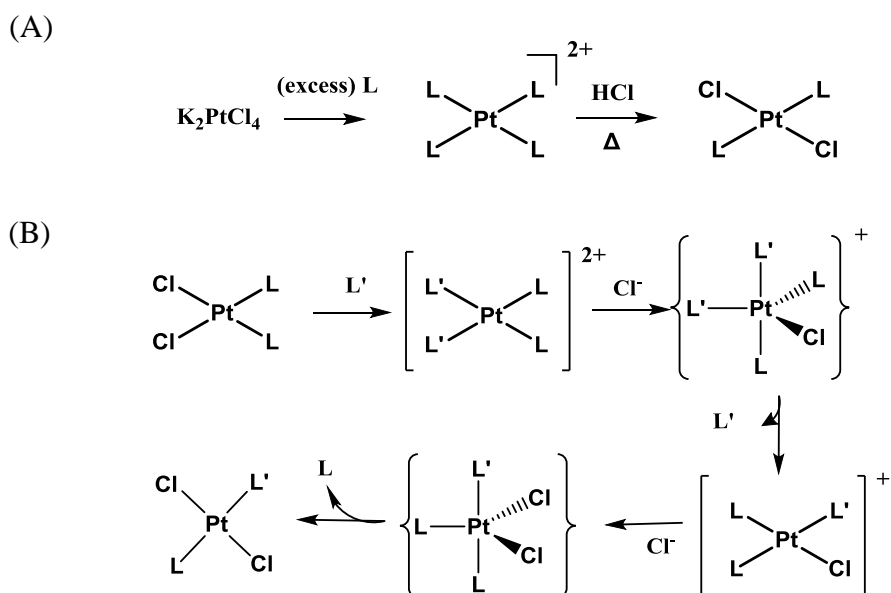


Figure 4.10: (A) Synthetic scheme and reaction mechanism for the synthesis of *trans*-[Pt(Cl)₂(L)₂], and (B) reaction mechanism for the synthesis of *trans*-[Pt(Cl)₂(L)(L')], where L and L' are nitrogen monodentate ligands.

In the case of complex **12**, the side product was *trans*-[Pt(Cl)₂(pyr)₂]. Since the 2-picoline ligand is bulky, it does not enter easily the coordination sphere of the platinum, leaving some of the starting material unreacted. In the presence of HCl (under heat), it isomerizes from *cis* to *trans*²⁵ which then is carried as an impurity

through the rest of the steps. Attempts to generate this compound starting from *cis*-[Pt(Cl)₂(2-pic)₂], **11**, and subsequent addition of pyridine were unsuccessful. This can be attributed to the steric hindrance created by the 2-picoline ligands, making the platinum centre inaccessible to the pyridine. The restricted rotation of the 2-picoline ligands is evident from the ¹H-NMR spectra of *cis*-[Pt(I)₂(2-pic)₂] **10** and *cis*-[Pt(Cl)₂(2-pic)₂] **11**. In the former, two sets of peaks are featured for each proton indicating the inequivalence of the picolines due to the presence of rotamers and in the latter the broadness of peaks proves the restricted rotation (Figure 4.6). The crystal structure of *cis*-[Pt(Cl)₂(2-pic)₂] was reported previously by Rochon *et al.*¹³

An increase in the amount of the picoline ligand in the reaction mixture (to 4 mol equivalents) diminished the side product but the use of these experimental conditions was not reproducibly successful. Nevertheless, the evidence suggests that the reaction could be successful, if an even greater proportion of picoline ligand is used.

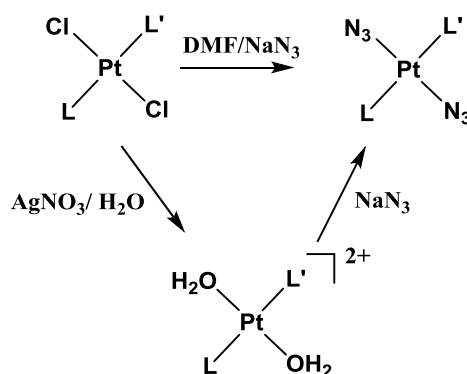
Trans-Diazido Pt(II) compounds

Figure 4.11: Scheme for the synthesis of *trans*-[Pt(N₃)₂(L)(L')] complexes.

Replacement of the chlorido ligands with azidos can be achieved by the use of AgNO₃ to form the diaqua complex and then subsequent addition of NaN₃ (Figure 4.11). Care must be taken during this reaction to use stoichiometric amount of AgNO₃, as excess amount of Ag⁺ could lead to the formation of AgN₃, which is a well-known explosive. Another method that can be employed is the direct replacement of the chlorides in a solution of the precursor in DMF with excess sodium azide.²⁶ This route, although less time efficient, resulted in a superior quality product, as the precipitation of the solid was in the form of crystalline material. Furthermore, the synthesis of *trans*-[Pt(N₃)₂(mim)₂] **31**, via the first route was unsuccessful.

Trans-diazido Pt(IV) compounds

The hydroxido ligands were added in the axial positions via oxidation of the Pt(II) precursor with hydrogen peroxide. Recrystallisation of the Pt(II)-diazido precursor in general has a beneficial effect on the oxidation step, as the production

of side products is minimized. In the case of *trans, trans, trans*-[Pt(N₃)₂(OH)₂(pyr)(3-pic)] **19**, isolation and analysis of the side product at the oxidation step indicated the production of [Pt(N₃)₃(OH)(pyr)(3-pic)], which demonstrated the importance of the complete removal of excess azide before oxidation.

All the novel Pt(IV)-diazido complexes (including *trans, trans, trans*-[Pt(N₃)₂(OH)₂(4-pic)₂] **26** and *trans, trans, trans*-[Pt(N₃)₂(OH)₂(tz)₂] **29** which have been synthesized before in our group but without any full characterization data)²⁷ were characterised by ¹H, ¹³C, ¹⁹⁵Pt-NMR, ESI-MS and HPLC.

The ¹⁹⁵Pt NMR peaks of all the complexes were found to lie in the range of 954-987 ppm. The only exception was complex *trans, trans, trans*-[Pt(N₃)₂(OH)₂(pyr)(2-pic)] **18**, with a δ_{Pt} of 1132 ppm, showing the platinum nucleus in this case is greatly deshielded. A systematic study has been carried out previously by Marzilli *et al.*²⁸ on the ¹⁹⁵Pt chemical shift of *cis*-[Pt(Xpy)(Me₂SO)Cl₂], *trans*-[Pt(Xpy)(Me₂SO)Cl₂], *cis*-[Pt(Xpy)₂(Me₂SO)Cl]⁺ and *cis*-[Pt(Xpy)(Me₂SO)₂Cl]⁺, where Xpy is a pyridine related compound. It was shown that the chemical shift is influenced not only by the basicity of the ligand but also by the *ortho* substituent. The *ortho* ligands influence δ_{Pt} from low (shielding) to high (deshielding) chemical shift values as follows: O⁻ > NHR > CH₃O ~ HOCH₂ ~ CH₃ ~ C₂H₅ ~ n-C₃H₇ > HC(O) > (C₆H₅)C(O) ~ 3-thienyl > C₆H₅. Therefore it is not surprising that a deshielding effect is observed for complex *trans, trans, trans*-[Pt(N₃)₂(OH)₂(pyr)(2-pic)] **18**, although the pK_a values of all the picoline ligands are similar (5.97, 5.68 and 6.02 for 2-, 3- and 4-picoline, respectively).²⁹ Furthermore, the theoretical calculations on complex **18**

predicted that the Pt–N (2-picoline) distance is 2.068 Å and Pt–N(pyridine) is 2.055 Å, which could suggest that the sterically hindered 2-picoline forms a longer σ -bond and therefore the platinum centre has less electron density.

The solubility results (Table 4.5) indicate the effect that the planar aromatic ligand has on the lipophilicity of the complex. A striking difference exists between complexes **29** and **32** with 1-methylimidazole and thiazole ligands, respectively, for which the solubility decreases 91-fold. Good aqueous solubility is a desirable attribute for platinum anticancer complexes as they tend to have a longer half life in the blood and they are excreted efficiently *via* the kidneys, avoiding systemic toxicity.³⁰ For example in the case of cisplatin, with an aqueous solubility of ~ 8 mM, excretion occurs 50% through kidneys and 50% through the bile which might require 2 months before complete excretion.³¹ As shown in Chapter 3, a significant proportion of this class of complexes enters the cell through passive diffusion. Although measurement of lipophilicity via logP was not carried out, it can be assumed that the highly soluble complexes (e.g. **29**) will be more hydrophilic and hence passive uptake will be hindered. This agrees with a recent work by Gao *et al* in which they showed that blocking active transport of their extremely soluble Pt(II) complex (aqueous solubility of 1.5 M), decreases the cytotoxicity.³²

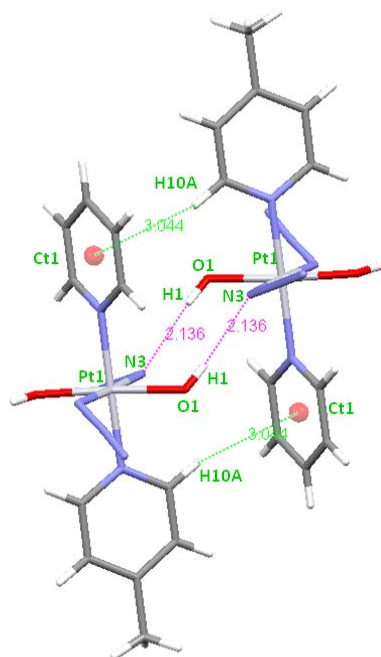
4.4.2 X-Ray crystallography

The Pt–N _{α} bond lengths and the N _{β} –N _{α} –Pt bond angle were found to compare well with other Pt(IV)-diazido complexes reported previously.^{33,34,35} Complexes

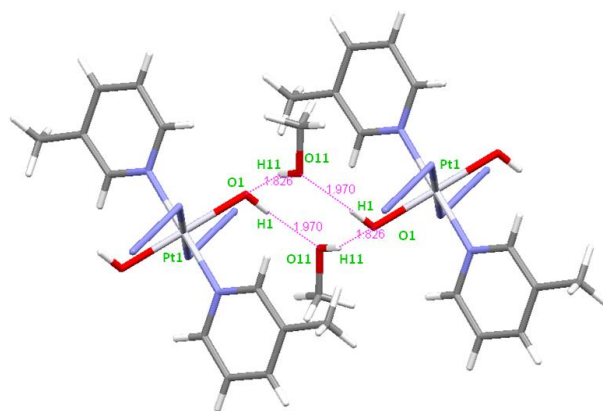
23 and **26** have no significant differences in bond distances or angles indicating that sterically and electronically are very similar. The Pt–N (aromatic ligand) bond length is significantly shorter in complex **32**, an effect which might be attributed to the higher pK_a of 1-methylimidazole (7.06) compared to the picoline ligands (5.68-6.02).

The intermolecular interactions in these complexes are dominated by H-bonding (Figure 4.12), frequently between the hydroxyl group and the N_α of the azide (e.g. in the case of **20**, **26** and **32**). The strength of these H-bonds is moderate (refer to Chapter 3), the strongest being in the case of **32**, for $O1'-H1'\cdots N2$ (2.066 Å). In complex **20** some weak $C-H\cdots\pi$ interactions ($Ct1-H10A$, 3.044 Å) also occur. In the case of **23**, H-bond bridges are formed between methanol molecules and neighbouring complexes using the -OHs on each face of the complex (Figure 4.12) to form an infinite chain along one crystal packing axis.

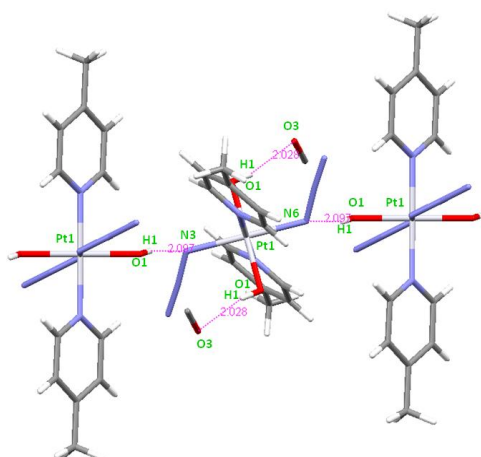
(A)



(B)



(C)



(D)

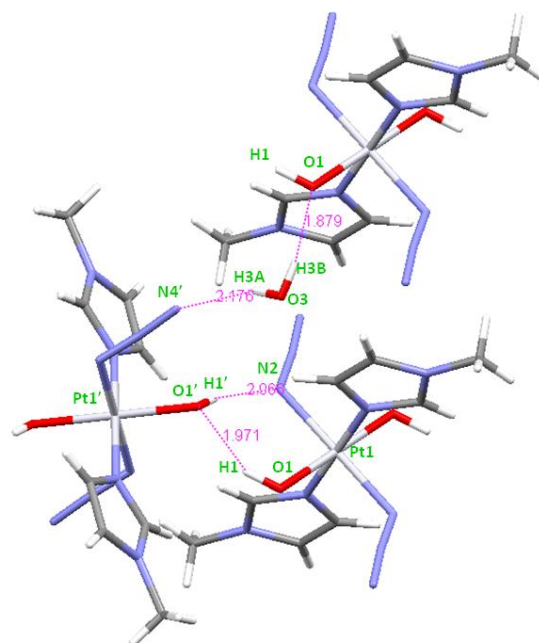


Figure 4.12: Intermolecular interactions for complexes **20** (A), **23** (B), **26** (C) and **32** (D). The pink lines denote H-bond interactions, and in the case of **20** the green lines illustrate C-H... π interaction.

4.4.3 Photoirradiations monitored by UV-Vis

The complexes were irradiated with blue light ($\lambda = 463$ nm) and the decrease in the absorbance of the main UV band, which corresponds to the $N_3 \rightarrow Pt$ LMCT was followed until 78% decrease. This decrease occurs because of the loss of an azide, which has been documented before in these systems.^{36, 33} The decay fits an exponential function (Figure 4.5) suggesting an irreversible first order photoreaction, from which a half-life was obtained and compared for the various complexes, given that the irradiation conditions were the same. The complexes listed from the highest to the lowest half-lives have the following order (Table 4.6) : $Pt(4-pic)_2 \sim Pt(3-pic)_2 > Pt(1-mim)_2 \sim Pt(pyr)_2 \sim Pt(pyr)(4-pic) \sim Pt(pyr)(3-pic) > Pt(tz)_2 > Pt(pyr)(2-pic)$.

In photoreaction kinetics, the rate of the disappearance of a product is proportional to the quantum yield and the energy absorbed in unit time by unit volume.³⁷ This relationship is described by the equation: $d[X]/dt = I_{abs} \times \phi$, where I_{abs} is the absorbed energy and ϕ , the primary quantum yield. A primary quantum yield is defined as the number of molecules undergoing the process of interest per number photons absorbed. The energy absorbed depends on the intensity of the light and the extinction coefficient of the molecule at that particular wavelength.

The extinction coefficient of the compounds at 463 nm was found to be very similar and lying within a narrow range of 32 to 36 $M^{-1}cm^{-1}$. The only exception is for compound **18**, *trans, trans, trans*-[Pt(N_3)₂(OH)₂(pyr)(2-pic)], which was found to be 64 $M^{-1}cm^{-1}$, double than the dipyridine compound *trans, trans, trans*-[Pt(N_3)₂(OH)₂(pyr)₂] **3** ($\epsilon = 32 M^{-1}cm^{-1}$), Figure 4.3. This fact can explain its

increased rate of photodecomposition when irradiated with blue light (half-life of 9.1 min versus 21.6 min). Although the *trans, trans, trans*-[Pt(N₃)₂(OH)₂(pyr)(3-pic)] and *trans, trans, trans*-[Pt(N₃)₂(OH)₂(pyr)(4-pic)] complexes have a half-life of 20 min, for the bis-picoline complexes (e.g. [Pt(N₃)₂(OH)₂(3-pic)₂], the half life increases to ~25 min. This increase cannot be accounted by a significant decrease in the extinction coefficient, suggesting that it might lie in the different quantum yields for these compounds. The same observation applies to comparison of the two complexes with 5-membered planar aromatic ligands (i.e. thiazole and 1-methylimidazole), *trans, trans, trans*-[Pt(N₃)₂(OH)₂(tz)₂] **29** and *trans, trans, trans*-[Pt(N₃)₂(OH)₂(mim)₂] **32**, with half lives of 21.7 and 16.7 min, respectively.

Interestingly, DFT and TDDFT calculations performed on complex **18**, showed the presence of transitions at 419 nm and 417 nm with oscillator strengths of 0.004 and 0.0003, respectively (Table 4.8). Calculations on *trans, trans, trans*-[Pt(pyr)₂(OH)₂(N₃)₂] resulted in transitions at lower wavelengths (414 nm, 404 nm) with smaller oscillator strengths (0.0027 and 0.0001).¹¹ As with most of *trans*-Pt(IV)-diazido complexes, the transitions are highly dissociative and occupation of the LUMO (Table 4.8 and Figure 4.8) would lead to dissociation of the azide and/or the hydroxide ligands. The facile chemical reduction of a Pt(IV) complex incorporating a 2-picoline ligand was noted by Hambley *et al* who showed that the reduction potential increases by 56 mV by replacing pyridine with 2-picoline in the complex *cis, trans, cis*-[PtCl₂(OH)₂(NH₃)(X)], where X is 2-picoline or pyridine. This was attributed to the steric clash between the N-ligand and the platinum which destabilizes the Pt–O bond facilitating reduction to Pt(II).³⁸ This destabilization proves to be beneficial for the photochemical

reduction of Pt(IV)-diazido complexes suggesting that steric hindrance is more important for photolability rather than the electronic effects caused through inductive effects of the methyl group.

It is worth mentioning that a theoretical study on Pt(IV)-diazido complexes showed that electron-donating substituents on the pyridine can have an effect on the absorption properties of Pt(IV)-diazido complexes by increasing the contribution of the frontier orbitals that are closer to the HOMO and LUMO.³⁹ The present work has shown that the position of the substituent may play a more crucial role.

4.5 Conclusions

In this Chapter, the first family of Pt(IV)-diazido complexes, with the general formula of *trans, trans, trans*-[Pt(N₃)₂(OH)₂(L₁)(L₂)], where L₁ and L₂ are N-heterocyclic ligands (pyridine, picolines, thiazole, 1-methylimidazole) has been constructed. The synthesis, characterisation (¹H, ¹³C, ¹⁹⁵Pt-NMR, ESI-MS) and X-ray crystal structures (in four cases) of seven novel complexes are described and discussed.

The planar ligands have an effect on the solubility, with thiazole and 1-methylimidazole producing the least and most water soluble complexes, respectively (0.9 mM and 84 mM). Also the use of picoline instead of pyridine ligands diminished the solubility by 5-fold.

Studying the photosensitivity of the compounds showed that incorporation of a sterically demanding 2-pic ligand as in the case for *trans, trans, trans*-

[Pt(N₃)₂(OH)₂(2-pic)(pyr)] can greatly enhance the photoactivity of the complex, as the half-life decreases to 9 minutes on irradiation with 463 nm, whereas the other complexes had half-lives in the range of 20-25 min. DFT-TTDFT calculations on complex *trans, trans, trans*-[Pt(N₃)₂(OH)₂(pyr)(2-pic)] **18**, showed that indeed this complex has higher intensity transitions at longer wavelength which are in agreement with its enhanced photoactivity. In the next chapter, phototoxicity data of these complexes will be presented.

References

1. G. Natile and M. Coluccia, *Coord. Chem. Rev.*, 2001, **217**, 383-410.
2. S. M. Aris and N. P. Farrell, *Eur. J. Inorg. Chem.*, 2009, **2009**, 1293-1302.
3. J. Holford, S. Y. Sharp, B. A. Murrer, M. Abrams, and L. R. Kelland, *Br. J. Cancer*, 1998, **77**, 366-373.
4. M. Ravera, E. Gabano, I. Zanellato, I. Bonarrigo, E. Escibano, V. Moreno, M. Font-Bardia, T. Calvet, and D. Osella, *Dalton Trans.*, 2012, **41**, 3313-3320.
5. K. S. Lovejoy, M. Serova, I. Bieche, S. Emami, M. D'Incalci, M. Broggini, E. Erba, C. Gespach, E. Cvitkovic, S. Faivre, E. Raymond, and S. J. Lippard, *Mol. Cancer Ther.*, 2011, **10**, 1709-1719.
6. N. Farrell, 2002, US6350740(2002).
7. N. Farrell, L. F. Povirk, Y. Dange, G. DeMasters, M. S. Gupta, G. Kohlhagen, Q. A. Khan, Y. Pommier, and D. A. Gewirtz, *Biochem. Pharmacol.*, 2004, **68**, 857-866.
8. Y. Najajreh, J. M. Perez, C. Navarro-ranninger, and D. Gibson, *J. Med. Chem.*, 2002, **45**, 5189-5195.
9. N. J. Farrer, J. A. Woods, V. P. Munk, F. S. Mackay, and P. J. Sadler, *Chem. Res. Toxicol.*, 2010, **23**, 413-421.

10. F. S. Mackay, J. A. Woods, P. Heringová, J. Kaspárková, A. M. Pizarro, S. A. Moggach, S. Parsons, V. Brabec, and P. J. Sadler, *Proc. Natl. Acad. Sci. USA.*, 2007, **104**, 20743-20748.
11. N. J. Farrer, J. A. Woods, L. Salassa, Y. Zhao, K. S. Robinson, G. Clarkson, F. S. Mackay, and P. J. Sadler, *Angew. Chem. Int. Ed.*, 2010, **49**, 8905-8908.
12. G. B. Kauffman and R. J. Thompson, *Inorg. Synth.*, 1963, **7**, 249-253.
13. C. Tessier and F. D. Rochon, *Inorg. Chim. Acta*, 1999, **295**, 25-38.
14. N. Farrell, L. R. Kelland, J. D. Roberts, N. Farteli, R. Lloyd, and M. V. Beusichem, *Cancer Res.*, 1992, **15**, 5065-5075.
15. M. Cossi, N. Rega, G. Scalmani, and V. Barone, *J. Comput. Chem.*, 2003, **24**, 669-681.
16. F. S. Mackay, N. J. Farrer, L. Salassa, H.-C. Tai, R. J. Deeth, S. A. Moggach, P. A. Wood, S. Parsons, and P. J. Sadler, *Dalton Trans.*, 2009, **7**, 2315-2325.
17. A. F. Westendorf, L. Zerzankova, L. Salassa, P. J. Sadler, V. Brabec, and P. J. Bednarski, *J. Inorg. Biochem.*, 2011, **105**, 652-662.
18. R. N. Keller, T. Moeller, and J. V. Quagliano, *Inorg. Synth.*, 2007, **2**, 250-253.
19. S. C. Dhara, *Indian J. Chem.*, 1970, **8**, 193.
20. P. W. Atkins, T. L. Overton, J. P. Rourke, M. T. Weller, and F. A. Armstrong, *Inorganic Chemistry*, Oxford University Press, Oxford, Fourth., 2006.
21. R. A. Alderden, M. D. Hall, and T. W. Hambley, *J. Chem. Educ.*, 2006, **83**, 728-734.
22. L. K. Thompson, *Inorg. Chim. Acta*, 1980, **38**, 117-119.
23. S. Shamsuddin, A. S. Mohammad, S. Huang, and A. R. Khokhar, *J. Coord. Chem.*, 2002, **55**, 659-665.
24. L. Maresca and G. Natile, *Comments Inorg. Chem.*, 1993, **14**, 349-366.
25. P.-C. Kong and F. D. Rochon, *Can. J. Chem.*, 1978, **56**, 441-445.
26. S. S. Kamath, V. Uma, and T. S. Srivastava, *Inorg. Chim. Acta*, 1989, **161**, 49-56.

27. F. Mackay, *Photoactive Platinum(IV) Azide Complexes (Report)*, 2007.
28. L. G. Marzilli, Y. Hayden, and M. D. Reily, *Inorg. Chem.*, 1986, 974-978.
29. R. J. Bansal, *Heterocyclic Chemistry*, New Age International (P) Ltd., New Delhi, 3rd edn., 1999.
30. M. Galanski and B. K. Keppler, *Anticancer Agents Med. Chem.*, 2007, **7**, 55-73.
31. J. Reedijk, *Pure Appl. Chem.*, 2011, **83**, 1709-1719.
32. P. Liu, Y. Lu, X. Gao, R. Liu, D. Zhang-Negrerie, Y. Shi, Y. Wang, S. Wang, and Q. Gao, *Chem. Commun.*, 2013, **49**, 2421-2423.
33. F. S. Mackay, S. A. Moggach, A. Collins, S. Parsons, and P. J. Sadler, *Inorg. Chim. Acta*, 2009, **362**, 811-819.
34. P. Muller, B. Schroder, J. A. Parkinson, N. A. Kratochwil, R. A. Coxall, A. Parkin, S. Parsons, and P. J. Sadler, *Angew. Chem. Int. Ed.*, 2003, **42**, 335-339.
35. F. S. Mackay, J. A. Woods, H. Moseley, J. Ferguson, A. Dawson, S. Parsons, and P. J. Sadler, *Chem. Eur. J.*, 2006, **12**, 3155-3161.
36. J. S. Butler, J. A. Woods, N. J. Farrer, M. E. Newton, and P. J. Sadler, *J. Am. Chem. Soc.*, 2012, **134**, 16508-16511.
37. C. E. Wayne and R. P. Wayne, *Photochemistry*, Oxford University Press, New York, 1996.
38. A. R. Battle, R. Choi, D. E. Hibbs, and T. W. Hambley, *Inorg. Chem.*, 2006, **45**, 111-115.
39. H.-C. Tai, Y. Zhao, N. J. Farrer, A. E. Anastasi, G. Clarkson, P. J. Sadler, and R. J. Deeth, *Chem. Eur. J.*, 2012, **18**, 10630-10642.

Chapter 5

Nucleobase binding and cellular behaviour of Pt(IV)- diazido complexes

5.1 Introduction

Irradiation of Pt(IV)-diazido, dihydroxo complexes in the presence of nucleotides has shown to form monofunctional as well as bifunctional Pt(II) adducts, following the loss of one or both azides.¹ Furthermore, CT-DNA binding studies have indicated that these complexes bind irreversibly to DNA. The rate at which this occurs depends greatly on the presence or absence of the pyridine ligand (for example the *trans, trans, trans*-[Pt(N₃)₂(OH)₂(NH₃)₂] binding faster than the *trans, trans, trans*-[Pt(N₃)₂(OH)₂(NH₃)(pyridine)] complex) and the extent of the binding is dependent upon the irradiation conditions: the presence of the DNA *in situ* (as opposed to mixing the irradiated complex with DNA) and the absence of competing nucleophiles, (e.g. chloride and GSH) enhance the binding yield.^{2, 3} Characterization of DNA adducts by plasmid transcription studies using *trans, trans, trans*-[Pt(N₃)₂(OH)₂(NH₃)(pyr)] showed that the preferred binding sites are mainly guanines and cytosines and less frequently adenines (similarly to transplatin).³ Studies with ethidium bromide, thiourea and gel electrophoresis illustrated that the Pt(IV)-azido complexes can potentially form monofunctional adducts which rapidly close to form bifunctional adducts. Only 6% of these adducts are interstrand, suggesting a potential majority of 1,3-intrastrand lesions.³ Similar studies with *trans,trans,trans*-[Pt(N₃)₂(OH)₂(pyr)₂] resulted in an analogous outcome in which monofunctional and intrastrand crosslinks are the major DNA adducts (51% and 37%, respectively) upon irradiation with either UVA or visible light.⁴ These lesions are able to stall RNA polymeraseII thus inhibiting RNA synthesis.⁴ DNA isolated from treated cells with aforementioned

complex (*trans,trans,trans*-[Pt(N₃)₂(OH)₂(pyr)₂]) provide direct evidence that it enters cells and binds to nuclear DNA after photoactivation.⁴

In order to determine whether the mechanism of cell death involves an apoptotic pathway, the caspase activity as well as the phosphatidylserine (PS) redistribution (both hallmarks of apoptosis) have been studied in cells treated with *trans, trans, trans*-[Pt(N₃)₂(OH)₂(pyridine)(NH₃)].⁵ Neither activation of caspase 3 or 7 nor the significant translocation of PS from the inner to the outer leaflet of the plasma membrane were observed. In contrast, cisplatin gave positive results in these tests.^{3, 5} Staining of nuclei of A2780 cells treated with *trans, trans, trans*-[Pt(N₃)₂(OH)₂(pyr)₂] with Hoechst dye showed that the nuclei did not fragment or condense, as opposed to the cisplatin-treated cells. Chromatin condensation and fragmentation is generally associated with a cell undergoing apoptosis.⁶ Overall these results indicated a non-apoptotic mechanism of cell death, which is distinct from cisplatin. Furthermore, morphological studies carried out on cells treated with *cis, cis, trans*-[Pt(N₃)₂(NH₃)₂(OH)₂] showed rounding of the cells, cellular shrinkage and loss of contact with neighbouring cells had occurred. In addition an excessive nuclear packing but no budding or formation of apoptotic bodies, expected for apoptosis, was seen.⁷

In the search for a possible mechanism of cell death, autophagy became a reasonable possibility due to the expected alteration of key autophagic proteins (e.g. LC3, p62) when HL60 cells were irradiated in the presence of *trans, trans, trans*-[Pt(NH₃)(pyr)(N₃)₂(OH)₂]. However this still needs to be confirmed.⁵

The work described in this chapter assesses the binding of the photoactivatable complexes, described in Chapter 4, to the nucleotide 5'-GMP; since the

preferential binding of platinum complexes to guanines is well established. Of specific interest is the complex *trans, trans, trans*-[Pt(N₃)₂(OH)₂(2-pic)(pyr)] as it is sterically hindered, showing fast photodegradation kinetics (refer to Chapter 4). Furthermore, the phototoxicity of the complexes in different cell lines A2780, A2780cis (ovarian cancer cell line) and OE19 (oesophageal cancer cell line) will be presented and discussed. The incidence of oesophageal cancer is increasing in the UK. Currently it is the ninth most common cancer and it is one of the most difficult cancers to treat.^{8,9} Therefore novel anticancer drugs which can tackle this serious problem are required. Moreover, both organs, the ovaries and the oesophagus, are accessible for PDT treatment.^{10,11}

The mechanism of cell death and the cellular targets of the Pt(IV)-diazido complexes have only recently been studied and further research is required for a better understanding. Herein, methods which have been employed for the first time in the study of photoactivatable Pt(IV)-diazido complexes will be presented and discussed.

5.2 Materials

Yeast strains for the *S. pombe* cell survival experiments were provided by Dr Jacob Dalgaard, University of Warwick (Life Sciences). The optical densities of the yeast cultures were determined on a NanoDrop 2000 spectrophotometer (Thermo Scientific). The microscopy slides for the confocal microscopy were sterile 15 µ-slide 8 well, purchased from Ibidi (Thistle Scientific). The fluorescent dyes (LIVE/DEAD Cell-mediated cytotoxicity kit (L7010) and the MitoTracker (Mitochondrion-Selective Probes)) were bought from Molecular Probes and Invitrogen, respectively.

5.3 Methods

5.3.1 5'-GMP binding studies

5'-GMP binding studies were carried out by irradiating the complexes (2 mM, except in case of **29**, *trans, trans, trans*-[Pt(N₃)₂(OH)₂(tz)₂] where 1 mM was used) in the presence of 5'-GMP (2 mol eq) with 420 nm light source (photoreactor, 1 h, 14 mW/cm²) and recording ¹H-NMR spectra immediately after the irradiation on a 500 MHz NMR spectrometer. The binding was quantified by integrating the peaks of the C₁H' bound protons for bound GMP (numbering scheme for 5'-GMP can be seen in the Appendix). Extensive irradiation studies for complex **18** (*trans, trans, trans*-[Pt(N₃)₂(OH)₂(pyr)(2-pic)]) were carried out (9 mM, PBS/ D₂O) in the presence of 2 mol eq of 5'-GMP at 420 nm light (7 mW/cm², 45 minutes). The ¹H-NMR spectra were recorded on a 600 MHz NMR spectrometer. The LC-MS analysis was undertaken on the HTC-Ultra mass spectrometer (Bruker) by diluting 50-fold the NMR samples in H₂O. An aliquot of 20 µL was injected into a ZORBAX Eclipse Plus C18 (4.6×150 mm, 5-Micron) column and eluted with H₂O (A)/ MeOH (B), both containing 0.1% formic acid. The gradient used was the following: 0 min- 7% B, 5 min-7% B, 25 min-70% B, 29 min- 70% B, 29.01-7% B, 30 min-7% B. The detection wavelength was 254 nm.

5.3.2 Phototoxicity testing

The phototoxicity testing was carried out in collaboration with Dr Julie Woods, University of Dundee, as outlined in Chapter 2.

5.3.3 Light dose dependence on cell survival (Action spectra)

Cells (A2780, OE19, HT1197) were seeded at a density of 1×10^6 in Petri dishes (diameter 53.5 mm) 24 hours before treatment, in order to adhere to the plate. The medium was removed and the cells were washed with PBS (2×5 mL) prior to the addition of the drug (15 μ M, 5 mL). The cells were incubated with the drug for 1 hour at 37 °C, 5% CO₂ atmosphere in the dark. Following this step, removal of the cells from the plate surface was carried out by gentle scraping and then broken apart by pipetting and release. Irradiations at 430 nm or 515 nm were carried in sterilized quartz cuvettes (2.5 mL) equipped with a magnetic stirrer. For each dose of irradiation 3 aliquots (3×30 μ L) of the irradiated or sham irradiated sample were taken and placed in a 96-well plate containing pre-warmed media at 37 °C. The monochromator used (Figure 5.1) was a Bentham 450 W Xenon Light Sources (IL 450 Xe), the output of which was measured before any experiment. The slit widths were set to 9 mm. Depending on the wavelength, the appropriate filter type was used: for 430 nm and 515 nm, GG375 and GG475, respectively. The cells were allowed to recover for 72 hours (in the case of A2780 and OE19) or 96 hours (for HT1197). Then cell viability was determined using the MTT assay as outlined in Chapter 2.

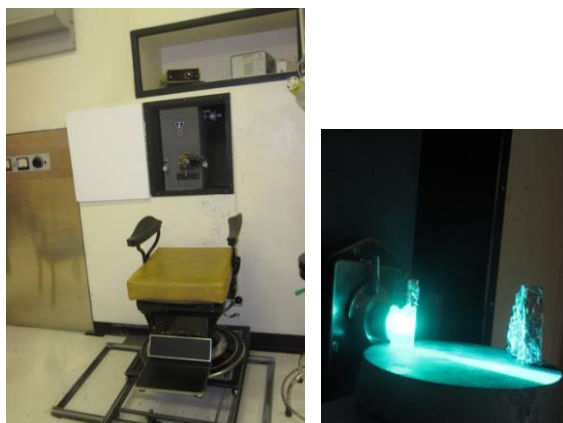


Figure 5.1: The monochromator (Bentham 450 W) employed for the action spectra, which is normally used for PDT on patients at the Photobiology Unit of Ninewells Hospital (Dundee, UK).

5.3.4 Yeast studies

Colonies from two strains of *Schizosaccharomyces pombe* ($h^{90}leu$ 1-32, *ade* 6-210, *ura4*- Δ 18 and h^{90} , *ade* 6-210, *ura4*- Δ 18, $\Delta rad3::ura4$) were collected and allowed to grow overnight in ~ 5 mL of complete yeast extract medium supplemented with adenine (YEA, 5 g/L yeast extract, 30 g/L dextrose, 0.075 g/L adenine) at 33 °C with shaking. Then, they were inoculated in 5 mL of pre-warmed medium at an $OD_{600\text{ nm}}$ of ~0.5 and were allowed to grow for a further 2 hours. The cells were then spun down for the removal of the medium, resuspended in PBS and kept on ice during the experiment to prohibit further growth. A stock solution with an $OD_{600\text{ nm}}$ 0.02 was prepared and used to plate the cells in a 96-well plate with OD_s of 0.01, 0.005, 0.0025 and 0.00125 ($OD_{600\text{ nm}}$ 0.01 corresponds to ~100000 cells). Complex **3** (*trans, trans, trans*-[Pt(N₃)₂(OH)₂(pyr)₂]) was then added at different concentrations (300, 200, 100 and 0 μ M) and the plate was placed on the shaker for 5 minutes. The drug was

allowed to be taken up for 1 hour on ice in the dark and then the cells were irradiated with 420 nm light (45 min, 12 mW/cm²), using the photoreactor. Following this step, the plate was placed on a plate centrifuge (10 minutes, 5000 g). The supernatant was removed and the cells resuspended in YEA media (100 µL). The contents of each well were spread on YEA agar plates and were allowed to grow for 3 days at 33 °C. The survival was estimated by colony counting which was plotted against the non-treated controls. A modified protocol was also applied, where the number of cells plated was equivalent to OD_{600 nm} = 0.1 in 2 mL. Following irradiation under the same experimental conditions as described above, the cells were counted using a cellometer (Nexcelom Bioscience) and diluted to a concentration of 4000 cells/mL before spreading onto the YEA agar plates.

5.3.5 Confocal Microscopy

A2780 cells were seeded on a microscopy chamber (Figure 5.2) at densities of 2×10^5 and 1×10^5 and were allowed to adhere for 24 or 48 hours, for the contrast and confocal microscopy experiments, respectively. The walls of the empty middle wells of the microscopy chamber were blacked out using a black permanent marker pen to avoid leakage of light to the control wells.

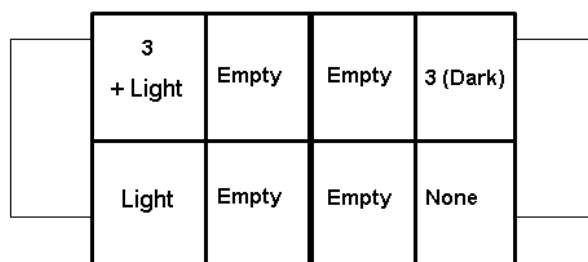


Figure 5.2: The chamber used for the live-cell confocal microscopy experiment, showing the setup of each well. The thick middle line represents the blackened out walls.

After the adhesion period, cells were washed with PBS (300 μL) prior to addition of the drug in PBS (50 μM) and mitotracker (213 nM) and incubated in the dark for 1 hour. Cells were irradiated for 5 min (64 mW/cm^2 , 17 J/cm^2) resulting in a comparable dosage, according to number of cells and irradiation time used for the phototoxicity studies of complex **3** reported previously⁶ (5 J/cm^2 for 6×10^4 cells/ cm^2). Following irradiation, media was replaced with fresh RPMI-1640 (300 μL) and propidium iodide (10 μL of 7.5 μM stock solution) was added. Cells were then incubated for 5 minutes at 37 $^\circ\text{C}$ and viewed using a SP5 Leica confocal microscope equipped with a temperature control chamber set to 37 $^\circ\text{C}$. Focusing of the cells was carried out by visualizing the mitotracker using a 633 nm laser, therefore prohibiting exposure to white light, which can photoactivate the complex. Cells were imaged using a 594 nm (HeNe) laser during 12-15 hours using a 40 X oil immersed objective. The first image was captured *ca* 30 minutes after the photoactivation of the cells. Images were taken every 15 minutes.

5.4 Results

5.4.1 5'-GMP binding studies

Irradiation of the *trans*-diazido diamine complexes (2 mM) (Figure 5.3) at 420 nm (1 hour, 24.7 mW/cm², 88920 mJ/cm²) in the presence of 5'-GMP (2 mol equivalents) in PBS/ D₂O (pH* 7.4) resulted in binding of all the complexes to form two adducts which can be assigned by analogy with previous studies to the mono and bis GMP adducts.⁶ The extent of binding of individual complexes to 5'-GMP is depicted in Table 5.1. Release of the N-heterocyclic ligand was not observed in any of the cases.

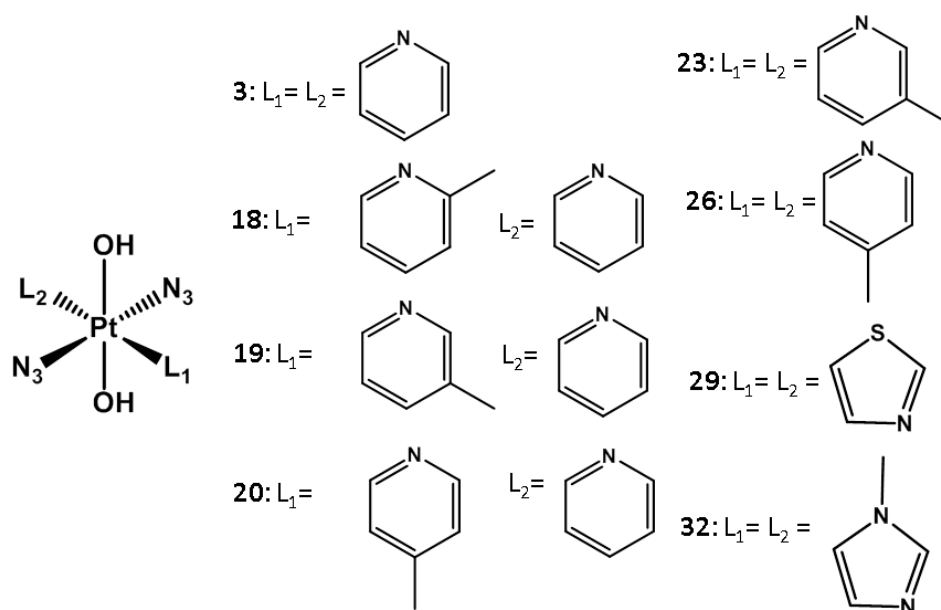


Figure 5.3: Structures of complexes studied in this chapter.

In order to examine the photoproducts of the sterically hindered *trans, trans, trans*-[Pt(N₃)₂(OH)₂(pyr)(2-pic)] (**18**), the irradiation was carried out using the

same concentration and irradiation conditions as published previously for *trans*, *trans*, *trans*-[Pt(N₃)₂(OH)₂(pyr)₂] (9 mM, 420 nm, 7 mW/cm²).⁶ Upon irradiation, the solution turned cloudy and the appearance of bubbles was observed. Precipitation was not observed when the irradiations are carried out at lower concentrations (e.g. 2 mM).

Table 5.1: 5'-GMP binding of Pt(IV)-diazido complexes upon blue light irradiation (420 nm, 1 hour, 14 mW/cm²). The error is approximated to 5-10% due to errors in integration of NMR peaks.

Complex	%Binding
18	52
19	58
20	64
23	68
26	64
29*	80
32	48

Irradiation of complex **18** (9 mM) in PBS with a low dose of 420 nm resulted in the formation of only one major 5'-GMP photoproduct as illustrated by the ¹H-NMR (Figure 5.4 B). ¹⁹⁵Pt: 129 MHz NMR spectrum showing the Pt(IV) region proved the almost complete disappearance of the Pt(IV) peak suggesting a nearly complete reduction to Pt(II) had occurred (Figure 5.5 A). In the Pt(II) region the formation of a major and minor products, (X) and (Z) respectively, is shown (Figure 5.5 B). The major peak (X) can be assigned to the mono-GMP adduct, *trans*-[Pt(N₃)(2-pic)(pyr)(5'-GMP)], as confirmed by the LC-MS studies (Figure

5.6). Over time (2 weeks in the dark) it was shown that a second 5'-GMP product is formed and its appearance was evident as early as 3 days after the irradiation (Figure 5.4 C and Figure 5.6 B). The LC-MS chromatogram indicated that this photoproduct is the bis-5'-GMP adduct (Y). It can be deduced that the minor Pt(II) product, Z shown in the ^{195}Pt -NMR spectrum, had formed immediately after irradiation and is slowly being converted into the bis-GMP adduct. This species can be tentatively assigned to the species $[\text{Pt}(2\text{-pic})(\text{pyr})(\text{OH})(5'\text{-GMP})]^+$ (theoretical $M^+ = 747.1\ m/z$) as in the LC-MS chromatogram, there is a minor peak with the corresponding mass spectrum containing a peak with $m/z = 747.0$.

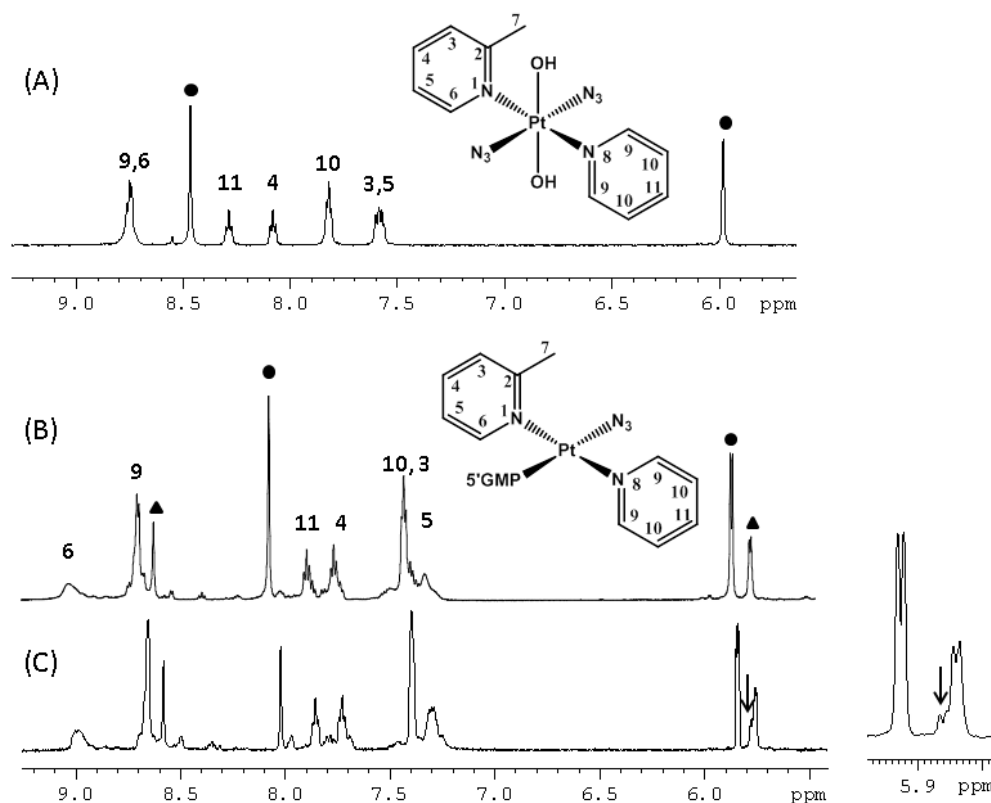


Figure 5.4: 600 MHz ^1H -NMR of complex **18** (9 mM) in the presence of 5'-GMP (2 mol eq) in PBS/ D_2O (pH* 7.4) of: (A) In the dark. (B) Immediately after irradiation (420 nm, 45 min, 7 mW/cm²). The formation of the mono-GMP adduct is shown, with the assignment of the peaks corresponding to the pyridine ligands on the platinum. The assignment was aided by 2D ^1H correlation spectroscopy (COSY). The circle and the triangle represent free and bound 5'-GMP, respectively. (C) Two weeks after the irradiation, where the evolution of a second 5'-GMP adduct is observed, as shown by the arrows. The spectrum on the right hand side is zoomed in, on the C_1 proton of the sugar ring to illustrate the evolution of the second product 3 days after irradiation.

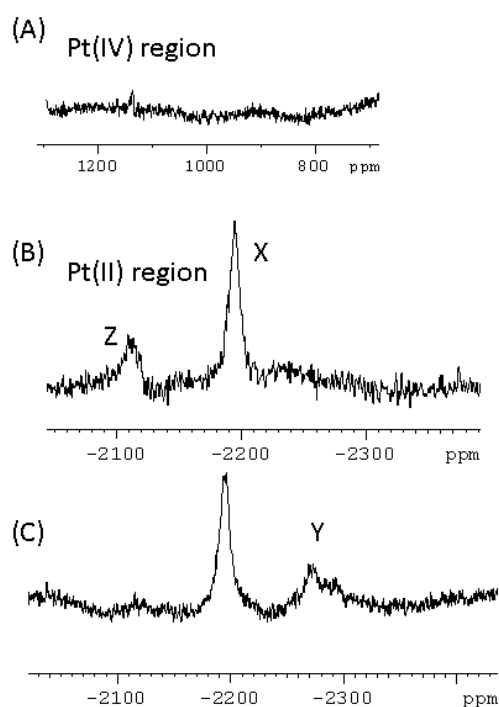


Figure 5.5: ^{195}Pt -NMR spectra of the Pt(IV) and Pt(II) regions after irradiation (420 nm, 45 min, 7 mW/cm²) of complex **18** (9 mM) in the presence of 5'-GMP. Spectra A and B were obtained immediately after irradiation whereas spectrum C was recorded 2 weeks after the sample was allowed to stand in the dark at ambient temperature. Products X and Y have been assigned to the mono-GMP and bis-GMP adducts, respectively whereas product Z was tentatively assigned to *trans*-[Pt(2-pic)(pyr)(OH)(5'-GMP)].

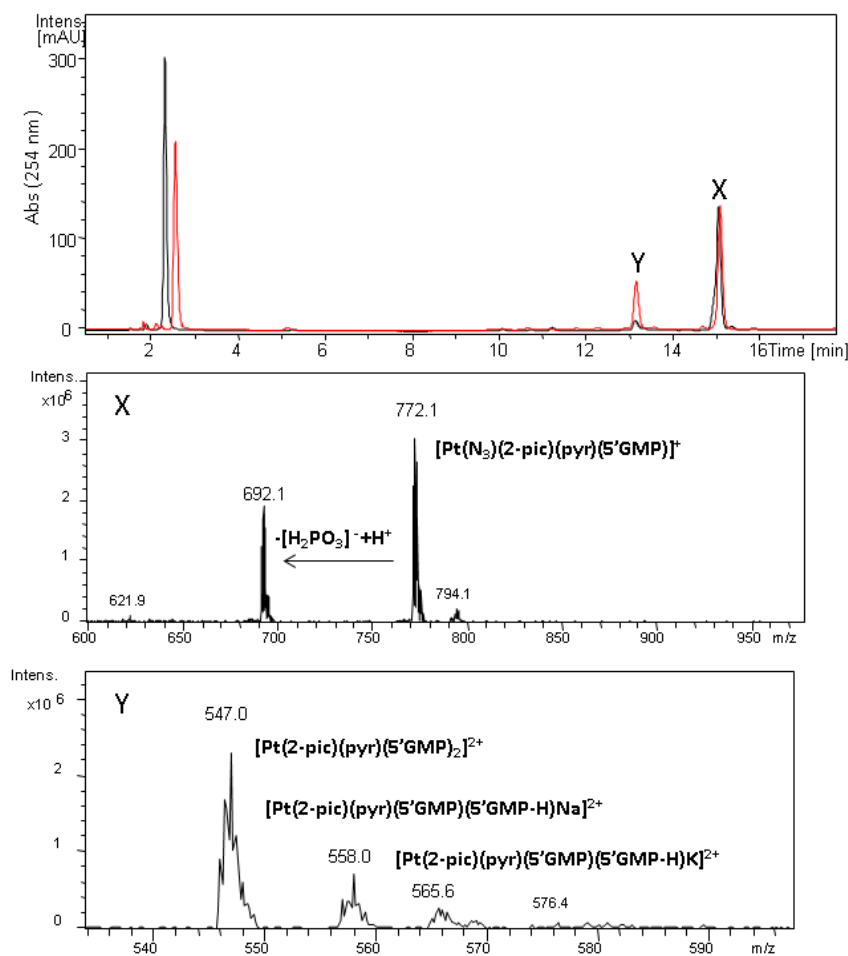


Figure 5.6: LC-MS of the irradiated sample of complex **18** a day after irradiation (black) and two weeks (red). Product X (major) corresponds to $[\text{Pt}(\text{N}_3)(2\text{-pic})(\text{pyr})(5'\text{-GMP})]^+$ (theoretical $M = 772.1\text{ m/z}$, $[\text{M}-\text{H}_2\text{PO}_3^- + \text{H}^+] = 692.2\text{ m/z}$). Product Y evolves over time and is assigned as $[\text{Pt}(5'\text{-GMP})(2\text{-pic})(\text{pyr})]^{2+}$ (theoretical $[\text{M}]^{2+} = 546.6\text{ m/z}$, $[\text{M}-\text{H} + \text{Na}]^{2+} = 557.6\text{ m/z}$, $[\text{M}-\text{H} + \text{K}]^{2+} = 565.6\text{ m/z}$).

5.4.2 Phototoxicity studies

The phototoxicity studies were performed on ovarian cell lines (A2780 and A2780 cisplatin resistant cells A2780cis) and oesophageal cancer cells (OE19). The results are depicted in Table 5.2. Activity in cisplatin resistant cell lines is usually indicative of a cell death mechanism distinct of that from cisplatin which is a favourable feature for potential anticancer therapeutics.

Table 5.2: Phototoxicity of the complexes reported in Chapter 4, with the general structure of *trans, trans, trans*-[Pt(N₃)₂(OH)₂(L₁)(L₂)] where L₁ and L₂ are defined in Figure 5.3. Irradiation of the complexes was carried out with 420 nm (5 J/cm², TL03), filtered below 400 nm.

*PI= phototoxic index, ** ND= not determined, ***FM165= *trans, trans, trans*-[Pt(N₃)₂(OH)₂(NH₃)(pyr)]

Complex	A2780			A2780cis			OE19		
	IC ₅₀	95% CI	*PI	IC ₅₀	95% CI	PI	IC ₅₀	95% CI	PI
18	14.5	12.7-16.7	7.3	15.5	11.2-21.5	5.3	ND	ND	ND
19	4.0	3.0-5.4	>51.5	3.3	1.9-5.9	>71.0	5.5	3.2-9.4	>38
20	5.4	4.3-6.8	>38	4.6	3.8-5.6	>45	12.3	7.9-19.1	>17
23	7.2	6.0-8.7	>27.8	10.4	8.7-12.2	>19.3	ND	ND	ND
26	2.1	1.6-2.7	>95	4.1	3.3-5.1	>48.8	8.2	5.5-12.0	>24
29	2.4	2.2-2.7	48	2.9	1.6-5.2	>71.0	7.6	5.4-10.7	>27
32	56.3	40.2-78.9	>3.7	164.2	wide	>1.3	ND	ND	ND
FM165 ***	25.4	22.2-29.1	>9.6	**ND	ND	ND	ND	ND	ND
3	6.7	3.6-13.7	>45	ND	ND	ND	8.4	ND	>45

Photofrin (a known PDT agent) has an IC₅₀ of 46.8 ng/mL. This is in the nanomolar range but photofrin is a mixture of oligomers, so an IC₅₀ in molar units cannot be accurately provided. Nevertheless, it is significantly more active than the current Pt(IV)-diazido complexes.

The dose-response of the activity of complex **20** ([Pt(N₃)₂(OH)₂(pyr)(4-pic)]) upon irradiation at 430 nm and 515 nm in A2780 and OE19 cells was also assessed (Figure 5.7). The complex showed no phototoxicity on activation at 515

nm in either A2780 or OE19 cells. Upon use of 430 nm irradiation, there was 8% and 57% survival with a dose of 100 J/cm² in A2780 and OE19 cells, respectively.

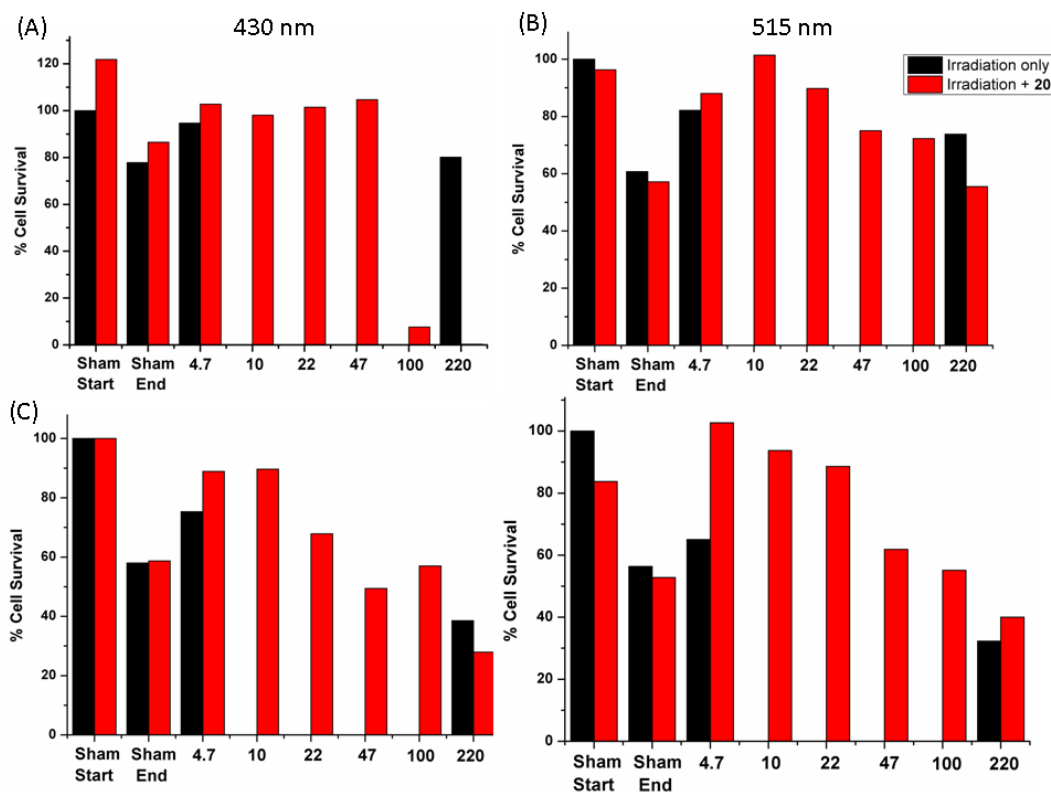


Figure 5.7: Survival of A2780 (A and B) and OE19 (C and D) cells treated with complex **20**, upon irradiation with different doses (in J/cm²) of 430 nm and 515 nm light. Sham cells were not exposed to any light.

5.4.3 Cell survival in *Schizosaccharomyces pombe* in response to Pt(IV)-diazido drug

Two strains of *S. pombe* were used, a wild-type strain and a Δ rad3 (i.e. deletion of the Rad3 kinase which is responsible for DNA repair) to study the effects of the complex *trans, trans, trans*-[Pt(N₃)₂(pyr)₂(OH)₂], **3**.

When the experiment was carried out under conditions of a low drug concentration (2 μ M and 0.04 μ M), no apparent difference between the two strains

was observed and when 400 μM drug concentrations was used there was no colony growth for either WT or ΔRad3 cells. However with Pt concentrations of 300 and 200 μM , the difference between the two strains became obvious. No difference in cell survival was observed for the non-treated cells, indicating that the light alone did not cause any cell death (Figure 5.8 and Figure 5.9).

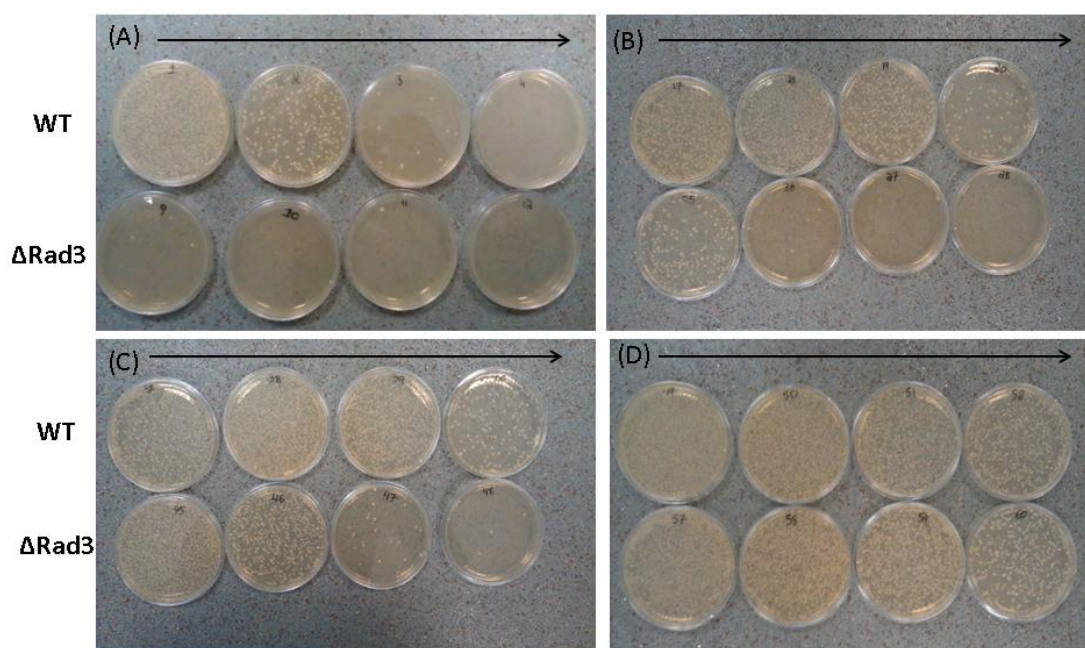


Figure 5.8: Images of colony growth of *S. pombe* cells. The arrow shows the decreasing amount of cells in each plate (OD 0.01, 0.005, 0.0025, 0.00125). (A) 300 μM of complex **3** (B) 200 μM (C) 100 μM and (D) 0 μM . The cells were irradiated with 420 nm (45 min, 12 mW/cm^2 , 45 min). The top row of dishes in each of the images consists of WT cells whereas the bottom the Δrad3 mutant. The image shows the difference in survival between the two strains.

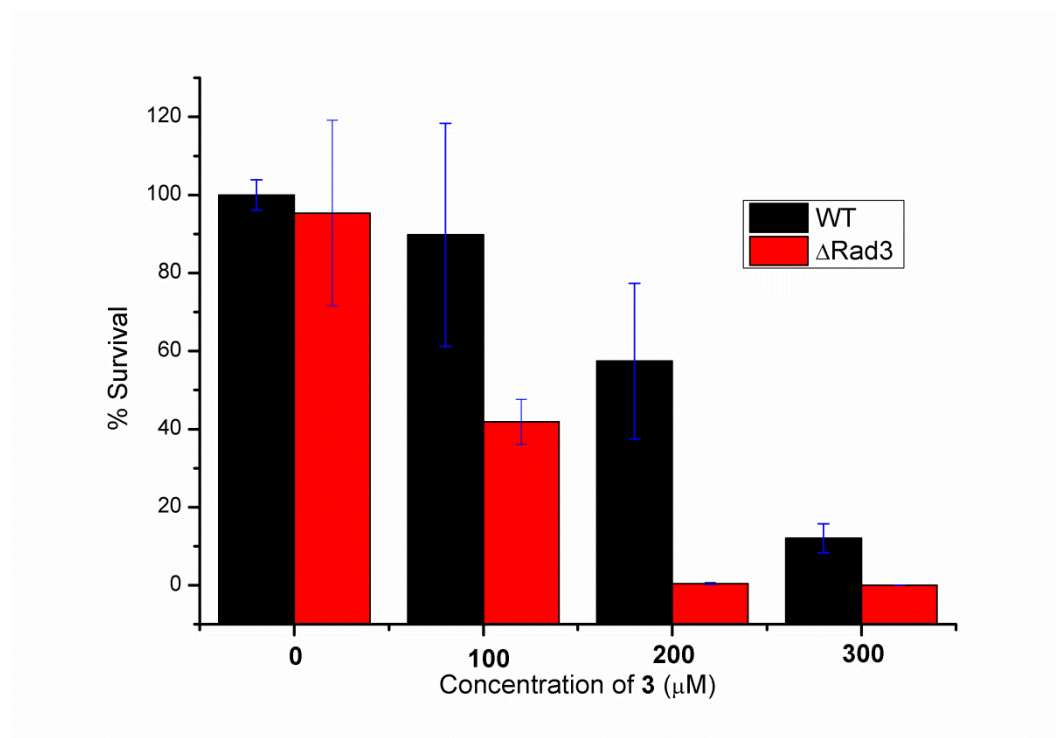


Figure 5.9: Effect of complex 3 concentration on the % survival of *S. pombe* cells as measured by colony counting between the two strains. The data were plotted with the initial concentration of seeded cells as an OD = 0.005. The error bars were produced from two experimental repeats.

5.4.4 Live-cell confocal microscopy

The aim of this experiment was to establish a protocol to allow changes in cells after the photoactivation of a Pt(IV)-diazido drug such as *trans, trans, trans*-[Pt(N₃)₂(OH)₂(pyr)₂] to be monitored. The concentration chosen was low enough to avoid any dark toxicity (20 μM) although it was unknown whether the prolonged exposure to the confocal microscope's laser would cause any complex activation and subsequent cell death. Finding the appropriate focus was achieved using the purple dye, mitotracker (λ_{ex} = 644 nm), a specific dye which targets mitochondria only, to avoid exposure to white light. However some non-specific binding was observed and the cytoplasm was also partially stained (Figure 5.10).

Cell death was assessed by following the uptake of propidium iodide (red dye) which binds to nucleic acids only when the integrity of the cell membrane is compromised. Activation of the drug using LED light source (463 nm, 5 min) allowed phototoxicity to be obtained for treated cells without unwanted death of control cells (Figure 5.11). The first indication of cell staining with propidium iodide occurred as early as 1 h 45 min after the activation, suggesting that the membranes may have been compromised very early on. This represents the first example of live imaging of cell death caused by a Pt(IV)-diazido complex.

Morphological changes of the treated cells with phase contrast images captured 16 hours after activation showed rounding of the cells, loss of contact with the neighbouring cells as well as detachment from the surface of the chamber. No such changes were observed when the cells were treated with the complex alone without irradiation or for untreated irradiated controls (Figure 5.12).

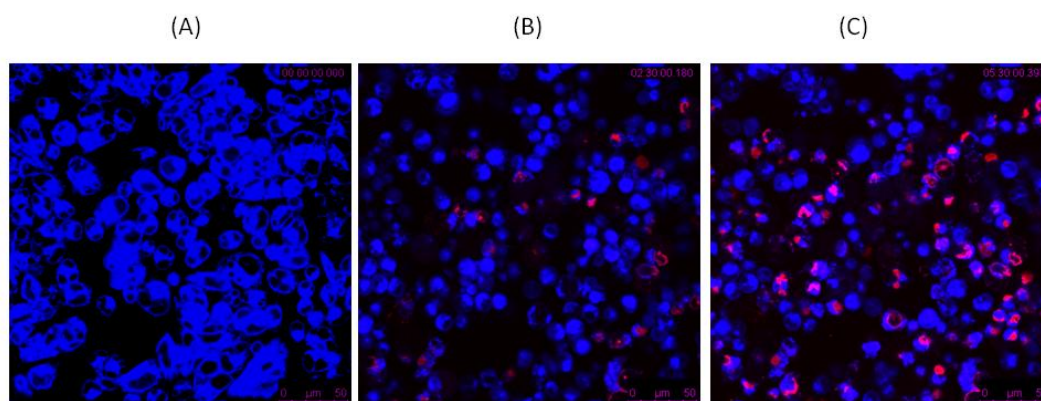


Figure 5.10: Confocal microscopy images of A2780 cells treated with complex **3** and irradiated with blue light (463 nm) at $t=0$ (A), 2 h 30min (B) and 5h 30 min(C) post-irradiation. The blue and the red fluorescent dyes are a result of the mitotracker and propidium iodide, respectively. The colour of the mitotracker was changed from purple to blue using ImageJ in order for clarity.

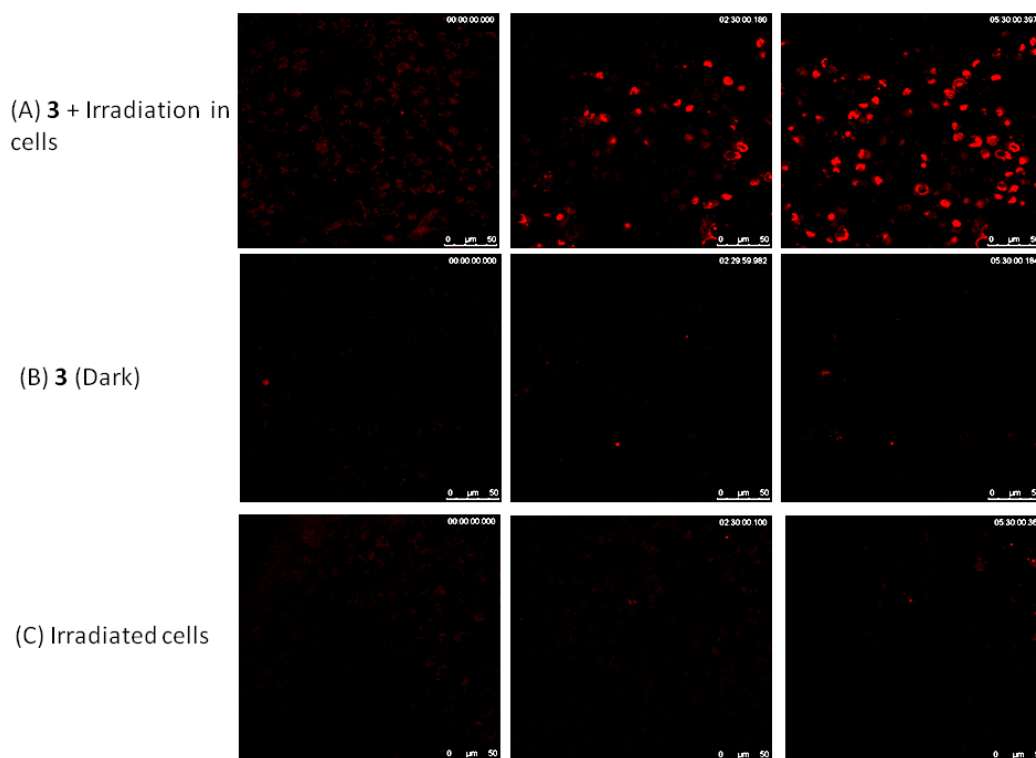


Figure 5.11: Confocal microscopy images obtained at $t=0$, 2 h 30 min and 5 h 30 min during the live cell experiment of A2780 cells treated with complex **3** and irradiated with blue light (463 nm) ($t=0$ corresponds to *ca* 30 min after the photoactivation of the cells). A, B and C represent the different conditions, under which the cells were exposed. The red staining (Propidium Iodide) illustrates the nuclei of the dead cells.

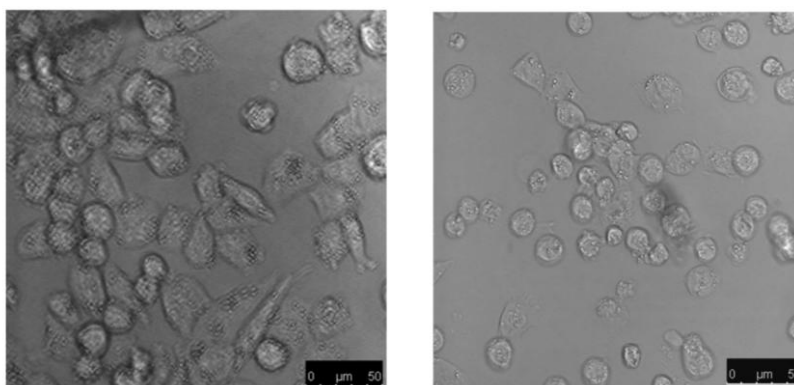


Figure 5.12: Phase-contrast images of A2780 cells after exposure to complex **3** (*trans, trans, trans*-[Pt(N₃)₂(OH)₂(pyr)₂] for 1 hour in the dark (left) or irradiated with 463 nm light (right). The images were obtained 16 hours after the exposure to the drug alone (left) or the drug plus light (right).

5.5 Discussion

5.5.1 5'-GMP binding studies

Irradiation of the *trans*-Pt(IV)-diazido complexes reported in the previous chapter was shown to lead to formation of 5'-GMP adducts with an average extent of 59% conversion with respect to the platinum complex. Similar reactions for complexes with (pyr)(3-pic), (3-pic)₂ and (4-pic)₂ as the N-heterocyclic ligands resulted in almost identical binding yields, between 64-68%. A lower extent of binding was observed for the (1-methylimidazole)₂ complex, 48% (Table 5.1). Although no excessive photoproduct analysis was undertaken for all these complexes, it can be reasonably assumed that the photoproducts are the mono [Pt(N₃)(GMP)(n-heterocycle)₂]⁺ and bis [Pt(GMP)₂(n-heterocycle)₂]²⁺ adducts.

Complex **18**, Pt^{IV}(2-pic)(pyr), irradiated at 420 nm as a 9 mM solution in PBS (D₂O) was studied more extensively with ¹H, ¹⁹⁵Pt- NMR and LC-MS. The mono-GMP adduct is the only adduct formed first and the bis-GMP is generated when the irradiated sample is allowed to stand over time in the dark at room temperature (Figure 5.4 and Figure 5.6). The methyl group creates steric constraint on the platinum centre which can reduce the substitution kinetics of the Pt(II) photoproduct. In fact, the restricted rotation about the Pt^{II}-2-picoline bond of the [Pt(N₃)(2-pic)(pyr)(5'-GMP)] product is evident from the broadening of the 6 and 5 protons (Figure 5.4 B). The analogous protons exhibited most of the broadening observed for *cis*-[Pt(2-pic)₂Cl₂] (Chapter 4, Figure 4.6).

The evolution of various DNA adducts over time is commonly observed amongst platinum compounds. For example transplatin shows a few interstrand crosslinks

in cells and this was accounted by the slow conversion of the monofunctional to bifunctional adducts.¹²

In studies performed with the *trans, trans, trans*-[Pt(N₃)₂(OH)₂(pyr)₂], re-oxidation of the Pt(II) product was observed over time,⁶ a result which was not obtained in this work for complex **18**. This difference could be attributed to the fact that in this work PBS (0.01 M phosphate, 0.0027 M KCl, 0.137 M NaCl) was employed instead of D₂O only.

5.5.2 Phototoxicity and structure-activity relationships

The N-heterocyclic ligand appears to play an important role in the biological properties of the *trans, trans, trans*-Pt(IV)-diazido-dihydroxo complexes. Comparing the compounds with pyridine as one ligand and n-picoline as the second ammine ligand, it is evident that the complex **18** containing 2-picoline is the least phototoxic ($\lambda = 420$ nm, IC₅₀ = 14.5 μ M). Along with the findings from the [Pt(N₃)₂(OH)₂(NH₃)(n-picoline)] family of compounds, which were photoactivated with UVA light, it is confirmed that steric hindrance close to the platinum centre does not favour phototoxicity.¹³ A possible explanation for this could be the slow formation of bifunctional adducts, as in the case of picoplatin. It was shown that picoplatin forms interstrand DNA crosslinks and binds plasma proteins more slowly than cisplatin.¹⁴ The phototoxicity and dark toxicity IC₅₀ values are tabulated in Table 5.2. The difference in IC₅₀ values between the Pt^{IV}(pyridine)(3-picoline) (**19**) and Pt^{IV}(pyridine)(4-picoline) (**20**) complexes is minimal (4.0 vs 5.4 μ M in A2780) however in OE19 cells the Pt^{IV}(pyr)(3-pic) complex is 2-fold more active (5.5 μ M vs 12.3 μ M). In the Pt^{IV}(n-picoline)₂

family of complexes, there is almost a 2-fold decrease in cytotoxicity between the $\text{Pt}^{\text{IV}}(3\text{-picoline})_2$ (**23**) and $\text{Pt}^{\text{IV}}(4\text{-picoline})_2$ (**26**) complexes. Variations in cytotoxicity between picoline analogues is not unusual, as it has been reported that in complexes $\text{trans-}[\text{Pt}^{\text{II}}\text{X}_2(3\text{-pic})_2]$ and $\text{trans-}[\text{Pt}^{\text{II}}\text{X}_2(4\text{-pic})_2]$, where X is Cl^- or OAc^- , the 4-picoline complexes were more cytotoxic in Pam 212 and Pam 212-*ras* cell lines (murine keratinocytes).¹⁵ Furthermore, it was shown by Rakic *et al.* that changing the position of substituent on the pyridine has a significant effect on the cytotoxic properties of the complexes, as studying the cytotoxicity of $\text{trans-}[\text{PtCl}_2(3\text{-acetylpyridine})_2]$ and $\text{trans-}[\text{PtCl}_2(4\text{-acetylpyridine})_2]$ in a range of cell lines showed that the para-substituted complex was more cytotoxic.¹⁶ The results in the present work show that for the bis-picoline complexes, a *para* substitution enhances the cytotoxicity but in the (pyridine)(*n*-picoline) complexes the *meta* substitution is slightly favoured. None of the complexes in this series was found to be dark-toxic with the exception of the $\text{Pt}^{\text{IV}}(\text{pyridine})(2\text{-picoline})$ complex, with a PI of 7.3 (i.e. $\text{IC}_{50} \sim 106 \mu\text{M}$ in the dark).

The $\text{trans-Pt}^{\text{IV}}(\text{thiazole})_2$ (complex **29**) is a very potent compound ($2.4 \mu\text{M}$ in A2780), constituting another example of a compound with bis-aromatic ligands more phototoxic than having only one aromatic amine, as the IC_{50} of the complex $\text{trans, trans, trans-}[\text{Pt}(\text{N}_3)_2(\text{OH})_2(\text{NH}_2\text{CH}_3)(\text{thiazole})]$ was $28.2 \mu\text{M}$.¹⁷ However this complex exhibited some dark toxicity in the A2780, although it was the most toxic compound in the A2780cis cell line. The least phototoxic compound from the family was that bearing 1-methylimidazole ligands (complex **32**). This lack of activity might be attributable to its high hydrophilicity, as shown by the high aqueous solubility, leading to low cellular uptake.

In order to test cell viability with different doses of light at 430 nm, and 515 nm, action spectra were recorded for the A2780 and OE19 cell lines (Figure 5.7). They were also attempted with the HT1197 bladder cell line but these cells were highly sensitive to the blue light as well as the conditions under which the experiment was conducted (e.g. stirring, scraping, pipetting to form a single cell suspension). The light sensitivity of these cells can be attributed to the high intracellular porphyrin content (twice as high as OE19) causing phototoxicity.¹⁸ It is also evident from the action spectra as well as the phototoxicity values for A2780 and OE19 cells that there is a resistance factor in the oesophageal cancer cell line. This effect might involve antioxidant defence, drug uptake, drug efflux, drug localisation or DNA repair, for example.

5.5.3 Cell survival assessed in *S. pombe*

During the cell cycle of eukaryotes, accurate DNA replication is crucial for genomic stability and thus the survival of the organism. DNA lesions can be caused endogenously, for example by base-pair mismatch or strand breaks occurring during replication, and exogenously by UV exposure, DNA damaging agents (e.g. hydroxyurea, methyl methanesulfonate) making cells non-viable or susceptible to mutation.^{19, 20} For these reasons, eukaryotic cells have developed sophisticated mechanisms to control responses to DNA damage which happen at checkpoints at different times of the cell cycle.^{11, 21} When damage is detected, the appropriate signalling is triggered to delay the cell mitosis and for DNA repair to take place. Checkpoint sensor proteins are responsible for detecting the DNA damage and then activating the mediator proteins, which in turn promote protein-

protein interactions between sensors and effectors, thus mediating signal transduction to the effectors. Once these become activated, most of the biological effects take place in the cell which can lead to procession to the next stage of the cell cycle, to DNA repair, remodelling or to cell death.¹⁹ Most of the proteins involved in the repair pathways have been identified in budding and fission yeast and loss of function in these (by mutation) can result in significant cell death in the presence of a damaging agent.²² In *Schizosaccharomyces pombe* there are two known checkpoint pathways: the first one is controlled by the effector *Cds1* (acting in the S-phase) and the second by the *Chk1* (acting in the G2 phase and in the G₂ phase in the absence of *Chk1*). Both of these are activated (by phosphorylation) by the upstream sensor protein Rad3²³ that detects replication blocks as well as DNA damage (e.g. double strand breaks) (Figure 5.13).²⁴ The orthologous protein in mammals is the ATR kinase. Disruption or mutation of Rad3 can lead to serious inhibition of the DNA checkpoint signalling. Due to the functional overlap of the two signalling pathways (*Cds1* and *Chk1*), deletion of either one of them does not lead to a striking effect in the replication pathway but a Rad3 deletion has a profound effect in cell survival, when exposed to a DNA damaging agent.^{25, 26}

Yeast is a widely used model to study the effects of drugs due to the fact that it is a eukaryotic organism with many of the cellular processes conserved in mammals.²⁷ *S. cerevisiae* has been used previously to study cisplatin toxicity, drug transport, DNA repair and also genes involved in drug resistance and sensitivity.^{24, 28, 29} Nevertheless, best to the author's knowledge, this work represents their first use to study the mechanism of action of light activated drugs.

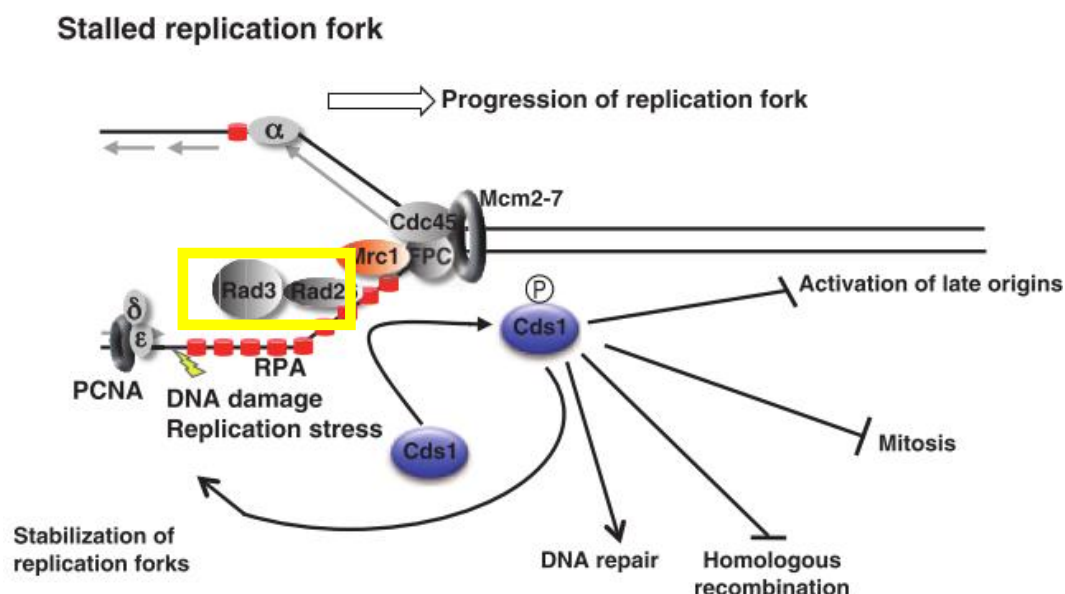


Figure 5.13: Schematic illustration of the S-phase checkpoint in fission yeast, where the Rad3 is recruited on the ssDNA region through the binding partner Rad26. Then Rad3 phosphorylates Mrc1 which is required for the efficient phosphorylation of Cds1 by Rad3. Cds1 switches on DNA repair. Taken from reference.³⁰

The sensitivity of the Rad3 mutant towards the Pt(IV)-diazido complex (Figure 5.8) indicates that the DNA is a target for this kind of compound. However, the WT strain also showed toxicity especially at high drug concentrations ($>200 \mu\text{M}$), suggesting the existence of multiple mechanisms of action (e.g. oxidative stress caused by the complex). For the 100 and 200 μM concentrations, the difference in survival between the two strains is significant, suggesting that the DNA damage triggered can be repaired, thus enhancing the survival of the WT cells (Figure 5.9). The Pt(IV)-diazido complexes can damage DNA through the release of radicals or through DNA platination (Figure 1.15, Chapter 1). Reactive oxygen species can produce DNA lesions via base modification, induction of inter and

intrastrand crosslinks, promotion of DNA-protein crosslinks or creating strand breaks.³¹ However the ROS can cause oxidation of other vital cellular components such as proteins and membrane lipids, therefore triggering a DNA-independent cell death. These results suggest a concentration-dependent mechanism of action, where DNA damage can potentially play a major role.

Notably the amount of complex **3** that is required to cause an effect is *ca* 20-fold higher than in mammalian cells. A similar result was observed for the cisplatin studies although in that case it was attributed to the reactivity and subsequent deactivation of the drug with the sulphur-rich culture media.²⁷ In this case however, the inertness of Pt(IV) drugs, especially in PBS, could not account for this effect. A reasonable explanation can be the poor cell uptake of the Pt(IV) drugs, which is likely due to the presence of a cell wall, that can impede the uptake of some agents.³²

The assay was carried out by diluting first the yeast cells and then treating them with the drug, in this way only a small amount of compound is required. The experiment was also attempted with a different protocol, in which the cells were seeded in larger numbers and counted, diluted, photoactivated and then plated on YEA media. The distinction between the cell survival of the two strains was then less obvious, leading to complete cell death in most of the cases. This can be due to the fact that the time between activation and plating into the YEA culture media was longer (*ca* 2 hours), allowing longer exposure to the irradiated medium and also a longer time before cells were allowed to recover, making this approach less suitable for this assay.

5.5.4 Live-cell confocal microscopy

The determination of the cell death pathway for a drug is not straight forward requiring the use of multiple markers. The application of real-time techniques can lead to significant improvements.³³ Morphological changes can usually provide initial information about the cell death mechanism triggered. For example, in apoptosis cell shrinkage, nuclear condensation, blebbing and formation of apoptotic bodies usually take place. Necrosis on the other hand is usually manifested by an increasing translucent cytoplasm, organelle swelling and cell volume expansion.³³ In autophagy, the appearance of autophagosomes within the cytoplasm can become evident.³⁴

Live cell imaging is a useful technique that can be used to visualize cells with minimal artefacts, as opposed to fixed cell microscopy. Furthermore, it is the best method for following kinetic events and it also gives the opportunity to study whole cells rather than looking at organelle-specific techniques which can lead to erroneous results.³⁵ Nevertheless, challenges in performing live cell experiments include the difficulty of maintaining the cells healthy for prolonged periods of time outside the incubator, the focal drift due to cell movement, as well as potential phototoxicity induced by the continuous exposure to the laser of the microscope.³⁵

The original idea was to activate the drug in cells *in situ* using the microscope's laser. This proved to be difficult, as control cells which were exposed for long times to the laser light underwent cell death. This was attributed to components within the cell media that cause oxidative stress via radical production when exposed to light. Studies reported in the literature confirmed that the riboflavin

contained in the media (e.g. 0.2 mg/ L in RPMI-1640) is likely to be the main component responsible for such effects, although L-tryptophan (5 mg/ L) enhances the effects of riboflavin.^{36, 37, 38} Therefore for this method to be successful more optimization is required (e.g. potential addition of antioxidants).

Irradiation of the complex in PBS with a blue LED (463 nm, 5 min) resulted in a better survival of the untreated controls, allowing imaging of the uptake of propidium iodide (PI), a marker of cell death without artefacts. PI-related fluorescence was only observed in the drug-treated plus irradiated cells approximately 2 h 30 min post activation (Figure 5.11), indicating a relatively fast process.

In comparison, morphological changes for cisplatin treated ASTC-a-1 cells (human lung adenocarcinoma) showed the typical hallmarks of apoptosis 16 hours post-treatment.³⁹ A similar result was also reported with 5637 cells,⁷ suggesting that the DNA-damaging effect of cisplatin -which eventually leads to apoptosis- is a relatively slow process. Also, time-lapse analysis of actinomycin D (a strong apoptosis inducer) has shown propidium iodide uptake 5 hours 48 min after drug exposure.³⁵

The morphological images captured after 16 hours following photoactivation resemble those reported for the autophagic cell death of HL60 cells treated with *trans, trans, trans*-[Pt(N₃)₂(OH)₂(pyr)(NH₃)] and activated by UVA (image in Chapter 1).⁵ Although morphological changes cannot be used as a stand-alone method for identifying cell death, the absence of the typical apoptosis markers along with the timing of cell death (Figure 5.12), can lead to the conclusion that also in the case of *trans, trans, trans*-[Pt(N₃)₂(OH)₂(pyr)₂], apoptosis is not

induced. However it must be noted that the pathway which a cell uses to die upon exposure to an agent is dose-dependent. It was shown that at low and high concentrations of a drug apoptosis or necrosis respectively can be triggered.⁴⁰ In photodynamic therapy all three types of cell death have been identified.¹¹

5.6 Conclusions

Complexes of the general formula *trans, trans, trans*-[Pt(N₃)₂(OH)₂(L₁)(L₂)], where L₁ and L₂ are ligands such as pyridine, 2, 3, 4-picoline, thiazole or 1-methylimidazole, synthesized and characterized in the previous chapter, were irradiated in the presence of 5'-GMP and showed to form adducts with an average yield of 59% with respect to the platinum centre.

Irradiation studies of the sterically hindered 2-picoline complex, *trans, trans, trans*-[Pt(N₃)₂(OH)₂(2-pic)(pyr)], followed by ¹H, ¹⁹⁵Pt-NMR and LC-MS showed the formation of the [Pt(N₃)(2-pic)(pyr)(5'-GMP)] whereas the bis-GMP adduct ([Pt(2-pic)(pyr)(5'-GMP)₂]) only formed slowly over time in the dark.

In phototoxicity studies (λ= 420 nm) on A2780, A2780cis and OE19 cell lines with the (pyridine)(n-picoline) family, the 2-picoline complex was the least toxic with an IC₅₀ 3.6 μM, 2.7 fold higher than that of 3-picoline and 4-picoline, respectively. This suggests that steric hindrance close to the platinum centre does not favour phototoxicity, possibly due to the slow formation of bifunctional adducts. The most active complexes were the *trans,trans,trans*-[Pt(N₃)₂(OH)₂(4-pic)₂] (IC₅₀ = 2.1 μM) and *trans,trans,trans*-[Pt(N₃)₂(OH)₂(thiazole)₂] complexes (IC₅₀ = 2.4 μM), although the latter showed some dark toxicity (PI (phototoxic index) = 48). Most of the complexes studied here were equally potent in cisplatin resistance ovarian cancer cell line (A2780cis), except *trans,trans,trans*-

[Pt(N₃)₂(OH)₂(3-pic)₂] and *trans,trans,trans*-[Pt(N₃)₂(OH)₂(4-pic)₂] which exhibited some cross resistance. All of the complexes tested in both A2780 and oesophageal (OE19) cell lines showed less sensitivity to OE19 cancer cells (average IC₅₀ in A2780 and OE19, 3.5 μM and 8.4 μM, respectively).

Studies of *trans,trans,trans*-[Pt(N₃)₂(OH)₂(pyr)₂] in *S. pombe* yeast strains (WT and ΔRad3) to probe the role of DNA in photocytotoxicity resulted in a decrease in the survival of the Rad3 mutant (e.g. with the use of 200 μM complex, survival reduced from 57% to 0.4%) due to impaired DNA repair in ΔRad3, suggesting that DNA is potentially an important target for this class of compounds. However the fact that there is significant cell death in the WT (with 200 and 300 μM) also suggests that these complexes are multi-targeting.

Live-cell confocal microscopy performed on A2780 cells treated with the aforementioned complex (**3**) and irradiated with a low dose of blue light (463 nm, 17 J/cm²) resulted in cell death 2 h 30 min post-activation. The phase-contrast images did not illustrate the morphological changes typical of apoptosis, suggesting that the cell death mechanism could be either via necrosis or autophagy. This work appears to be the first example of a real-time study of photoactivation of a Pt(IV)-diazido complex in cells and it shows that with the use of appropriate conditions and lasers, these photoactivatable complexes can be studied with confocal microscopy.

References

1. P. J. Bednarski, K. Korpis, A. F. Westendorf, S. Perfahl, and R. Grünert, *Phil. Trans. R. Soc. A*, 2013, **371**, 371:20120118.
2. A. F. Westendorf, A. Bodtke, and P. J. Bednarski, *Dalton Trans.*, 2011, **40**, 5342-5451.
3. F. S. Mackay, J. A. Woods, P. Heringová, J. Kaspárková, A. M. Pizarro, S. A. Moggach, S. Parsons, V. Brabec, and P. J. Sadler, *Proc. Natl. Acad. Sci. USA.*, 2007, **104**, 20743-20748.
4. J. Pracharova, L. Zerzankova, J. Stepankova, O. Novakova, N. J. Farrer, P. J. Sadler, V. Brabec, and J. Kasparkova, *Chem. Res. Toxicol.*, 2012, **25**, 1099-111.
5. A. F. Westendorf, J. A. Woods, K. Korpis, N. J. Farrer, L. Salassa, K. Robinson, V. Appleyard, K. Murray, R. Grünert, A. M. Thompson, P. J. Sadler, and P. J. Bednarski, *Mol. Cancer Ther.*, 2012, **11**, 1894-18904.
6. N. J. Farrer, J. A. Woods, L. Salassa, Y. Zhao, K. S. Robinson, G. Clarkson, F. S. Mackay, and P. J. Sadler, *Angew. Chem. Int. Ed.*, 2010, **49**, 8905-8908.
7. P. J. Bednarski, R. Grünert, M. Zielzki, A. Wellner, F. S. Mackay, and P. J. Sadler, *Chem. Biol.*, 2006, **13**, 61-67.
8. CRUK, *Accesed on 02/09/2013*, <http://www.cancerresearchuk.org/cancer-info/cancer>.
9. NHS, *Accessed on 02/09/2013*, <http://www.nhs.uk/conditions/Cancer-of-the-oesopha>.
10. S. G. Bown, *Phil. Trans. R. Soc. A*, 2013, 371:20120371.
11. P. Agostinis, K. Berg, K. A. Cengel, T. H. Foster, A. W. Girotti, S. O. Gollnick, S. M. Hahn, M. R. Hamblin, A. Juzeniene, and D. Kessel, *CA-Cancer J. Clin.*, 2011, **61**, 250-281.
12. S. M. Aris and N. P. Farrell, *Eur. J. Inorg. Chem.*, 2009, **2009**, 1293-1302.
13. N. J. Farrer, J. A. Woods, V. P. Munk, F. S. Mackay, and P. J. Sadler, *Chem. Res. Toxicol.*, 2010, **23**, 413-421.
14. Y. Chen, Z. Guo, J. A. Parkinson, and P. J. Sadler, *Dalton Trans.*, 1998, 3577-3585.

15. A. G. Quiroga, J. M. Pérez, C. Alonso, C. Navarro-Ranninger, and N. Farrell, *J. Med. Chem.*, 2006, **49**, 224-231.
16. G. M. Rakić, S. Grgurić-Sipka, G. N. Kaluderović, S. Gómez-Ruiz, S. K. Bjelogrić, S. S. Radulović, and Z. L. Tesić, *Eur. J. Med. Chem.*, 2009, **44**, 1921-1925.
17. Y. Zhao, *PhD Thesis, University of Warwick*, 2012.
18. J. A. Woods, *Unpublished Data*, 2013.
19. S. P. Jackson and J. Bartek, *Nature*, 2010, **461**, 1071-1078.
20. E. Sommariva, T. K. Pellny, N. Karahan, S. Kumar, J. A. Huberman, and J. Z. Dalggaard, *Mol. Cell. Biol.*, 2005, **25**, 2770-2784.
21. B. Alberts, A. Johnson, J. Lewis, M. Raff, K. Roberts, and P. Walter, *Molecular biology of the cell*, Garland Science, New York, 4th edn., 2002.
22. T. A. Weinert, G. L. Kiser, and L. H. Hartwell, *Genes Dev.*, 1994, **8**, 652-665.
23. N. Rhind and P. Russell, *J. Cell Sci.*, 2000, **113**, 3889-96.
24. J. L. Nitiss and J. Heitman, Eds., *Yeast as a Tool in Cancer Research*, Springer Netherlands, Dordrecht, 2007.
25. Y. Zeng, K. C. Forbes, Z. Wu, S. Moreno, H. Piwnica-Worms, and T. Enoch, *Nature*, 1998, **395**, 507-510.
26. M. N. Boddy, *Science*, 1998, **280**, 909-912.
27. A. A. Hostetter, M. F. Osborn, and V. J. DeRose, *ACS Chem Biol.*, 2012, **7**, 218-225.
28. D. Paparatto, D. Fletcher, K. Piwowar, K. Baldino, C. Morel, and S. Dunaway, *PLoS ONE*, 2009, **4**, e6181.
29. S. Ishida, J. Lee, D. J. Thiele, and I. Herskowitz, *Proc. Natl. Acad. Sci. USA.*, 2002, **99**, 14298-14302.
30. K. Tanaka, *Biosci. Biotechnol. Biochem.*, 2010, **74**, 2367-2373.
31. N. R. Jena, *J. Biosci.*, 2012, **37**, 503-517.
32. M. Zhang, M. Hanna, J. Li, S. Butcher, H. Dai, and W. Xiao, *Toxicol. Sci.*, 2010, **113**, 401-411.

33. O. Kepp, L. Galluzzi, M. Lipinski, J. Yuan, and G. Kroemer, *Nat. Rev. Drug Discov.*, 2011, **10**, 221-237.
34. F. C. Dorsey, M. A. Steeves, S. M. Prater, T. Schröter, and J. L. Cleveland, *Meth. Enzymol.*, 2009, **453**, 251-271.
35. L. Bouchier-Hayes, C. Munoz-Pinedo, S. Connell, and D. R. Green, *Methods*, 2008, **44**, 222-228.
36. B. Tracy and J. Wangt, *Photochem. Photobiol.*, 1977, **26**, 589-593.
37. A. M. Edwards, E. Silva, B. Jofré, M. I. Becker, and A. E. De Ioannes, *J. Photochem. Photobiol. B*, 1994, **24**, 179-186.
38. F. M. Griffin, G. Ashland, R. L. Capizzi, and L. Cells, *Cancer Res.*, 1981, **41**, 2241-2248.
39. L. Liu, D. Xing, W. R. Chen, T. Chen, Y. Pei, and X. Gao, *Int. J. Cancer*, 2008, **122**, 2210-2222.
40. S. V. Lennon, S. J. Martin, and T. G. Cotter, *Cell Prolif.*, 1991, **24**, 203-214.

Chapter 6

Conclusions and future outlook

6.1 Conclusions

This thesis describes the synthesis, characterisation as well as chemical and biological photochemical studies of *trans*-diazido Pt(IV) complexes with the prospect of being used as anticancer agents for photoactivated chemotherapy. A variety of techniques have been employed such as NMR, HPLC, LC-MS, UV-Vis, mammalian and yeast cell studies and confocal microscopy.

Functionalization of an axial hydroxido group to obtain Pt(IV)- azido complexes with general formula *trans, trans, trans*-[Pt(N₃)₂(OH)(OCOR)(pyr)₂], reported in Chapter 3, was achieved by reaction of the dihydroxido precursor *trans, trans, trans*-[Pt(N₃)₂(OH)₂(pyr)₂] with anhydrides (succinic anhydride and N-methylisatoic anhydride). Further derivatisations of the *trans, trans, trans*-[Pt(N₃)₂(OH)(Succ)(pyr)₂] were carried out via coupling to 1-propanol, in order to afford a neutral and more lipophilic complex, as well as to the (RGD)f peptide (a tumour targeting peptide) to increase the selectivity of the complex towards cancer cells. The synthesis of the seven *trans, trans, trans*-[Pt(N₃)₂(OH)₂(L₁)(L₂)] complexes reported in Chapter 4, where L₁ and L₂ can be pyridine, picoline, thiazole or 1-methylimidazole ligands, was achieved by oxidation of the Pt(II)-diazido precursors *trans*-[Pt(N₃)₂(L₁)(L₂)].

The X-ray crystal structures of seven Pt(IV)-diazido complexes have been obtained in this work, including the first examples of mono-carboxylato diazido Pt(IV) complexes reported up to date. All complexes show an octahedral geometry with [N₄O₂] coordination environment around the platinum centre. Slight distortions from the ideal geometry were observed in the complexes bearing two different ligands in *trans* position, as indicated by deviations from the

180° angle between ligands. In the case of the monocarboxylato complexes the average lengths of the Pt–O(H) and Pt–O(COR) bonds were 1.978 Å and 2.035 Å, respectively, indicating a potential lability of the carboxylate with respect to the hydroxido ligand. The intermolecular forces in all of the cases are dominated by moderately strong H-bonding between the hydroxido and the Pt-bound Nα of the azide.

The photodegradation kinetics were studied by UV-Vis spectroscopy and the exponential decrease in intensity of the $N_3 \rightarrow Pt$ LMCT band was followed to determine the half-lives of the complexes. For *trans, trans, trans*-[Pt(N₃)₂(OH)₂(L₁)(L₂)] family of complexes, the steric hindrance created by the methyl group in the ortho position of the 2-picoline ligand, favoured an increased rate of photodegradation upon irradiation with blue light (463 nm) as the half-life decreased by 2.5-fold when compared to the average half-life of the other complexes (20-25 minutes). A 3-fold decrease in the half-lives of the *trans, trans, trans*-[Pt(N₃)₂(OH)(OCOR)(pyr)₂] complexes was observed in comparison to the dihydroxido complex when irradiated with green light (517 nm). Therefore it can be concluded that axial ligand modifications with the carboxylato functionality as well as the steric effect induced by the methyl substitution on the pyridine ligand are beneficial in the photolability of the complexes.

DFT and TDDFT calculations on the complexes of [Pt(N₃)₂(OH)(Succ)(pyr)₂] **4** and [Pt(N₃)₂(OH)₂(pyr)(2-pic)] **18** show higher and longer intensity transitions in the 410-470 nm region when compared to complex *trans, trans, trans*-[Pt(N₃)₂(OH)₂(pyr)₂], which support the experimental data of improved photoactivity at the longer wavelengths.

^1H and ^{195}Pt -NMR were used for photoproduct analysis from irradiations of selected complexes with 2 mol eq of 5'-GMP in order to follow the photochemical behaviour of these complexes in the presence of biomolecules. Irradiation of complex *trans, trans, trans*-[Pt(N₃)₂(OH)(Succ)(pyr)₂] resulted in the formation of the mono-GMP adduct in a 2.6-fold greater proportion than for [Pt(N₃)₂(pyr)₂(OH)₂] **3** when irradiated with the same dose of 463 nm light. Studies of complex [Pt(N₃)₂(OH)(N-MI)(pyr)₂] **6** were carried out in MeOD due to the poor solubility of the complex in water. The release of the axial ligand N-MI was observed, but no significant 5'-GMP binding was found. Furthermore, the release of pyridine was observed, especially when the irradiation was carried out with a low dose of UVA which is a result similar to that obtained when the dihydroxido complex [Pt(N₃)₂(OH)₂(pyr)₂] **3** was irradiated under the same conditions, indicating the effect of the solvent on the type of photoproducts formed. However, the release of the axial N-methylisatoate (N-MI) ligand in an aqueous environment was confirmed by fluorescence emission studies where an increase in the intensity of the fluorescence band at 420 nm was observed upon continuous irradiation. This fluorescence band matches the emission wavelength of the free ligand (N-MIA), which was synthesized independently for comparison purposes.

Irradiation of complex [Pt(N₃)₂(OH)₂(pyr)(2-pic)] **18** at a high concentration (9 mM) in the presence of 5'-GMP (2 mol eq) showed the production of the mono-GMP adduct. The presence of the bulky 5'-GMP ligand caused restricted rotation of the 2-picoline ligand, as shown by the broadness of H₆ and H₅ ^1H -NMR

resonances (Figure 5.4, Chapter 5). Slow formation of the bis-GMP adduct was observed over time after keeping the solution in the dark at room temperature.

To obtain further information with regard to the photoproducts upon irradiation with 420 nm of the complexes *trans, trans, trans*-[Pt(N₃)₂(OH)(Succ)(pyr)₂] **4** and *trans, trans, trans*-[Pt(N₃)₂(OH)(Succ-(RGD)f)(pyr)₂] **7** in the presence of 5'-GMP (2 mol eq), LC-MS studies were undertaken. The photoproducts in this case were shown to be identical with a major product, the mono-GMP Pt(II) adduct. The release of the intact peptide moiety from *trans, trans, trans*-[Pt(N₃)₂(OH)(Succ-(RGD)f)(pyr)₂] **7** was observed, showing that in a cellular environment, as soon as the complex selectively enters the tumour cells, light activation will liberate the active Pt(II) moiety.

The pathway of the photoreduction of these complexes, regardless of the nature of the axial ligand (OH or OCOR) involves the release of azidyl radicals, which were shown by previous reports to play an important role in the phototoxicity of this type of complexes. The fact that the carboxylato complexes *trans, trans, trans*-[Pt(N₃)₂(OH)(Succ)(pyr)₂] **4** and *trans, trans, trans*-[Pt(N₃)₂(OH)(Succ-Pr)(pyr)₂] **5** (at 1 mM concentration) show release of azidyl radicals in water upon green light (517 nm) activation constitutes an important advantage of this class of complexes. The highest yield of trapped radicals [DMPO-N₃] was observed for the complex [Pt(N₃)₂(OH)(Succ-Pr)(pyr)₂] at a concentration 68 μM, whereas the dihydroxido complex [Pt(N₃)₂(OH)₂(pyr)₂] **3** did not generate any radicals at this wavelength.

Cellular uptake studies in A2780 cells after 1 hour incubation in the dark, were performed on the complexes reported in Chapter 3: *trans, trans, trans*-[(Pt(N₃)₂

(OH)₂(pyr)₂] **3**, *trans, trans, trans*-[Pt(N₃)₂(pyr)₂(OH)(Succ)] **4**, [Pt(N₃)₂(pyr)₂(OH)(Succ-Pr)] **5** and *trans, trans, trans*-[Pt(N₃)₂(pyr)₂(OH)(N-MI)] **6**. The uptake increased by 1.7-fold when comparing **4** and **5** and interestingly by 10-fold when comparing complexes **3** and **6**. Temperature dependence studies on complexes **3** and **6** showed that the uptake is greatly facilitated by active transport as there is an increase in uptake when the temperature increases from 4 °C to 37 °C (5-fold and 2-fold in the cases of **3** and **6**, respectively). However the fact that there is still uptake even at 4°C shows that passive uptake is also involved.

The phototoxicity of the complexes reported in this thesis was tested in the dark and with a low dose of blue light (420 nm, 5 J/cm²) against ovarian (A2780 and A2780cis) and also oesophageal (OE19) cancer cell lines. The only complexes that showed dark toxicity towards A2780 were complex [Pt(N₃)₂(OH)₂(thiazole)₂] **29** (Phototoxic Index (PI)= 48) and [Pt(N₃)₂(OH)₂(pyr)(2-pic)] **18** (PI= 7.3). The least phototoxic complexes were [Pt(N₃)₂(OH)₂(1-methylimidazole)₂] **32** (IC₅₀ 56.3 µM) and [Pt(N₃)₂(OH)₂(2-pic)(pyr)] **18** (IC₅₀ 14.5 µM). The lack of activity of the former could be attributed to low cellular uptake as the high solubility of the complex (82 mM) implies high hydrophilicity. The steric hindrance close to the platinum centre created by the 2-picoline ligand in the latter could hinder the formation of bifunctional DNA adducts.

Complexes [Pt(N₃)₂(OH)(Succ)(pyr)₂] **4** and [Pt(N₃)₂(OH)(Succ-Pr)(pyr)₂] **5** also showed an improved activity (IC₅₀ values of 3.6 µM and 3.7 µM) when compared to [Pt(N₃)₂(OH)₂(pyr)₂] **3** (IC₅₀= 6.7 µM) although all of them gave rise to the

same Pt(II) photoproducts. This suggests that the enhanced photoactivity is beneficial for obtaining more active complexes.

Finally, yeast and confocal microscopy studies carried out on complex **3** provided new tools for the study of Pt(IV)-diazido photoactivatable complexes. Survival studies with WT and Δ Rad3 mutants of *S. pombe* showed a decrease in survival (from 57% to 0.4%) when the complex was irradiated with blue light (420 nm). Since the mutant is unable to repair DNA, these results suggest that the DNA can be a significant target for this class of complexes. Live cell confocal microscopy performed on A2780 cells with the same complex captured for the first time the live-cell death triggered only by photoactivation with blue light (463 nm). The uptake of propidium iodide was monitored over time and the first signs of cell death were captured 2h 30 min post activation.

6.2 Future Work

This section will explore possible future work which can be carried on based in the results described in the previous chapters.

6.2.1 Axial ligand modifications

Several axial ligand modifications could be carried out by derivatising an already existing axial ligand or by substitution of the hydroxide ligands in the precursor Pt(IV)-dihydroxido complexes.

Complex $[\text{Pt}(\text{N}_3)_2(\text{OH})(\text{succ})(\text{pyr})_2]$, **4** described in Chapter 3, provides the potential for coupling with moieties which can confer imaging or targeting capabilities to the Pt(IV)-diazido prodrugs. A chromophore attachment can enhance the light harvesting capabilities of the complex. For example Ford *et al*¹

have shown that attachment of RSE chromophore to Roussin's red salt ester ($[\text{Fe}_2(\mu\text{-RS})_2(\text{NO})_4]$) resulted in efficient energy transfer from the chromophore to the metal centre enabling the release of NO at longer wavelength.

Attachment of L-tryptophan (Figure 6.1 A) onto complex **4** is also an interesting possibility to explore the effect on the phototoxicity since L-tryptophan is a radical quencher. A preliminary synthesis was carried out through a CDI-mediated (carbonyldiimidazole) coupling reaction to the monocarboxylato complex **4**. However, further purification is required since two tryptophans were found to be coupled to the platinum complex: potentially one through the carboxylic acid and the second through the axial hydroxide ligand.

Other functional groups (e.g. various alcohol or amines) can be incorporated onto the carboxyl group of complex **4** to enable the study of structure-activity relationship with regards to the axial group. Furthermore, a potential correlation between photoreactivity with electrode potentials is an interesting avenue to be explored.

Different molecules can also be incorporated as axial ligands, such as TFA (trifluoroacetate) or DCA (dichloroacetate), as shown in Figure 6.1 B and C. Incorporation of TFA ligands in the $\text{Pt}(\text{dach})(\text{L})(\text{L}')$, where L= acetate or TFA and L'=oxalate showed that the TFA bearing complexes had superior *in vivo* activity due to increased cellular accumulation.² The facile reaction of the hydroxide ligands of the Pt(IV)-diazido complexes with TFA (trifluoroacetic acid) has already been shown in the present work (Chapter 3) therefore it will be interesting to demonstrate the effect of the TFA ligands on the photolability of the Pt(IV) complexes. Another ligand which would be interesting to attach instead of

the axial hydroxides is dichloroacetate (DCA), a pyruvate dehydrogenase inhibitor. The incorporation of DCA in mitaplatin, *cis*, *trans*, *cis*-[Pt(NH₃)₂(dca)₂Cl₂] led to the formation of a potent complex with dual mode of action.³

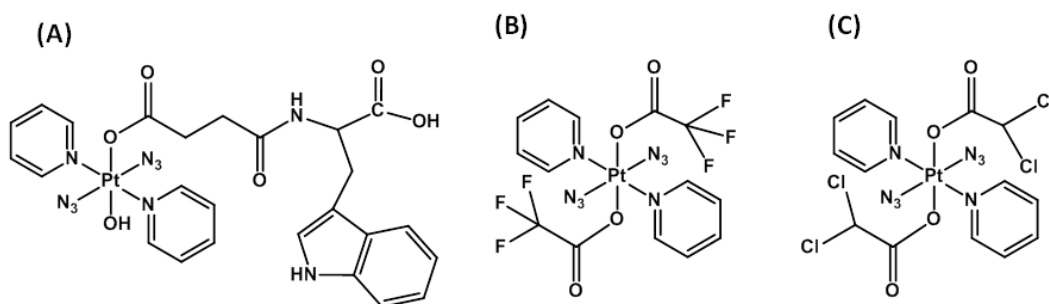


Figure 6.1: Proposed complexes to be explored. A and B have been synthesized in preliminary attempts but their synthesis requires further optimization.

Complex [Pt(N₃)₂(OH)(N-MI)(pyr)₂] **6**, has two important features which provide beneficial application for imaging experiments in cells: its high cellular accumulation and a fluorophore ligand that could be released for confocal microscopy studies. IR-mapping of the azides within cells (collaboration with Prof Clotilde Policar) was attempted in MCF-7 cells treated with complex **3** after fixing them onto ZnS and CaF₂ windows but no signals were observed under these conditions. However, the high cellular uptake of the complex [Pt(N₃)₂(OH)(N-MI)(pyr)₂] **6**, could lead to successful Pt-azide IR mapping.

6.2.2 Further work on equatorial ligand modifications

Firstly, cell uptake studies are important to be carried out for the $[\text{Pt}(\text{N}_3)_2(\text{OH})_2(\text{L}_1)(\text{L}_2)]$ (Chapter 4) family of complexes which can provide an insight to explain the lack of activity of $[\text{Pt}(\text{N}_3)_2(\text{OH})_2(1\text{-mim})_2]$, **32**.

Furthermore the lower phototoxicity of $[\text{Pt}(\text{N}_3)_2(\text{OH})_2(2\text{-pic})(\text{pyr})]$ compared to the $[\text{Pt}(\text{N}_3)_2(\text{OH})_2(\text{n-pic})(\text{pyr})]$ or $[\text{Pt}(\text{N}_3)_2(\text{OH})_2(\text{n-pic})_2]$ family of complexes, despite its fast photoreduction kinetics, could be explained by the mode of interaction of Pt(II) photoproducts with DNA. Therefore characterisation studies of adducts with plasmid DNA interactions analysed by electrophoresis, similar to those reported by Pracharova *et al*⁴ are proposed future experiments.

The survival studies with *S. pombe* reported in Chapter 5 can be utilized to explore other cellular targets and modes of action of Pt(IV)-diazido complexes. For example, it has been shown by Farrell *et al.*, that *trans* planar amine Pt(II) complexes have the ability to form crosslinks with DNA and topoisomerase I, suggesting that topoisomerases can be a potential target for the Pt(IV)-diazido complexes.^{5, 6} Studies comparing the survival of TopI mutant versus WT in the presence of a Pt(IV)-diazido drug should show an increase of survival in the TopI mutant if enzyme inhibition takes place.

Further modifications of the equatorial ligands can also involve modifications via the azide. The azide-alkyne cycloadditions have long been known in the literature but a great majority require Cu(I) catalysts.⁷ Preliminary work within our group (Farrer *et al*, unpublished data) on complex *trans, trans, trans*- $[\text{Pt}(\text{N}_3)_2(\text{OH})_2(\text{pyr})_2]$ **3** has shown that the azides can react with only electron-withdrawing acetylenes (dimethyl acetylenedicarboxylate, DMAD and diethyl

acetylenedicarboxylate, DEACD) on one or both azides to produce monofunctional and bifunctional adducts. A pure product was obtained by the reaction (Figure 6.2) of complex *trans*-[Pt(N₃)₂(pyr)₂] **2**, with DMAD. The azides coordinated to Pt(II) are more electron rich⁸ thus facilitating the cycloaddition reaction. The presence of the two different resonances corresponding to methyl groups in the ¹H-NMR spectra (Appendix) suggested that the triazole is coordinated to the Pt through the N α .

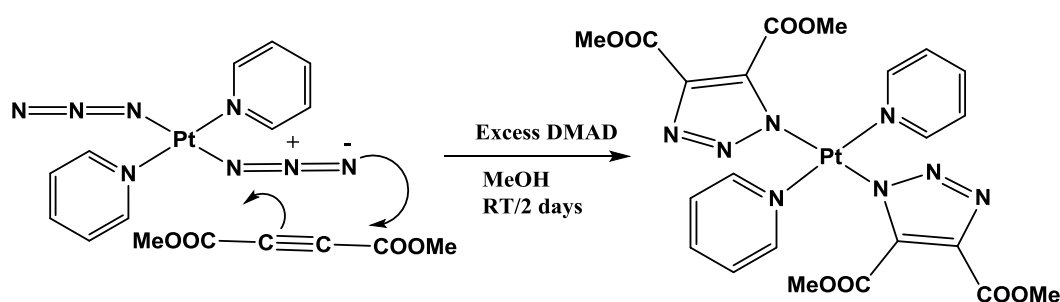


Figure 6.2: Synthetic scheme for reaction between complex *trans*-[Pt(N₃)₂(pyr)₂] **2**, and DMAD.

The controlled functionalization of the azides via cycloaddition can provide an easy method for the derivatisation of the complexes with fluorescent tags or peptides.

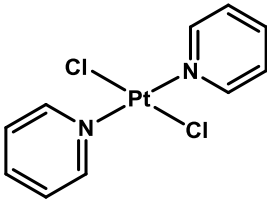
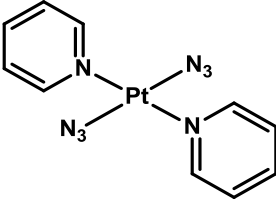
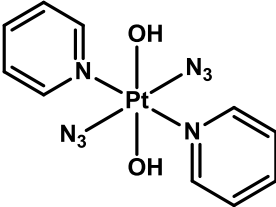
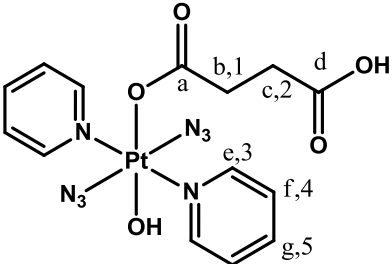
References

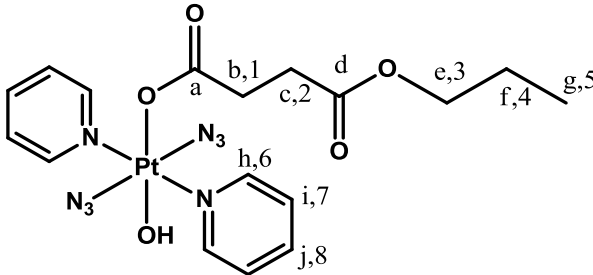
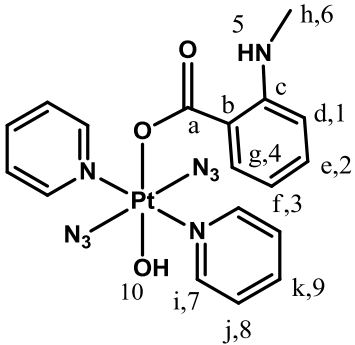
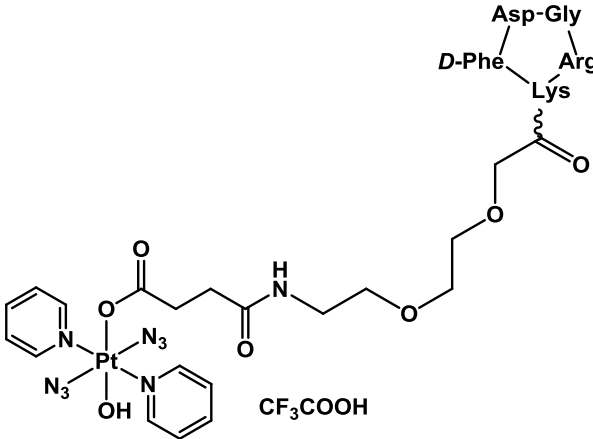
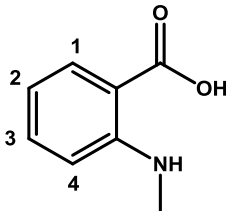
1. A. D. Ostrowski and P. C. Ford, *Dalton Trans.*, 2009, 10660-10669.
2. E. Wexselblatt, E. Yavin, and D. Gibson, *Angew. Chem. Int. Ed.*, 2013, **52**, 1-5.
3. S. Dhar and S. J. Lippard, *Proc. Natl. Acad. Sci. USA.*, 2009, **106**, 22199-22204.

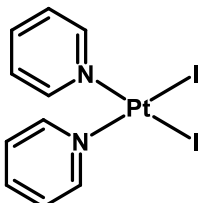
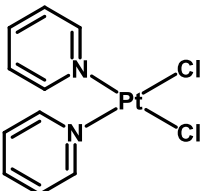
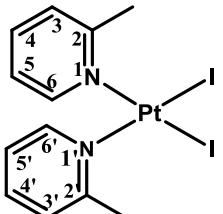
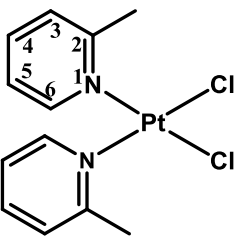
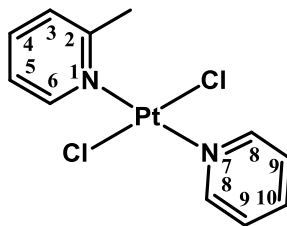
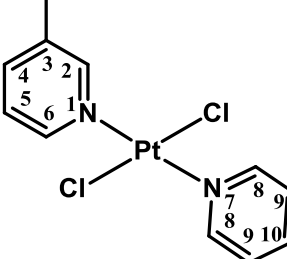
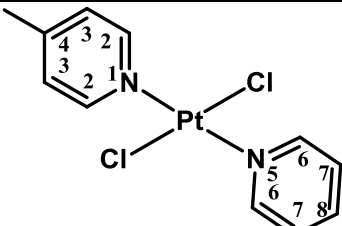
4. J. Pracharova, L. Zerzankova, J. Stepankova, O. Novakova, N. J. Farrer, P. J. Sadler, V. Brabec, and J. Kasparikova, *Chem. Res. Toxicol.*, 2012, **25**, 1099-111.
5. S. M. Aris and N. P. Farrell, *Eur. J. Inorg. Chem.*, 2009, **2009**, 1293-1302.
6. N. Farrell, L. F. Povirk, Y. Dange, G. DeMasters, M. S. Gupta, G. Kohlhausen, Q. A. Khan, Y. Pommier, and D. A. Gewirtz, *Biochem. Pharmacol.*, 2004, **68**, 857-866.
7. S. Díez-González, *Catal. Sci. Technol.*, 2011, **1**, 166-178.
8. N. J. Farrer, P. Gierth, and P. J. Sadler, *Chem. Eur. J.*, 2011, **17**, 12059-12066.

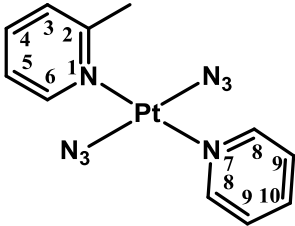
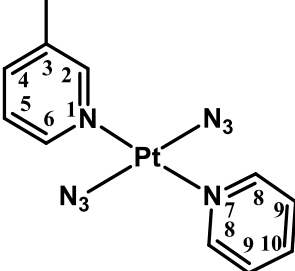
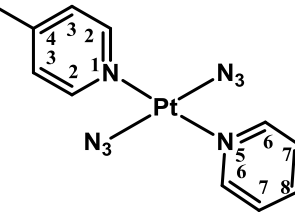
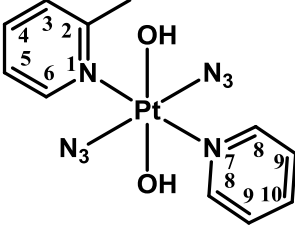
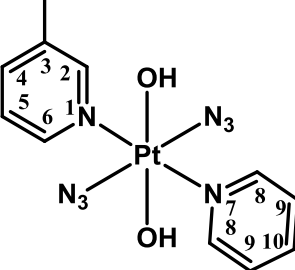
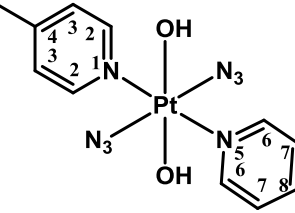
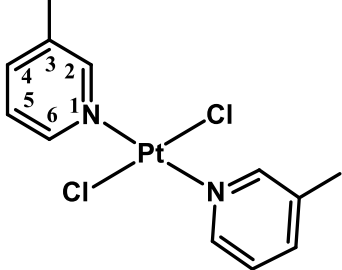
APPENDIX

Table A1: Compounds and atom numbering. Ligands are denoted as: **Pyr**= pyridine; **Succ**= succinate; **Succ-Pr**= 4-oxo-4-propoxybutanoate; **N-MI**= N-methylisatoate; **Succ-(RGD)f**= succinate coupled with (RGD)f peptide; **pic**= picoline; **tz**= thiazole; **mim**= 1-methylimidazole.

Name	Nº	Structure
<i>trans</i> -[Pt(Cl) ₂ (pyr) ₂]	1	
<i>trans</i> -[Pt(N ₃) ₂ (pyr) ₂]	2	
<i>trans, trans, trans</i> -[Pt(N ₃) ₂ (OH) ₂ (pyr) ₂]	3	
<i>trans, trans, trans</i> -[Pt(N ₃) ₂ (OH)(Succ)(pyr) ₂]	4	

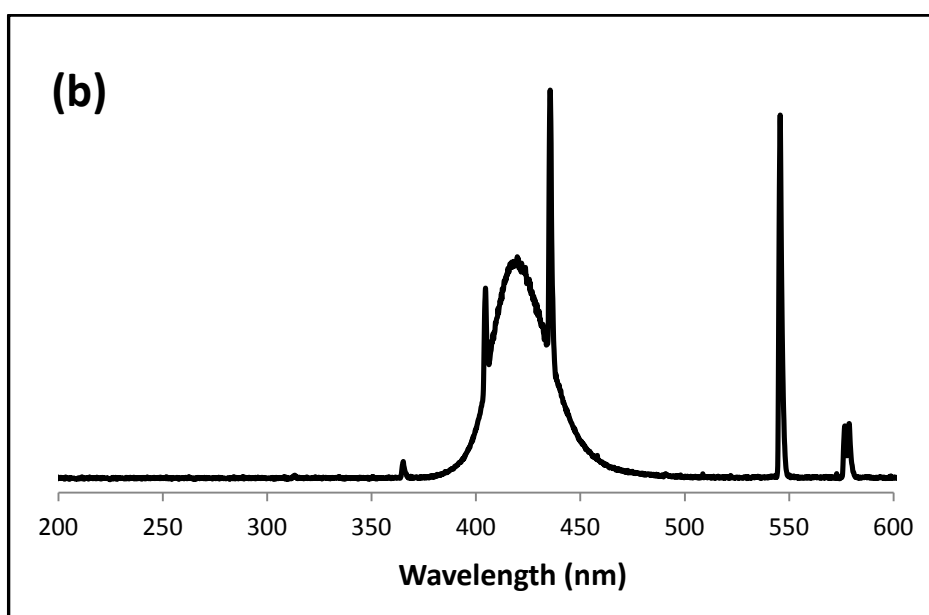
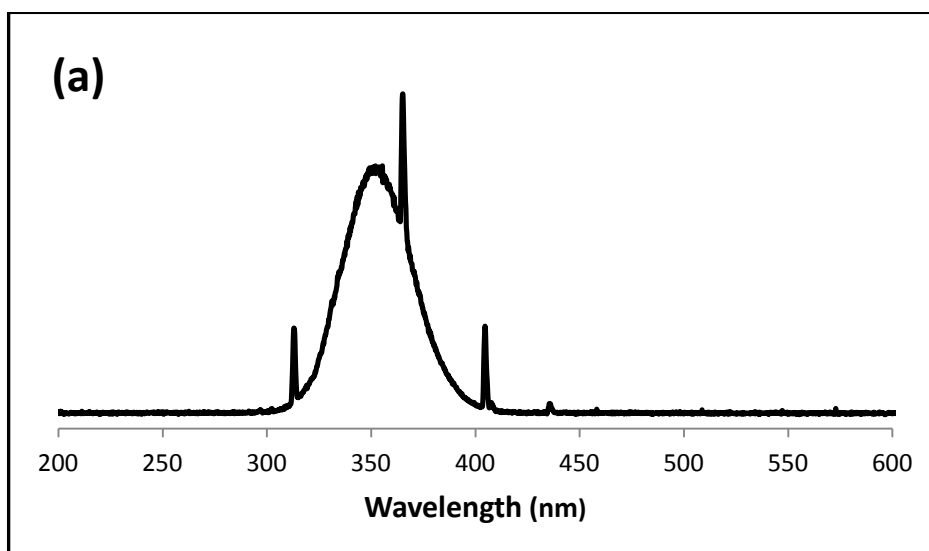
<p><i>trans, trans, trans-</i> [Pt(N₃)₂(OH)(Succ-Pr)(pyr)₂]</p>	5	
<p><i>trans, trans, trans-</i> [Pt(N₃)₂(pyr)₂(OH)(N-MI)]</p>	6	
<p><i>trans, trans, trans-</i> [Pt(N₃)₂(OH)(pyr)₂(Succ-(RGD)f)]</p>	7	
<p>N-methylisatoic acid (N-MIA)</p>	L1	

<i>cis</i> -[Pt(I) ₂ (pyr) ₂]	8	
<i>cis</i> -[Pt(Cl) ₂ (pyr) ₂]	9	
<i>cis</i> -[Pt(I) ₂ (2-pic) ₂]	10	
<i>cis</i> -[Pt(Cl) ₂ (2-pic) ₂]	11	
<i>trans</i> -[Pt(Cl) ₂ (pyr)(2-pic)]	12	
<i>trans</i> -[Pt(Cl) ₂ (pyr)(3-pic)]	13	
<i>trans</i> -[Pt(Cl) ₂ (pyr)(4-pic)]	14	

<i>trans</i> -[Pt(N ₃) ₂ (pyr)(2-pic)]	15	 The structure shows a central platinum atom (Pt) in a square planar geometry. It is coordinated to two azido (N ₃) groups in a trans configuration. The other two coordination sites are occupied by a pyridine (pyr) ring and a 2-picoline (2-pic) ring. The pyridine ring is numbered 1 to 6, and the 2-picoline ring is numbered 1 to 10, with the methyl group at position 2.
<i>trans</i> -[Pt(N ₃) ₂ (pyr)(3-pic)]	16	 The structure shows a central platinum atom (Pt) in a square planar geometry. It is coordinated to two azido (N ₃) groups in a trans configuration. The other two coordination sites are occupied by a pyridine (pyr) ring and a 3-picoline (3-pic) ring. The pyridine ring is numbered 1 to 6, and the 3-picoline ring is numbered 1 to 10, with the methyl group at position 3.
<i>trans</i> -[Pt(N ₃) ₂ (pyr)(4-pic)]	17	 The structure shows a central platinum atom (Pt) in a square planar geometry. It is coordinated to two azido (N ₃) groups in a trans configuration. The other two coordination sites are occupied by a pyridine (pyr) ring and a 4-picoline (4-pic) ring. The pyridine ring is numbered 1 to 6, and the 4-picoline ring is numbered 1 to 8, with the methyl group at position 4.
<i>trans, trans, trans</i> -[Pt(N ₃) ₂ (OH) ₂ (pyr)(2-pic)]	18	 The structure shows a central platinum atom (Pt) in an octahedral geometry. It is coordinated to two azido (N ₃) groups in a trans configuration, two hydroxyl (OH) groups in a trans configuration, and a pyridine (pyr) ring and a 2-picoline (2-pic) ring in a trans configuration. The pyridine ring is numbered 1 to 6, and the 2-picoline ring is numbered 1 to 10, with the methyl group at position 2.
<i>trans, trans, trans</i> -[Pt(N ₃) ₂ (OH) ₂ (pyr)(3-pic)]	19	 The structure shows a central platinum atom (Pt) in an octahedral geometry. It is coordinated to two azido (N ₃) groups in a trans configuration, two hydroxyl (OH) groups in a trans configuration, and a pyridine (pyr) ring and a 3-picoline (3-pic) ring in a trans configuration. The pyridine ring is numbered 1 to 6, and the 3-picoline ring is numbered 1 to 10, with the methyl group at position 3.
<i>trans, trans, trans</i> -[Pt(N ₃) ₂ (OH) ₂ (pyr)(4-pic)]	20	 The structure shows a central platinum atom (Pt) in an octahedral geometry. It is coordinated to two azido (N ₃) groups in a trans configuration, two hydroxyl (OH) groups in a trans configuration, and a pyridine (pyr) ring and a 4-picoline (4-pic) ring in a trans configuration. The pyridine ring is numbered 1 to 6, and the 4-picoline ring is numbered 1 to 8, with the methyl group at position 4.
<i>trans</i> -[Pt(Cl) ₂ (3-pic) ₂]	21	 The structure shows a central platinum atom (Pt) in a square planar geometry. It is coordinated to two chlorine (Cl) atoms in a trans configuration and two 3-picoline (3-pic) rings in a trans configuration. The 3-picoline rings are numbered 1 to 10, with the methyl group at position 3.

<i>trans</i> -[Pt(N ₃) ₂ (3-pic) ₂]	22	<p>The structure shows a platinum (Pt) center in a trans configuration. It is coordinated to two azido (N₃) groups and two 3-picoline (3-pic) ligands. One 3-pic ligand is shown with atom numbering: 1 for the nitrogen, 2 for the carbon attached to the ring, 3 for the carbon at the meta position, 4 for the carbon at the para position, 5 for the carbon at the other meta position, and 6 for the carbon at the other para position. The other 3-pic ligand is shown without numbering.</p>
<i>trans, trans, trans</i> -[Pt(N ₃) ₂ (OH) ₂ (3-pic) ₂]	23	<p>The structure shows a platinum (Pt) center in a trans configuration. It is coordinated to two azido (N₃) groups, two hydroxyl (OH) groups, and two 3-picoline (3-pic) ligands. One 3-pic ligand is shown with atom numbering: 1 for the nitrogen, 2 for the carbon attached to the ring, 3 for the carbon at the meta position, 4 for the carbon at the para position, 5 for the carbon at the other meta position, and 6 for the carbon at the other para position. The other 3-pic ligand is shown without numbering.</p>
<i>trans</i> -[Pt(Cl) ₂ (4-pic) ₂]	24	<p>The structure shows a platinum (Pt) center in a trans configuration. It is coordinated to two chlorine (Cl) atoms and two 4-picoline (4-pic) ligands. One 4-pic ligand is shown with atom numbering: 1 for the nitrogen, 2 for the carbon attached to the ring, 3 for the carbon at the meta position, 4 for the carbon at the para position, and 5 for the carbon at the other meta position. The other 4-pic ligand is shown without numbering.</p>
<i>trans</i> -[Pt(N ₃) ₂ (4-pic) ₂]	25	<p>The structure shows a platinum (Pt) center in a trans configuration. It is coordinated to two azido (N₃) groups and two 4-picoline (4-pic) ligands. One 4-pic ligand is shown with atom numbering: 1 for the nitrogen, 2 for the carbon attached to the ring, 3 for the carbon at the meta position, 4 for the carbon at the para position, and 5 for the carbon at the other meta position. The other 4-pic ligand is shown without numbering.</p>
<i>trans, trans, trans</i> -[Pt(N ₃) ₂ (OH) ₂ (4-pic) ₂]	26	<p>The structure shows a platinum (Pt) center in a trans configuration. It is coordinated to two azido (N₃) groups, two hydroxyl (OH) groups, and two 4-picoline (4-pic) ligands. One 4-pic ligand is shown with atom numbering: 1 for the nitrogen, 2 for the carbon attached to the ring, 3 for the carbon at the meta position, 4 for the carbon at the para position, and 5 for the carbon at the other meta position. The other 4-pic ligand is shown without numbering.</p>
<i>trans</i> -[Pt(Cl) ₂ (tz) ₂]	27	<p>The structure shows a platinum (Pt) center in a trans configuration. It is coordinated to two chlorine (Cl) atoms and two thiazole (tz) ligands. One thiazole ligand is shown with atom numbering: 1 for the sulfur, 2 for the carbon attached to the ring, 3 for the nitrogen, 4 for the carbon at the other end of the double bond, and 5 for the carbon at the other end of the single bond. The other thiazole ligand is shown without numbering.</p>

<i>trans</i> -[Pt(N ₃) ₂ (tz) ₂]	28	<p>The structure shows a platinum (Pt) center in a square planar geometry. It is coordinated to two azide (N₃) ligands in a trans configuration and two thiazole (tz) ligands in a trans configuration. The thiazole ring is numbered 1 to 5, with the nitrogen atom at position 3. The azide ligands are represented as N₃ groups.</p>
<i>trans, trans, trans</i> -[Pt(N ₃) ₂ (OH) ₂ (tz) ₂]	29	<p>The structure shows a platinum (Pt) center in a square planar geometry. It is coordinated to two azide (N₃) ligands in a trans configuration, two hydroxyl (OH) ligands in a trans configuration, and one thiazole (tz) ligand. The thiazole ring is numbered 1 to 5, with the nitrogen atom at position 3.</p>
<i>trans</i> -[Pt(Cl) ₂ (mim) ₂]	30	<p>The structure shows a platinum (Pt) center in a square planar geometry. It is coordinated to two chloride (Cl) ligands in a trans configuration and two 1-methylimidazole (mim) ligands in a trans configuration. The imidazole ring is numbered 1 to 5, with the nitrogen atoms at positions 1 and 3.</p>
<i>trans</i> -[Pt(N ₃) ₂ (mim) ₂]	31	<p>The structure shows a platinum (Pt) center in a square planar geometry. It is coordinated to two azide (N₃) ligands in a trans configuration and two 1-methylimidazole (mim) ligands in a trans configuration. The imidazole ring is numbered 1 to 5, with the nitrogen atoms at positions 1 and 3.</p>
<i>trans, trans, trans</i> -[Pt(N ₃) ₂ (OH) ₂ (mim) ₂]	32	<p>The structure shows a platinum (Pt) center in a square planar geometry. It is coordinated to two azide (N₃) ligands in a trans configuration, two hydroxyl (OH) ligands in a trans configuration, and two 1-methylimidazole (mim) ligands in a trans configuration. The imidazole ring is numbered 1 to 5, with the nitrogen atoms at positions 1 and 3.</p>
5'-Guanosine Monophosphate (5'-GMP)	33	<p>The structure shows the chemical structure of 5'-Guanosine Monophosphate (5'-GMP). It consists of a guanine base (a purine ring system with an amino group at position 2 and a carbonyl group at position 6) attached to a ribose sugar at the 1' position. The ribose sugar is numbered 1' to 5', and the phosphate group is attached to the 5' carbon. The phosphate group is shown as a phosphorus atom double-bonded to an oxygen atom and single-bonded to three hydroxyl groups.</p>



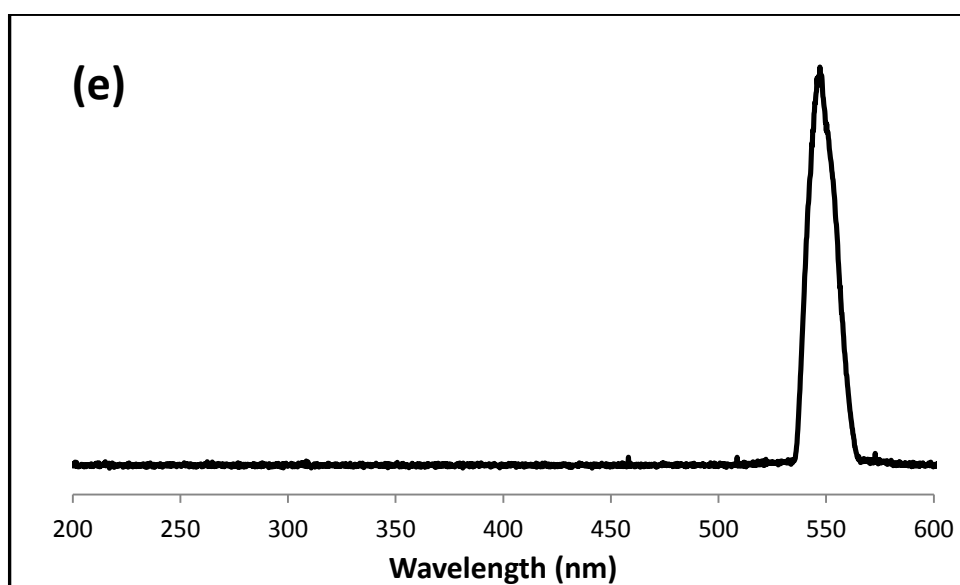
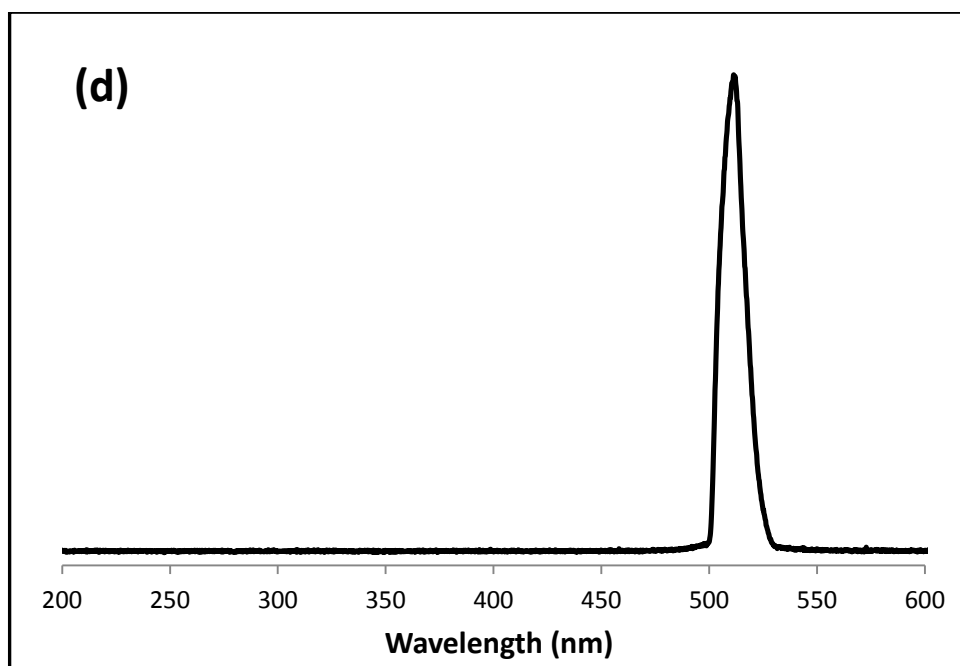
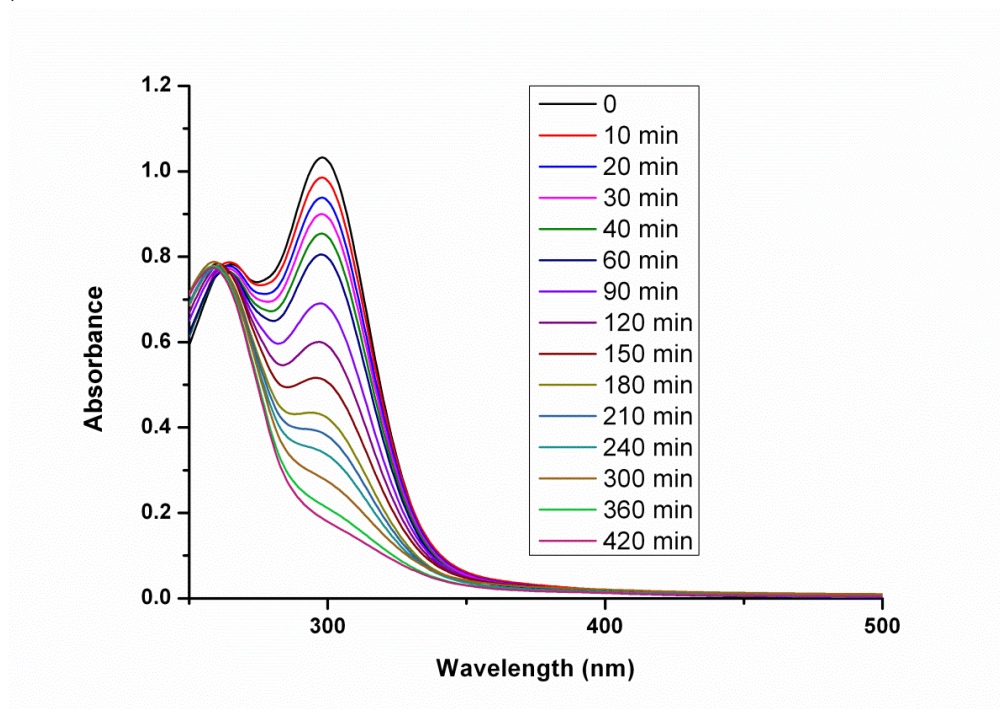
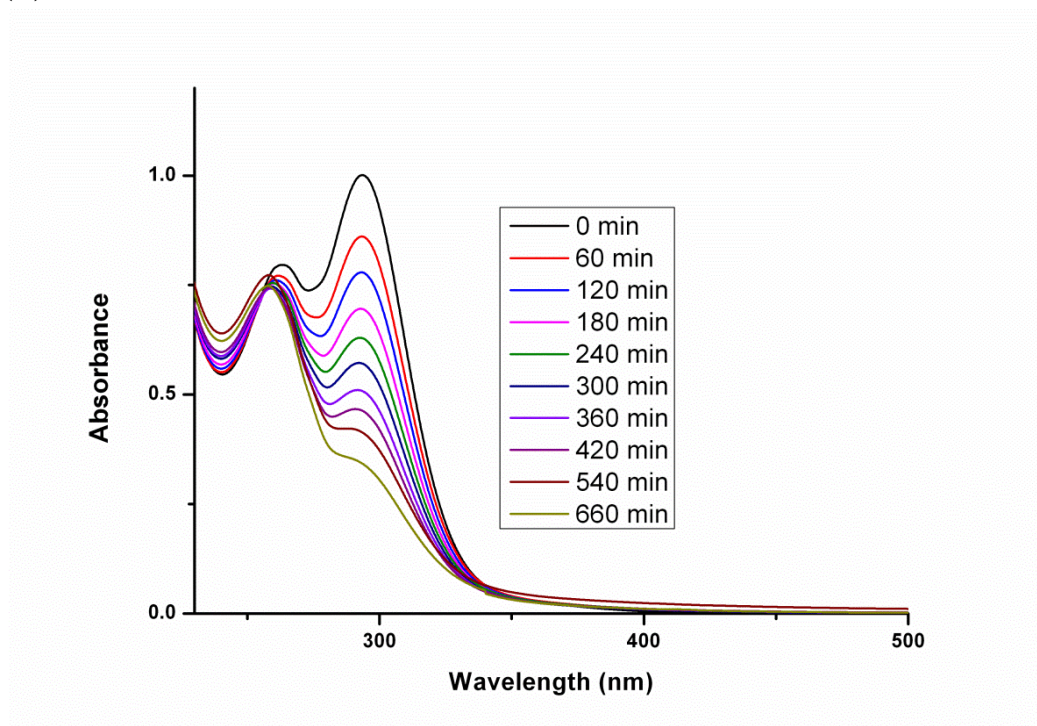


Figure A1: Output of Light Sources. (a) UVA lamps (Hitachi) fitted in the LZC-ICH2 photoreactor; (b) 420 nm lamps (Luzchem) fitted in the LZC-ICH2 photoreactor; (c) 463 nm, LED; (d) 517 nm, LED; (e) 550 nm KiloArc, fitted with GG530 filter, 4 nm slit widths.

(a)**(b)**

(c)

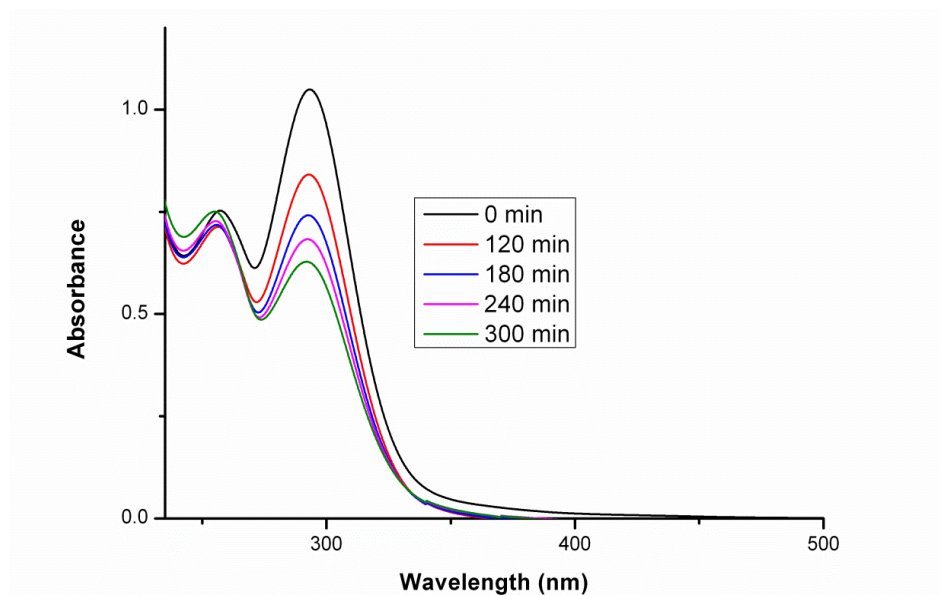


Figure A2: UV-Vis spectra of some complexes presented in Chapter 4 upon photoirradiation with 517 nm (30 mW/cm^2): (a) complex *trans, trans, trans*-[Pt(N₃)₂(OH)₂(pyr)(2-pic)] **18**, (b) complex *trans, trans, trans*-[Pt(N₃)₂(OH)₂(pyr)(3-pic)] **19** and (c) complex *trans, trans, trans*-[Pt(N₃)₂(OH)₂(pyr)(4-pic)] **20**, respectively. The graphs show the decrease in intensity of the N₃→Pt LMCT absorption band upon continuous irradiation at *ca.* 20 °C.

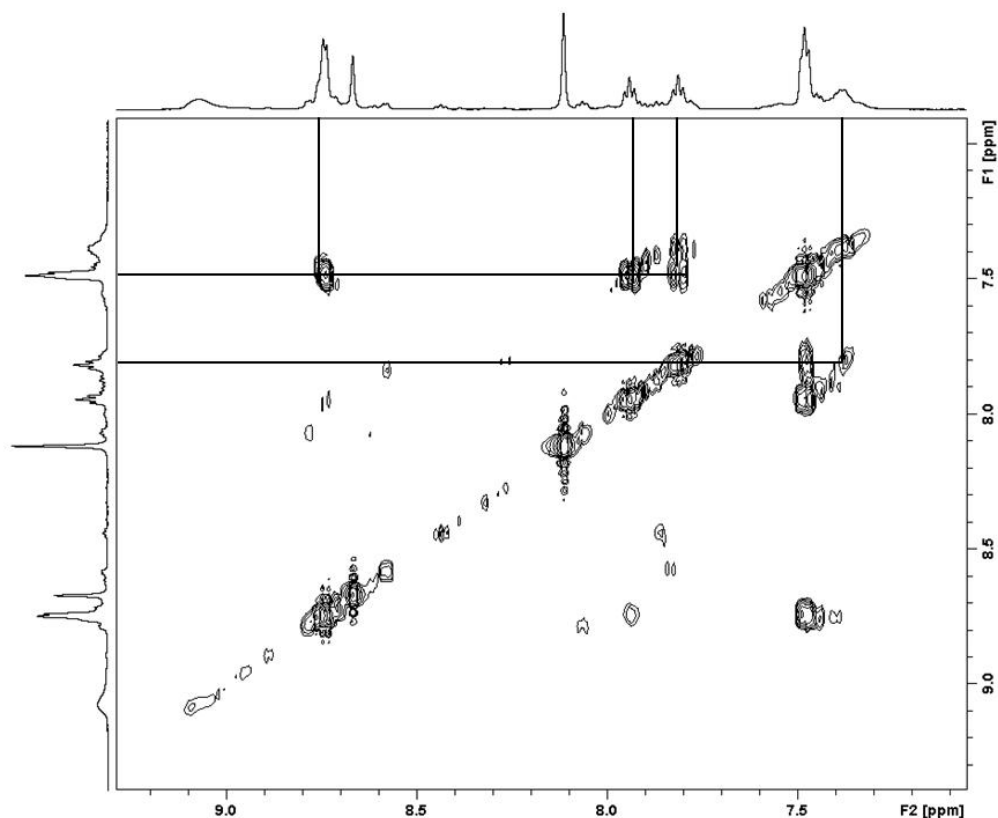


Figure A3: ¹H-COSY NMR spectrum (600 MHz) of complex *trans, trans, trans*-[Pt(N₃)₂(OH)₂(pyr)(2-pic)] **18** upon photoirradiation (420 nm, 7 mW/cm², 45 min) in the presence of 5'-GMP (2 mol equiv). The correlated signals correspond to the *trans*-[Pt(N₃)(5'-GMP)(pyr)(2-pic)] adduct.

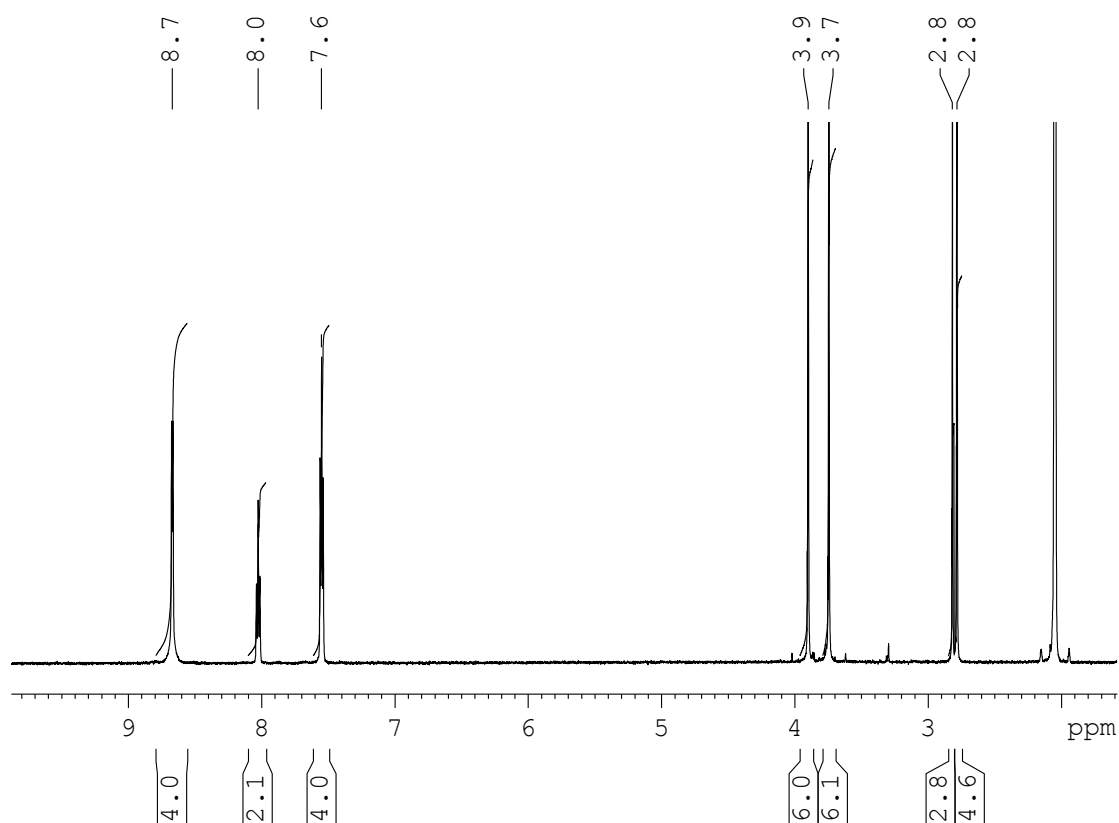


Figure A4: ^1H -NMR (600 MHz) of the $[\text{Pt}^{\text{II}}(4,5\text{-dicarbamethoxy-1,2,3-triazole})_2(\text{pyr})_2]$ produced by the click reaction of DMAD to $[\text{Pt}(\text{N}_3)_2(\text{pyr})_2]$. The peaks at 3.9 and 3.7 ppm are assigned to the two methyl groups on the triazole.